



**This electronic thesis or dissertation has been  
downloaded from Explore Bristol Research,  
<http://research-information.bristol.ac.uk>**

*Author:*

**Brown, Jamie R C**

*Title:*

**Assessing the combined effect of Carbon-Water dynamics on hydrological processes  
in Brazil**

**General rights**

Access to the thesis is subject to the Creative Commons Attribution - NonCommercial-No Derivatives 4.0 International Public License. A copy of this may be found at <https://creativecommons.org/licenses/by-nc-nd/4.0/legalcode> This license sets out your rights and the restrictions that apply to your access to the thesis so it is important you read this before proceeding.

**Take down policy**

Some pages of this thesis may have been removed for copyright restrictions prior to having it been deposited in Explore Bristol Research. However, if you have discovered material within the thesis that you consider to be unlawful e.g. breaches of copyright (either yours or that of a third party) or any other law, including but not limited to those relating to patent, trademark, confidentiality, data protection, obscenity, defamation, libel, then please contact [collections-metadata@bristol.ac.uk](mailto:collections-metadata@bristol.ac.uk) and include the following information in your message:

- Your contact details
- Bibliographic details for the item, including a URL
- An outline nature of the complaint

Your claim will be investigated and, where appropriate, the item in question will be removed from public view as soon as possible.

# **Assessing the combined effect of Carbon-Water dynamics on hydrological processes in Brazil**

By

JAMIE BROWN



Department of Civil Engineering

UNIVERSITY OF BRISTOL

A thesis submitted to the University of Bristol in accordance with the requirements of the degree of DOCTOR OF PHILOSOPHY in the Faculty of Engineering

JUNE 2023

Word count: 35448



## ABSTRACT

Vegetation dynamics optimally adapt to given environmental conditions by maximising their net carbon profit. If we model these processes, can they help us understand hydrological fluxes across different climates? Furthermore, can this optimality modelling further our understanding on the sensitivity of carbon-water mechanisms in vegetation to changes in CO<sub>2</sub>? This thesis uses a vegetation optimality model across multiple biomes in Brazil to examine the extent to which it can answer these questions. Firstly, we examine the reliability and suitability of five high-resolution meteorological gridded products (ERA5-Land, GLDAS2.0, GLDAS2.1, the BNMD and MSWEPv2.2 (precipitation only)) for seven variables (precipitation, air temperature, wind speed, pressure, specific humidity and downward shortwave and longwave radiation) against eleven flux towers spanning five biomes across Brazil. At the daily scale analysis showed that MSWEPv2.2 outperformed the others for precipitation whilst ERA5-Land showed the most consistency for all other variables. Secondly, we show that the Vegetation Optimality Model (VOM), is successfully able to reproduce patterns of evapotranspiration (ET) at several sites, with a stronger correlation at more seasonal sites ( $r$  values ranging 0.25 – 0.69 across sites). VOM is a developed model that attempts to quantify the physiological processes of a plant growth carbon-capture cost-benefit system through describing carbon-water dynamics. Results show the importance of root dynamics in the success of the model; the minimal calibration needed per site reflects the strong physiological understanding behind it. Finally, we show declines in ET across an increasing atmospheric CO<sub>2</sub> gradient, with dampened impacts on hydrological processes through modelling long-term adaptations in vegetation (reductions from 0.7-6.0% over an increase of 77 ppm CO<sub>2</sub>). Overall, this thesis advances our knowledge in relation to the questions above improving our understanding of modelling hydrological processes in vegetation dominated environments across Brazil.



## ACKNOWLEDGEMENTS

This research was funded as part of the Water Informatics Science and Engineering Centre for Doctoral Training (WISE CDT) through a grant from the Engineering and Physical Sciences Research Council (EPSRC), grant number EP/L016214/1. The research was also partially supported by the Brazilian Experimental datasets for Multi-Scale interactions in the critical zone under Extreme Drought (BEMUSED) project, which is funded by UK Natural Environment Research Council (NERC; grant number NE/R004897/1) and the Fundação de Amparo à Pesquisa do Estado de São Paulo (FAPESP).

First and foremost, I wish to thank my supervisors Dr Rafael Rosolem and Dr Ross Woods for their continuous support and their contributions to this thesis in the form of direction, ideas, critical review, encouragement, and incredible patience. Rafael, thanks for the unbelievable amount of effort and support you gave consistently over the course of my research, steering me through the jungle of hydrometeorology and motivating me through your passion of your incredible home country, Brazil. Thanks also for being more than a supervisor, always checking up and asking important questions outside of the academic bubble and sharing the odd evening at the bar with a glass of whisky. Ross, thank you for always listening and helping me see the wider picture throughout, encouraging novel approaches, stimulating interesting debates, and most importantly reminding me that its always more important to ask questions rather than to know the answers. Thanks to Dr Stan Schymanski, without whom there would be no vegetation model. Thank you, Stan, and Remko for making me feel welcome in Luxembourg and for always offering guidance and help navigating the waters of VOM. Thanks to the rest of room A008 who made the office an enjoyable workplace. I also would like to acknowledge Prof Humberto Ribeiro da Rocha at Universidade de São Paulo, and Prof Debora Regina Roberti at the Universidade Federal de Santa Maria for providing additional data for

Cruz Alta (CRA), Votorantim Fazenda Cara Preta (VCP) and Usina Santa Rita (USR). An additional mention to data contributions should also go to Celso von Randow who supplied closed energy balance data and providing important direction regarding the latent heat measurements for Reserva Jarú (RJA) and Fazenda Nossa Senhora (FNS) addressed in Appendix B.

I am also indebted to my WISE colleagues and my office mates at Woodland Road. Thank you especially to Bert and Elisa for becoming strong friends and relating to the many struggles a PhD entails offering frequent ad-hoc advice on both scientific and personal matters from the beaches of Devon to the back gardens of Bath. In addition, I would like to give a special mention to; Briony, for her constant support and encouragement over the final year who helped edit this thesis and probably learned more than she ever wanted to about tropical hydrometeorology, Penney, for interesting conversations regarding academia and personal support throughout, who won't believe the thesis is finally finished, and Will for the squash games, a moment of much needed calm in the final onslaught to the finish line.

Finally, I would like to thank my family for the unwavering support they have provided over the course of my studies and especially through the pandemic. Both my siblings for understanding efforts and always offering to read, and edit, the younger of whom motivating me through competition to the PhD finish line (who may have *just* beaten me). My mum for keeping my fridge well stocked and always reminding me there are other things to worry about, and my dad who was an unofficial third supervisor, for his wisdom, direction, and interest, and for both of their encouragement, without which this thesis would not exist.





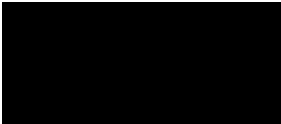
*Water is the blood of the Earth and rivers, its veins.*

– Leonardo da Vinci



## AUTHOR'S DECLARATION

I declare that the work in this dissertation was carried out in accordance with the requirements of the University's Regulations and Code of Practice for Research Degree Programmes and that it has not been submitted for any other academic award. Except where indicated by specific reference in the text, the work is the candidate's own work. Work done in collaboration with, or with the assistance of, others, is indicated as such. Any views expressed in the dissertation are those of the author.

SIGNED:  .....

DATE: .....18/09/2023.....



## TABLE OF CONTENTS

1.	Chapter 1: Introduction .....	1
1.1	Background .....	1
1.1.1	The role of carbon-water dynamics in hydrological models.....	1
1.1.2	The importance of Brazilian Biomes .....	6
1.2	Aims and objectives .....	10
1.3	Thesis Outline .....	12
2.	Chapter 2: The Study Sites .....	16
2.1	Introduction.....	16
2.2	The Study Sites .....	19
2.2.1	Manaus Kilometer 34 (K34) ( <i>Araújo et al. 2002</i> ).....	19
2.2.2	Santarém Kilometer 67 (K67) ( <i>Saleska et al., 2003</i> ) .....	21
2.2.3	Santarém Kilometer 83 (K83) ( <i>Goulden et al., 2004</i> ).....	22
2.2.4	Santarém Kilometer 77 (K77) ( <i>Sakai et al., 2004</i> ) .....	23
2.2.5	Reserva Jarú (RJA) ( <i>von Randow et al., 2004</i> ) .....	24
2.2.6	Fazenda Nossa Senhora (FNS) ( <i>Kirkman et al., 2002</i> ) .....	25
2.2.7	Ilha do Bananal (BAN) ( <i>Borma et al., 2009</i> ).....	26
2.2.8	Reserva Pé de Gigante (PDG) ( <i>da Rocha et al., 2002</i> ) .....	27
2.2.9	Usina Santa Rita (USR) ( <i>Cabral et al., 2013</i> ) .....	28
2.2.10	Votorantim Fazenda Cara Preta (VCP) ( <i>Cabral et al., 2010</i> ).....	29
2.2.11	Cruz Alta (CRA) ( <i>Webler et al., 2012</i> ) .....	30
3.	Chapter 3: How can we choose accurate meteorological forcing data in the region? ..	32
3.1	Introduction.....	32
3.1.1	Chapter Contained Research Questions .....	35
3.2	Datasets .....	35
3.2.1	In-situ observations .....	35
3.2.2	Regional Products .....	36
3.3	Methodology .....	39
3.3.1	Quality control.....	39
3.3.2	Temporal averaging.....	39
3.3.3	Wind Speed vertical interpolation.....	40

3.3.4	Pressure .....	41
3.3.5	Specific humidity .....	41
3.3.6	Decomposition of the mean square error .....	41
3.3.7	Ranking .....	42
3.4	Results.....	43
3.4.1	Precipitation .....	43
3.4.2	Air Temperature .....	45
3.4.3	Other Meteorological Variables .....	48
3.4.4	Seasonality in Errors .....	50
3.5	Discussion.....	53
3.5.1	Which product is recommended overall?.....	53
3.5.2	Which product is recommended for each variable?.....	53
3.5.3	What are the dominant types of error?.....	54
3.5.4	How do these errors vary by location and time of year?.....	54
3.5.5	Comparative literature.....	55
3.6	Implications and Conclusions .....	57
4.	Chapter 4: How can we use Carbon-Water mechanisms to understand hydrological fluxes?.....	60
4.1	Introduction.....	60
4.1.1	Chapter Contained Research Questions .....	64
4.2	The Vegetation Optimality Model.....	65
4.2.1	Vegetation model .....	65
4.2.2	Carbon costs and benefits.....	66
4.2.3	Water balance model.....	68
4.2.4	Model Optimisation.....	70
4.3	Methodology .....	70
4.3.1	Model forcing data .....	70
4.3.2	Soil hydraulic properties .....	71
4.3.3	Adjustable vegetation parameters .....	72
4.3.4	Tuning vegetation parameters .....	72
4.3.5	Model evaluation.....	74
4.4	Results.....	75
4.4.1	VOM parameter sensitivity analysis using K83.....	75

4.4.2	Model performance at sites representing natural ecosystems .....	79
4.4.3	Model performance at sites representing cultivated ecosystems .....	84
4.5	Discussion .....	85
4.6	Conclusions.....	92
4.6.1	To what extent can the VOM predict ET across different climates? .....	92
4.6.2	To what extent can the VOM predict ET in natural ecosystems?.....	93
4.6.3	To what extent can the VOM predict ET in cultivated ecosystems? .....	94
4.6.4	What is the sensitivity of the VOM to poorly constrained parameters in these environments? .....	94
4.6.5	What are the important water and plant interactions captured by vegetation optimality in the study areas? .....	95
4.6.6	Overall conclusions .....	95
5.	Chapter 5: How sensitive are hydrological processes in vegetation to changes in atmospheric CO <sub>2</sub> concentration? .....	98
5.1	Introduction.....	98
5.1.1	Chapter contained research questions .....	102
5.2	Methodology .....	102
5.2.1	Selection of sites.....	102
5.2.2	Justification of simulated atmospheric CO <sub>2</sub> concentrations.....	103
5.2.3	Simulating short and long-term vegetation responses.....	105
5.2.4	Variables showing simulated response .....	106
5.3	Results.....	106
5.3.1	Evapotranspiration, Discharge and Roots .....	106
5.3.2	Water Use Efficiency .....	109
5.3.3	Fractional Vegetation Cover .....	110
5.4	Discussion .....	115
5.4.1	Hydrological responses to eCO <sub>2</sub> across natural ecosystems .....	115
5.4.2	Hydrological responses to eCO <sub>2</sub> across cultivated ecosystems .....	118
5.4.3	The importance of perennial responses to eCO <sub>2</sub> on hydrological processes	119
5.4.4	Synthesis and limitations.....	120
5.5	Conclusions.....	121
6.	Chapter 6: Conclusions and Outlook .....	125
6.1	Summary .....	125

6.2	Overarching remarks.....	128
6.3	Directions for future research .....	131
A.	Appendix A: Supporting Information for Chapter 3.....	138
A.1	An overview of errors and their contribution to the MSE .....	138
A.2	Seasonality in errors.....	139
A.3	Gridded meteorological forcing data availability .....	139
A.3.1	Seasonal errors in precipitation (mm) .....	149
A.3.2	Seasonal errors in Air Temperature (°C) .....	151
A.3.3	Seasonal errors in Incoming Solar Radiation ( $\text{W m}^{-2}$ ).....	153
A.3.4	Seasonal errors in specific humidity ( $\text{kg kg}^{-1}$ ) .....	155
B.	Appendix B: Supporting Information for Chapter 4.....	158
B.1	Energy balance closure at RJA and FNS .....	158
B.2	Parameter values for the Vegetation Optimality Model .....	159
B.3	Data and model code availability.....	159
C.	Appendix C: Supporting Information for Chapter 5.....	162
C.1	Results for sites excluded sites .....	162
7.	References.....	166





## LIST OF TABLES

Table 2.1 Summary of the abbreviated names, lat, lon, location, period of observation, vegetation type, elevation (abs), and references for the 11 flux tower sites analysed in this thesis. All sites were provided directly by the principal investigator. * .....	20
Table 3.1 Selected variables from each flux tower site with variables that were unavailable noted. ....	36
Table 3.2 Description of variables listed in Table 3.1 .....	36
Table 3.3 Summary of gridded data products used in this study <sup>a</sup> .....	37
Table 3.4 Overall ranks for MSE. MSE is taken per variable per site and ranked. Ranks are then averaged for all sites to produce an overall rank for daily and monthly data. Both the lowest (bold) value (i.e. best performance) and highest (italics) value (i.e., worst performance) in each row are identified. Dashed cells (-) indicate no data available. Ranking for precipitation has been scaled to be included in the average rank. ....	44
Table 4.1 Soil characteristics of the Brazilian study sites, based on the High resolution South American hydraulic parameter map (Marthews et al., 2014). $\Theta_r$ and $\Theta_s$ refer to residual and saturated soil moisture content, respectively, $\alpha$ and $n$ the Van Genuchten soil parameters (Van Genuchten, 1980) and $K_{sat}$ the saturated hydraulic conductivity. ....	72
Table 4.2 The initial conditions and for water table depth and maximum rooting depth set in VOM with the minimum and maximum depths of the grid cells surrounding the site. Water table depths taken from Fan et al. (2013), and maximum rooting depths taken from Fan et al. (2017). All depths are given in meters above ground level to provide a negative value. ....	73
Table 4.3 ET errors between VOM results and observations at site K83 for different $c_{rv}$ values. Table a) represents initial sensitivity analysis whilst table b) represents finer analysis. Units for $c_{rv}$ , $(\sigma_s - \sigma_o)$ , $(\mu_s - \mu_o)$ and RMSE are given in $(\mu\text{mol m}^3 \text{s}^{-1})$ . The value of $c_{rv}$ with the lowest combination of errors has been highlighted and this was used to run the final simulation. ....	78
Table 4.4 Errors between VOM simulation and flux tower observations at all sites seperated into natural and cultivated ecosystems. Showing the land cover type, Pearson's correlation coefficient ( $r$ ), difference in standard deviations $(\sigma_s - \sigma_o)$ , difference in means $(\mu_s - \mu_o)$ and the root mean square error (RMSE). Units for $(\sigma_s - \sigma_o)$ , $(\mu_s - \mu_o)$ and the RMSE are in $\text{mm d}^{-1}$ . ....	80
Table 4.5 All study sites grouped by their Köppen climate classification. Derived from (Alvares et al., (2014) and literature. ....	86
Table 5.1 Sites analysed in this chapter with their respective land cover and Köppen climate classification (Alvares et al., 2013).....	103
Table 5.2 Simulated responses to increasing $C_a$ . The first column in each variable block gives actual values for $C_a = 339$ ppm, while the subsequent columns in italics give the percentage difference from this value. Decreases, or negative differences, are shown in red. P, precipitation, ET, evapotranspiration, Q, discharge, WUE, water use efficiency (Equation(5-1), FVC, fractional vegetation cover of all vegetation (perennial and seasonal), RAI, root area index (fine root surface area per ground area), $R_i$ depth, maximum rooting depth of perennials, $R_g$ depth, maximum rooting depth of seasonal vegetation. a) shows vegetation short-term adaptation, b) shows long-term adaptation.	

Shaded cells indicate that the means of ET were significantly different ( $p < 0.05$ ) when compared to the mean of the lowest  $C_a$  run (339ppm). ..... 114

Table A.1 Data Sources for Chapter 3 ..... 140

Table A.2 The correlation contribution to the MSE scaled to the RMSE of each gridded data set and the meteorological variables against all observation sites at the DAILY scale.. .... 141

Table A.3 The bias contribution to the MSE scaled to the RMSE of each gridded data set and the meteorological variables against all observation sites at the DAILY scale..... 142

Table A.4 The variation contribution to the MSE scaled to the RMSE of each gridded data set and the meteorological variables against all observation sites at the DAILY scale. .... 143

Table A.5 The MSE scaled to the RMSE of each gridded data set and the meteorological variables against all observation sites at the DAILY scale ..... 144

Table A.6 The correlation contribution to the MSE scaled to the RMSE of each gridded data set and the meteorological variables against all observation sites at the MONTHLY scale. .... 145

Table A.7 The bias contribution to the MSE scaled to the RMSE of each gridded data set and the meteorological variables against all observation sites at the MONTHLY scale. .... 146

Table A.8 The variation contribution to the MSE scaled to the RMSE of each gridded data set and the meteorological variables against all observation sites at the MONTHLY scale. .... 147

Table A.9 The MSE scaled to the RMSE of each gridded data set and the meteorological variables against all observation sites at the MONTHLY scale..... 148

Table B.1 Description of the parameters set in VOM to achieve the results presented in Chapter 4. From left to right the parameters are soil depth (m), capital gamma S (m), average channel bed elevation (m) (above the bottom of the profile), the slope to channel (radians), saturated hydraulic conductivity ( $m\ s^{-1}$ ), residual soil moisture, saturated soil moisture, the van Genuchten soil parameter n, the van Genuchten soil parameter alpha ( $1/m$ ), the thickness of the soil sublayers (m), min and max tree root depth (m), min and max grass root depth (m), water transport cost factor ( $\mu mol\ m^3\ s^{-1}$ ). ..... 160

Table B.2 Data Sources used in Chapter 4..... 160



## LIST OF FIGURES

Figure 2.1 Schematic of a typical flux tower showing the types of instrumentation that may be used to take meteorological measurements. Depending on the tower there may be more instruments up the body of the tower to measure gas exchanges. ....	17
Figure 2.2 Map of Brazil split into its six major biomes showing the location of the study sites analysed in this thesis and their measured average monthly precipitation (blue), air temperature (red), and incoming irradiance (green). ....	18
Figure 2.3 K34 flux tower near Manaus. Source: <a href="https://lba2.inpa.gov.br/">https://lba2.inpa.gov.br/</a> .....	19
Figure 2.4 K67 primary forest tower near Santarém (Hutyra et al., 2008).....	21
Figure 2.5 Instruments positioned at the top of the flux tower located at K83 (Miller et al., 2009) 22	
Figure 2.6 K77 flux tower at the pasture site near Santarem (Fitzjarrold and Sakai, 2010).....	23
Figure 2.7 RJA flux tower site, Rebio Jaru. Source: <a href="https://lba2.inpa.gov.br/">https://lba2.inpa.gov.br/</a> .....	24
Figure 2.8 View from PDG tower overlooking cerrado vegetation in (a) wet-January and (b) dry-September seasons (Cabral et al., 2015) .....	27
Figure 2.9 USR tower site. (Xin et al., 2020) .....	28
Figure 3.1 Air temperature at site BAN where a). shows partial contributions to the MSE for each gridded dataset and b). shows the monthly time series of all gridded datasets for air temperature over the operation period of the flux tower (observation data in bold). .....	43
Figure 3.2 Partial contributions to the MSE between each observation site and gridded dataset (x-axis) for each variable (y-axis) at the daily scale. Precipitation includes MSWEPv2.2 errors. ....	46
Figure 3.3 Partial contributions to the MSE between each observation site and gridded dataset (x-axis) for each variable (y-axis) at the monthly scale. Precipitation includes MSWEPv2.2 errors. ....	47
Figure 3.4 Partial contributions to the MSE averaged by month over all operational observation years for MSWEPv2.2 precipitation across all sites. Sites are in descending order from distance from equator.....	51
Figure 3.5 Partial contributions to the MSE averaged by month over all operational observation years for ERA5-Land air temperature across all sites. Sites are in descending order from distance from equator.....	52
Figure 4.1 A simplified visual conception of the Vegetation Optimality Model coupling a vegetation dynamics model with a water balance model detailing inputs, outputs and main interactions between carbon and water. ....	69
Figure 4.2 Comparison of ET, precipitation, and soil moisture saturation for a). observation measurements taken at site K83 (Bruno et al., 2006) and b). the VOM modelled soil moisture and ET results predicted by the VOM .....	76
Figure 4.3 VOM ET results for altered values of the cost factor ( $c_{rv}$ ) (colour bar) for site K83 overlapping with observations (black line) July 2000-March 2004. $c_{rv}$ values for the more coarse sensitivity seen in a) are associated with those in Table 4.3a whilst $c_{rv}$ values for the finer sensitivity analysis are found in Table 4.3b. All data are weekly averages of daily total ET. ....	78

Figure 4.4 Final VOM simulation (red) and flux tower observation (black) ET for the overlapping period for sites representing natural ecosystems. Results are displayed descending with distance from the equator.....81

Figure 4.5 Final VOM simulation (red) and flux tower observation (black) ET for the overlapping period for sites representing cultivated ecosystems. Results are displayed descending with distance from the equator.....82

Figure 4.6 ET rate averaged by month for the final VOM simulations (red) and flux tower observations (black) at all sites, natural and cultivated. Average monthly forcing precipitation is shown with grey bars on the secondary axis. Simulations were only averaged for the overlapping period with observations.....83

Figure 5.1 Annual average atmospheric CO<sub>2</sub> concentrations from Mauna Loa observatory (blue), and temperature (red) and precipitation (blue) over Brazil from ERA5 1980 – 2021. Black triangles indicate the selected [CO<sub>2</sub>] used in this study at years 1980, 2004 and 2021. .... 104

Figure 5.2 Simulated mean annual ET rates for varying C<sub>a</sub>. ‘Long-term’ (blue) refers to simulations where all vegetation properties were optimised for each C<sub>a</sub>. ‘Short-term’ (red) refers to simulations where ‘long-term’ optimised parameters for C<sub>a</sub> = 339 ppm were kept for C<sub>a</sub> = 377 and 416 ppm simulations. The black dashed line is ET at C<sub>a</sub> = 339 ppm simulations for reference. .... 111

Figure 5.3 Simulated mean monthly ET rates for varying C<sub>a</sub> at natural Brazilian ecosystems. ‘Long-term’ (right) refers to simulations where all vegetation properties were optimised for each C<sub>a</sub>. ‘Short-term’ (left) refers to simulations where ‘long-term’ optimised parameters for C<sub>a</sub> = 339 ppm were kept for C<sub>a</sub> = 377 and 416 ppm simulations. Grey bars represent precipitation for reference between water limiting and energy limiting periods..... 112

Figure 5.4 Simulated mean monthly ET rates for varying C<sub>a</sub> at cultivated Brazilian ecosystems. ‘Long-term’ (right) refers to simulations where all vegetation properties were optimised for each C<sub>a</sub>. ‘Short-term’ (left) refers to simulations where ‘long-term’ optimised parameters for C<sub>a</sub> = 339 ppm were kept for C<sub>a</sub> = 377 and 416 ppm simulations. Grey bars represent precipitation for reference between water limiting and energy limiting periods..... 113

Figure A.1 Partial contributions to the MSE averaged by month over all operational observation years for precipitation across all sites for gridded datasets a) BNMD, b) ERA5-Land, c) GLDAS2.0, and d) GLDAS2.1. Sites are in descending order from distance from equator. .... 150

Figure A.2 Partial contributions to the MSE averaged by month over all operational observation years for Air Temperature across all sites for gridded datasets a) BNMD, b) GLDAS2.0, and c) GLDAS2.1. Sites are in descending order from distance from equator. .... 152

Figure A.3 Partial contributions to the MSE averaged by month over all operational observation years for precipitation across all sites for gridded datasets a) BNMD, b) ERA5-Land, c) GLDAS2.0, and d) GLDAS2.1. Sites are in descending order from distance from equator. .... 154

Figure A.4 Partial contributions to the MSE averaged by month over all operational observation years for specific humidity across all sites for gridded datasets a) BNMD, b) ERA5-Land, c) GLDAS2.0, and d) GLDAS2.1. Sites are in descending order from distance from equator..... 156

Figure B.1 Average diurnal cycles comparing evaporation after applying the energy balance closure to latent heat flux and unaltered measured latent heat flux at site FNS. .... 158

Figure B.2 Average diurnal cycles comparing evaporation after applying the energy balance closure to latent heat flux and unaltered measured latent heat flux at site RJA. .... 159

Figure C.1 Simulated mean annual ET rates for varying  $C_a$  at excluded sites BAN and VCP. 'Long-term' (blue) refers to simulations where all vegetation properties were optimised for each  $C_a$ . 'Short-term' (red) refers to simulations where 'long-term' optimised parameters for  $C_a = 339$  ppm were kept for  $C_a = 377$  and  $416$  ppm simulations. The black dashed line is ET at  $C_a = 339$  ppm simulations for reference. .... 162

Figure C.2 Simulated mean monthly ET rates for varying  $C_a$  at excluded sites a) BAN and b) VCP. 'Long-term' (right) refers to simulations where all vegetation properties were optimised for each  $C_a$ . 'Short-term' (left) refers to simulations where 'long-term' optimised parameters for  $C_a = 339$  ppm were kept for  $C_a = 377$  and  $416$  ppm simulations. Grey bars represent precipitation for reference between water limiting and energy limiting periods. .... 163





## LIST OF ABBREVIATIONS

Abbreviation	Definition
4D-Var	4D-Variational Data Assimilation
BNMD	Brazilian National Meteorological Database
$C_a$	Atmospheric Carbon Concentration
CO <sub>2</sub>	Carbon Dioxide
$c_{rv}$	Water Transport Cost Factor
ECMWF	European Centre for Medium Range Forecasts
eCO <sub>2</sub>	Elevated Atmospheric CO <sub>2</sub> Concentrations
ECMWF	European Centre for Medium-Range Weather Forecasts
ERA5-Land	Fifth Generation European Reanalysis for Land
ET	Evapotranspiration
FACE	Free Air CO <sub>2</sub> Enrichment
FPC	Fractional Percentage Cover of Vegetation
FVC	Fractional Vegetation Cover
GLDAS	Global Land Data Assimilation System
GMAO	Global Modelling and Assimilation Office
GPCP	Global Precipitation Climatology Project
GPP	Gross Primary Productivity
GSFC	Goddard Space Flight Centre
HYBRAS	Hydrophysical Database for Brazilian Soils
IBAMA	Brazilian Environmental Protection Agency
INMET	Instituto Nacional de Meteorologia
K-S test	Kolmogorov-Smirnov test
LAI	Leaf Area Index
LBA	Large-Scale Biosphere-Atmosphere Experiment
LSM	Land Surface Model
MSE	Mean Square Error
MSWEP	Multi-Source Weighted-Ensemble Precipitation
NASA	National Aeronautics and Space Administration
NCP	Net Carbon Profit
NOAA	The National Oceanic and Atmospheric Administration
P	Precipitation
Q	Discharge
RAI	Root Area Index
RMSE	Root Mean Square Error
SYNOP	Surface Synoptic Observations
VOM	Vegetation Optimality Model
WUE	Water Use Efficiency



# Chapter 1: Introduction

## 1.1 Background

### 1.1.1 The role of carbon-water dynamics in hydrological models

Hydrological processes can be realistically represented in small catchments and ungauged basins using current models (Devia et al., 2015; Q. Huang et al., 2020; Wagner et al., 2022), but the drivers of the hydrological system are much more complex at large spatial and temporal scales (Tijerina et al., 2021). Macro-scale hydrological models have been able to simulate runoff from large river basins somewhat realistically in the past for use in predicting global water resources (Arnell, 1999; Vörösmarty et al., 2000; Döll et al., 2003). However, their predictive power has frequently been questioned and several studies have found that often, hydrological models, commonly used worldwide, statistically fail to replicate observations, especially in tropical regions (Trambauer et al., 2013; Allasia et al., 2016; Wannasin et al., 2021; Ávila et al., 2022).

In principle, a hydrological system balances water based on the theory of conservation of mass, whereby water entering a system or area must either leave or be stored within that system. Precipitation is partitioned into runoff and infiltration, then infiltration is partitioned into evapotranspiration (ET) and drainage. The temporal distribution of precipitation controls the system, and water storage balances it. The water cycle and vegetation are intrinsically coupled (e.g., Hutjes et al., 1998; Sprenger et al., 2019) as water balance determines the productivity (e.g., Churkina et al., 1999; Jiao et al., 2021) and distribution (e.g., Stephenson, 1990; Zhang

et al., 2016) of terrestrial vegetation around the world. As such the distribution and composition of vegetation communities are fundamentally important for runoff generation and evapotranspiration (Penman, 1951; Dunn & Mackay, 1995; Zhao et al., 2013; Sood & Smakhtin, 2015; McLaughlin et al., 2017).

Plants have been proven to have considerable effects on runoff through features such as transpiration and stomatal behaviour (e.g., Skiles & Hanson, 1994; Matthews & Lawson, 2018), interception and albedo (Eckhardt et al., 2003), leaf area (Neilson & Marks, 1994; Kergoat, 1998; Tesemma et al., 2015), rooting strategy (Milly, 1997; Liu et al., 2018), and phenology (Peel et al., 2001). For example, it is recognised that deforestation increases runoff (Khaleghi, 2017) and decreases ET (Zeng et al., 2021), while reforestation typically lowers runoff (Bosch & Hewlett, 1982; Francis et al., 2023). Aside from the global distribution of vegetation (Peel et al., 2001), the level of atmospheric CO<sub>2</sub> influences regional and global ET and runoff through impacting the water use efficiency of plants (Lockwood, 1999; Keenan et al., 2013). Atmospheric CO<sub>2</sub> levels have risen consistently over the last few decades showing signs of continued increase into the future (Olivier & Peters, 2020). It has become important to predict the impact of these increased levels on hydrological processes to ensure the future of global water security. For example, at elevated atmospheric CO<sub>2</sub> concentrations, vegetation productivity and photosynthetic rate (carbon uptake) are generally higher per unit of water transpired, while stomatal conductance of water is reduced. Some experimental evidence suggest that this stomatal conductance may even decrease by 30-40% at doubled atmospheric CO<sub>2</sub> concentrations (e.g., Eamus & Jarvis, 1989, Lammertsma et al., 2011) as plants optimise between water loss and CO<sub>2</sub> absorption (Lockwood, 1999). Understanding and quantifying these interactions is essential to understanding hydrological processes at an ecosystem and global level and could be pivotal in predicting the distribution of water under environmental change. Here they are collectively defined in this thesis as carbon-water dynamics.

Parameterisation of vegetation can be inadequate in traditional hydrological models (Duethmann et al., 2020), and the cross-relationship between water and vegetation is not described as a process-based approach. Consequently, crucial hydrosphere-biosphere interactions may be neglected by independent hydrological models, particularly their temporal dynamics (Gerten et al., 2004). As an example, they lack the ability to sufficiently capture hydrological effects that result from alterations in vegetation distribution and composition. These effects are likely to arise in response to climate change (Gitay et al., 2001), inhibiting our ability to model/predict the eco-hydrological processes of certain regions. However, these processes are considered in vegetation dynamics models (Franklin et al., 2020) and have been highlighted as one of the main reasons of failure in conceptual hydrological models, especially in response to climate change (Duethmann et al., 2020).

Over the last two decades there have been efforts to improve representation of carbon-water dynamics in hydrological models. In 2001, Zhang et al., were one of the first to do this by coupling a vegetation model to a water balance model. Since then, vegetation coverage, type, and rooting depth have been dynamically incorporated into such models to explain the decadal and inter-annual variations in water balance (McVicar et al., 2007; Schymanski et al., 2008, 2009; D. Yang et al., 2009; Donohue et al., 2012). However, the diversity of these models is large, with some adopting a process-based approach that generally need large numbers of parameters (Shen et al., 2013; Lei et al., 2014). As our understanding of biophysical processes increases, so does the complexity of vegetation dynamics models (Franklin et al., 2020). The tendency for models to become dependent on an ever-increasing number of parameters mean they become poorly constrained by observations. This in turn decreases model robustness, transparency, and predictive power due to aggregation of uncertainty (Prentice et al., 2015). Important limitations of current vegetation dynamics models have arisen over the last decade,

with predictions of vegetation cover and carbon fluxes shown to differ significantly amongst state-of-the-art global models (Prentice et al., 2015; Whitley et al., 2017; Pugh et al., 2018).

Whilst understanding individual plant processes may improve predictions of hydrological processes, the challenge remains to predict vegetation dynamics in a changing environment. One way of tackling this is to look at the global drivers on vegetation communities and what impacts their structure. It is well known that vegetation type and coverage is strongly influenced by climate and water availability (Stephenson, 1990; Franklin et al., 2020; Gan et al., 2021). There is strong resemblance in growth forms in phylogenetically unconnected plants growing under comparable climates, resulting in similarities in vegetation communities (Keeley & Johnson, 1977; Smith & Wilson, 2002) suggesting that vegetation coevolves with climate. Franklin et al., (2020) argue that three general organisation principals; self-organisation, natural selection, and entropy maximisation, can help in producing more reliable vegetation models. Although not novel ideas, they have only been explored primarily in theoretical and small-scale studies. Recent approaches to modelling vegetation dynamics focus on a single controlling factor that forces the direction of vegetation coevolving with climate, which, if coupled with a traditional hydrological model could enhance predictive power in changing environments.

Troch et al. (2013) considered that vegetation's coevolution with climate leads to long-term hydrologic partitioning and catchments develop signatures based on their climate, vegetation, and soil interactions. Biophysical processes that take climate, water, and soil interactions into account can then be used to find the limitations to vegetation growth and hence help explain hydrological processes. For example, vegetation water use efficiency (Caylor et al., 2009; Troch et al., 2009, 2013; Medlyn et al., 2011; Manzoni et al., 2013; Creed et al., 2014) and net carbon gain/profit (Raupach, n.d.; Schymanski et al., 2007b, 2009, 2015a; Del Jesus et al., 2012; Manzoni et al., 2013) might control the direction of vegetation coevolving with climate.

## *Chapter 1: Introduction*

Rooting depth and density, and vegetation coverage and type can be estimated assuming that plants will naturally want to maximise growth and productivity whilst reducing their water stress to achieve an optimal state (Kleidon & Heimann, 1998; Van Wijk & Bouten, 2001; Collins & Bras, 2007).

The original concept of vegetation optimality modelling can be traced back to Cowan and Farquhar (1977) who explored the concept of stomatal function acting as a way to minimise water loss while maximising total carbon uptake in the most efficient way constrained by environmental conditions. This ideology has led to several recent developments in modelling vegetation, for example, Anderegg et al. (2018) present two hypotheses, maximising either carbon profit or water use efficiency and analysing results against empirical data from vegetation spanning global forest biomes. They model these two hypotheses and find evidence to support the evolution of stomatal function to maximise carbon profit. Furthermore, Sabot et al. (2020) test a new profit maximisation model, where plant hydraulic function is traded optimally against photosynthetic uptake of CO<sub>2</sub>. Wolf et al. (2016) also presented a carbon-maximisation optimisation model as an alternative for the empirical based models and it has been found in these studies that this alternative modelling technique produces promising results minimising error and outperforming classic stomatal modelling techniques.

Some studies show other benefits of using this optimality approach, when the optimisation of stomatal conductance to minimise the amount of water used per carbon gained is modelled (Lei et al., 2008; Schymanski et al., 2008, 2009; Chen et al., 2022; Zhu et al., 2023). This has been proven to correctly capture responses to changing atmospheric CO<sub>2</sub> and can be used to analyse responses at elevated CO<sub>2</sub>, important in studying global change biology (Medlyn et al., 2011; Manzoni et al., 2013; Buckley & Schymanski, 2014; Schymanski et al., 2015b; Wolf et al., 2016; Dewar et al., 2018). There is also increasing experimental and theoretical evidence that vegetation optimises carbon gain by dynamically adapting its root system to environmental

conditions, balancing the carbon cost of root growth with the benefit of increasing water uptake to meet canopy demand across climates (Schymanski et al., 2009; Guswa, 2010; Brunner et al., 2015; Tron et al., 2015; Y. Yang et al., 2016). Furthermore, promising results have been found optimising the allocation of carbon with the objective of maximising tree height growth rate to explain growth patterns in height, rooting depth, and leaves in conifers (Valentine & Mäkelä, 2012). However, despite successful experiments and vegetation optimality gaining global recognition, this type of modelling has not yet been extensively tested worldwide, particularly in the tropics.

### **1.1.2 The importance of Brazilian Biomes**

Tropical and subtropical areas exhibit strong interactions between water and carbon (Wohl et al., 2012; Hamel et al., 2018; Wright et al., 2018). For example, Brazil contains seven major biomes each with unique vegetation types that have coevolved with climate; Amazonia occupying 49.5% of the Brazilian territory (4.2 million km<sup>2</sup>), followed by the Cerrado (23.3%), Mata Atlantica (13%), the Caatinga (10.1%), the Pampas (2.3%), and the Pantanal (1.8%) (IGBE, 2023). Each bring with them their own unique hydrological importance but the two largest, Amazonia and the Cerrado, which cover 72% of Brazilian land mass, are among the most biodiverse areas in the world, and are the most threatened biomes in Brazil (Marris, 2005).

The Amazonia biome contains ~35% of the world's natural forest and has been estimated to contain tens of thousands of species of flora (estimates reviewed by Hopkins, 2019). The biome comprises of a mosaic of ecosystems including rainforests, deciduous forests, flooded forests, seasonal forests, and savannas (Prance, 1979). These forests influence global and regional climate and weather as well as the global carbon cycle (Davidson et al., 2012; Spracklen & Garcia-Carreras, 2015). Furthermore, they regulate the Amazon basin river flow and water balance providing ecosystem services critical for sustaining biodiversity, water supply, transport, and regulating climate (Foley et al., 2007; Lima et al., 2014; Ruiz-Vásquez et al.,



## *Chapter 1: Introduction*

2020; Manciu et al., 2022; Sierra et al., 2022), and economic resources such as industry, agriculture, hydroelectric power, urban dwellings, fisheries, and tourism (Guo et al., 2000; Postel & Thompson, 2005; Kirkby et al., 2011; Castello et al., 2013). These ecosystem services are maintained by the close relationship between vegetation dynamics and the hydrology of the region. On average the rainforest receives more than 2,000 mm of precipitation per annum, often through seasonal cycles the vegetation has coevolved to depend on (Hilker et al., 2014; Zemp et al., 2017). The vegetation in turn captures and transpires large quantities of precipitation recycling it through time, maintaining and regulating the local seasonal climate (Eltahir & Bras, 1994; Van Der Ent et al., 2010; Zemp et al., 2014, 2017; Spracklen & Garcia-Carreras, 2015). Where strong seasonality occurs, vegetation has developed adaptive strategies such as deeper root systems and are able maintain water uptake through the drier seasons and evapotranspiration then exceeds precipitation (Bruno et al., 2006). In addition, over the large areas susceptible, seasonal flooding brings nutrient-rich sediments onto the floodplain to support the growth or alter the composition of vegetation (Koschorreck & Darwich, 2003; Hawes et al., 2012).

Meanwhile, the Cerrado biome covers an area of 2 million km<sup>2</sup> and comprises of ecosystems varying from savannas, grasslands, wetlands and shrublands to dry and wet forests (Ruggiero et al., 2002). It is home to more than 7000 species of flora and has high levels of endemism among both flora and vertebrates (Klink & Machado, 2005) leading to its classification as one of the 36 global biodiversity hotspots, along with Brazil's Atlantic Forest (Mata Atlantica) (Myers et al., 2000; Kong et al., 2021). The region distributes fresh water to major Brazilian and South American basins, including the Tocantins, São Francisco, Paraguai and Paraná. As with the Amazon, these watersheds supply water for animals and people, help maintain ecohydrological functions, and are a source for agriculture, industry, tourism, navigation, and hydroelectric power (Oliveira et al., 2014; Resende et al., 2019, 2021). The biome is

## *Chapter 1: Introduction*

characterised by distinct wet and dry seasons where almost 90% of annual precipitation falls during the wet season (~1500 mm annual average) spanning October to April, while mean annual temperatures vary between 20°C in the south and 26°C in the north (Klink & Machado, 2005). Vegetation therefore has seasonal growth patterns, and many native species have deep root systems observed down to 10 m in depth maintaining some level of transpiration through the dry months (May-August) (R. S. Oliveira et al., 2005; Ferreira et al., 2007). Mechanisms of vegetation demand and water supply govern the magnitude and seasonality of evapotranspiration across both Amazonia and the Cerrado (Christoffersen et al., 2014a) and changes to land use such as the replacement of natural vegetation by shallow-rooted pasture and crops could alter the hydrology of the region (R. S. Oliveira et al., 2005; Silva et al., 2006).

Natural vegetation clearing for infrastructure development and agricultural expansion, namely pasture and cropland (Solar et al., 2016; Silva Junior et al., 2021), not only alters the water balance but can impair ecosystem services (Fujisaka et al., 1998; Foley et al., 2007; Castello et al., 2013; Lima et al., 2014; Ruiz-Vásquez et al., 2020; Sierra et al., 2022). Recent amendments in Brazil's environmental policies, including deregulating indigenous lands and reducing environmental licencing constraints, have led to increases in deforestation, wildfires, and damage to protected areas (Nature Editorials, 2018a; 2018b; Andrade, 2019; Escobar, 2019; Tollefson, 2019; de Oliveira Serrão et al., 2020, Rajão et al., 2020). Over the last five decades, the Cerrado has increasingly been replaced by pasture and cropland (Marris, 2005; Jepson et al., 2010) and to date, over 50% has been cleared for anthropogenic use and clearing continues to meet the world demand for exported crops such as soy, sugar cane, corn and coffee, and pastures for beef (Klink & Machado, 2005; Hunke et al., 2015). The augmented expansion of agriculture is reliable for the substantial boost in yields and economic wealth in the region over a short period (Martinelli et al., 2010). However, it has also contributed to severe environmental issues related to water shortages, eutrophication, soil degradation,

pesticide contamination and disease control (Martinelli et al., 2010; Schiesari & Grillitsch, 2011; Schiesari et al., 2013; Raulino et al., 2021).

Increases in these deforestation rates across the biomes within Brazil place its environmental systems and water balance at considerable risk (Coe et al., 2009; Nepstad et al., 2014; Lamparter et al., 2018; Serrão et al., 2019; de Oliveira Serrão et al., 2020). With less than 3% of the country's agriculture irrigated (The World Bank, 2017), land use-climate feedback will almost certainly affect the regional energy and water balances underlying the importance of understanding the potential impact changes in land use will have on the hydrological cycle and regional climate (Betts et al., 2008; Lima et al., 2014; Cabral et al., 2015; Lawrence & Vandecar, 2015; P. T. S. Oliveira et al., 2015; Spera et al., 2018; Anache et al., 2019).

Current trends in global climate exert further pressure on the hydrological systems in Brazil (Lawrence & Vandecar, 2015; Avila-Diaz et al., 2020; Alves et al., 2021; Raulino et al., 2021). Changes in patterns of precipitation, intensity of flooding and droughts, and increased concentrations of CO<sub>2</sub> characterise global climate change (Alves et al., 2021; Intergovernmental Panel on Climate Change, 2022). Simulations excluding climate response to deforestation predict increases in runoff and river discharge relative to the region deforested (Coe et al., 2011; Levy et al., 2018). However, when including climate response, reductions in mean annual precipitation are predicted and some basins, such as the Juruá and Purus, are expected to decrease mean annual discharge (Lima et al., 2014; Y. Yang et al., 2019). Predicting vegetation response to climate is scale dependent and complex but is critical to understanding future hydrological trends in water availability. For example, elevated atmospheric CO<sub>2</sub> concentrations may increase water-use efficiency in vegetation, decreasing evapotranspiration and local precipitation in non-water stressed environments (Bruno et al., 2006; Farris et al., 2015). However, it may also minimise the effect of drought on native species in water-stressed environments (Lima et al., 2014; Souza et al., 2016; V. F. Oliveira et

al., 2016), leading to alterations in water storage across different regions, and either enhancing or diminishing negative climate forcing (Bonan, 2008).

Changes in climate could cause a shift in vegetation composition in turn altering climate feedback systems. A study carried out by Esquivel-Muelbert *et al.* (2018), looked at the potential changes in species composition in Amazonian forests due to climate change. They found that a slow shift towards more dry-affiliated genera is underway, with changes in composition in-line with climate-change drivers. They conclude that the increase in atmospheric CO<sub>2</sub> is forcing a shift within tree communities but there is a lag caused by the long generation times of tropical trees. If energy or water becomes more limited in a region, perennial communities could shift more towards seasonal communities. One thing for certain is that these changes in vegetation composition would involve changes in water use efficiency ultimately impacting the hydrology of the region (Troch *et al.*, 2009; Keenan *et al.*, 2013; Schymanski *et al.*, 2015). It is therefore important to understand why and how this may occur to predict future trends in hydrology in response to climate change.

## 1.2 Aims and objectives

The overall aim of this thesis is to test an alternative method of modelling hydrology over different climates and land-uses, both natural and cultivated, by focusing on the relationship between carbon and water dynamics and the potential of this to predict hydrological responses under elevated atmospheric CO<sub>2</sub>. We have employed one of the recently developed model approaches which combine carbon and water dynamics based on vegetation optimality theory first presented by Schymanski *et al.* (2008, 2015), but not yet tested in the Brazilian tropics and subtropics, the Vegetation Optimality Model (VOM). By using vegetation optimality as a modelling technique, we eliminate over parameterisation and the potential uncertainty this brings by focusing on maximising net carbon gain in plants. Plant biophysical processes are

constrained by climate and natural changes in vegetation composition can occur over longer time periods allowing us to assess changes in hydrological fluxes. In theory this cost-benefit system should predict changes in hydrological fluxes across biomes if natural vegetation was not influenced by anthropogenic change. However, we also look at the potential of the model to predict hydrological fluxes at cultivated monocrop sites by forcing seasonal vegetation cover to dominate. Following this, if we can successfully predict hydrological fluxes such as evapotranspiration, we can then adjust the atmospheric CO<sub>2</sub> concentration used as an input to the model and look at the implications this could have across multiple biomes and land-use types.

To do this our study focuses on answering the following research questions focusing on tropical and sub-tropical regions:

*(1): How can we use Carbon-Water mechanisms to understand hydrological fluxes?*

*(2): How sensitive are hydrological processes in vegetation to changes in atmospheric CO<sub>2</sub> concentration?*

We compare the model results against eleven flux tower sites representing both key natural biomes and human-impacted land in Brazil (Chapter 2). However, the VOM requires long term records of meteorological variables which are not necessarily available in most data-scarce regions. Therefore, to first setup the model, we have extensively analysed widely used high-resolution global gridded data to identify the most suitable dataset combination for the model runs (Chapter 3).

Once the recommended forcing dataset combination has been identified, we set up model experiments tailored to the specific characteristics of each site and compare our model against independently measured fluxes (Chapter 4). Here we look at the impacts of introducing carbon dynamics into a hydrological model to key Brazilian regions under current climate conditions

leading us to answer *Question (1)*. Model adjustments are kept to minor changes in parameters to assess how robust and transferable the model is.

With the VOM working satisfactorily at the study sites and having assessed its limitations we investigate the isolated impact of CO<sub>2</sub> changes to the overall evapotranspiration at sites in key Brazilian regions and try to understand why we obtain the results we do (Chapter 5), linking back to answer *Question (2)*. We look at both the long and short-term vegetation responses as it optimally adapts through maximising net carbon profit to changes in atmospheric CO<sub>2</sub> concentrations. Long-term responses consist of changes in ecosystem structure such as vegetation cover and maximum rooting depth while short-term effects are solely related to stomatal closure and water-use efficiency. Finally, in Chapter 6, we summarise our findings, discuss their overall conclusions and ponder what this new knowledge might lead to in terms of future research and the impact of linking vegetation optimality to hydrological modelling.

### 1.3 Thesis Outline

The thesis is divided into a study site overview chapter, three research chapters, a conclusion chapter, and appendices, structured as follows:

- **Chapter 2: The Study Sites**

Descriptions of each Flux Tower site used in this thesis providing their locations and representative climate and ecosystems.

- **Chapter 3: How can we choose accurate meteorological forcing data in the region?**

This chapter answers the following self-contained questions.

- a). Which high-resolution data product is most suitable overall?
- b). Which product is most suitable for each variable?

- c). What are the dominant types of error?
- d). How do these errors vary by location and time of year?

- **Chapter 4: How can we use Carbon-Water mechanisms to understand hydrological fluxes in (sub)tropical regions?**

This chapter answers the following self-contained questions.

- a). To what extent can the VOM predict evapotranspiration across different climates in (sub)tropical regions?
- b). To what extent can the VOM predict evapotranspiration in:
  - ii. natural ecosystems?
  - iii. cultivated ecosystems?
- c). What is the sensitivity of the VOM to poorly constrained parameters in these environments?
- d). What are the important water and plant interactions captured by vegetation optimality in the study areas?

- **Chapter 5: How sensitive are hydrological processes in (sub)tropical regions to changes in atmospheric CO<sub>2</sub> concentration?**

This chapter answers the following self-contained questions:

- a). What would be the difference in predicted average annual evapotranspiration rates if only daily to sub-annual varying vegetation properties were permitted to respond to elevated CO<sub>2</sub> (short-term response)?
- b). What would be the difference in predicted average annual evapotranspiration rates if all vegetation properties were permitted to optimally adapt to elevated CO<sub>2</sub> (long-term response)?

c). Does increased atmospheric CO<sub>2</sub> concentrations have comparable effects on evapotranspiration across different Brazilian ecosystems for both the short and long-term responses?

- **Chapter 6: Summary and Conclusions**
- **Appendices**

Appendices A, B, and C contain supporting information for Chapters 3, 4 and 5 respectively.

Each research chapter (Chapters 3, 4 & 5) follows on from the previous and is dependent upon the results of the preceding chapter. For this reason, each of these chapters contains its own results and discussion for the fluidity of the thesis.





## Chapter 2: The Study Sites

### 2.1 Introduction

Global and regional networks of eddy-covariance towers (Figure 2.1), such as FLUXNET (Olson et al., 2004) offer in situ datasets of water, carbon, energy, and momentum fluxes between the Earth's atmosphere and surface. These sites are carefully chosen so that the climate, vegetation, and soil characteristics are representative of a wider ecosystem or land-use type (Chu et al., 2021). Occasionally these representative areas are also chosen to enable intercomparison between land uses, for example, a pasture site cleared of rainforest relatively close to an untouched rainforest site. Most importantly, the towers provide a network of calibration and validation sites key for global and regional vegetation monitoring (Running et al., 1999) and are widely used to benchmark remote sensing products and models (Chen et al., 2018; Ricciuto et al., 2018).

A network of such towers, some described by da Rocha et al. (2009), exists across Brazil spanning multiple biomes and representing natural ecosystems, operated within the Large-Scale Biosphere-Atmosphere Experiment in Amazonia (LBA) (Restrepo-Coupe et al., 2021). As a consequence of the vast quantity of agriculture and its economic importance in Brazil, experimental sites are also set up to study fluxes linked with commercial crops and plantations (Cabral, et al., 2010, Webler et al., 2012, Cabral et al., 2013).

To accurately model hydrological processes and validate results it is important to understand and represent the physical properties of the observation site in the model. Ecohydrological modelling requires prior knowledge regarding climate, soil profile, ecology and location before

attempts can be made to replicate hydrological processes. This Chapter describes just that for the study sites used in this thesis so that we may justify our model set-up and understand the site characteristics before describing the relationship between carbon and water dynamics.

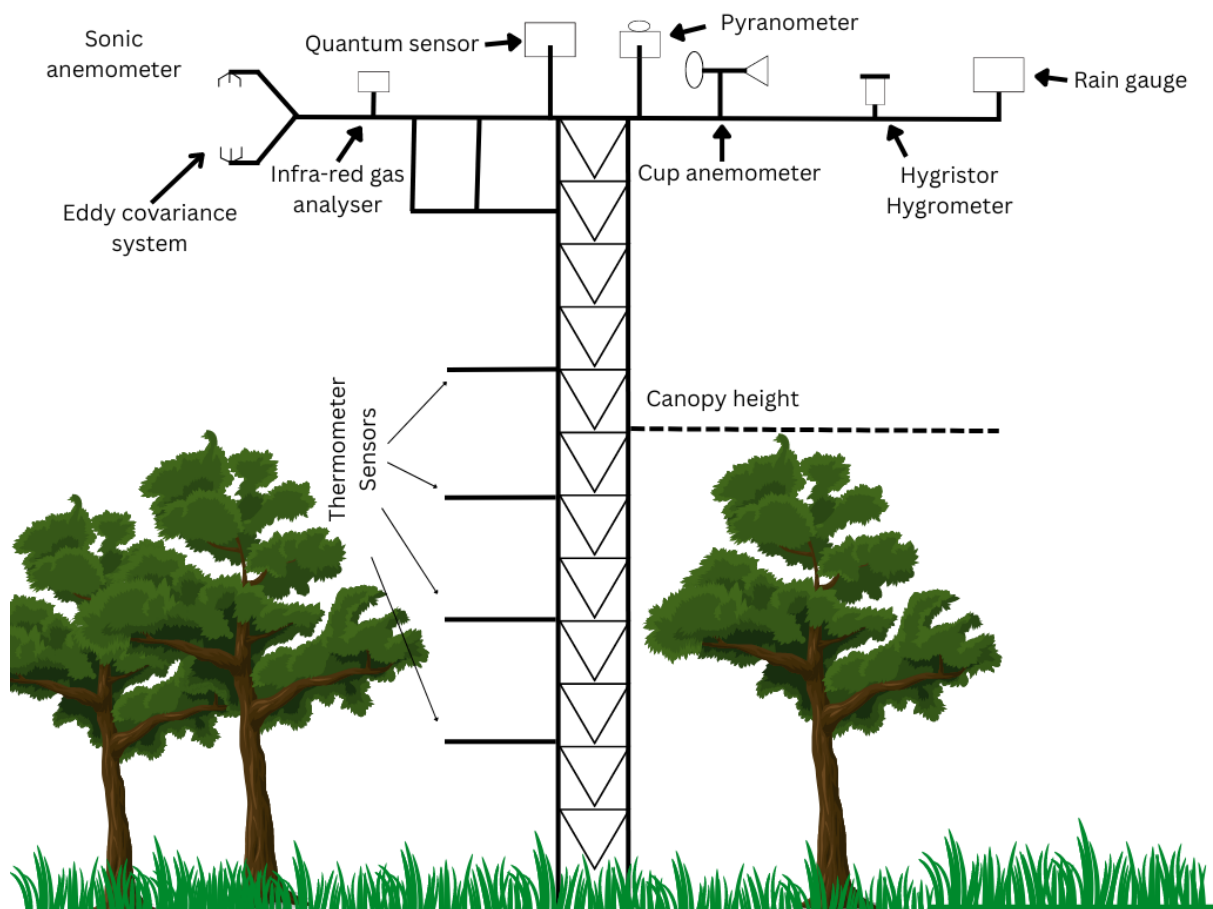


Figure 2.1 Schematic of a typical flux tower showing the types of instrumentation that may be used to take meteorological measurements. Depending on the tower there may be more instruments up the body of the tower to measure gas exchanges.

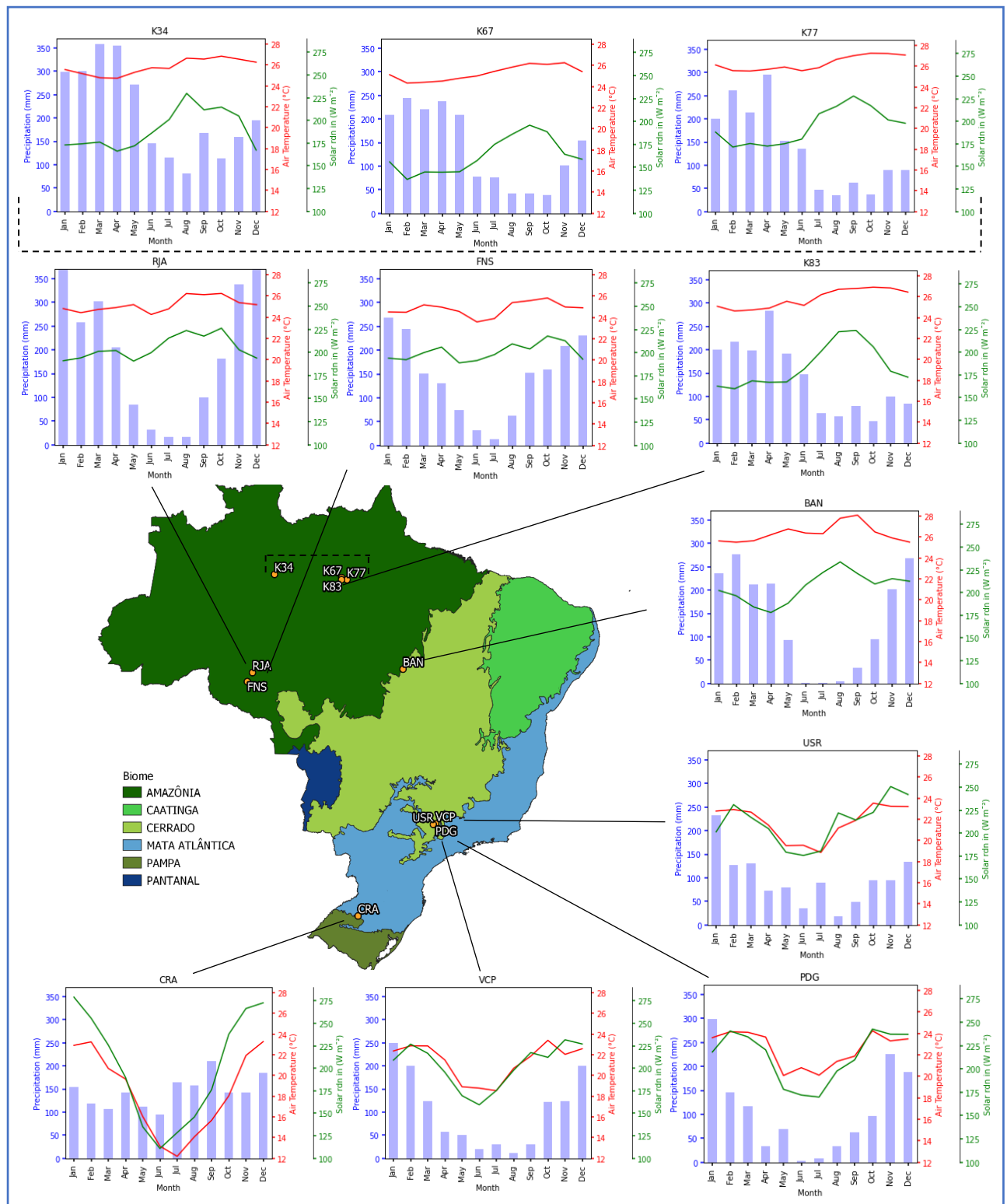


Figure 2.2 Map of Brazil split into its six major biomes showing the location of the study sites analysed in this thesis and their measured average monthly precipitation (blue), air temperature (red), and incoming irradiance (green).

## 2.2 The Study Sites

Meteorological data for 11 sites across Brazil were obtained directly from the site principal investigators, eight of which are from the LBA-ECO CD-32 flux tower network (Restrepo-Coupe et al., 2021). All these towers are equipped with various measurement instrumentation including an eddy covariance system (Figure 2.1) to measure these fluxes above canopy height to avoid interference from the vegetation column (Aubinet et al., 2012). Table 2.1 specifies the abbreviated name, location, temporal coverage, dominant land cover and papers describing the site characteristics and initial analysis on the measurements. They correspond to several land covers across Brazil including tropical rainforest, tropical dry forest, savanna, woodland savanna, and a variety of agricultural sites, the locations of which are depicted in Figure 2.2.

### 2.2.1 Manaus Kilometer 34 (K34) (Araújo et al. 2002)

Located in the Cuieiras Reserve deep in the Amazon ~60 km north of Manaus, K34 is the western most tropical rainforest site (Figure 2.2, Table 2.1). At least 1600 km from the coast, oceanic influence has little impact on the climate (Araújo et al. 2002). Deforestation rates are lower in comparison to sites located further east near Santarem (K67, K83 and K77), but as population and industrial and agricultural development in Manaus increase so does the deforestation rate. To acquire measurements not influenced by deforestation and pollution, the site was installed in



Figure 2.3 K34 flux tower near Manaus. Source: <https://lba2.inpa.gov.br/>

the Cuieiras reserve of the Instituto Nacional de Pesquisas da Amazonia (INPA), some 60 km north of Manaus in the heart of the rainforest (Andreae et al., 2002). The tower is 50 m tall and was erected in 1999, situated on a flat plateau 130 m asl.

Table 2.1 Summary of the abbreviated names, lat, lon, location, period of observation, vegetation type, elevation (m), and references for the 11 flux tower sites analysed in this thesis. All sites were provided directly by the principal investigator. \*

Name	Lat (°N)	Lon (°E)	Location (State)	Start	End	Land Cover	Elevation (m)	Reference
K34	-2.6091	-60.2093	Manaus (AM)	2000	2006	Tropical Rainforest	130	Araujo et al. 2002
K67	-2.8567	-54.9589	Tapajos (PA)	2002	2006	Tropical Rainforest	130	Rice et al. 2004
K83	-3.017	-54.9707	Tapajos (PA)	2000	2004	Tropical Rainforest	130	Goulden et al. 2004
K77	-3.0119	-54.5365	Tapajos (PA)	2000	2005	Cropland - Pasture	130	Sakai et al. 2004
RJA	-10.083	-61.9309	Jaru (RO)	2000	2002	Tropical Dry Forest	191	Andreae et al. 2002
FNS	-10.774	-62.3374	Ji-Parana (RO)	2000	2004	Cropland - Pasture	306	Kirkman et al. 2002
BAN	-9.8244	-50.1591	Araguaia (TO)	2003	2017	Woodland Savanna	120	Borma et al. 2009
PDG	-21.621	-47.63	Luis Antonio (SP)	2000	2017	Savanna	690	Rocha et al. 2002
USR	-21.637	-47.7903	Luis Antonio (SP)	2005	2008	Cropland - Sugarcane	552	Cabral et al. 2013
VCP	-21.583	-47.602	Ribeirao Preto (SP)	2006	2009	Cropland (Eucaliptus)	761	Cabral et al. 2010
CRA	-28.603	-53.6736	Cruz Alta (RS)	2009	2014	Cropland (soybean)	432	Webler et al. 2012

\*The site names are abbreviations used throughout this thesis. K stands for Kilometer followed by a number which the name of the access road to the site within the Amazon. The other sites are abbreviations also regarding their location listed here: CRA – Cruz Alta, FNS – Fazenda Nossa Senhora, RJA – Rebio Jaru, PDG – Pé de Gigante, VCP – Votorantim, Fazenda Cara Preta, BAN – Bananal Island, USR – Usina Santa Rita

The land cover consists of a closed canopy evergreen broadleaf tropical rainforest with a vegetation cover fraction of 0.98, an average canopy height of 35 m and an average leaf area index (LAI) of 5-6  $\text{m}^2 \text{m}^{-2}$  (Malhi et al., 2002). A more detailed description of the vegetation can be found in Jardim and Hosokawa (1987). The soil type of the plateau is a clayey yellow oxisol (latosol) (66% clay, 21% sand, 13% Silt) (Malhi et al., 2009).

The climate is tropical monsoon (Koppen Am climate) and the site receives an average yearly rainfall of 2200 mm with marked wetter (November-May) and reduced rain (June-October) periods (Andreae et al., 2002). The mean temperature is 26-27°C and relatively constant throughout the year (Figure 2.2). During La Niña years the dry season becomes wetter and during El Niño years the wet season becomes drier (Andreae et al., 2002).

### 2.2.2 Santarém Kilometer 67 (K67) (Saleska et al., 2003)

K67 is in the Tapajós National Forest near kilometer 67 along the Santarém-Cuiabá Highway (BR-163). The forest is bounded by highway on the east and the Tapajós River on the west, 50-150 km south of the city of Santarém. To the east the land-use is extensively established for agriculture (Hutyra et al., 2007). The forest is classified as a moist tropical forest, drier than the more substantial wet forests. As the dry season in the Amazon increases in length with climate change, this type of forest may be a model for the future Amazon (Cox et al., 2000; Esquivel-Muelbert et al., 2019).



Figure 2.4 K67 primary forest tower near Santarém (Hutyra et al., 2008)

The 64 m tall tower is located on a flat, broad plateau (130 m asl) and characterised as broadleaf evergreen (Oliveira et al., 2005, Hutyra et al., 2007) with a closed canopy at an average height of 35 m and an average LAI of 5-6  $\text{m}^2 \text{m}^{-2}$  (Domingues et al., 2005). The forest is considered primary and, at the time of the

observation period, showed no signs of deforestation or other anthropogenic disturbance (Rice et al., 2004). The soils are predominantly nutrient poor clay oxisols with some sandy ultisols present (68% clay, 32% sand) (Silver et al., 2000) and a deep water table nearly 100 m below the surface (Nepstad et al., 2002).

The climate is also tropical monsoon (Köppen Am climate) with an average temperature of 25°C, annual average rainfall 1920 mm and humidity 85% (Saleska et al., 2003; Rice et al., 2004) (Figure 2.2). The dry period is between 3-5 months (August-December), during which less than 15% of the annual precipitation falls. However, El Niño events can cause the forest to suffer severe drought and annual rainfall can fall to 800 mm (Oliveira et al., 2005).

### 2.2.3 Santarém Kilometer 83 (K83) (Goulden et al., 2004)

Also located in the Tapajós National Forest, around 70 km south of Santarem and around 5 km east at kilometer 83 of the BR-163, lies the tower site for K83 (Goulden et al., 2004). The forest around the site extends 5 km to east, 8 km to the south, and 40 km to the north before reaching pasture, and 8 km west to the



Figure 2.5 Instruments positioned at the top of the flux tower located at K83 (Miller et al., 2009)

edge of the plateau before sloping down to the Tapajós River around 14 km away. As part of a broader experiment the site was selectively logged in September 2001, using reduced-impact techniques whereby ~5% of aboveground biomass was removed (around 2-3 trees per ha) creating a patchwork of undisturbed forest surrounding the new clearings (Miller et al., 2007).

As with K67, the 67 m tall tower, K83 is also located on a flat, broad upland plateau (153 m asl) with well drained soils, characterised by broadleaf evergreen vegetation with an average canopy height of 35 m (Hernandez Filho et al., 1993; Miller et al., 2004) and LAI between 4.5-5.5  $\text{m}^2 \text{m}^{-2}$  (Doughty & Goulden, 2008). The soils are mostly clay oxisols, distributed in a



similar pattern as described for K67 (Silver et al., 2000) and the water table is assumed to be similar also (>100 m deep). The climate is almost identical to K67, tropical monsoon (Köppen Am) with an annual average rainfall of 1911 mm, average temperature of 26°C and a dry season from August to mid-December, when around 11% of the mean annual precipitation falls (da Rocha et al., 2004, 2009) (Figure 2.2).

Soil moisture measurements were also taken at this site after the logging in an intact patch of the forest ~50 m from the nearest clearing from March 2002 to December 2003. A 10 m deep soil pit lies ~20 m southeast of the tower and recorded soil moisture at high spatial and temporal resolution for an experiment to study the relationship between soil water dynamics and surface energy exchange. The experiment concluded that during dry periods soil moisture withdrawal from the top 10 m of soil agreed well with evapotranspiration rates recorded by the eddy covariance technique (Bruno et al., 2006).

#### 2.2.4 Santarém Kilometer 77 (K77) (Sakai et al., 2004)

K77 is a pasture site situated around 8 km east of site K83 in the Tapajós National Forest, about 5 km east of the kilometer 77 road after the BR-163 highway (Sakai et al., 2004). It sits 25 km from the Tapajós River in a 500-ha field surrounded by both primary and secondary forest which has an average canopy height of ~40 m. The site underwent deforestation in 1991 to make way for a cattle ranch and a commonly used C4 grass species, *Brachiaria brizantha*, was planted for grazing. In late 2001 the pasture was burned, ploughed, and a rice crop was planted which was harvested in mid-2002, after which it was not replanted. However, rice that was not harvested spontaneously regrew after.



Figure 2.6 K77 flux tower at the pasture site near Santarém (Fitzjarrold and Sakai, 2010)

The 20 m tower is also located on the plateau ~130 m asl but the terrain slopes about 4.8° from west to east with the pasture LAI estimated to be ~2.5 m<sup>2</sup> m<sup>-2</sup> (Negrón Juárez et al., 2009). Due to their proximity, the climate and soils for K77 are similar to K83 and K67 (Köppen Am, tropical monsoon with annual averages of 1911 mm for precipitation, 26°C temperature and a July-November dry season, and mostly clay oxisol) (Figure 2.2). Around 460 m to the east of the tower lies a spring-fed lake at the bottom of the slope suggesting that the water table depth is not below 39 m, assuming homogenous geology.

### 2.2.5 Reserva Jarú (RJA) (von Randow et al., 2004)

On the southern fringe of the Amazon basin, in the state of Rondônia, about 100 km north of Ji-Paraná lies the primary forest, Rebio Jaru and site RJA (von Randow et al., 2004). The area comprises of ~268,000 ha of tropical wet and dry (Peel et al., 2007) forest whose altitude varies between 100-150 m asl. In 1968 the Cuiabá-Porto Velho highway (BR-364) was constructed and since then the rainforest in Rondônia



Figure 2.7 RJA flux tower site, Rebio Jaru. Source: <https://lba2.inpa.gov.br/>

has been increasingly cleared by colonisation in a “fishbone” pattern of pastures, plantations, and degraded land so extensive that they can be seen on satellite images (Andreae et al., 2002). Despite being owned by the Brazilian Environmental Protection Agency (IBAMA) the reserve has experienced some slash and burn events close to the western border. However, during the observation period the forest around the site remained undisturbed for at least 1 km in the direction of the shortest fetch (southwest).

The tower stands 60 m tall and is situated on flat floodplains confined by a low hill range several kilometers to the south and east with the Ji-Paraná River about 800 m west forming the boundary of the reserve. An extra 2.7 m mast was later built at the top of the tower (Andreae

et al., 2002). Many springs and streams keep the vegetation moist throughout the year which comprises mainly of open tropical forest interspersed with palm trees (IBAMA., 2006). The average canopy height is 35 m and vegetation LAI averages 5-6  $\text{m}^2 \text{m}^{-2}$ , however, some trees can reach up to 45 m. The climate is considered tropical savanna, dry winter (Köppen Aw climate) with annual averages of precipitation ~2100 mm, temperature 25°C (relatively constant) and a dry season spanning May-September (Figure 2.2) (da Rocha et al., 2009).

The soil at the site has derived from in situ weathering of the bedrock and varies in depth from <1 m to ~2 m and classified as sandy loam (80% sand, 10% clay, 10% silt) with a high sand content near the top, and clay and silt quantities increasing with depth (Hodnett et al., 1996). The first 0.05 m of soil contain a dense mat of fine roots and Wright et al. (1996) have reported strong evidence of roots penetrating deeper than 3.5 m at the site to extract water suggesting the root systems grow deeper into the weathered/fractured bedrock.

#### **2.2.6 Fazenda Nossa Senhora (FNS) (Kirkman et al., 2002)**

Also located in the state of Rondônia, around 8 km southwest of the town Ouro Preto do Oeste on the cattle ranch, *Fazenda Nossa Senhora Aparecida*, lies the pasture site FNS (Kirkman et al., 2002). The surrounding land was originally deforested by fire in 1977 and has consisted of a fire sensitive, fairly drought tolerant perennial C4 African grass since 1991 stretching from about 4 km wide and tens of kilometers long (Andreae et al., 2002). This deforested land, along with many other areas, is part of the “fishbone” pattern characteristic of the rapid land conversion in the area known as the “arc of deforestation”(Lawrence & Vandecar, 2015).

The tower stands 8 m tall on flat terrain around 315 m asl and the soils are highly weathered, sandy (>75%) red-yellow podzols (Hodnett et al., 1996, Andreae et al., 2002). The average grass height and LAI is 0.16 m and 1.7  $\text{m}^2 \text{m}^{-2}$ , respectively (Kirkman et al., 2002), and the

soils are >6 m deep, comprising of weathered, sandy/loamy-sand texture (~80% sand and 10% clay) having the same classification as RJA (Hodnett et al., 1996). Like RJA the climate is also tropical savanna dry winter (Köppen Aw) with average annual values of precipitation and temperature around 1750 mm and 25°C, respectively. FNS also has a well-defined dry season spanning May-September (Figure 2.2).

### 2.2.7 Ilha do Bananal (BAN) (Borma et al., 2009)

The tower site is in the reserve of Cantão State Park which lies around 260 km west of Palmas, in the Tocantins state (Borma et al., 2009). The reserve protects 89,000 ha of an area separating two of Brazil's dominant biomes, the Amazon rainforest to the west and the Cerrado (Brazilian savanna) to the east and bounded by Bananal Island to the southwest. Bananal Island is the largest river island in the world (80 x 260 km), found at the confluence of the Araguaia and Javaés rivers and is composed of grassland and savanna that is seasonally flooded. The four main ecosystems found in the reserve are (1) the seasonally flooding forest (*mata de igapó*) ~24,000 ha, found around the water channels and lakes (in which the tower is located), (2) the semideciduous forest (*mata de torrão*) ~47,000 ha, (3) the *inner waters*, which is a system over 8148 ha comprising of lakes interconnected by channels during the floods but become separated during the dry period, and (4) the swamps (*varjão*), natural grasslands with high nutrient content deposited during the floods, 724 ha. The 40 m tower, BAN, sits on the ecotone 2 km east of the Javaezinho river, a tributary of the Javaés river which forms the eastern border of the island. Annual floods affect most of the reserve raising the water level 1-5 m above the land surface for up to 5 months between January and June (da Rocha et al., 2004, Borma et al., 2009).

The landcover at the site is a mixture of Cerrado (dense shrub with 5 m tall trees and grass undergrowth), cerradão (tall woodland savanna with 18 m trees and occasional shrubs) and campo (natural grassland) (da Rocha et al., 2004). The soils are classified as hydromorphic

sandy soil (Gley humic). Despite the convergence of ecosystems in this area the transition zones around the site form well-defined boundaries (Neiff, 2003).

The climate is hot and seasonally humid with low precipitation during the winter months (Köppen Aw) (Alvares et al., 2013). The temperature is relatively consistent with an annual average of 25°C whilst the mean annual precipitation is 1755 mm and the dry season spans May to September with ~90% of the annual precipitation occurring in the wet season (Figure 2.2) (da Rocha et al., 2004, Borma et al., 2009).

### 2.2.8 Reserva Pé de Gigante (PDG) (da Rocha et al., 2002)

The tower at PDG was erected in the state of São Paulo, located at Santa Rita do Passa Quatro city in the Vassununga state park (da Rocha et al., 2002).

The site was placed in a contiguous 1060 ha area of savanna vegetation in the Gleba Pé de Gigante, with altitudes varying between 660-740 m asl. The area comprises of a number of meso ecosystems within the area of ecological interest; (1) Cerrado Sensu stricto (79%) closed shrub and small trees (5 m tall), occasional taller trees (7-11 m), and dense herbaceous story, (2) Cerradão (11%) nearly closed

canopy taller trees (10 m tall) with dense litter, (3) Campo cerrado (8%) sparse tall trees (7-10 m), open shrubland, and dense herbaceous story, (4) other open grasslands and seasonal forest (2%) (Batalha, 1997, Ruggiero et al., 2002). Much of the Cerrado has undergone deforestation

to be replaced by intensive agriculture (Hunke et al., 2015) and the reserve is surrounded by sugarcane, eucalyptus, and citrus plantations (Pivello et al., 1996). The site is therefore representative of an area that once covered 23% of Brazilian territory.



Figure 2.8 View from PDG tower overlooking cerrado vegetation in (a) wet-January and (b) dry-September seasons (Cabral et al., 2015)

The 21 m high flux tower was established in the northwest sector of the protected area in October 2000 around 690 m asl (Table 2.1). The main vegetation surrounding the site was cerrado sensu stricto (da Rocha et al., 2002) that has an annual average LAI of  $2.3 \text{ m}^2 \text{ m}^{-2}$  (Bitencourt et al., 2007), while the soil is mostly quartz sand neosol with ~10% clay (Ruggiero et al., 2002). The climate is humid subtropical with a dry winter (Köppen Cwa) from April-September and a hotter summer with increased precipitation from October-March (da Rocha et al., 2009). The annual average precipitation is 1284 mm, and the average monthly temperatures range from 20°C in the winter to 25°C in the summer.

### 2.2.9 Usina Santa Rita (USR) (Cabral et al., 2013)

On the São José do Pulador Farm, 552 m asl in the municipality of Luiz Antonio, São Paulo state, lies the flux tower owned by Usina Santa Rita (USR) (Cabral et al., 2013). Previously natural Cerrado, the site has been deforested and replaced with a sugarcane (a C4 plant) plantation over 351 ha (Tatsch, 2009). Brazil is the largest sugarcane



Figure 2.9 USR tower site. (Xin et al., 2020)

producer in the world (FAO, 2020) and the state of São Paulo accounts for 70% of all cultivated sugarcane in Brazil (USDA, 2022). The sugarcane was planted in 2003 and subsequently underwent stubble burning before crop re-growth in April 2004 and May 2005.

The continuous area of sugarcane sits on a slope (<2%) surrounded by citrus orchards, pasture and the native Cerrado (Cabral et al., 2012). The 9 m tower is situated amongst the crop which had a maximum canopy height of 5 m. The average annual LAI for the site has been estimated as  $3.1 \text{ m}^2 \text{ m}^{-2}$  (Caudra et al., 2012) and the soil type is red-yellow latosol (oxisol) with a sandy texture (74% sand, 22% clay, 3% silt) to at least a depth of 2.6 m (Tatsch, 2009, Cuadra et al., 2012). As with PDG the climate is humid subtropical with dry winter (Köppen

Cwa) with an average annual precipitation of 1517 mm and average monthly temperature ranging from 19°C in July to 24°C in January (Figure 2.2). The well-defined dry season occurs from April-September.

#### **2.2.10 Votorantim Fazenda Cara Preta (VCP) (Cabral et al., 2010)**

Brazil is also a major global producer of Eucalyptus and around 3.5 km northeast of the Pé de Gigante reserve (site PDG) is a plantation located on the Cara Preta farm near Santa Rita do Passa Quatro. In the middle of this farm lies the tower, VCP standing 27 m tall (Cabral et al., 2010; Cabral et al., 2011). The area of Brazil covered by Eucalyptus plantations has increased from 3.5 M ha in 2006 to 5.7 M ha in 2020 (MapBiomas Project, accessed October 2022). High growth and productivity rates are frequently linked to high rates of water use and there are concerns that the production of Eucalyptus may alter the hydrological regime and reduce water availability from supply catchments (Bosch and Hewlett, 1982; Viola et al., 2014; Almeida et al., 2016).

The site sits 761 m asl on an eastward 3.5% slope with a 1 km fetch containing Eucalyptus plants of the same age and hybrid. In the other directions the fetch was at least 2 km of continuous vegetation but of differing ages. During the measuring period the canopy height surrounding the site grew from 12 m to 21 m and the average LAI was  $2.8 \text{ m}^2 \text{ m}^{-2}$  (Schleppi et al., 2007). The soil type was a quartz sand (Typic Quartzipsamment) with <12% clay present throughout the 3.5 m profile (Cabral et al., 2010). As with PDG and USR, the climate is humid subtropical with dry winter (Köppen Cwa) with an annual average precipitation of ~1500 mm and average monthly temperature varying from 19-24°C. Again, the dry season occurs from April-September (Figure 2.2).

**2.2.11 Cruz Alta (CRA)** (*Webler et al., 2012*)

CRA is the southernmost site in the study and is located at the Research and Experimental Foundation Center, Cruz Alta, in the state of Rio Grande do Sul (*Webler et al., 2012*). The natural vegetation at the site consisted of Araucaria open forest, which is a coniferous forest in the Atlantic Forest biome, and natural grassland. However, in the 1950's, the vicinity was deforested and transformed to commercial agriculture that used a conventional tillage system for soybean/wheat on a 3-year rotation (*Chavez et al., 2009; Bortolotto et al., 2015*).

The site is 452 m asl and the tower stands 3 m tall surrounded by cropland. The LAI changed with crop age and rotation but averaged around  $3.4 \text{ m}^2 \text{ m}^{-2}$  (*Moreira et al., 2018*). The soil type is a Typic Haplorthox (52% clay, 24% silt and 24% sand), with a total depth of 2.5 m and without slope.

The climate of Cruz Alta is subtropical humid (Köppen Cfa) (*Peel et al., 2007*), with an average annual rainfall of 1755 mm consistently distributed throughout the year (*Figure 2.2*). There is strong seasonality in temperature with monthly averages reaching lows of 12°C in July and highs of 24°C in December. A national weather station owned by the Instituto Nacional de Meteorologia (INMET) is located 400 m from the tower site and has been recording meteorological variables continuously since 1974 (*Moreira et al., 2015*).





## Chapter 3: How can we choose accurate meteorological forcing data in the region?

### 3.1 Introduction

The predictive power of any model is dependent upon the quality of its input data. Often models, such as the VOM, require forcing data with an extensive meteorological record (+20 years). Data collected from the tower sites described in Chapter 2 ranges from four to seven years, therefore, an alternative to the observation data is needed to force the model.

In regions that lack high-density meteorological monitoring networks or have sporadic historical observations, gridded weather products provide valuable historical references to aid studies for many purposes, including water resources (Syed et al., 2008; Vissa et al., 2019), flood forecasting and heatwaves (Miralles et al., 2019), prediction of vegetation dynamics and agricultural yields (Tian et al., 2019), and climate change impacts (Dullaart et al., 2020; Xi et al., 2021; Terzago et al., 2020). These products provide a method to integrate available weather station data both temporally and spatially consistent, whilst taking into consideration factors of influence such as topography, prevailing winds, and distance (Thornton et al., 2021). They are becoming more readily available worldwide and are helping with regional to large-scale applications globally where ground-based observations are not available or more consistent temporally extensive datasets are needed (e.g.,; Soti et al., 2010; Gebere et al., 2015; Cantoni et al., 2022; Tladi et al., 2022). However, limitations in the forcing data can result in

### *Chapter 3: How can we choose accurate meteorological forcing data in the region?*

disinformation in data which can lead to incorrect conclusions (Beven, 2011; Kauffeldt et al., 2013) and therefore the validation of such products is key for the performance of models. Comparison studies between these products and ground-based observations over the study area is one way to validate and determine its reliability and suitability.

New efforts are being made to validate global data products for important hydrological applications. For example, Sikder et al. (2019) tested three GLDAS versions and ERA-Interim/Land products over South and Southeast Asia (the Ganges-Brahmaputra-Meghna and Mekong River basins) against discharge observations to determine which product better describes the system. Gebrechorkos et al. (2020) used rainfall observations to analyse the competency of two gridded high-resolution datasets to detect climate variability and droughts across East Africa, whilst Weber et al. (2021) compared multiple gridded products against an Alpine observation centre to determine their capability for snow hydrological modelling.

The selection of a gridded product is based on its suitability for this study, for hydrological application of the VOM, which requires consistent meteorological forcing data spanning over 20 years, but it is also important to compare them in data sparse areas whenever ground-based observations are available to provide insight to risk of error associated with the product. Higher risk of error leads to greater uncertainty potentially affecting a country or area's ability to prepare for climate events. Furthermore, increased data in data poor areas strengthens model representation of Earth system processes (IPCC, 2012).

Global data products make extensive use of data from ground-based weather stations. The distribution of weather stations tends to be biased toward populated areas leaving large areas underrepresented (Viana et al., 2021). For example, in a study carried out by Filho et al. in 2018 that utilised 11,427 rain gauges covering Brazil, the Amazon basin which contains 70% of the country's freshwater has the lowest density of gauges with only 199 in the state of

### *Chapter 3: How can we choose accurate meteorological forcing data in the region?*

Amazonas. Places of ecological importance such as large forests and savannas like the Amazon and Cerrado influence the hydrological cycle through a variety of factors including biodiversity, vegetation dynamics, and root distribution (Oliveira et al., 2005; Diaz et al., 2007, Bonal et al., 2016, Coe et al., 2016) despite low meteorological station density. To combat this meteorological observation data from measurement stations such as flux towers and eddy covariance stations provide valuable insight into representative areas across the country.

FluxNet is an international network of flux towers where eddy covariance techniques are used to measure energy, water and carbon fluxes between the biosphere and atmosphere (Baldocchi et al. 2001), however, their distribution is highly biased towards North America and Europe. This network of towers has provided opportunities to validate gridded products over data rich areas such as North America (Decker et al., 2012) and China (Wang and Zeng, 2012) but less has been done in comparatively data poor areas such as South America. The tower sites in this study are part of the FluxNet but no attempt thus far has been made to validate gridded products using these locations.

With centres such as the European Centre for Medium Range Forecasts (ECMWF), and the National Aeronautics and Space Administration (NASA) Goddard Space Flight Center (GSFC)'s Global Modelling and Assimilation Office (GMAO) producing openly available high-resolution global gridded products using different techniques it can be difficult to know which products may be better suited for each application. Different products may excel in some areas over others due to the nature of their interpolation/reanalysis method and the ground observations used. For example, products like the ECMWF's ERA5-Land (Muñoz-Sabater, 2019) are developed from blending observations with past short-range weather forecasts rerun with modern weather forecasting models to produce many land-surface flux variables. MSWEPV2.2 (Beck et al. 2019), however, focuses only on precipitation data and combines satellite remote sensing data with multiple sources of reanalysis products, then bias corrects

and weights between multiple nearby observation gauges. Multiple studies have been undertaken showing that different products provide contrasting results depending on the environment or climate in question (Decker et al., 2012; Wang and Zeng, 2012; Sikder et al., 2019; Beck et al., 2021).

In this chapter we compare the accuracy of one regional and four global high-resolution gridded meteorological products over 11 ecologically different flux tower sites spanning multiple biomes across Brazil, described in Chapter 2, with the intention of selecting the most suitable to force the VOM. The assessment of these products can be broken down into four main research questions set out below.

### **3.1.1 Chapter Contained Research Questions**

1. Which product is most suitable overall?
2. Which product is most suitable for each variable?
3. What are the dominant types of error?
4. How do these errors vary by location and time of year?

## **3.2 Datasets**

### **3.2.1 In-situ observations**

Meteorological data obtained were from the 11 sites across Brazil and are described in Chapter 2. This chapter focuses on the main hydrometeorological variables used to force the VOM (see model description in Chapter 4). Variables for each site were selected based on their consistency and availability and, where needed, converted for uniformity and comparability. The variables analysed were air temperature, precipitation, wind speed, air pressure, thermal (longwave) and solar (shortwave) radiation, and specific humidity (Table 3.1 and Table 3.2).

### Chapter 3: How can we choose accurate meteorological forcing data in the region?

Table 3.1 Selected variables from each flux tower site with variables that were unavailable noted.

Name	Meteorological variables	Missing Data
K34	<i>wsed, ta, press, rg, rgl, prec, ee</i>	
K67	<i>wsed, ta, press, par, rgl, prec, ee</i>	<i>rgl</i>
K77	<i>ws, ta, press, rgs, rgl, prec, dpt</i>	
K83	<i>wsed, ta, press, rgs, rgl, prec, ee</i>	
CRA	<i>Wind Speed (ms-1) (INMET), Temperature (°C) (INMET), Pmb (INMET), Rg (Wm<sup>-2</sup>) (INMET), Lwin (Wm<sup>-2</sup>), Prec (mm) (INMET), Dew Point (°C) (INMET)</i>	<i>Lwin (Wm<sup>-2</sup>)</i>
FNS	<i>ws, ta, press, rgs, rgl, prec, ee</i>	
RJA	<i>wsed, ta, press, rgs, rgl, prec, ee</i>	
PDG	<i>ws, ta, press, rgs, rgl, prec, ee</i>	<i>rgl</i>
VCP	<i>WS_sonic, T_air, Pres, Ki, LW In, Rain, RH</i>	<i>LW In</i>
BAN	<i>wsed, ta, press, rgs, rgl, prec, ee</i>	<i>rgl</i>
USR	<i>WindSpeed, Air_temp, Press, Global_In, LW In, Rain, Air_humidity</i>	<i>LW In</i>

Table 3.2 Description of variables listed in Table 3.1

Meteorological variable	Description
<i>wsed</i>	<i>Win Speed Sonic</i>
<i>ws</i>	<i>Wind Speed Cup</i>
<i>ta</i>	<i>AWS Air temperature</i>
<i>Press, pmb</i>	<i>AWS Pressure</i>
<i>par</i>	<i>PAR Incident Radiation</i>
<i>rg, Global_In, Ki</i>	<i>Global Incident Radiation</i>
<i>rgs</i>	<i>Short wave radiation in</i>
<i>rgl, Lwin, LW In</i>	<i>Long wave radiation in</i>
<i>prec, Rain</i>	<i>precipitation</i>
<i>ee</i>	<i>Vapour pressure</i>
<i>Dpt, Dew Point</i>	<i>Dew point temperature</i>
<i>RH, Air_humidity</i>	<i>Relative Humidity</i>

#### 3.2.2 Regional Products

There are relatively few freely available high resolution national meteorological datasets covering Brazil. However, efforts have been made to produce high-resolution datasets through interpolation of weather stations (Xavier et al., 2016). The meteorological station network across Brazil varies spatially and temporally with few data available before 1980. There has been a steady increase in weather stations and rain gauges over the last 40 years but with heavy bias to densely populated areas such as São Paulo and Rio de Janeiro (Alvares et al., 2013;

### Chapter 3: How can we choose accurate meteorological forcing data in the region?

Filho et al., 2018). These biases bring the quality of meteorological datasets under scrutiny and a strong need for validation especially over the more data poor areas. Gridded data products were selected based on their open access availability, a spatial resolution of 0.25 x 0.25 degrees or finer, and a daily or sub-daily temporal resolution (Table 3.3) referred to here on as high-resolution.

#### 3.2.2.1 Brazilian National Meteorological Gridded Database (BNMD)

A high-resolution gridded dataset developed from local interpolation of meteorological variables across Brazil was released in 2016 (the Brazilian National Meteorological Database, referred here as BNMD) (Xavier et al. 2016). The data were collected from 3625 rain gauges and 735 weather stations over the period of 1980-2013 and quality control procedures were performed to identify outliers based on Liebmann and Allured (2005). The novelty of the dataset and the rapid increase in stations/gauges over the 30-year period raises questions about its reliability, particularly over less data rich areas such as the Amazon.

Table 3.3 Summary of gridded data products used in this study<sup>a</sup>

Data Descriptor	Data Source	Variables accessed	Periods	Temp. res.	Spatial res.	Reference
BNMD	BNMD	Prec, maxTa, minTa, SWdn, Ps, Wind, Rh	1980-2017	Daily	0.25x0.25	Xavier et al. 2016
ERA5-Land	ERA5-Land	Prec, Ta, SWdn, LWdn, Ps, Wind, d2m	1981-2019	Hourly	0.1x0.1	Muñoz Sabater, 2019
GLDAS2.0	GLDAS_NOAH25_3H 2.0	Prec, Ta, SWdn, LWdn, Ps, Wind, q	1948-2014	3-hourly	0.25x0.25	Rodell et al. 2004
GLDAS2.1	GLDAS_NOAH25_3H 2.1	Prec, Ta, SWdn, LWdn, Ps, Wind, q	2000-2019	3-hourly	0.25x0.25	Rodell et al. 2004
MSWEPv2.2	MSWEP_v2.2_sh	Prec	1979-2017	3-hourly	0.1x0.1	Beck et al. 2019

<sup>a</sup>Prec, precipitation; Ta, air temperature; SWdn/LWdn, surface downward shortwave/longwave radiation flux; Ps, pressure; Wind, wind speed; d2m, dewpoint 2m temperature; Rh relative humidity; q, specific humidity. Note: temporal resolution was converted to the coarsest of that of the datasets –Daily. Monthly values were also generated.

#### 3.2.2.2 GLDAS2.0 and GLDAS2.1

High-resolution datasets have been around for some time now but are less common in regions outside the Western world. In 2004, however, NASA-GSFC and NCEP released a reanalysis data product called the Global Land Data Assimilation System (GLDAS) (Rodell et al. 2004). Since then, GLDAS has been reprocessed leading to the updated release of

### *Chapter 3: How can we choose accurate meteorological forcing data in the region?*

GLDAS2.0 in November 2019 and GLDAS2.1 in January 2020. GLDAS products are one of the few datasets that provide consistent quality-controlled high-resolution (0.25 x 0.25 degrees, 3-hourly) meteorological variables available over the South American continent. GLDAS2.0 data are products of the new NOAH-3.6 LSM forced using the Princeton meteorological forcing dataset (Sheffield et al. 2006) producing a dataset from 1948 – 2014. GLDAS2.1 is a direct update from GLDAS-1 where NOAH-3.6 LSM is forced with combined forcing data including Global Precipitation Climatology Project (GPCP) version 1.3 produced by NOAA with available data from 2000-present.

#### *3.2.2.3 ERA5-Land*

More recently, the European Centre for Medium Weather Forecasting (ECMWF) released ERA5-Land (an upgraded form of ERA-Interim) providing a higher resolution global land-based dataset from 1981-present (0.1 x 0.1 degrees, hourly) (Muñoz-Sabater, 2019) generated using Copernicus Climate Change Service Information. The production of ERA5-Land is the result of the tiled ECMWF Scheme for Surface Exchanges over Land incorporating land surface hydrology (H-TESSSEL). The recent release sees it benefit from over a decade of developments in 4D-VAR data assimilation, core dynamics, and model physics relative to GLDAS and ERA-Interim. As it is built on the back of a previously well documented dataset confidence in the quality would be expected to be higher than that of new regional datasets such as ones produced by Xavier et al. (2016).

#### *3.2.2.4 MSWEPv2.2*

Another recent dataset that has received widespread praise recently is the Multi-Source Weighted-Ensemble Precipitation, version 2.2 (MSWEP V2.2) (Beck, et al., 2019). Although only precipitation data, it provides the highest temporal (3-hourly) and spatial (0.1 degrees) resolution based on gauges, satellites, and reanalysis with distributional bias corrections. The dataset merges multiple observation, satellite and reanalysis data across the globe and its



predecessors have proven to provide reliable estimates for precipitation patterns globally (Baez-Villanueva et al. 2018; Moreira et al. 2018; Alijanian et al. 2019; Xu et al. 2019).

Table 3.3 provides a summary of the gridded products used in this study with information about time periods covered, temporal and spatial resolution, the meteorological variables accessed and their references.

### 3.3 Methodology

This section describes the data manipulation necessary to quantify the differences between the gridded products and observations.

#### 3.3.1 Quality control

As previously mentioned, flux towers can often have gaps or periods of quality deficiency in the data. Therefore, variables were selected for each site based on their homogeneity and percentage of data available.

Some sites had already undergone some quality control and gap filling by the PI. Nonetheless, obvious instrument errors were eliminated from the data and linear regression was used to fill the seven meteorological variables. Only other variables from the same sites with strong correlations ( $R^2 > 0.8$ ) were used (strongest correlations first).

#### 3.3.2 Temporal averaging

Flux tower sites have different recording methods and temporal resolutions. All observation and gridded datasets were converted to the coarsest temporal resolution, the daily scale, for analysis (BNMD, Table 3.3). As the gridded datasets have no gaps this was a straightforward forward or backward averaging depending on the variable and averaging method. Two-sample Kolmogorov-Smirnov (K-S) tests were carried out on the observation data for each variable, where full days (24-hours) were used to create daily data and set as the reference distribution.

### *Chapter 3: How can we choose accurate meteorological forcing data in the region?*

Samples were then tested against this distribution using one less hour each iteration to determine whether samples significantly deviated from the reference sample. 12 hours of data (50% available) in a day was set as the minimum for daily conversion.

A similar averaging method was adopted to convert daily data to monthly. However, due to a shortage of data availability, instead of using 100% of days available in a month as the reference sample, 80% or above was used to acquire a more comprehensive sample to test against. The minimum conversion allowed was 50% of days in a month.

Precipitation was summed when converting to daily and monthly. Rainfall does not follow a regular pattern or known distribution, meaning taking anything less than all 24 hours of available data would result in an under-prediction. Therefore, only days with all data available were converted to daily. The same approach was taken converting daily to monthly but, in some cases, resulted in a high loss of data. To conserve data, each site was assessed uniquely looking at the two-sample K-S test results and changes in the mean after using fewer days in the month to convert (i.e., rejected if changes in the means and standard deviations were  $>2\%$ ). A factor was then applied to the monthly total depending on how the percentage of days missing to bring the total up to 100%.

#### **3.3.3 Wind Speed vertical interpolation**

The height at which the measurement instruments are located differ at each site. To compare data products to the observation data they are vertically interpolated to the height of the instrument at each site. The BNMD wind speed variable was calculated by interpolating laterally from the nearest Brazilian weather station which records wind speed over grass. The ERA5-Land 10m wind speed product is produced for comparison against SYNOP stations, also above grass. GLDAS 10m wind speed is adjusted down from the model's lowest level to 10m but it is unclear whether this is over grass or different vegetation types. For consistency, the

same vertical interpolation method was used for all data products. The wind speeds were interpolated up the log-wind profile using grass as the vegetation type at the height of the WMO weather station standard (30 cm) from either 2 m or 10 m depending on the data product.

### **3.3.4 Pressure**

The BNMD dataset does not include pressure as a variable therefore it was estimated as a single continuous value, dependent on altitude, using the FAO irrigation and drainage paper 56 method (Equation 7, Allen et al. 1998).

### **3.3.5 Specific humidity**

Specific humidity was available for both GLDAS datasets but needed to be calculated for ERA5-Land and the BNMD. ERA5-Land vapour pressure was calculated from the dew point temperature variable and then converted to specific humidity using pressure (Shuttleworth, 2012). For the BNMD, the vapour pressure at maximum and minimum temperatures was calculated using the FAO method (Equation 11, Allen et al. 1998). These were then used with the relative humidity, and estimated pressure to calculate specific humidity using ideal gas laws (Bolton, 1980).

### **3.3.6 Decomposition of the mean square error**

To quantify the differences, the mean square error (MSE) was calculated for each variable and data product against the observation data at each site. The MSE is a single quantity explaining little about the cause of the error, but it can be decomposed into parts to acquire a better understanding of contributions to the error (Gupta et al. 2009) (Equation (3-1)).

$$MSE = 2 \cdot \sigma_s \cdot \sigma_o \cdot (1 - r) + (\sigma_s - \sigma_o)^2 + (\mu_s - \mu_o)^2 \quad (3-1)$$

### *Chapter 3: How can we choose accurate meteorological forcing data in the region?*

In equation (3-1),  $\sigma_s$  and  $\sigma_o$  are the standard deviations of the sample (gridded product) and observations,  $r$  is the linear correlation between the sample and the observations, and  $\mu_s$  and  $\mu_o$  are the means of the sample and observations respectively. Written like this the equation is seen to have three parts. The first term is the correlation contribution to the MSE, the second, the variation contribution or differences in standard deviation, and the third term represents the bias contribution or differences in means. For a clearer understanding of the results the MSE was scaled to the RMSE to conserve the units for each variable. Whilst quantifying the relative contribution to the MSE does not allow us to determine which gridded product is superior to another it does allow us to understand the reasons as to why there is discrepancy between the observation measurements and the gridded products.

#### **3.3.7 Ranking**

The extent of the data analysed makes it difficult to quantify the results into a coherent structure. For this reason, a ranking system was used to ascertain which data product for each variable performed best due to its simplicity (Brunke et al. 2003). The MSE for each variable was given a rank dependant on how many data products have that variable recorded (for incoming longwave radiation this was 1-3; precipitation, 1-5; and all other variables 1-4, 1 being the best performing/lowest MSE). This was done for each site and then the ranks were averaged across all 11 sites to provide a single rank for each variable and each data product. A product with the lowest MSE for a variable over all 11 sites would score a rank of 1. An overall average rank was then also given to each data product which only included ranks of variables that were present for all products. This method of ranking was performed for both the daily and monthly data.

### 3.4 Results

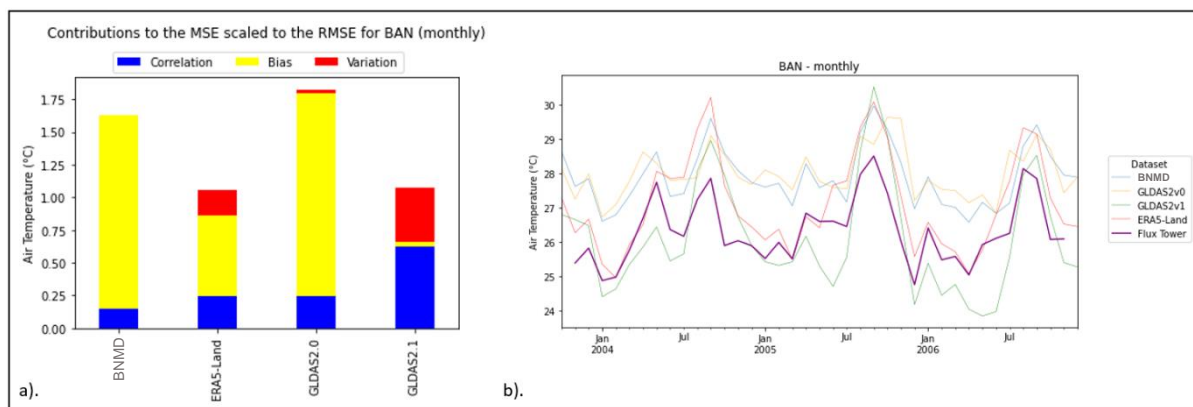


Figure 3.1 Air temperature at site BAN where a). shows partial contributions to the MSE for each gridded dataset and b). shows the monthly time series of all gridded datasets for air temperature over the operation period of the flux tower (observation data in bold).

Partial contributions to the MSE have been assigned a colour and plotted as stacked columns. An example of this can be seen in Figure 3.1a where the whole column equates to the MSE (scaled to the RMSE to conserve units). Figure 3.1a can be interpreted with the help of Figure 3.1b. The large bias contributions seen for the BNMD and GLDAS2.0 datasets are due to consistent overpredictions of the observed data with higher mean temperatures. However, both datasets follow the seasonality of the observation data leading to a low variability contribution to the error. Relatively high variability error for GLDAS2.1 is most likely due to its overprediction of temperatures in the hot months and underpredicting them in the cooler months. There is a low bias contribution as the mean of the data is similar to the observation data. Table 3.4 shows the ranking scores of the MSE for each dataset and variable averaged over the 11 flux tower sites and includes an overall average rank across all variables.

#### 3.4.1 Precipitation

Precipitation was statistically analysed across all five of the gridded datasets at two temporal resolutions (daily and monthly). MSWEPv2.2 has the best score at the daily scale whilst GLDAS2.0 has the poorest score at both daily and monthly scales. However, the results show

### Chapter 3: How can we choose accurate meteorological forcing data in the region?

that the BNMD dataset has the best overall monthly precipitation out of all gridded products compared.

Table 3.4 Overall ranks for MSE. MSE is taken per variable per site and ranked. Ranks are then averaged for all sites to produce an overall rank for daily and monthly data. Both the lowest (**bold**) value (i.e. best performance) and highest (*italics*) value (i.e., worst performance) in each row are identified. Dashed cells (-) indicate no data available. Ranking for precipitation has been scaled to be included in the average rank.

	Daily				
	BNMD	ERA5-Land	GLDAS2.0	GLDAS2.1	MSWEPv2.2
Wind Speed (m s <sup>-1</sup> )	2.55	<b>1.64</b>	3.27	2.55	-
Air Temperature (°C)	3.36	<b>1.09</b>	3.64	1.91	-
Pressure (hPa)	2.18	<b>1.82</b>	2.82	3.18	-
Solar rdn in (W m <sup>-2</sup> )	3.55	<b>1.36</b>	2.36	2.73	-
Thermal rdn in (W m <sup>-2</sup> )	-	<b>1</b>	2.2	2.8	-
Precipitation (mm)	2.04	2.62	3.42	2.33	<b>1.6</b>
Specific Humidity (kg kg <sup>-1</sup> )	4	<b>1.18</b>	2.45	2.36	-
Average Rank (exc. Thermal)	2.95	<b>1.62</b>	2.99	2.51	-

	Monthly				
	BNMD	ERA5-Land	GLDAS2.0	GLDAS2.1	MSWEPv2.2
Wind Speed (m s <sup>-1</sup> )	<b>1.91</b>	2	3.36	2.73	-
Air Temperature (°C)	3.27	<b>1</b>	3.27	2.45	-
Pressure (hPa)	2.18	<b>1.82</b>	2.82	3.18	-
Solar rdn in (W m <sup>-2</sup> )	2.73	3	<b>1.91</b>	2.36	-
Thermal rdn in (W m <sup>-2</sup> )	-	<b>1</b>	2.6	2.4	-
Precipitation (mm)	<b>1.6</b>	3.13	3.2	2.26	1.82
Specific Humidity (kg kg <sup>-1</sup> )	4	<b>1.27</b>	2.36	2.36	-
Average Rank (exc. Thermal)	2.62	<b>2.04</b>	2.82	2.56	-

Figure 3.2 and Figure 3.3 illustrate the partial contributions to the MSE at daily and monthly temporal resolutions respectively. From Figure 3.2 we can see that the correlation contribution to the MSE is the predominant source of error, but some sites also show errors due to variability (e.g. RJA and K34). It is worth noting that the bias contribution at the daily scale contributes almost nothing to the overall MSE but this changes at the monthly scale (Figure 3.3). Large spikes in the bias contribution can be seen at the northern Amazonian flux tower sites (K67, K77 and K83) for the ERA5-Land dataset which arise due to the consistent overprediction of monthly rainfall. Contributions to the variability are larger at sites RJA and USR as although

most datasets adequately reflect the total rainfall for the dry months the wet season is consistently overpredicted. MSWEPv2.2 did not perform best at all sites; in fact, it performed worst at site K83 at the daily scale where the timing of rainfall peaks was predicted less well during the wet season causing a large MSE with a high correlation contribution. Furthermore, at the monthly scale, it performed worst at site BAN where an overprediction of peaks during the wet months lead to larger contributions to bias and variability.

### **3.4.2 Air Temperature**

Air temperature was analysed across four of the gridded datasets. ERA5-Land performed best whilst GLDAS2.0 performed least well at both daily and monthly scales (Table 3.4). The ranking of 1 and 1.09 indicates that ERA5-Land had the lowest MSE when compared with every other dataset across all sites at the monthly scale and all sites except one (CRA) at the daily scale respectively. The monthly BNMD dataset performed equally as poorly as GLDAS2.0 meaning the ranking system is unable to identify which dataset reflects the in-situ observations least well. Correlation error has the largest contribution to the MSE for the daily datasets with the bias contribution also having some influence (Figure 3.2). However, at the monthly scale, the bias contribution is the greatest source of error across all datasets and sites whilst the correlation error carries less weight (Figure 3.3).

Both the BNMD and GLDAS2.0 datasets consistently overpredict temperature explaining the bias contributions for both monthly and daily datasets. Although performing well overall, the monthly GLDAS2.1 dataset had the largest variability contributions which are explained by overpredicting temperatures in the hotter months and underpredicting them in the cooler months (K34, K67, K77 & BAN). The ERA5-Land dataset followed the mean of the observation data most closely but varied in either overpredicting or underpredicting temperature at different sites.

### Chapter 3: How can we choose accurate meteorological forcing data in the region?

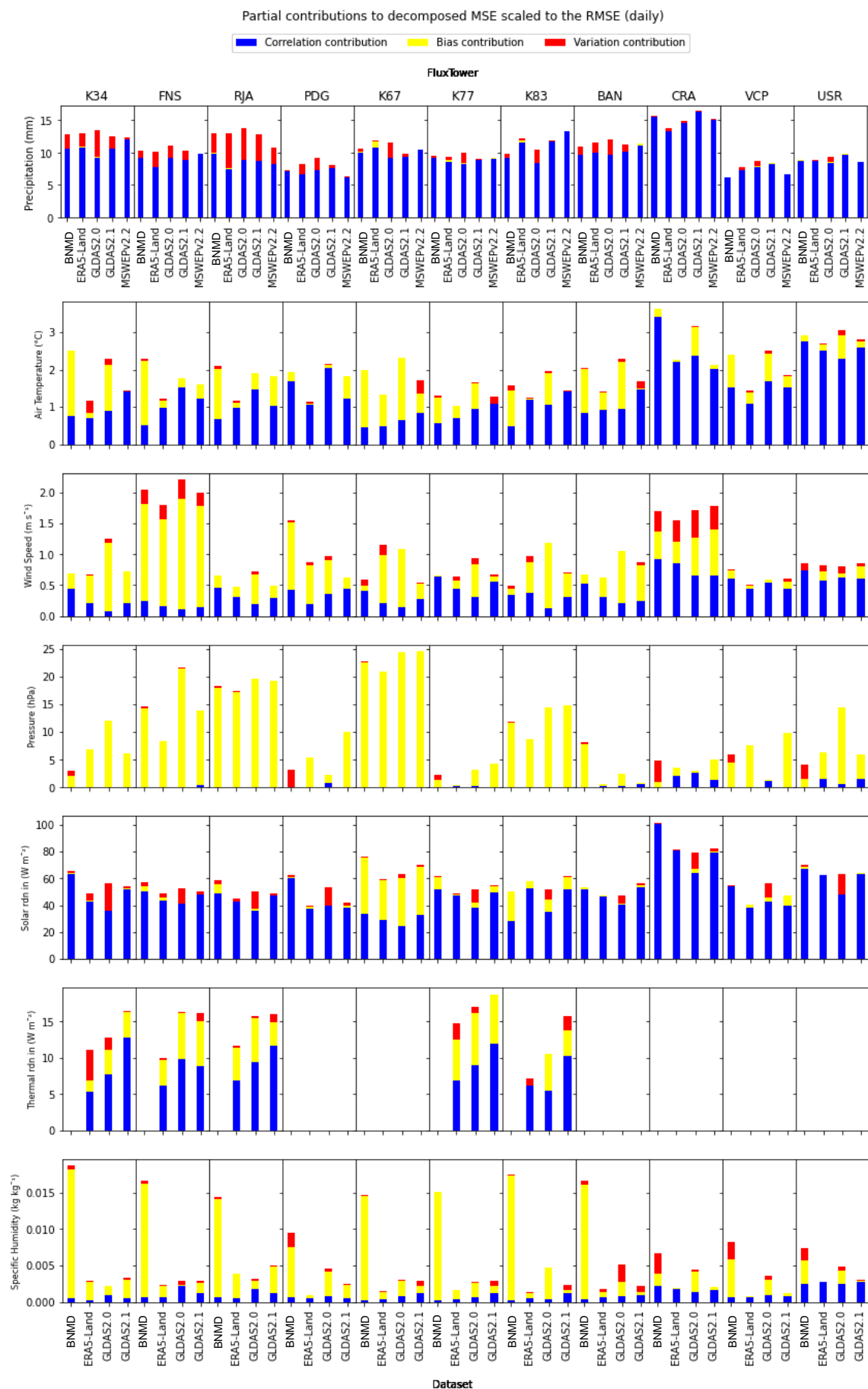


Figure 3.2 Partial contributions to the MSE between each observation site and gridded dataset (x-axis) for each variable (y-axis) at the daily scale. Precipitation includes MSWEPv2.2 errors.



### Chapter 3: How can we choose accurate meteorological forcing data in the region?

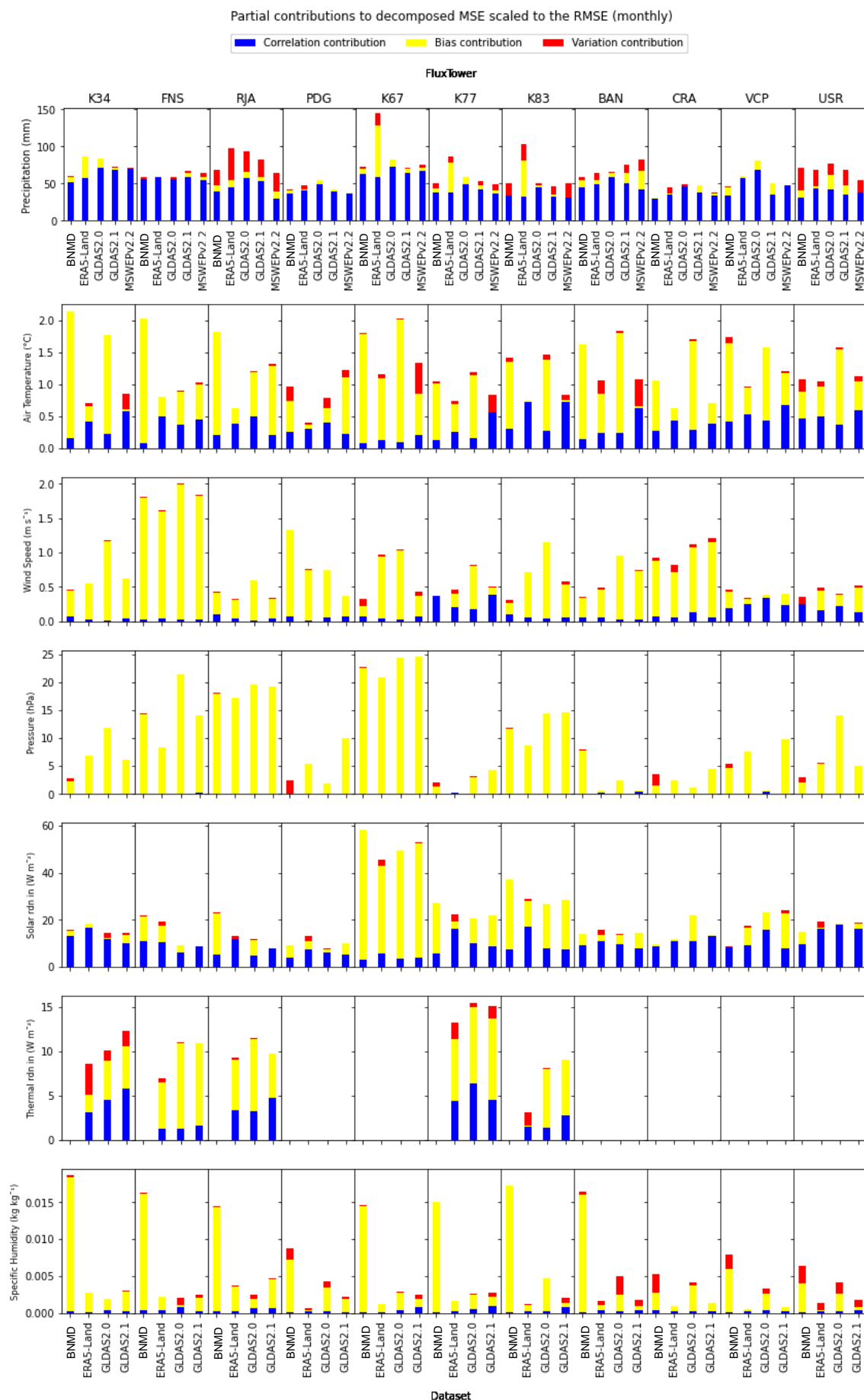


Figure 3.3 Partial contributions to the MSE between each observation site and gridded dataset (x-axis) for each variable (y-axis) at the monthly scale. Precipitation includes MSWEPv2.2 errors.

### **3.4.3 Other Meteorological Variables**

Besides precipitation and temperature, five other meteorological variables were analysed; wind speed, pressure, downward shortwave and longwave radiation fluxes (solar and thermal in Table 3.4 respectively), and specific humidity.

For wind speed, GLDAS2.0 performed most poorly at both temporal resolutions whilst ERA5-Land performed best at the daily scale and BNMD at the monthly scale. Large bias errors can be seen at site FNS over all datasets due to the gridded datasets underpredicting the observation data by means ranging 45-75% lower than that of the observation data. The large variability and bias contribution to the MSE can be seen at site CRA whereby the datasets underpredict the observation data from 2009-2013 after which the observation data drops uncharacteristically leaving the gridded products overestimating for the final year (2013-14).

ERA5-Land proved to have the lowest MSE on average whilst GLDAS2.1 performed least well at both temporal resolutions when analysing pressure. It is worth noting that the ranking did not change between daily and monthly scales for pressure as performance consistency was unaffected between daily and monthly datasets. The errors associated with pressure are heavily dominated by the bias contribution (Figure 3.2 and Figure 3.3). Contributions to the variability error are visible for the BNMD dataset as pressure was estimated using the elevation of the site using the standard FAO method (Allen et al. 1998) and kept as a constant figure. Its relatively low MSE when compared to other datasets tells us that estimating a single value for pressure can sometimes more accurately reflect the observation data. The large consistent biases at sites K67 and RJA are due to an overprediction and underprediction of 23 hPa and 19 hPa on average, respectively, for all datasets.

ERA5-Land performed best again at the daily scale for the variable, downward shortwave (solar) radiation whilst the BNMD dataset performed least well. Surprisingly, however, ERA5-

### *Chapter 3: How can we choose accurate meteorological forcing data in the region?*

Land performed least well at the monthly scale while GLDAS2.0 performed best. The correlation contribution to the MSE dominated across all sites at both daily and monthly scales, but as temporal resolution decreases, so does the correlation contribution resulting in lower overall MSEs. Large bias contributions are evident at site K67 over both temporal resolutions as the gridded datasets consistently overpredict the observation data by around  $40 \text{ W m}^{-2}$ . The observation data tends to have a downwards trend over the entire recording period resulting in an increased bias towards the end of the time series when comparing to the gridded products.

Only three of the gridded data products and five sites recorded measurements of downward longwave (thermal) radiation leading to its exclusion in the overall ranking across all variables in Table 3.4. ERA5-Land performed best at all sites across both time scales whilst GLDAS2.1 and 2.0 performed least well at the daily and monthly scales, respectively. All datasets tend to underpredict at every site, with contributions to all three components of the MSE visible at both time scales. However, the scale of the errors is not large, ranging between 1-7% error across the spread of the data.

With regards to specific humidity, ERA5-Land outperformed the other gridded datasets again whilst the BNMD had the weakest performance at both time scales. The BNMD's large biases are due to the estimation of vapour pressure from the minimum and maximum temperatures and a constant estimate for pressure (see Methodology, 3.3.5). Biases associated with air temperature for the BNMD can therefore be expected to be seen in specific humidity. Similarly, the variability contributions to the BNMD MSEs found at sites PDG, CRA, VCP and USR are associated with the variability errors in pressure as this was also utilised in the calculation.

The ranks were averaged for all shared variables for the BNMD, ERA5-Land, GLDAS2.0 and GLDAS2.1 across both time scales. ERA5-Land performed best on average whilst GLDAS2.0 performed least well at both monthly and daily scales.

#### **3.4.4 Seasonality in Errors**

Errors throughout the year can change if the datasets fail to capture the correct range of seasonality. For example, dry seasons may have low errors in precipitation because the mean rainfall will be closer to 0. Figure 3.4 shows this behaviour across almost all sites for the best performing precipitation dataset, MSWEPv2.2. Similarly, biases may occur if datasets overpredict temperatures in the warmer seasons as seen in Figure 3.5 at sites, BAN and FNS. It is clear from Figure 2.2 (Chapter 2) that seasonality changes with latitude and that sites located further south have a higher range of temperature between seasons. This increased seasonality helps explain the relatively large errors seen at sites CRA and USR in Figure 3.5. Comparing the errors spread over of the year between datasets helps us determine which ones best predict the seasonality. For example, with BNMD air temperature, the correlation component's contribution to the MSE increases in the summer months the further south the site, suggesting there is a weakness in the datasets ability to predict seasons. Further graphical representations of this can be found in Appendix A.

Chapter 3: How can we choose accurate meteorological forcing data in the region?

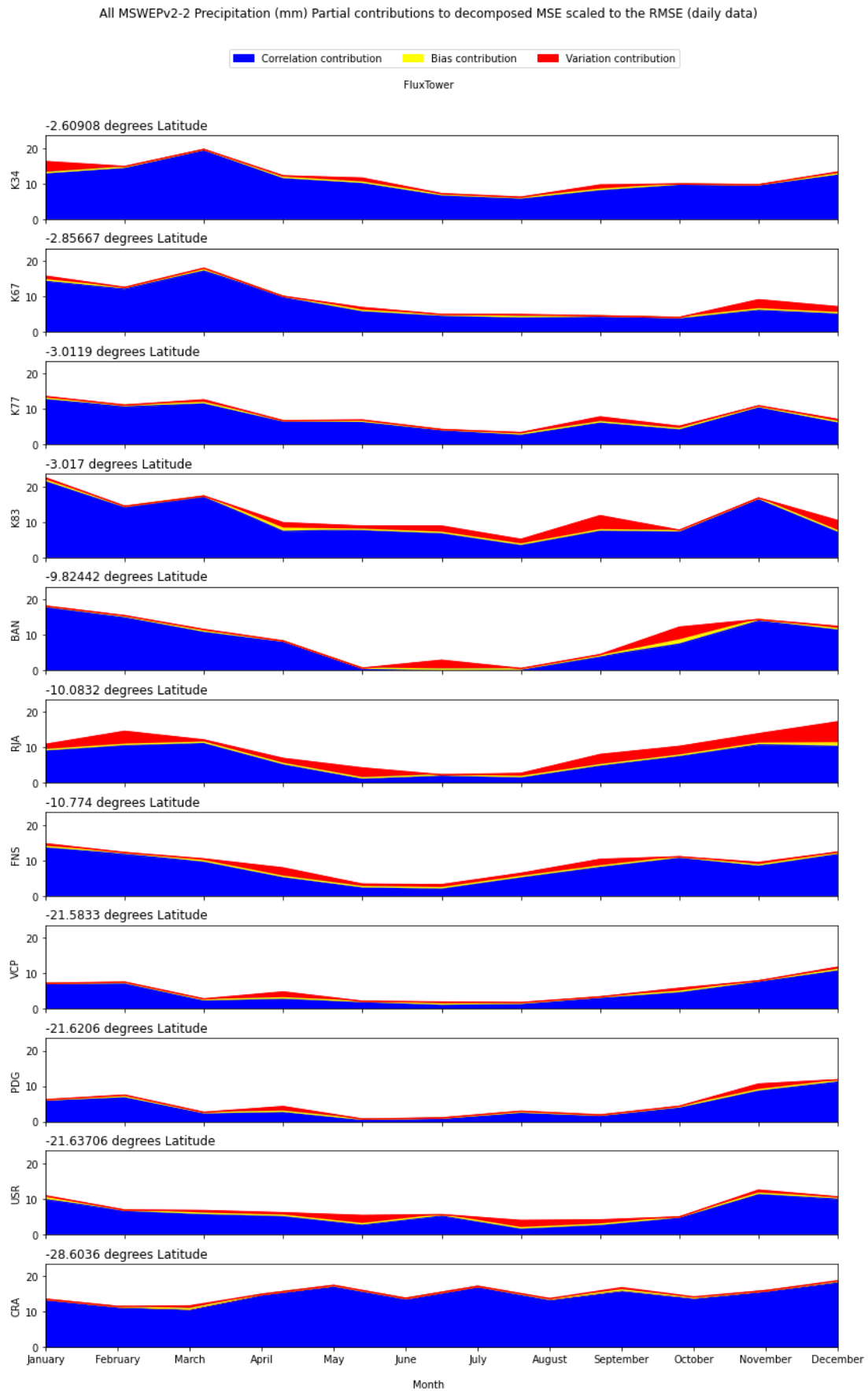


Figure 3.4 Partial contributions to the MSE averaged by month over all operational observation years for MSWEPv2.2 precipitation across all sites. Sites are in descending order from distance from equator.

### Chapter 3: How can we choose accurate meteorological forcing data in the region?

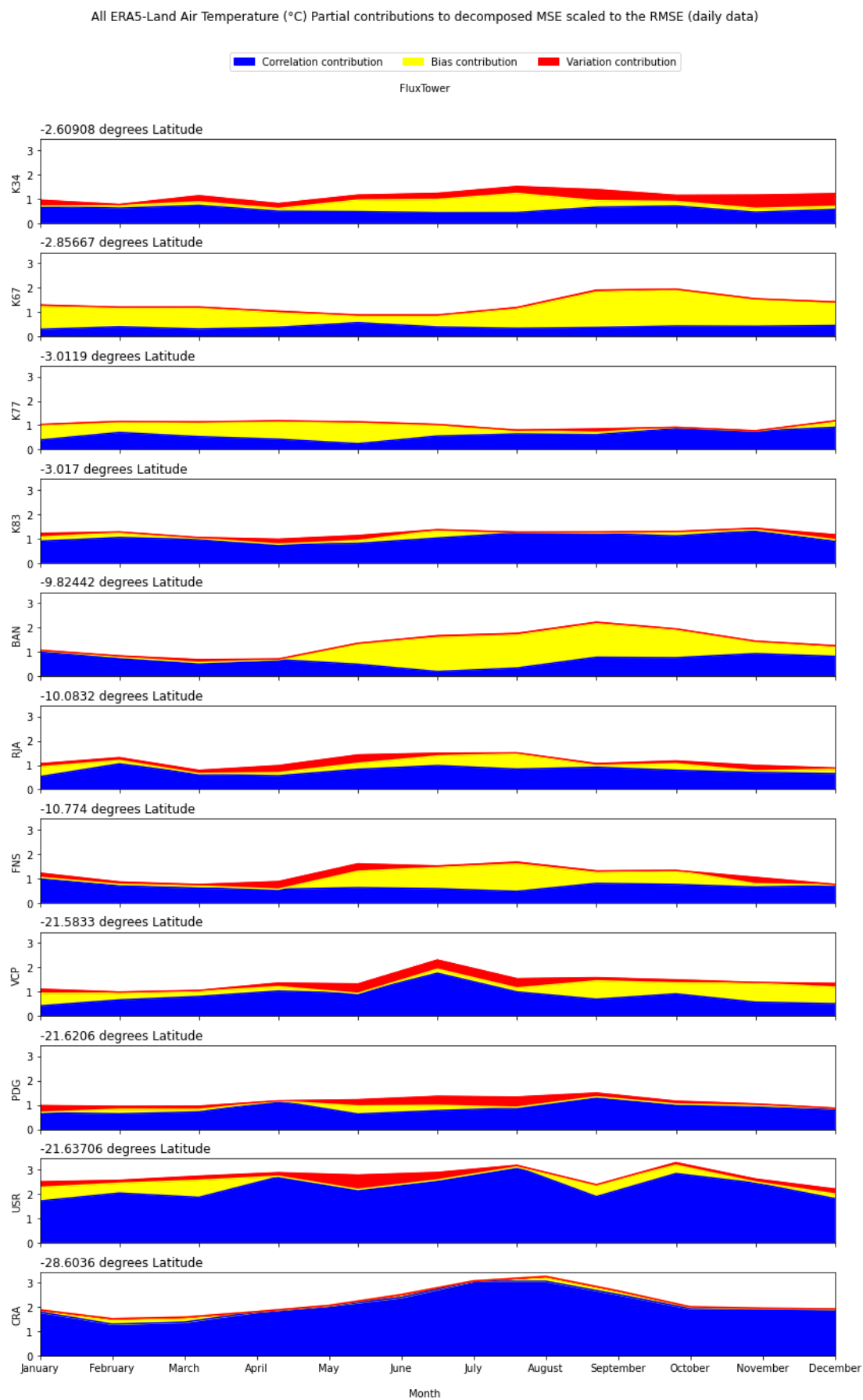


Figure 3.5 Partial contributions to the MSE averaged by month over all operational observation years for ERA5-Land air temperature across all sites. Sites are in descending order from distance from equator.

## 3.5 Discussion

Five gridded data products (BNMD, GLDAS2.0, GLDAS2.1, ERA5-Land, and MSWEPv2.2) were evaluated with in situ measured meteorological variables across multiple biomes in Brazil. The products were evaluated against 11 flux tower stations for seven meteorological variables (air temperature, wind speed, pressure, downward shortwave and longwave radiation, and specific humidity). Stations are spread over a variety of different Brazilian climates, and daily and monthly observational averages (or totals) were compared against the gridded products. The MSE scaled to the RMSE was calculated and intercompared among different products using a ranking system. Three statistical moments (the correlation contribution, the variance contribution, and the bias contribution) were also computed to provide further insight into the cause of error.

### 3.5.1 Which product is recommended overall?

It was found that the data product that performed best collectively, taking all meteorological variables into consideration for the ranking, was ERA5-Land at both the monthly and daily scales. Considering its place in this study as the newest and highest resolution global dataset, these findings coincide with multiple reports arguing its superiority as a global meteorological dataset (Jiang et al. 2020; Pelosi et al. 2020; Zandler et al. 2020).

However, as found with similar studies exploring errors with gridded datasets over different climates (Decker et al. 2012; Wang et al. 2012; Blankenau et al. 2020), we also found that no single data product is superior to others for all variables at both the daily and monthly scales.

### 3.5.2 Which product is recommended for each variable?

At the daily scale ERA5-Land outperformed in all variables except precipitation where MSWEPv2.2 matched the observations more closely. At the monthly scale ERA5-Land has the best representation of pressure, air temperature, longwave radiation, and specific humidity,

whilst it was the BNMD dataset for wind speed and precipitation, and GLAS2.0 represented shortwave radiation best.

### **3.5.3 What are the dominant types of error?**

The dominant sources of error change depending on variable and time scale. At the smaller time scale the correlation error appears to be the largest contribution for most variables (precipitation, air temperature, solar radiation, and thermal radiation), whilst errors associated with bias contribute majorities for pressure and specific humidity. Wind speed has similar overall contributions from both correlation and bias errors over the sites. A shift in the dominant contribution of error can be seen when moving from the daily to monthly time step. The relative contribution of bias increases over all variables whilst the relative contribution of correlation decreases. This is expected as the time lag associated with correlation contributions is smoothed out by decreasing temporal resolution, consequently increasing the relative contribution of bias to the error.

The bias associated with wind speed is most likely due to assumptions when vertically interpolating each dataset. Pressure is a relatively stable variable and therefore the errors associated with it are simply either an over prediction or underprediction resulting in bias. Specific humidity utilises the pressure variable meaning it will be sensitive to its errors.

### **3.5.4 How do these errors vary by location and time of year?**

It was found that some errors, such as precipitation and solar radiation, were seasonal resulting in smaller errors in the drier seasons and increased errors in the wetter season. Precipitation error is expected as there is higher chance for error with more rain. Solar radiation error could be associated with increased cloud cover as it follows a similar pattern and are more difficult to replicate in modelled systems such as LSMs.



It is more difficult to speculate on latitudinal impact on error, as there do not appear to be patterns. This does not necessarily mean latitude has no influence, other factors such as the dominant vegetation type may obscure potential patterns. One notable finding was the correlation contribution in air temperature did appear to be affected, with most errors increasing with distance from the equator.

### **3.5.5 Comparative literature**

Several similarities can be drawn from the study carried out by Decker et al. (2012) who compared meteorological variables from several reanalysis products against flux towers across North America. Although they compared previous versions of some of the gridded products analysed in this study (ERA-Interim, ERA-40 and GLDAS1.0), they concluded ERA-Interim (the predecessor of ERA5/ERA5-Land) outperformed the other products across most variables. Furthermore, they acknowledged that the correlation contribution was more prominent at the daily and sub-daily scale and the bias contribution more so at the monthly scale, similarly also found in this study.

Furthermore, as mentioned earlier, similar studies also found that there was no single reanalysis that was superior to others for all variables at different time scales (Decker et al. 2012; Wang et al. 2012; Blankenau et al. 2020) suggesting that the use of multiple datasets could be beneficial if forcing models with different meteorological variables. ERA-Interim also performed well when compared to flux tower measurements across the Tibetan Plateau (Wang et al. 2012) performing best at both daily and monthly air temperatures and producing low biases and high correlations in other variables such as precipitation. As the predecessor of ERA5-Land, where many of the techniques in producing the dataset are parallel, we can assume a similar performance should be expected in this study. More surprisingly GLDAS performed best in Wang et al.'s study whilst its successor (GLDAS2.0) performed worst at both time scales. The implication is that different datasets are not performing consistently globally and

### *Chapter 3: How can we choose accurate meteorological forcing data in the region?*

may be superior to others over different regions and climates underlining the importance of regional validation on global products.

MSWEP has been proven to perform well consistently at various regions around the globe where limited data products are available (Alijanian et al. 2019; Xu et al. 2019), as well as in South America (Moreira et al. 2019), therefore, its superior performance at the daily scale was expected. However, when the temporal resolution is increased to the monthly scale the BNMD dataset performs best suggesting that despite capturing daily patterns less well it captures the overall seasonality better than MSWEP. An explanation for this could be that the BNMD dataset has a greater correlation error but lower errors in variation and bias at the daily scale. When both datasets are “smoothed out” with the increase in temporal resolution the BNMD’s correlation error drops the overall MSE more than MSWEP. Both products use an extensive network of rain gauges to create the gridded product but use different methods of interpolation (as well as inevitably a few different sources). It is with interest that they outperform each other at different scales as this proves that different approaches to the creation of data products could prove suitable depending on the concerning temporal scale.

GLDAS2.0 outperformed other data products only in incoming short-wave radiation at the monthly scale. Similar studies found former GLDAS products to perform well for this variable on different continents (Decker et al. 2012; Wang et al. 2012). The GLDAS2.0 product is forced using the Princeton dataset which combines the incoming short-wave radiation from NCEP reanalysis and NASA Langley which is monthly data which could explain its superiority at the monthly scale as the monthly signal from the Langley data is conserved.

The observation data underwent some quality control, but Flux Tower instrument errors and deterioration of accuracy can still cause some concern when comparing results (Hollinger and Richardson, 2005). All data that was inside the scope of the variability, and therefore could not

be rejected, was kept. Flux Towers are expensive to operate and maintain and therefore, are often only operational episodically. Due to the intermittent operation of the flux towers the availability of ground truth data varies through time. Furthermore, differences in reanalysis and interpolation methodology are in part responsible for discrepancies in error as well as a range of sensitivity factors associated with the spread of the sites. The spatial resolution also appears to be a limitation at shorter time-steps, but this seems to become less so as the temporal resolution decreases.

### 3.6 Implications and Conclusions

This study evaluated five high-resolution meteorological global data products against 11 flux tower observations across Brazil. It is found that no one data product is superior for all variables at both daily and monthly scales although the higher spatial and temporal resolution products (ERA5-Land and MSWEP) appear to outperform the lower resolution ones (GLDAS2.0, GLDAS2.1 and BNMD) at the daily scale. As an overall product, the ERA5-Land dataset outperformed the others at both daily and monthly time-steps.

Decomposition of the MSE provides useful insight into understanding the dominant sources of error for certain variables which could help in the selection of a product for model use. The study spans multiple climates and uses high quality observation data covering different time periods giving useful insight into the robustness of each product.

Combined high-resolution reanalysis products such as ERA5-Land and MSWEP have the potential to increase model predictive power, but site-specific validation would always benefit the performance before selection of any dataset is made. A lack of observation data or time constraints can prevent this and studies validating the gridded datasets over multiple climatological regions become important.

### *Chapter 3: How can we choose accurate meteorological forcing data in the region?*

This chapter, along with other comparative studies mentioned throughout, makes it clear that caution should be taken before selecting a gridded data product for use in applications. Bias correction methods and data processing not considered in this study could alter the ability of one product to outperform another. Furthermore, application use should also be considered when selecting a suitable data product, for example, if evaluating evapotranspiration for agricultural farming then products that perform best in the dry season may be most suitable (Blankenau et al. 2020). However, to study long term responses of naturally growing ecosystems over time then data products that perform best annually over extended periods of time would be most appropriate (Schymanski et al. 2015).



## Chapter 4: How can we use Carbon-Water mechanisms to understand hydrological fluxes?

### 4.1 Introduction

In this chapter we look at how the concept of vegetation optimally adapting to its environment to maximise growth can be used across multiple land uses and climates to describe hydrological fluxes such as evapotranspiration (ET).

Vegetation plays an important role in hydrology as it acts as the main conduit for water in land-surface interactions (Graham & Bergström, 2000). It directly affects the surface water balance through root absorption, canopy interception, and stomatal transpiration, as it maintains and maximises growth, sometimes referred to as gross primary productivity (GPP). This impacts various hydrological processes through horizontal distribution and vertical structure redistributing both water and energy (Makarieva and Gorshkov, 2010). These interactions are often simplified in hydrological models and quantifying them to gain reliable estimates of ET remains a significant challenge (Duethmann et al., 2020).

Hydrological models, which primarily focus on solving the water balance, contain rather conceptual ET components (Graham and Bergström, 2000; Overgaard et al., 2006). Current models tend to use either integrated converting methods or classification gathering methods to estimate ET (Zhao et al., 2013). The former includes methods such as estimating potential evapotranspiration and converting it to actual evapotranspiration applying the Soil Moisture Extraction Function (Dyck, 1985; Maidment, 1992; Zhao et al., 2013), while the latter

estimates water surface, soil and vegetation evaporation and transpiration separately before combining them based on land use patterns, usually associated with physically based hydrological models (Refsgaard, 1996). However, the use of empirical equations in integrated converting methods have been reported to cause large uncertainties in evaporation simulations despite achieving good fits between simulated and observed (Bai et al., 2016; Rakovec et al., 2016).

Compared with land surface models, conceptual hydrological models tend to generalise vegetation functionality to decrease complexity. However, this requires intensive model calibration and in areas where vegetation dominates, such as the Amazon basin, these models can struggle to estimate the influence of vegetation on hydrological processes such as ET or soil moisture dynamics (Ávila et al., 2022). Distributed physically based hydrological models can provide a better representation of the movement of water through vegetation but tend to require a large number of parameters to do so creating greater uncertainty (Beven, 2001; Troch et al., 2013). Yet, if parameters can follow a certain ‘goal’ function, they have the potential to be optimised by the system and therefore can be calculated a priori and do not need intensive parameterisation or calibration (Schymanski et al., 2009).

New approaches in modelling plant physiological interactions through the adaptive nature of vegetation in response to its environment can lead to an improved understanding of hydrological fluxes (Franklin et al., 2020). If parameters controlling dynamically changing traits such as root depth, stomatal conductance, water use efficiency and coverage are based on informed guesses or accepted as static, the ability of vegetation to adapt to seasonal or long-term environmental shifts is constrained. Understanding how plants or plant communities adapt to control their water use over different climates can help us quantify their physiological processes and play an important part in the development of hydrological models (Donohue et al., 2007).

In contrast to hydrological models, land surface models, which focus on solving the energy balance, tend to have extensive soil, rooting, and vegetation parameters. However, despite land surface models attempt to simulate vegetation dynamics, model intercomparison studies have revealed persistent deficiencies in estimating gross primary productivity (GPP) (Christoffersen et al., 2014; Whiteley et al., 2016; Restrepo-Coupe et al., 2017; Restrepo-Coupe et al., 2021; Teckentrup et al., 2021). For example, Restrepo-Coupe et al. (2017) compared how well four state-of-the-art dynamic global vegetation models simulated seasonality of carbon fluxes in the Amazon tropical rainforests and found that the modelled dry season periods produced a reduction in GPP in contrast to the observed increases. These were found to be driven by modelled ‘soil-water stress’ which was not apparent at any of the observed northern Amazonian sites. In the case of tropical rainforests, they conclude that simulated flux seasonality requires a greater understanding of the internal biophysical mechanisms in future model developments.

This highlights the need for a better representation of carbon-water dynamics in models if we are to successfully capture hydrological processes in vegetation dominated areas. The incorporation of plant physiology could significantly progress the predictive power of hydrological models but transferability over different climates and land-uses remains an issue. An alternative approach at modelling vegetation that uses physical principals rather than conceptual ones may be necessary.

Over millennia vegetation has evolved along with the changing environment to create unique ecosystems across the planet driven by natural selection. This natural progression is a result of vegetation optimally adapting to these given environmental conditions (Givnish, 1988). Therefore, regardless of the inherent complexity of interactions between communities, organisms, and ecosystems, natural selection can be a source of predictability in vegetation driven systems (Franklin et al., 2020). This concept allows models to predict while requiring less parameter information ultimately improving their predictive capability and our



understanding of the systems they describe. For example, as vegetation growth is constrained by either energy, water, or carbon dioxide then it may be assumed that vegetation will grow to its maximum potential until one of these constraints prevents it. It is then possible to group plants in a collectively spatial manner which can produce patterns in vegetation structure that offer both feasible ways to reduce model complexity and improve scientific insight at the ecosystem level.

Vegetation optimality modelling assumes that through natural selection, vegetation has adapted to self-optimize by maximising the difference between carbon used on maintenance of its uptake organs and carbon acquired through photosynthesis (i.e., carbon available for growth called here the Net Carbon Profit, NCP), finding the optimal vegetation for given environmental conditions (Schymanski et al., 2007). The theory of ecological optimality is not novel and has been well described by Eagleson in terms of maximizing net primary productivity (Eagleson 1982; Eagleson and Tellers, 1982; Eagleson and Segarra 1985). However, despite its growing use in land-surface models to improve vegetation responses to climate (Eller et al., 2018; Eller et al., 2020), its application in hydrological models is still relatively uncommon but is gaining recognition through positive results (Schymanski et al., 2015; Franklin et al., 2020; Nijzink et al., 2021; Nijzink and Schymanski, 2022).

The Vegetation Optimality Model (VOM) (Schymanski et al., 2008, 2009, 2015) is a coupled vegetation dynamics – water balance model. It provides an approach to understanding hydrological processes based on the concept of vegetation optimality and has been applied successfully over multiple land-uses and climates from wheat and maize crops in northern China (Lei et al., 2008) to tropical savanna sites of different climates in Australia (Nijzink et al., 2021). Using vegetation optimality to understand hydrological processes in Brazil is relatively unexplored territory. The tropical rainforests and savannas of Brazil contribute considerably to regional and global water balance and a better understanding of the role

mechanisms in vegetation play is needed from a hydrological modelling perspective. If vegetation optimality can successfully describe key hydrological processes, such as ET, across major biomes in Brazil, either naturally formed or cultivated, it could enhance our understanding of how these processes may change under predicted land use or climate changes. It can also improve our awareness of crucial regions of hydrological importance based on vegetation cover in areas lacking observation data. This can benefit studies in water resources planning, prediction of agricultural yields, and the hydrological impacts of climate change. Furthermore, testing optimality across multiple environments and ecosystems leads to a clearer understanding of the shortcomings and highlight areas for improvement in the model.

As the VOM is based on natural evolution theory and maximises carbon profit for growth under given environmental conditions, it aims to represent a naturally occurring ecosystem. Cultivated land differs from this due to the strong impacts of anthropogenic activities such as deforestation, irrigation, harvesting, planting, and maintaining. The model may therefore struggle to represent heavily modified or cultivated ecosystems without undergoing some alterations.

In this chapter we apply the VOM over five biomes across Brazil using the 11 flux tower sites described in Chapter 2. The chapter contained research questions we will try to answer are defined below.

#### **4.1.1 Chapter Contained Research Questions**

1. To what extent can the VOM predict ET across
  - a. different climates in Brazil?
  - b. natural ecosystems?
  - c. cultivated ecosystems?

2. What are the important water and plant interactions captured by vegetation optimality in the study areas?

## 4.2 The Vegetation Optimality Model

The VOM (<https://github.com/schymans/VOM>) can be split into two sub-models, one which simulates vegetation dynamics and the other that controls water balance. These sub-models are coupled together by root water uptake and leaf transpiration feedback. VOM optimizes vegetation properties to maximise the NCP. Schymanski et al. (2008, 2009, 2015) describe the model in more detail and recent alterations relevant to the version of the model used in this study can be found in the technical note by Nijzink et al. (2021). For comprehensiveness the model is briefly described below, and a simplified visual conception of the model is illustrated in Figure 4.1.

### 4.2.1 Vegetation model

The model canopy is represented by two ‘big leaves’, one of variable size representing seasonal vegetation (e.g., grasses) and the other of constant size representing perennial vegetation (e.g., trees). Photosynthesis is calculated through a canopy gas exchange model using the optimal water-use hypothesis (Schymanski et al., 2007a). This is achieved by adjusting stomatal conductance, which controls water loss and gas exchange, in response to environmental conditions to optimise its water use efficiency (Buckley et al., 2017). Root depths, foliage cover and photosynthetic capacity dynamically change under this theory to ultimately maximise the NCP for the complete simulation period. Carbon spent to allow the process of photosynthesis is defined by maintenance costs in respiration, projected cover to the maintenance and turnover of leaf area. Stomatal conductance is connected to transpiration and therefore root water uptake costs and limitations. The root system is vertically distributed in

the soil profile and is optimised to satisfy the water demand of the canopy with the least total root surface area.

#### 4.2.2 Carbon costs and benefits

Different plant organs require maintenance which costs carbon. These costs are defined by the cost functions for the maintenance of foliage, the root system, and the plant hydraulic system. The cost function for foliage maintenance is defined in equation (4-1), where  $M_{A,p}$  is

$$R_f = L_{AIC} \cdot c_{tc} \cdot M_{A,p} \quad (4-1)$$

the perennial vegetation cover fraction,  $c_{tc}$ , the turnover cost factor of a leaf (set to  $0.22 \mu\text{mol}^{-1} \text{s}^{-1} \text{m}^{-2}$ ; Schymanski et al., 2007a), and  $L_{AIC}$  is the clumped leaf area (set to 2.5).

The cost function for root system maintenance is defined in equation (4-2) as root respiration

$$R_r = c_{Rr} \cdot \left( \frac{r_r}{2} \cdot S_{A,r} \right) \quad (4-2)$$

per unit catchment area ( $R_r$ ,  $\text{mol s}^{-1} \text{m}^{-2}$ ) which is a function of root surface area per unit ground area ( $S_{A,r}$ ,  $\text{m}^2 \text{m}^{-2}$ ), and root radius ( $r_r$ , m), where  $c_{Rr}$  is the respiration rate per fine root volume ( $0.0017 \text{ mol s}^{-1} \text{m}^{-3}$ ) and  $r_r = 0.3 \times 10^{-3} \text{ m}$  for citrus fine roots (Schymanski et al., 2008).

Water absorbed by fine roots needs to be transported upwards to leaves where it is transpired. The cost for this transportation changes with root depth and structure, however, due to a lack of literature, it has been assumed here that the carbon costs related to the maintenance of the vascular system ( $R_v$ ) are a linear function of the horizontal extent of the vegetation ( $M_A$ ) and rooting depth ( $y_r$ ). This is described in equation (4-3) where  $c_{rv}$  ( $\text{mol m}^{-3} \text{s}^{-1}$ ) is an unknown

$$R_v = c_{rv} \cdot M_A \cdot y_r \quad (4-3)$$

proportionality constant acting as a cost factor for water transport. As this factor relates water transport costs to rooting depth and fractional cover of the respective vegetation type (perennial or seasonal) it may vary depending on the ecosystem. Deeper root systems and larger above-

ground extents require more water transport infrastructure which is determined by  $c_{rv}$ . Vegetation types with shallow root systems and varying fractional vegetation cover (such as seasonal grasses) will have a higher cost factor than deeper rooted systems (such as trees). This cost factor cannot be easily estimated from empirical data and was previously set to  $1.2 \mu\text{mol m}^{-3} \text{s}^{-1}$  by Schymanski et al. (2009) after sensitivity analysis on Howard Springs. More recently Nijzink et al. (2022) carried out sensitivity analysis on this cost factor ranging the value between 0.2 to  $3.0 \mu\text{mol m}^{-3} \text{s}^{-1}$  for multiple sites. They found that values of the cost factor that best represented observed vegetation cover ranged between 0.6 and  $2.6 \mu\text{mol m}^{-3} \text{s}^{-1}$  across sites. For this reason,  $c_{rv}$  has been “tuned” between 0.01 and  $3 \mu\text{mol m}^{-3} \text{s}^{-1}$  in this study to account for this uncertainty. It is also worth noting that  $R_v$  should increase with canopy height, however, as this has not been modelled the effect has not been included.

The carbon benefits are defined as total  $\text{CO}_2$  assimilation across all plants. These have been calculated following a physiological canopy gas exchange model described by Schymanski et al. (2007) and modified so that the canopy was represented by both perennial and seasonal vegetation components. These were modelled separately as a function of their respective stomatal conductivities and electron transport rates. The photosynthetic pathway was modelled to represent C3 plants neglecting the C4 pathway. This increases model uncertainty but was accepted in return for greater generality. Despite this Schymanski et al. (2008, 2009, 2015) were able to capture the observed daily and diurnal dynamics of the fluxes as accurately in the C4-dominated season as in the C3-dominated season suggesting that the ET assimilation curves may not be entirely dissimilar for the different photosynthetic pathways. Furthermore, Lei et al. (2008) were able to adequately represent photosynthetic trends in C4 maize through parameter alteration potentially capturing the costs and benefits associated with this alternate pathway but this has not been explored here.

The objective function of the optimisation is the maximization of the NCP which is defined as the total CO<sub>2</sub> uptake of all seasonal and perennial plants over the entire period, take away the maintenance costs described above. This is described in equation (4-4) where  $A_{g,tot}$  is the assimilation of CO<sub>2</sub> by all plants,  $R_f$  (equation (4-1)) represents foliage costs of all plants,  $R_r$  (equation (4-2)) are the root costs of all plants totaled over all soil layers, and  $R_v$  (equation (4-3)) are the costs related to the vascular systems of all plants. As the cost factors are fixed for each model run there is no appreciation of how temperature might affect this value which may need to be explored in future model developments.

$$NCP = \int \left( A_{g,tot}(t) - R_f(t) - R_r(t) - R_v(t) \right) dt \quad (4-4)$$

### 4.2.3 Water balance model

The simple coupled water balance model is an adaptation of a ‘Representative Elementary Watershed’ approach outlined by Reggiani et al., (2000). It comprises of a drainage block containing a saturated and unsaturated zone both of dynamically changing thickness (Schymanski et al., 2008). The approach is extended to allow the vertical distribution of water to be calculated within the unsaturated zone which occurs through each soil layer (set to 0.2m in this study). For simplicity, the hydrological parameters represent a freely draining system whereby precipitation falling onto the soil block can either immediately run off the surface or infiltrate. In the case of the latter, soil evaporation, root water uptake or free drainage through the bottom of the profile can occur. Details of their formulations can be found in Schymanski et al. (2008, 2015). Soil parameters, defined by Van Genuchten, (1980) control the hydraulic conductivity and water transport rates through soil layers. The catchment geometry parameters for the model include the soil profile depth and water table depth. To compensate for the singular dimensionality of the model the slope angle to the channel (set to 0.02 radians for all

sites) and a hydrological length scale (set to 2 m across all sites) represent the speed at which water can reach the channel and drain from the model.

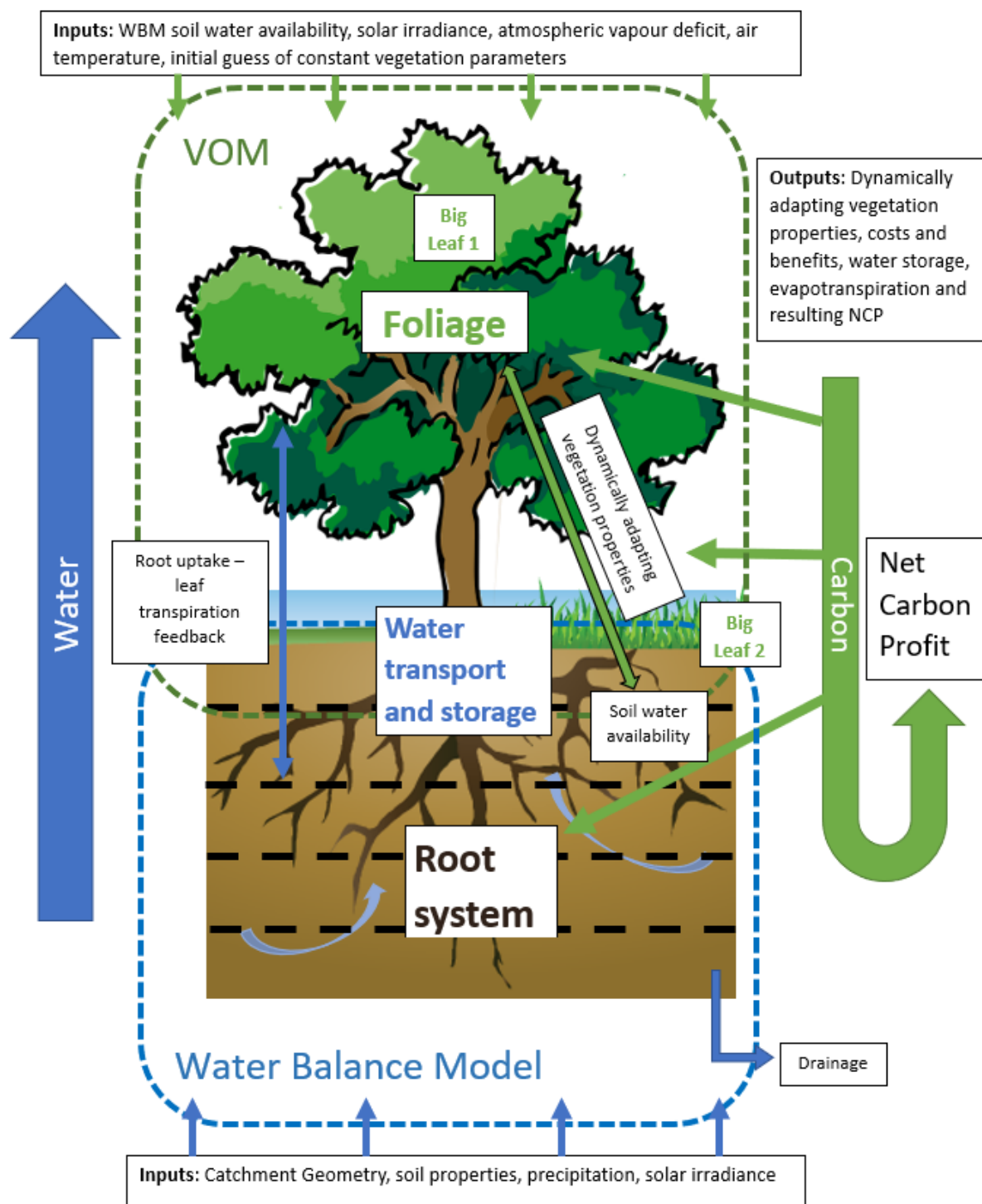


Figure 4.1 A simplified visual conception of the Vegetation Optimality Model coupling a vegetation dynamics model with a water balance model detailing inputs, outputs and main interactions between carbon and water.

#### **4.2.4 Model Optimisation**

The model allows for both long and short-term optimisation of adaptive vegetational traits. Long-term parameters are assumed to be static and not undergo considerable change over a 20–30-year period and are optimised for the full length of the simulation. These include the foliage projected cover of the perennial vegetation, the rooting depths of both seasonal and perennial vegetation, and water use strategy parameters for both seasonal and perennial vegetation. However, root surface area distributions of both seasonal and perennial vegetation, photosynthetic capacities and seasonal vegetation cover vary at the daily scale to maximise daily NCP.

The model optimises the vegetation properties for maximum NCP using the Shuffled Complex Evolution algorithm (SCE, Duan et al., 1994) spanning the simulation period of 36 years (1-1-1981 to 31-10-2017). The complex starts with a random seed and then the algorithm splits the parameter sets into a predetermined number of complexes (here set to 2), where it performs local optimisation within its complex then mixes complexes to converge to a global optimum. The model requires a longer period to reach optimality and therefore the first 5 years are disregarded when viewing results.

### **4.3 Methodology**

#### **4.3.1 Model forcing data**

For optimisation purposes the VOM requires a long time series of daily meteorological data (20-30 years) and therefore flux tower observation data were not suitable for forcing. Instead, the datasets that produced the lowest errors at the daily timestep in Chapter 3 were used to force the model. All meteorological forcing data used were obtained from ERA-Land, except for precipitation, which was obtained from MSWEPv2.2. A static concentration from the Mauna Loa CO<sub>2</sub> record (Keeling et al., 2005) was selected for the mean crossover year for all study



sites (377 ppm, in 2004). Perennial coverage, rooting depth and some water use parameters are known to adapt over time to trends in CO<sub>2</sub> (J. G. Huang et al., 2007; Franks et al., 2013; Quirk et al., 2019). However, as the VOM assumes that these parameters are static, it would not capture trends in these (Hutley et al., 2022; Nijzink et al., 2022). Nevertheless, there is capacity to assess how far the static properties might change in response to CO<sub>2</sub> using simulations at different static CO<sub>2</sub> concentrations. This is evaluated extensively in Chapter 5.

### **4.3.2 Soil hydraulic properties**

The VOM also requires soil parameters to govern hydraulic conductivities and soil water retentions. Tomasella and Hodnett (1998, 2004; Tomasella et al., 2000; Hodnett and Tomasella, 2002) conducted analysis on soil water retention characteristics and pedotransfer functions across Brazil. They developed a linear regression for estimating soil parameters (Cosby et al., 1984) for tropical soils across Brazil, which has since been adapted by Marthews et al. (2014) to create high-resolution hydraulic parameter maps for surface soils in across tropical South America, which is used in this study. These parameters describe the spatial soil profile water movement to 30 cm depth. In this study, the soil profile is vertically uniform, and accounts for consistency across all sites and which has been crosschecked against site specific literature (Table 4.1). Homogeneity of soil layers is common across the central Brazilian plateau (Reatto et al., 2007), and while there is limited data available across all sites, properties in water retention at the Amazonian site K83 have been found to be relatively uniform in depths down to 10m (Bruno et al., 2006). Saturated hydraulic conductivity ( $K_{sat}$ ) measurements were cross checked against the Hydrophysical database for Brazilian Soils (HYBRAS) (Ottoni et al., 2018) and where there was discrepancy the value most consistent with similar literature was selected.

Table 4.1 Soil characteristics of the Brazilian study sites, based on the High resolution South American hydraulic parameter map (Marthews et al., 2014).  $\theta_r$  and  $\theta_s$  refer to residual and saturated soil moisture content, respectively,  $\alpha$  and  $n$  the Van Genuchten soil parameters (Van Genuchten, 1980) and  $K_{sat}$  the saturated hydraulic conductivity.

	Site	Soil type	$\theta_r$	$\theta_s$	$\alpha$ (1/m)	$n$	$K_{sat}$ (m/s)
Natural	K34	Clay oxisol	0.18135	0.45469	5.95964	1.53543	3.34E-07*
	K67	Clay oxisol	0.23003	0.51454	4.46687	1.58093	3.34E-07*
	K83	Clay oxisol	0.23003	0.51454	4.46687	1.58093	3.34E-07*
	BAN	Sandy soil	0.18296	0.47791	2.91314	1.42782	6.73E-06
	RJA	Sandy loam	0.2188	0.49146	3.82617	1.4397	4.82E-06
	PDG	Quartz sand	0.1796	0.4542	3.62293	1.49797	7.25E-06
Cultivated	K77	Clay oxisol	0.23003	0.51454	4.46687	1.58093	7.06E-06
	FNS	Sandy loam	0.15532	0.45826	2.80064	1.41704	7.47E-06
	VCP	Quartz sand	0.1796	0.45422	3.62293	1.49727	7.25E-06
	USR	Sandy oxisol	0.1796	0.45422	3.62293	1.49727	7.25E-06
	CRA	Typic Haplorthox	0.14318	0.44485	3.82237	1.56442	1.14E-05

\*  $K_{sat}$  measurements taken from HYBRAS (Ottoni et al., 2018)

### 4.3.3 Adjustable vegetation parameters

Some aspects of the model were adjusted to represent the land-use type of the site more accurately. For natural rainforest sites with closed canopies, no seasonal grasses/plants are present, therefore, this part of the model is “switched off” (big leaf 2, Figure 4.1). Similarly with deforested pasture and crop sites, the perennials section of the model (big leaf 1, Figure 4.1) was “switched off”. This was done by setting the maximum and minimum rooting depth parameters both to 0 to switch off either the seasonal or perennial vegetation. Sites that have both perennial and seasonal vegetation such as the savanna sites were left unaltered. A more in-depth explanation of the adjustable vegetation properties and associated trade-offs can be found in Schymanski et al. (2015).

### 4.3.4 Tuning vegetation parameters

The soil profile depth, water table depth, and rooting depth were initially derived from literature (Fan et al., 2013; Fan et al., 2017). Together these parameters determine the potential access vegetation has to water through dry periods. Fan et al. (2013) have derived a 30 arc-second (~1 km) map of global observations of water table depth, assembled from literature,

government archives and groundwater modelling which was used as a starting point for water table depth. This figure was followed loosely due to the variability of the surrounding grid depths (Table 4.2) and a noticeable lack of observation data across the less densely populated areas of Brazil. A combination of the mapped data, surrounding variability and literature for each site were used to fine tune the model. Similarly, Fan et al. (2017) also produced a global map of maximum rooting depths using observations across multiple climates and species at a 30 arc-second grid scale which have been extracted for vegetation starting parameters (Table 4.2). However, they concluded that observed rooting depths reveal strong sensitivities to local soil water profiles governed by groundwater table depth from beneath and precipitation infiltration from above. Again, with poor representation of observations across Brazil these depths are taken somewhat sceptically and fine-tuned in the model.

Table 4.2 The initial conditions and for water table depth and maximum rooting depth set in VOM with the minimum and maximum depths of the grid cells surrounding the site. Water table depths taken from Fan et al. (2013), and maximum rooting depths taken from Fan et al. (2017). All depths are given in meters above ground level to provide a negative value.

Site	Water Table Depth (m)			Max root depth (m)
	3x3 Grid Min	At Location	3x3 Grid Max	
K83	-37.49	-28.66	-12.12	-10.15
K34	-28.70	-7.40	0.00	-3.86
K77	-44.97	-0.03	-0.03	-0.09
K67	-28.99	-16.53	-11.60	-9.00
CRA	-45.15	-34.30	-0.02	-2.88
VCP	-104.74	-104.74	-78.89	-7.06
PDG	-81.24	-49.74	-20.68	-12.85
USR	-51.55	-32.38	0.00	-11.15
BAN	-0.67	0.00	0.00	-0.00
FNS	-36.59	-36.59	0.00	-8.59
RJA	-33.31	-33.31	-0.37	-12.12

The rate at which roots uptake water from the soil is determined in the model by a cost factor for water transport ( $c_{rv}$ ). It is difficult to estimate this factor from empirical data, and a lack of literature lead us to initially set this to  $1.2 \mu\text{mol m}^{-3} \text{s}^{-1}$  based on previous studies by Schymanski et al. (2009, 2015). Bruno et al. (2006) tested the sensitivity of this value at site K83, where

soil moisture through a 10m column had been measured from March 2002 to December 2003 for comparability. The sensitivity of water uptake varied across different land uses and a range between 0.01-3.0  $\mu\text{mol m}^{-3} \text{ s}^{-1}$  was explored for each site.

#### 4.3.5 Model evaluation

Observational data from the flux tower sites (Chapter 2) of latent heat flux (LE), which was converted to evapotranspiration (ET), assuming the evaporative energy cost of water is 2256 J  $\text{g}^{-1}$ , is compared to the VOM outputs. Prior to conversion, nighttime LE was determined by analysing hours per month to acquire a more complete dataset. Solar irradiance which fell below 15  $\text{W m}^{-2}$  were set to 0. Daytime hours were then linearly interpolated for a maximum of one hour before converting full days (no hourly gaps) to daily totals. The VOM was evaluated for the comparable period for flux tower observations and model runs for each site (Chapter 2, Table 2.1).

The parameter interaction of the VOM is complex due to the number of vegetation properties it optimises. As mentioned earlier, the availability of soil moisture content data at K83 allowed soil water dynamic comparisons using a saturation index. To do this volumetric soil moisture data from Bruno et al. (2006) was converted to soil saturation degree using the function described by Vogel et al. (2001) (Equation (4-5), where  $s_{u,i}$  represents the soil saturation degree,  $\theta_i$  the volumetric water content, and  $\theta_r$  and  $\theta_s$  the empirical soil properties (residual and saturated soil moisture content respectively) (van Genuchten, 1980). Measurements for  $\theta_r$  were unavailable, therefore, the value was taken from Marthews et al. (2014), consistent with the model input.

$$s_{u,i} = \frac{\theta_i - \theta_r}{\theta_s - \theta_r} \quad (4-5)$$

The irregular depth measurements of the observation data were broken into smaller layers and then filled to interfaces between each measurement height, changing at the interface layer for comparability with the finer modelled layers. This is done to ensure that observations follow the same layering prescribed in VOM while preserving the total amount of soil water obtained at each measurement depth.

Performance was assessed through a combination of metrics including the root mean square error (RMSE), Pearson's correlation coefficient ( $r$ ), the difference in means (referred to as bias hereon) ( $\mu_s - \mu_o$ ), and the difference in standard deviations (referred to as variability hereon) ( $\sigma_s - \sigma_o$ ). Observed means were subtracted from simulated to work out the variability and bias, therefore, positive bias and variability equate to an overprediction of the mean and greater variability for the simulated ET. Conversely, a negative bias and variability equates to an underprediction of the mean and a lack of variability for the simulated ET. This provides an informative view into the deficiencies of the model at a site-specific level. Differences in levels of these metrics are expected due to the diversity of climate and land use therefore errors must be assessed on an individual basis.

## 4.4 Results

### 4.4.1 VOM parameter sensitivity analysis using K83

To investigate the model's ability to represent soil moisture dynamics, comparisons were made at site K83 between data collected by Bruno et al. (2006) and the VOM outputs. This comparison helped explore the parameter interaction and sensitivity whilst improving understanding of soil water storage and response rate of the water balance model to vegetation dynamics and ET and hence the models' ability to simulate observed physical processes.

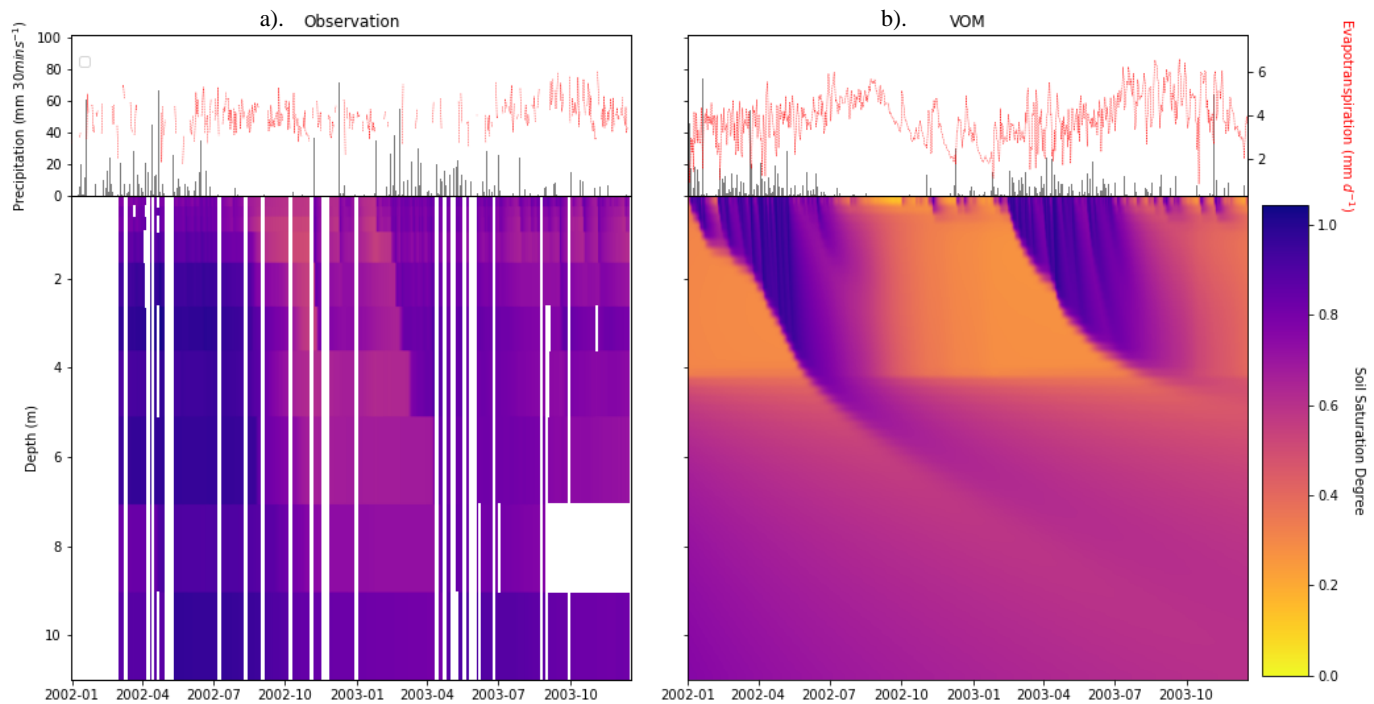


Figure 4.2 Comparison of ET, precipitation, and soil moisture saturation for a). observation measurements taken at site K83 (Bruno et al., 2006) and b). the VOM modelled soil moisture and ET results predicted by the VOM

Figure 4.2 exemplifies this and we can see from the observation data (Figure 4.2a) that the top soil layers (1-2 m) have the greatest variability in saturation degree losing moisture through the dry season (Aug-Dec). At a depth of 10 m, however, the moisture content in the soil remains close to fully saturated all year round. An explanation for evapotranspiration increasing in the dry period, could reflect available energy suggesting soil moisture is not limiting hence suggesting deeper roots are able to access the saturated soil layers during this time. Although this is maintained throughout the dry season in the observation data ET decreases after a few months when soil moisture becomes a limiting factor.

We can see much more definition of soil response looking at the modelled soil saturation degree. In this simulation the optimal root depth found to maximise the NCP was 4 m, which explains the distinct change in saturation content through time at that depth. The speed at which precipitation drains through the soil occurs at temporal periods which coincide with the two

wet seasons. We can also see that the soil drains slowly after precipitation events causing an increase in ET through the beginning of the dry season (Jul-Aug 2007). However, as the roots take in more moisture, soil saturation degree drops to  $<0.5$  and ET falls (except for short rainfall bursts).

Simulations using the literature-based water transport cost factor ( $c_{rv}$ ) ( $1.2 \mu\text{mol m}^{-3} \text{s}^{-1}$ ) resulted in reduced ET during the dry season. This parameter was isolated through multiple simulations, to investigate its sensitivity on other factors. Values ranged from  $0.1$ - $1.8 \mu\text{mol m}^{-3} \text{s}^{-1}$  and were evaluated through its impact on ET (Figure 4.3) and the associated error with observations (Table 4.3). Within a small range  $c_{rv}$  had a considerable influence on ET, especially the vegetations ability to access water during the dry season (Figure 4.3a). Above  $1.0 \mu\text{mol m}^{-3} \text{s}^{-1}$  the cost factor has no impact on the vegetations ability to take up water (Table 4.3a) but when it drops below this the seasonality of ET changes to increased ET in the dry season. This means the vegetation is able to access water in the deeper soil which is consistent with results found by Nijzink et al. (2021). When they tested the sensitivity of  $c_{rv}$  across multiple sites in Australia, however, they recorded that the sensitivity and range changed dependent on site characteristics. Therefore, despite finding a suitable value of  $0.2 \mu\text{mol m}^{-3} \text{s}^{-1}$  for site K83, a range of values for  $c_{rv}$  was tested at each site using this method. Differences in seasonality between sites mean some discretion is needed when determining the most suitable  $c_{rv}$  value. For example, if there is strong seasonality in ET at a site, a correlation statistic may tell us the most about suitability of the parameters. However, in areas that lack seasonality (such as in the northern Amazon) a combination of bias ( $\mu_s - \mu_o$ ) and variability ( $\sigma_s - \sigma_o$ ) may be the most appropriate indicator.

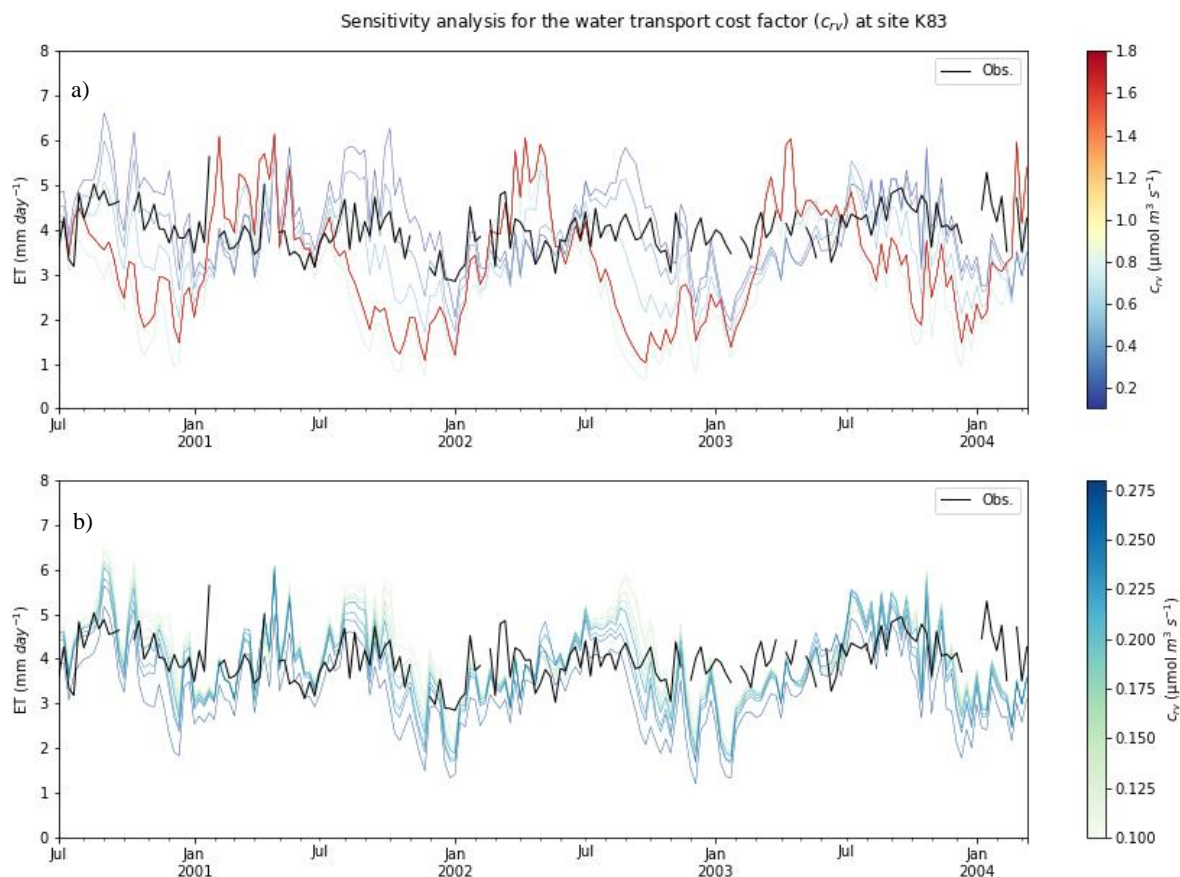


Figure 4.3 VOM ET results for altered values of the cost factor ( $c_{rv}$ ) for site K83 overlapping with observations (black line) July 2000-March 2004.  $c_{rv}$  values for the more coarse sensitivity seen in a) are associated with those in Table 4.3a whilst  $c_{rv}$  values for the finer sensitivity analysis are found in Table 4.3b. All data are weekly averages of daily total ET.

Table 4.3 ET errors between VOM results and observations at site K83 for different  $c_{rv}$  values. Table a) represents initial sensitivity analysis whilst table b) represents finer analysis. Units for  $c_{rv}$ ,  $(\sigma_s - \sigma_o)$ ,  $(\mu_s - \mu_o)$  and RMSE are given in  $(\mu\text{mol m}^3 \text{s}^{-1})$ . The value of  $c_{rv}$  with the lowest combination of errors has been highlighted and this was used to run the final simulation.

a)	$c_{rv}$	$r$	$(\sigma_s - \sigma_o)$	$(\mu_s - \mu_o)$	RMSE	b)	$c_{rv}$	$r$	$(\sigma_s - \sigma_o)$	$(\mu_s - \mu_o)$	RMSE
	0.1	0.274	0.426	0.312	1.21		0.10	0.274	0.426	0.312	1.21
	<b>0.2</b>	<b>0.305</b>	<b>0.339</b>	<b>-0.001</b>	<b>1.079</b>		0.12	0.294	0.384	0.342	1.172
	0.4	0.239	0.336	-0.53	1.24		0.14	0.304	0.373	0.294	1.145
	0.6	0.106	0.672	-1.381	2.033		0.16	0.32	0.357	0.177	1.096
	0.8	0.17	0.663	-1.385	2.029		0.18	0.322	0.358	0.115	1.087
	1.0	0.12	0.618	-0.976	1.736		<b>0.20</b>	<b>0.305</b>	<b>0.339</b>	<b>-0.001</b>	<b>1.079</b>
	1.2	0.12	0.616	-0.977	1.734		0.22	0.314	0.358	0.052	1.089
	1.4	0.12	0.616	-0.977	1.734		0.24	0.302	0.356	-0.108	1.1
	1.6	0.12	0.618	-0.976	1.736		0.26	0.293	0.343	-0.206	1.11
	1.8	0.121	0.61	-0.981	1.732		0.28	0.287	0.313	-0.686	1.273



#### **4.4.2 Model performance at sites representing natural ecosystems**

Figure 4.4 and Figure 4.5 present the daily ET rates for both VOM simulations and flux tower observations which are used to explain the seasonal differences presented in Figure 4.6. Table 4.4 presents the breakdown of errors numerically quantifying the visual graphical differences. Together these are used to assess the success of the model performance.

The model was optimised for only the perennial part of the model (representing trees) for closed canopy perennial forests which included (K34, K67, K83 and RJA). The savanna sites (BAN and PDG) were optimised for both perennial and seasonal (grasses) vegetation.

Through the northern Amazonian sites (K34, K67, and K83) the VOM simulations of ET had varying levels of success in following observations. There is a large bias at K34 ( $1.909 \text{ mm d}^{-1}$ , Table 4.4) with the model constantly overpredicting ET leading to the largest RMSE of all sites. However, variability is low and correlation shows reasonable capture of the annual signature. At K67 the overprediction of the mean was much lower but still noticeable ( $0.603 \text{ mm d}^{-1}$ ) as the model consistently overpredicted ET between March-September (Figure 4.6). However, the steep declines in ET in September (Figure 4.4) and an underprediction between October-February also led to some variability and a low correlation. The simulation at K83 had the strongest agreement with observations and followed the observed mean with some variation ( $0.339 \text{ mm d}^{-1}$ ). The model captured the slight increase in ET during the dry season although there were some sharp uncharacteristic declines in December and January (2002 and 2003) which resulted in the underpredictions for ET for these months (Figure 4.4).

At the tropical savanna site, BAN, the model was again able to capture the mean trend but struggled in maintaining variability ( $0.51 \text{ mm d}^{-1}$ ). Steep declines in ET led to underpredictions in the dry season (Figure 4.6) whilst consistently large spikes in ET uncharacteristic of the site

caused overpredictions in the wet season. Although minimal, there was seasonality in observed ET which the model captured.

Table 4.4 Errors between VOM simulation and flux tower observations at all sites separated into natural and cultivated ecosystems. Showing the land cover type, Pearson's correlation coefficient ( $r$ ), difference in standard deviations ( $\sigma_s - \sigma_o$ ), difference in means ( $\mu_s - \mu_o$ ) and the root mean square error (RMSE). Units for ( $\sigma_s - \sigma_o$ ), ( $\mu_s - \mu_o$ ) and the RMSE are in  $\text{mm d}^{-1}$ .

Natural Ecosystems					
Name	Land Cover	$r$	$(\sigma_s - \sigma_o)$	$(\mu_s - \mu_o)$	RMSE
K34	Tropical Rainforest	0.362	0.247	1.909	2.486
K67	Tropical Rainforest	0.253	0.441	0.603	1.461
K83	Tropical Rainforest	0.305	0.339	-0.001	1.079
BAN	Woodland Savanna	0.418	0.51	0.003	1.356
RJA	Tropical Dry Forest	0.216	0.297	1.832	2.34
PDG	Savanna	0.623	0.243	0.128	1.281

Cultivated Ecosystems					
Name	Land Cover	$r$	$(\sigma_s - \sigma_o)$	$(\mu_s - \mu_o)$	RMSE
K77	Cropland (Pasture)	0.453	-0.215	-0.327	1.416
FNS	Cropland (Pasture)	0.098	0.663	1.882	2.417
VCP	Cropland (Eucaliptus)	0.689	-0.713	-0.902	1.721
USR	Cropland (Sugarcane)	0.458	0.127	0.153	1.331
CRA	Cropland (Soybean)	0.472	-0.465	-0.12	1.727

The VOM simulation failed to follow the observed ET at the southern Amazonian site, RJA. The model overpredicted ET by an average of  $1.83 \text{ mm d}^{-1}$  (Table 4.4) and despite a weak correlation it was unable to maintain the lack of observed seasonality and steep declines in ET in July (mid-late dry season) can be found (Figure 4.4). In contrast, the model performed well at the most southerly site, PDG. There was low bias and variability and a high correlation because the model caught the strong seasonal signature of the site. There was a slight overprediction of ET during the wettest months in January and February.

## Chapter 4: How can we use Carbon-Water mechanisms to understand hydrological fluxes?

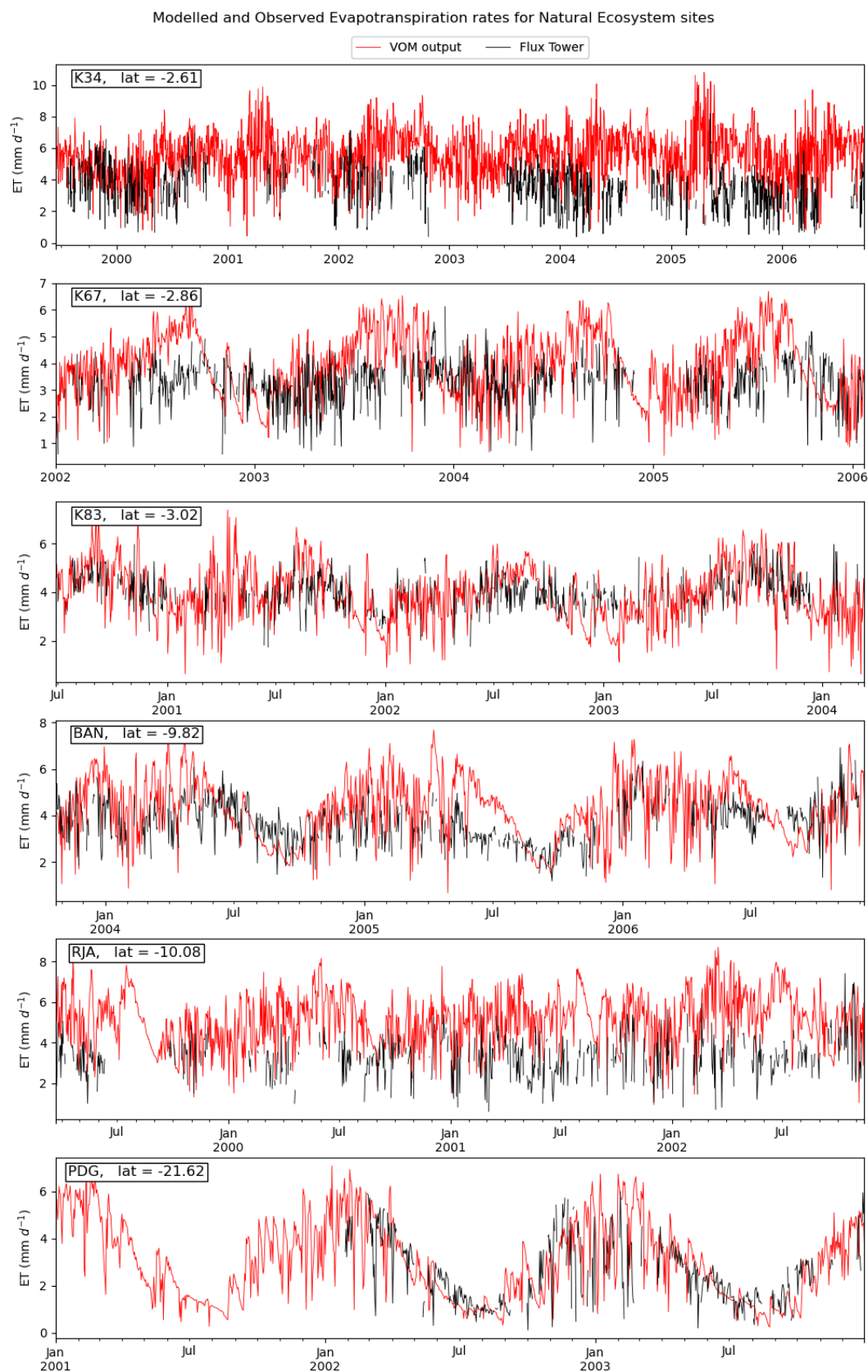


Figure 4.4 Final VOM simulation (red) and flux tower observation (black) ET for the overlapping period for sites representing natural ecosystems. Results are displayed descending with distance from the equator.

Chapter 4: How can we use Carbon-Water mechanisms to understand hydrological fluxes?

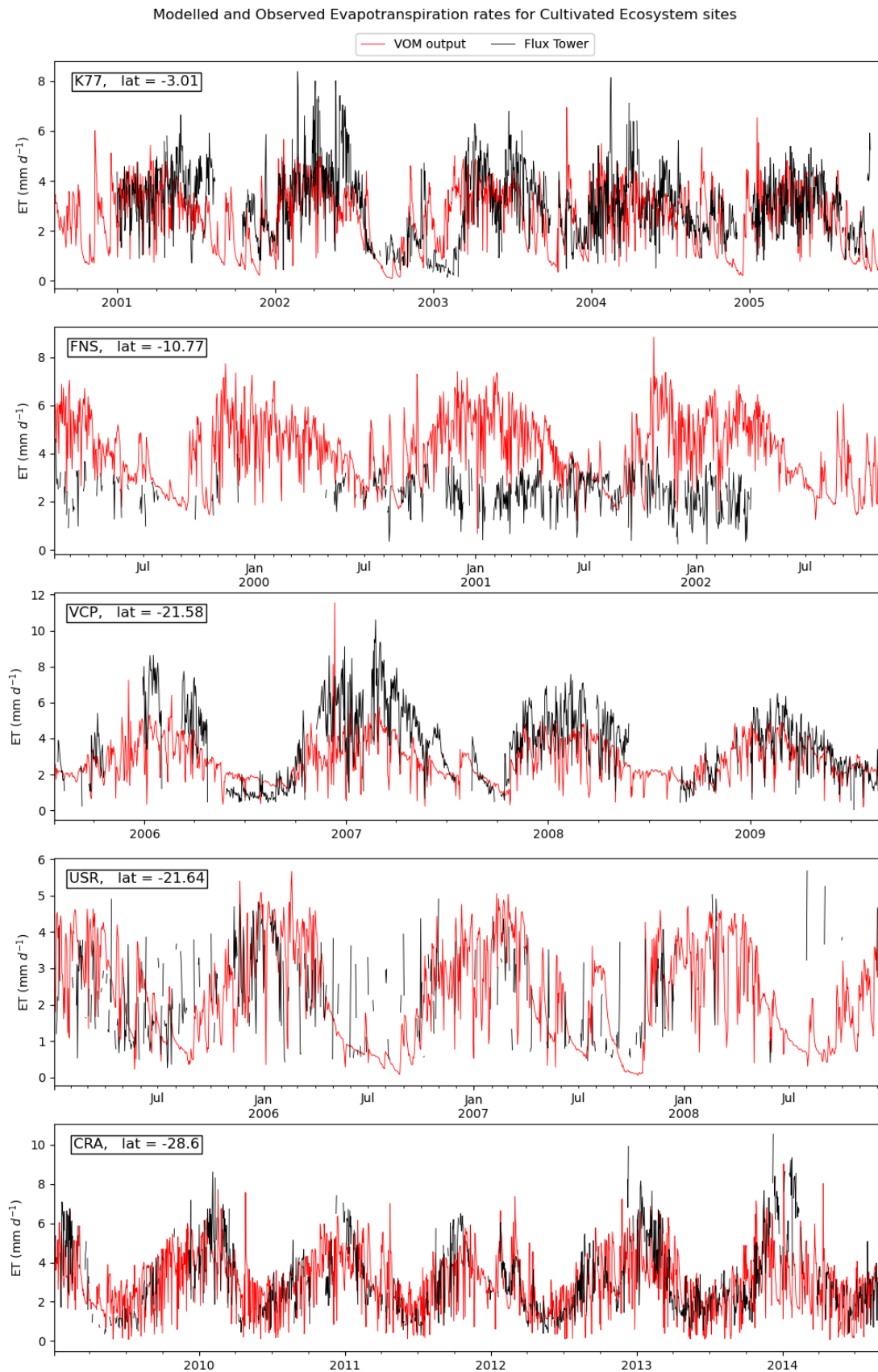


Figure 4.5 Final VOM simulation (red) and flux tower observation (black) ET for the overlapping period for sites representing cultivated ecosystems. Results are displayed descending with distance from the equator.

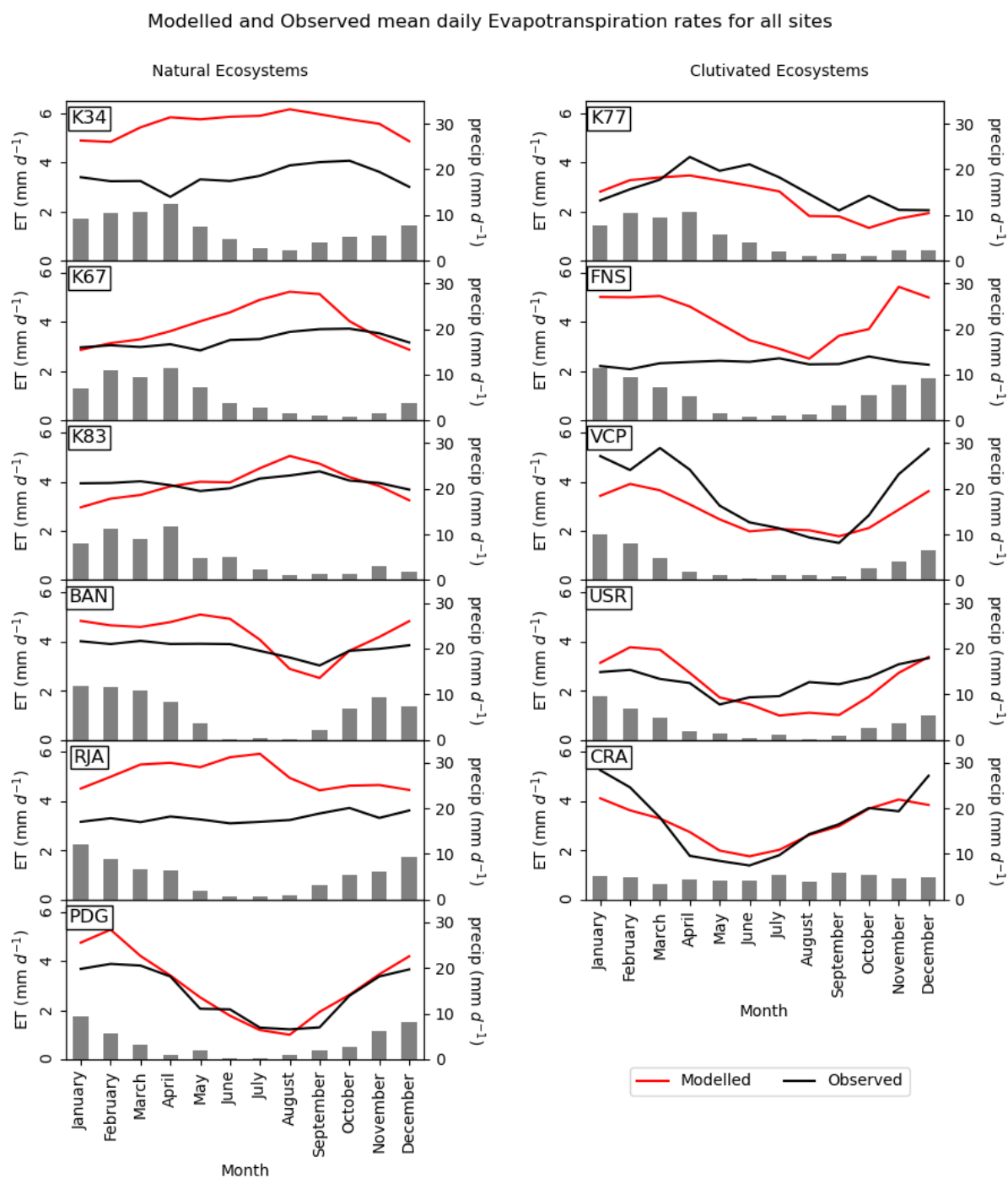


Figure 4.6 ET rate averaged by month for the final VOM simulations (red) and flux tower observations (black) at all sites, natural and cultivated. Average monthly forcing precipitation is shown with grey bars on the secondary axis. Simulations were only averaged for the overlapping period with observations.

### **4.4.3 Model performance at sites representing cultivated ecosystems**

The model was optimised for only the seasonal part of the model (grasses) for all cultivated sites except for the Eucalyptus plantation (VCP), where perennials were also optimised. The northern Amazon pasture site, K77, captured the observed seasonality of ET following increases in the wet season and decreases in the dry season. The mean was slightly underpredicted and the strength of the seasonality was slightly less than observed which had consistently higher rates of ET towards the end of the wet season (April-June) (Figure 4.5, Figure 4.6, Table 4.4). Conversely, the VOM was unable to capture observed trends in ET at the southern Amazonian pasture site, FNS. A high bias and variability combined with no visible correlation equates to the models lack in ability to replicate the hydrological processes at this site. The model shows strong seasonality with decreased ET in the dry season and high ET in the wet season which does not align with the lack of seasonality displayed by the flux tower observation data.

The VOM simulations for the Eucalyptus plantation, VCP, showed strong correlations as it captured ET seasonality. However, a constant underprediction during the wet season led to a greater difference in the means and not enough variability. The model did manage to capture ET in the dry season well as it did also in 2009 during the wet season (Figure 4.5). At site USR, the sugarcane crop, the model performed simulated ET well following the observed mean and variation. From Figure 4.5 it looks like the seasonality was also well captured but when averaged by month (Figure 4.6) there is a slight delay as observed ET increases during the dry season after May ( $r = 0.458$ ) whereas in the simulation recovery does not start until the wet season in September.

Unsurprisingly, the strongest observed seasonality occurred at the most southerly site, CRA. Simulated ET followed observations closely from May through to November capturing the

seasonal signature but consistently underpredicted during the hottest months (December-February) ( $(\sigma_s - \sigma_o) = -0.465$ ). Mean ET was almost identical for both simulated and observed.

## 4.5 Discussion

The sites are grouped into five different climates (Table 4.5). The northern Amazonian sites (K34, K67, K77 and K83) span two tropical climates, the most westerly of which receives more rainfall than the other sites. However, there is a markedly reduced rain period of 1-3 months varying between July and October at K34 (Araújo et al., 2002) and some studies have grouped the three forest sites together climatologically as they have a similar dry season spanning August-November (da Rocha et al., 2009; Restrepo-Coupe et al., 2013; Christofferson et al., 2014; Araújo et al., 2016; Almeida et al., 2018; Smith et al., 2020). Although less defined than other sites K34, K67 and K83 have seasonal ET cycles with a middle of the dry season peak due to a lack of soil moisture stress following trends in solar radiation suggesting they are light limited (Chapter 2, Figure 2) (da Rocha et al., 2004; Hutyra et al., 2007; Restrepo-Coupe et al., 2013, 2017, 2021; Christofferson et al., 2014). Nepstad et al. (1994) suggest that evergreen forests in the Af climate (e.g., K34) have a steady supply of water throughout the year and therefore roots do not need to penetrate deep soils to access more during dry seasons as Am forests do. The modelled and observed ET reflects this lack of soil moisture stress at all three sites with predictions matching dry season ET peaks which other models, during intercomparison studies, have struggled to predict (Restrepo-Coupe et al., 2017, 2021) suggesting VOM has a better understanding of hydrological processes. However, there is a consistent overprediction of ET at K34 by almost  $2 \text{ mm d}^{-1}$  (similar to Restrepo-Coupe et al., 2017, 2021). All the significant incoming and outgoing radiation terms are measured, so in principle, they should balance. However, it is common for there to be a mismatch owing to measurement uncertainty. Hasler and Avissar (2006) assessed the energy balance closure of

K34 by calculating the energy balance ratio using turbulent fluxes to net radiation. They calculated an energy balance closure of 77% throughout the wet and drier season concluding that the imbalance could cause an underprediction of observed latent heat flux, but due to a lack of temporal variation of imbalance over the forest, seasonal trends were not impacted confirming ET peaks in the late dry season. This is a standard lack of closure for forest sites and could account for a large percentage of the bias between observed and modelled (McMillen 1988; Baldocchi and Vogel 1996; Goulden et al., 1996; Wilson and Baldocchi 2000, Araújo et al., 2002, Mahli, et al., 2002).

Table 4.5 All study sites grouped by their Köppen climate classification. Derived from (Alvares et al., (2014) and literature.

Köppen climate		
Symbol	Description	Sites
Af	Tropical without dry season	K34
Am	Tropical monsoon	K67, K77, K83
Aw	Tropical with dry winter	BAN, FNS, RJA
Cwa	Humid subtropical with dry winter, hot summer	PDG, USR, VCP
Cfa	Humid subtropical without dry season, hot summer	CRA

Modelled water stress was reduced at K67 and K83 by altering the water transport cost factor ( $c_{rv}$ ) which allowed roots to penetrate deeper accessing more saturated soils over the dry period and sustaining ET throughout the year. The roots of perennial trees can grow down to 18m to access water throughout the dry period (Nepstad et al., 1994; Bruno et al., 2006). However, steep declines in ET towards the end of the dry season at K67 and K83 (Figure 4.4 and Figure 4.6) indicate that the modelled root system is not finding enough water to sustain the perennials throughout the dry period like we see in the observations. The freely draining nature of the water balance model could result in this underestimation of dry season water use (Nijzink et al., 2021). Energy balance closure was high at K83 (96%) but much lower at K67 (79%) which would account for the bias in predicted ET and bring observed ET up to a similar rate to that of K83 (Hasler and Avissar, 2006).



As K77 is a pasture site, only the part of the model representing seasonal vegetation was employed. The difference in observed ET seasonality at the perennial sites to K77, can be explained by water stress to short grass roots during the dry season caused a reduction in ET. The grass roots of the model only accessed the top 0.4 m of soil allowing a successful replication of site ET at this climate. Comparing the observations and simulations at this site to K67 and K83 outlines the importance of understanding rooting depths in this climate. Sakai et al (2004) calculated a reasonable average energy balance closure of 92%.

Three sites are classified as tropical dry winter climates: BAN, FNS and RJA. However, the model struggled to replicate observed ET at all three sites, overpredicting seasonality at BAN, mean ET at RJA and both mean and seasonality at FNS. Seasonal flooding occurs between February and June at BAN causing difficulties when prescribing static water table depth to the model (Borma et al., 2009). Fan et al. (2013) prescribed a water table depth at this location and the surrounding area between 0 – 0.6 m giving very little room for modelled root growth. Borma et al. (2009) measured groundwater at the tower which fell to ~4m depth between floods which was used instead in the model. They also measured soil moisture content down to 2 m and showed a slow top-down drying of the column which took around 4 months to dry out at 2 m depth to approximately 60% moisture during the dry season post flooding in 2004 and 2006. This correlated with a slow reduction of ET concluding that vegetation was able to extract water from below 2 m depth to maintain transpiration during the dry season. It is also likely that capillary action through the soil column driven by a high groundwater level helped keep moisture. The model struggled to replicate this overpredicting ET during floods and underpredicting ET during the dry season. Borma et al. (2009) calculated only a 78% energy balance closure on average over the wet and dry seasons and suggested that the eddy covariance measurements lead to underpredictions in ET. It was also noted that latent heat flux measurements were likely to be disturbed by evaporation from flooded areas leading to greater

uncertainty in observations over the wet season. If an underprediction of observation data increases mean ET throughout the wet and dry season, modelled ET in the late dry season is underpredicted even more (although wet season predictions may seem more in line). The model's only hydrological input is precipitation, and its singular dimensionality does not account for other external inputs raising the water table during the dry season such as streams, springs, and rivers. The VOM's inability to capture catchment dynamics, (i.e., catchment capture, storage, and release over the dry season) is a problem in runoff or groundwater fed areas that may sustain soil moisture throughout the dry season such as BAN. This along with the freely draining nature of the water balance model could then explain the underprediction in ET throughout the dry season.

Like at K34, VOM at RJA overpredicted ET throughout the year by  $\sim 1.7 \text{ mm d}^{-1}$ . Von Randow et al. (2004) analysed the energy fluxes at RJA and FNS and reported that the energy balance closure was poor at both sites. They applied two energy closure methods to adjust sensible and latent heat fluxes (from Twine et al., 2000) by identifying a potential range of values for the fluxes. When employed, average latent heat flux increases by 20-30% at RJA (the lack of seasonality remained the same). The observed results shown here are presented without closure correction which explains a large portion of the bias seen at RJA. Despite high seasonality in precipitation the forest is fed by many springs and streams suggesting there is a high water table (IBAMA, 2006). These supply moisture throughout the year to the vegetation, which are thought to help maintain ET levels throughout the dry season. It has also been reported that root systems grow beyond the soil layer often deep into weathered or fractured bedrock (Wright et al., 1996). Deep root access to water fed by springs or streams through fractured bedrock, may help maintain a constant level of ET throughout the year (von Randow et al., 2004). Bedrock is recorded from 1-2m depth (Hodnett et al., 1996) yet the water table depth is estimated to be 33 m deep (Fan et al., 2013, Table 4.2). As uniformity in soil structure

was assumed when modelling across all sites for consistency (as well as a lack of available data), the different hydraulic physical properties in bedrock compared to the top soil layer may account for some modelled water stress in the late dry season (July-August). Altering the soil structure profile and more site-specific knowledge of the profile's hydraulic properties might result in a better prediction.

When von Randow et al. (2004) applied the energy closure method at the pasture site, FNS, they documented a change in observed seasonality and a well-defined wet and dry season ET became obvious, supported by their measured soil moisture storage profiles. In their comparison study, average ET was 20% and 41% lower during the wet and dry season respectively at the pasture site (FNS) than the forest site (RJA). Similar results were also found by Hasler and Avissar (2006) when they applied energy closure corrections. As with RJA, observed results are presented without energy closure correction which would account for the difference between modelled and observed ET.

PDG, USR and VCP fall into the humid subtropical dry winter/hot summer climate category and are all located within 20 km of each other. All sites have strong climatic seasonality with hotter wetter summers (October-March) and drier winters (April-September). ET follows trends in precipitation, solar radiation, and temperature with peaks in the summer and lows in the winter. The model predicted these trends in ET correctly across all sites. Slight overpredictions in peak summer can be seen at PDG which could be due to a lack of data availability during these months, but these are considered marginal given the strong correlation and low differences in standard deviations and means (Table 4.4). The energy balance closure for PDG was 99% providing confidence in the observation measurements (Cabral et al., 2015).

A distinct lack of data availability (only 36.2%) at the sugarcane site, USR makes it difficult to draw conclusions regarding model performance. The model predicts lower rates of ET later

in the dry season than observed, increasing and decreasing with precipitation. Given the agreement in modelled results and observations at PDG, it is likely that this observed trend is due to a lack of data. Data that was available had a high energy balance closure of 97% (Cabral et al., 2012), however, cultivated sugarcane sites may be subject to irrigation during the dry season which could alter natural trends in ET unable to be captured by the model.

Strong seasonality in ET was seen at the Eucalyptus plantation, VCP. Cabral et al. (2010) established that full energy balance closure was accounted for, and very high daily rates of ET were observed up to 11 mm day<sup>-1</sup> during the wet summers. They calculated that ET over the Eucalyptus site was strongly dominated by transpiration (87%) and accounted for 77% of total rainfall. The rapid rate of growth and water use of Eucalyptus in Brazil has been documented by Stape (2002) and appears to be the highest recorded for woody vegetation (Whitehead and Beadle, 2004). As the VOM predicts natural vegetation adaptation based on NCP, the model will fail to reproduce rates of ET from monoculture and non-native trees that over exploit water availability, such as Eucalyptus, explaining the bias over the wet season. Rates of ET over the dry season were captured well by the model suggesting the rooting depth and soil moisture dynamics were represented well. Furthermore, the VOM assumes the prior establishment of perennial vegetation and that a growth equilibrium has already been reached. Trees grew rapidly at the site from 12 m to 21 m during the measurement period (2005-2009) which could not only explain the increased rates of ET during 2006 and 2007 but also account for well-matched ET during the 2009 wet season assuming vegetation was nearing full growth.

The most southerly site in this study is CRA, a soybean site with a humid subtropical climate without a dry season and with a hot summer. ET trends closely follow the well-defined winter-summer patterns of temperature and solar radiation. Confidence in observed latent heat flux is supported by an energy balance closure of 95% (Webler et al., 2012). Mean ET was well captured by the model although there was an underprediction at summer peaks. This could be

the product of a high soil saturated hydraulic conductivity parameter estimated by Marthews et al. (2014) which has been estimated to be lower around this region for pasture/crop (down to  $1.1 \times 10^{-6} \text{ m s}^{-1}$ ) in comparison to forest sites in southern Brazil (Lozano-Baez et al., 2018). Lower hydraulic conductivity could maintain soil moisture in the summer months increasing peak ET.

Although extreme biases may be partially attributed to a lack of energy balance closure at the site, the fact remains that five of the six strongest correlations were found at cultivated sites. This suggests that the model represents the biophysical processes over farmed ecosystems to a greater extent than its intended use over natural ecosystems. Biases suggest that the model consistently underpredicts ET at natural ecosystems implying that some physical processes are underrepresented. This could be partially explained by the greater uncertainties when modelling processes in perennial vegetation such as deeper, more complex rooting systems and the mechanisms in the vascular system that differ with differences in canopy height (which are not addressed in this model). Interestingly, biases for cultivated sites appear to be much more random suggesting that errors are not related to a consistent negligence of a particular process. Despite this, three of the five sites are dominated by vegetation with C4 photosynthetic pathways (K77, FNS, and USR) which could attribute to their errors. However, statistically K77 and USR perform no better or worse than the C3-dominated site CRA, whilst the C4-dominated site, PDG, outperformed almost all other sites. This suggests there is no obvious detriment in using the C3 photosynthetic pathway in this form of vegetation optimality modelling at these sites and that perhaps it is acceptable in return for greater generality (Schymanski et al., 2009).

It is important to acknowledge that disparities in simulated and observed ET could also be due to model incompetence. Other than the negligence of the C4 photosynthetic pathway and canopy height/structure the model also does not account for nutrient uptake which could have

a large impact on ecosystems that suffer from poor soil conditions and nutrient deficiencies causing this to limit growth affecting ET rates. Additionally, the model lacks site specific hydrological conditions allowing free drainage. This could lead to an underestimation of water use in dry seasons as found by Nijzink et al. (2022). Furthermore, the transport of water from deeper soil layers to the canopy and its distribution over vegetation require a complex water transport infrastructure here simplified resulting in the ‘tuning’ of the  $c_{rv}$  parameter. It was found that ET was very sensitive to the parameterisation of these costs and as such more research into how these water transport processes operate in relation to environmental conditions will most likely improve the modelling capabilities.

It is worth noting that improvement of the VOM’s performance over monocultural agriculture might be achieved by altering vegetation parameters in the model to represent that of the species rather than general vegetation (Lei et al., 2008), however, this decreases the generality of the model.

## 4.6 Conclusions

In this chapter we analysed the performance of the Vegetation Optimality Model, which optimises net carbon profit using carbon-water mechanisms, to understand hydrological fluxes across 11 different sites over Brazil by comparing measured and predicted ET. Performance was assessed by the ability to answer the original research questions below.

### **4.6.1 To what extent can the VOM predict ET across different climates?**

The VOM successfully captured observed trends in ET across five different climate classifications with no obvious failure linked to any one climate. Discrepancies in results at K34, K67, RJA and FNS were largely due to underpredictions in latent heat flux proven by poor energy balance closures (von Randow et al., 2004; Hasler and Avissar, 2006). With some calibration of the  $c_{rv}$ , the VOM correctly predicted dry season peaks in ET in the northern

Amazonian rainforest sites which has been a common challenge when modelling hydrological processes in tropical rainforests (Christoffersen et al., 2014; Restrepo-Coupe et al., 2017; Restrepo-Coupe et al., 2021). Soil moisture analysis at K83 proved that the model was able to successfully replicate moisture extraction from deeper soils for most of the dry season, however, apparent water stress in the late dry season at K67, K83 and RJA means either i) the model lacked of understanding of some carbon-water mechanisms enabling deeper root growth to access moisture during the dry season, ii) more knowledge is needed regarding the soil physical properties at the site (potentially impacting or changing free drainage from the water balance model), or iii) a combination of both.

The model also struggled to represent hydrological fluxes at the seasonally flooded site, BAN which maintained mean ET throughout the dry season. This highlighted 1-dimensional limitations in VOM and its inability to capture catchment dynamics where water may be supplied by a hydrological process other than precipitation. However, general seasonality was captured, and ET rates may be realistically modelled after energy balance closure during the wet season.

#### **4.6.2 To what extent can the VOM predict ET in natural ecosystems?**

The model was adjusted to represent either perennial only or perennial and seasonal vegetation depending on the characteristics of the natural ecosystem sites. K34, K67, K83 and RJA are classified as primary forest with no seasonal vegetation whilst BAN and PDG comprise of both. Realistic predictions of ET were made over three natural ecosystem types; tropical rainforest, savanna (Cerrado), and tropical dry forest suggesting this modelling approach is useful across multiple different vegetation types without the need to prescribe vegetation specific parameters. It shows that vegetation maximises the growth of carbon to the limitations of climatic and soil conditions across three major Brazilian biomes. However, modelled water stress in the late dry season at K67 and K83 implies it was unable to fully

capture the Amazon vegetation adaptive mechanisms of deep and efficient root systems. Furthermore, the VOM struggled to model ET over the transitional woodland savanna site, BAN, underlining limitations in modelling groundwater dominated ecosystems.

#### **4.6.3 To what extent can the VOM predict ET in cultivated ecosystems?**

Crop and pasture sites were represented by seasonal vegetation (CRA, FNS, K77 and USR) whilst the Eucalyptus plantation (VCP) was represented by both perennial and seasonal. The model realistically predicted ET at all crop and pasture sites without the adjustment of any vegetation parameters (aside from  $c_{rv}$ ) suggesting that these agricultural sites can be generalised across ecosystems. The inability of the model to capture high ET at the Eucalyptus plantation could be a combination of a) different hydrological processes that arise from the monoculture of a non-native species with high ET rates b) and a newly developing ecosystem with fast growth rates which hasn't yet reached stability. This conclusion can be drawn given its proximity to the natural savanna site, PDG, and shared soil hydraulic physical properties and climate.

#### **4.6.4 What is the sensitivity of the VOM to poorly constrained parameters in these environments?**

Alterations of water transport cost factor ( $c_{rv}$ ) had the ability to change seasonal ET by affecting the optimal rooting depth of vegetation at K83 resulting in the need for calibration of this parameter at all other sites. This proved that hydrological fluxes were highly sensitive to changes of  $c_{rv}$  and root water uptake in the vertical soil profile plays an important role that is not easily optimised. The value of the  $c_{rv}$  differed with land use type and climate to better predict observed variations in ET during the wet and dry (or summer and winter) seasons. The final values ranged from  $0.08 - 1.2 \mu\text{mol m}^{-3} \text{s}^{-1}$  (initially  $1.2 \mu\text{mol m}^{-3} \text{s}^{-1}$  (Schymanski et al., 2009,2015)). It is important to note that the alteration of this factor and its influence on ET may



be compensating for incorrect or generalised soil physical properties which were unaltered during calibration.

#### **4.6.5 What are the important water and plant interactions captured by vegetation optimality in the study areas?**

At the primary forest sites vegetation optimality allowed trees to search for the rooting depth that maximised the net carbon profit throughout the 30-year run period. The ability of vegetation to utilise water stored in deeper soil layers during the dry season to maximise growth was an important interaction when trying to realistically predict ET as it removed water stress as a limitation to growth and ET then followed patterns in temperature or light availability. Feedbacks between the catchment water balance and vegetation water use derive important rooting costs and vegetation optimality allows CO<sub>2</sub> and water fluxes to be modelled on a daily and yearly basis without prior vegetation assumptions across different ecosystems over Brazil.

#### **4.6.6 Overall conclusions**

The overall conclusion is that, through calibration of the water transport cost factor (controlling root water uptake rate) and prescribed soil physical properties, with no prior knowledge of vegetation other than seasonal or perennial growth, the VOM can consistently represent hydrological processes in both natural and cultivated ecosystems across multiple climates in Brazil. However, limitations in the model arise from its singular dimensionality and inability to represent ecosystems prone to two-dimensional hydrological influences such as seasonal flooding.

Using carbon-water mechanisms, vegetation optimality provides a novel approach to study hydrological processes in vegetation dominated ungauged catchments. Furthermore, there is potential to predict changes in hydrological fluxes between prospective natural vegetation and cultivated vegetation allowing assessments of the impact of land use change on the

*Chapter 4: How can we use Carbon-Water mechanisms to understand hydrological fluxes?*

hydrological cycle. ET predictions from vegetation optimality modelling could further be used as inputs to catchment runoff models that lack adequate representation of that component. Importantly it also allows for the potential to predict water use under long-term climate change scenarios based on vegetation properties.



# Chapter 5: How sensitive are hydrological processes in vegetation to changes in atmospheric CO<sub>2</sub> concentration?

## 5.1 Introduction

This chapter discusses potential long-term and short-term vegetation responses as it optimally adapts by maximising net carbon profit to changes in atmospheric CO<sub>2</sub> concentrations ( $C_a$ ). Long-term responses consist of changes in ecosystem structure including maximum rooting depth and vegetation cover whilst short term effects are linked to stomatal closure and water use efficiency. We look at how these responses affect hydrological processes across a variety of key Brazilian ecosystems. As discussed in Chapter 4 we now know that the VOM can predict key eco-hydrological fluxes in tropical and sub-tropical regions in Brazil in both naturally occurring and cultivated ecosystems. This allows us to isolate further impacts to these ecosystems using the VOM.

Understanding the ecosystem responses to changes in CO<sub>2</sub> concentration is important for eco-hydrology because of its potential impact on regional and global water balance. Increases in atmospheric CO<sub>2</sub> concentrations ( $C_a$ ) are largely thought to increase water use efficiency, reducing stomatal conductance and transpiration (Wong et al., 1979; Field et al., 1995; Sellers et al., 1996; Drake et al., 1997). This is known as the ‘physiological effect’ (e.g., Betts et al., 2007, 2011, 2012), and modelling this has led to some conclusions that elevated atmospheric CO<sub>2</sub> concentrations (eCO<sub>2</sub>) has resulted in regional to global shifts in the water balance due to

*Chapter 5: How sensitive are hydrological processes in vegetation to changes in atmospheric CO<sub>2</sub> concentration?*

increased river discharge (e.g. Costa et al., 1997; Gedney et al., 2006; Betts et al., 2007; Magrin et al., 2014), and shifting the Bowen ratio more in favour of sensible heat (Lemordant et al., 2018) which in turn enhances warming and decreases relative humidity reducing the fraction of low cloud cover (Cao et al. 2010; Andrews et al., 2011). In contrast, other studies have reported that eCO<sub>2</sub> increases leaf area index (LAI) and greening through the “CO<sub>2</sub> fertilisation” effect which counteracts the reduction in water use through transpiration (Wu et al., 2012; Donohue et al., 2013a; Niu et al., 2013).

It has been well documented that the physiological effect may play a bigger role than the radiative effect in driving changes in the hydrological cycle in the rainforests of Brazil (Costa et al., 1997; Abe et al., 2015; Chadwick et al., 2017; Skinner et al., 2017; Lemordant et al., 2018; Richardson et al., 2018). Through modelling elevated atmospheric CO<sub>2</sub> Richardson et al. (2018) argue that due to abundant vegetation and water recycling through evapotranspiration (ET), the physiological effect could cause a reduction in precipitation over the Amazon, whilst Lemes et al. (2022) provide evidence for large increases in temperature with decreases in ET, and changes in moisture balance causing large atmospheric circulation shifts due to deep convection. Considerably less research has been done on the effects of eCO<sub>2</sub> on natural vegetation in the Cerrado (Brazilian savanna). However, Souza et al. (2016) recorded that eCO<sub>2</sub> increased the biomass of native Cerrado woody species, even under water stress, due to increased water use efficiency (WUE) and potentially the growth of a deeper rooting system. This supported the hypothesis by Bond et al. (2003), that savanna ecosystems can become denser, reducing light availability to herbaceous species changing the composition of the natural vegetation strata. Additional studies have also been carried out investigating the physiological effect on Brazilian crops, confirming increased growth rates but suggesting dependence on precipitation, closely linked to the ET of the surrounding forests (Costa et al., 2009; Marin et al., 2013; Oliveira et al., 2013). They confirmed an increase in WUE under

*Chapter 5: How sensitive are hydrological processes in vegetation to changes in atmospheric CO<sub>2</sub> concentration?*

eCO<sub>2</sub> due to a decrease in stomatal conductance and a potential increase in yield, however, Oliveira et al. (2013) warn that the replacement of natural ecosystem with agricultural crops could decrease water availability offsetting the increases due to increased WUE.

These scenarios suggest that stomatal closure is the initial step in a deluge of potential effects of eCO<sub>2</sub>. These are not limited to, but could involve, shifts in ecosystem stratification, vegetation cover, perennial rooting depth, decreased annual ET and increased runoff linked to the reduction in water cost (through transpiration) to fix CO<sub>2</sub> in eCO<sub>2</sub>. However, changes in perennial ecosystem structure are only likely to be seen through decades of adaptational change.

There is much variation in modelled stomatal response which is impacted by both eCO<sub>2</sub> and temperature (Rogers et al., 2017). In a perturbed parameter experiment Booth et al. (2012) found the effect of temperature on photosynthetic rate to be the most prolific source of carbon cycle uncertainty, but that atmospheric CO<sub>2</sub>-temperature feedback systems are complex and poorly understood in current models. These uncertainties highlight the importance of isolating the effect of C<sub>a</sub> on vegetation. Efforts are being made to examine the separated effect of C<sub>a</sub> on different plant species from other climatic changes. These are known as large-scale free-air CO<sub>2</sub> enrichment (FACE) experiments but have primarily been focused on temperate ecosystems (Ainsworth and Long 2005). There is, however, one FACE experiment proposed by Norby et al. (2016) in the Amazon north of Manaus and site K34, which is currently ongoing and will provide important information on tropical broadleaf evergreen ecosystem response to eCO<sub>2</sub>, however, there has been a severe delay in the start of this project. Eventually, results will provide insight to the short-term vegetation responses, but this project is not intended to study long-term dynamics and is only limited to one ecosystem of Brazil.

*Chapter 5: How sensitive are hydrological processes in vegetation to changes in atmospheric CO<sub>2</sub> concentration?*

It is key to identify the difference between the short and long-term responses to eCO<sub>2</sub> across distinct ecosystems. As mentioned before long-term responses consist of changes in ecosystem structure, whilst short term effects are linked to stomatal closure and water use efficiency. These responses may differ in hydrological processes as, given time to adapt (long-term), increased perennial vegetation cover and root growth could increase ET rates and decrease runoff, dampening or even reversing short-term responses of decreased ET. For example, some authors have linked vegetation responses to increasing C<sub>a</sub> with observed global increases in perennial vegetation cover (known as ‘woody thickening’) (Bond & Midgley, 2000; Donohue et al., 2013a; Stevens et al., 2017; Melo et al., 2018). However, theoretical considerations differ as to the main drivers of this. As distinct ecosystems differ in energy and water limitations, perennial vegetation patterns and rooting depths, the long-term response to eCO<sub>2</sub> will be unique to each one, highlighting the importance to model potential changes to the water balance across climates.

Schymanski et al. (2015) were able to study the short and long-term effects of eCO<sub>2</sub> across four climatically different sites in Australia using the Vegetation Optimality Model (VOM), which incorporates dynamic feedbacks between vegetation and water balance (Schymanski et al., 2009). They presented theoretical support for decreases in ET due to a positive eCO<sub>2</sub> vegetation feedback causing reductions in plant water use from simulations. The benefit of this model is that it assumes that vegetation self-optimises maximising its net carbon profit (NCP) finding the optimal vegetation given environmental conditions rather than prescribing response to environmental change.

In this chapter, we conduct modelling experiments using VOM to evaluate both short and long-term vegetation responses to historic climate-C<sub>a</sub> combinations at selected sites in Brazil (Chapter 2) in which the model has previously shown good performance (Chapter 4). We use the model simulations to help answer the following chapter contained research questions.

### **5.1.1 Chapter contained research questions**

1. What would be the difference in predicted average annual ET rates in (sub)tropical regions if:
  - a. only daily to sub-annual varying vegetation properties were permitted to respond to eCO<sub>2</sub> (short-term response)?
  - b. all vegetation properties were permitted to optimally adapt to eCO<sub>2</sub> (long-term response)?
2. Does increased C<sub>a</sub> have comparable effects on ET across different Brazilian ecosystems for both the short and long-term responses?

## **5.2 Methodology**

### **5.2.1 Selection of sites**

Sites selected for analysis were based on model performance in Chapter 4 and how successfully simulations followed observed trends in ET seasonality and annual mean. The seasonally flooded dry forest site, BAN, has not been included in this study as the model was not able to capture the correct hydrological processes. The Eucalyptus site, VCP, was also excluded as the model was not able to capture the high ET rates in the wet season due to monoculture and the species unusually high ET rates. Due to their proximity (~15km apart) and the presence of both perennial and seasonal vegetation at both sites, the climate and model parameters at VCP are almost identical to the natural tropical savanna site, PDG, therefore, vegetation responses to eCO<sub>2</sub> in this climate are assessed at PDG. Similarly, due to their proximity and hence similarities in climate forcing, vegetation, and soil properties the northern tropical forest sites K67 is excluded and assumed to be represented by K83 in this chapter (chosen over K67 due to the availability of soil moisture analysis carried out in Chapter 4). In contrast to some studies (e.g., da Rocha et al., 2004; Restrepo-Coupe et al., 2013;



*Chapter 5: How sensitive are hydrological processes in vegetation to changes in atmospheric CO<sub>2</sub> concentration?*

Christoffersen et al., 2014) K34 was not grouped with K67 and K83 because of its significantly higher rainfall and the potential difference this may have on root depth and distribution to sustain perennial vegetation throughout the drier period (Nepstad et al., 1994).

Despite clear differences in observed and modelled ET seasonality, the southern Amazonian pasture site, FNS, has been included due to energy balance closure failures and corrections that imply the model better represents ET than the observations (von Randow et al., 2004). The same reasoning follows for the northern and southern Amazonian forest sites, K34 and RJA respectively. For clarity Table 5.1 lists the sites used in this chapter giving their land use type and Köppen climate classification. Results from sites excluded in this chapter are still available in Appendix C.

*Table 5.1 Sites analysed in this chapter with their respective land cover and Köppen climate classification (Alvares et al., 2013).*

Name	Land Cover	Climate
K34	Tropical Rainforest	Af
K83	Tropical Rainforest	Am
K77	Cropland - Pasture	Am
RJA	Tropical Dry Forest	Aw
FNS	Cropland - Pasture	Aw
PDG	Savanna	Cwa
USR	Cropland - Sugarcane	Cwa
CRA	Cropland -Soybean	Cfa

## **5.2.2 Justification of simulated atmospheric CO<sub>2</sub> concentrations**

The same climatological forcing data that was used to run simulations for the VOM in Chapter 4 (Table 4.1) has been used in this chapter spanning 36 years of data (1980-2016). According to the Mauna-Loa records (Keeling et al., 2001) observed C<sub>a</sub> over this period increased by 19.37% from 339 to 404ppm coinciding with an 1°C rise in average temperature over Brazil (Figure 5.1).

Chapter 5: How sensitive are hydrological processes in vegetation to changes in atmospheric CO<sub>2</sub> concentration?

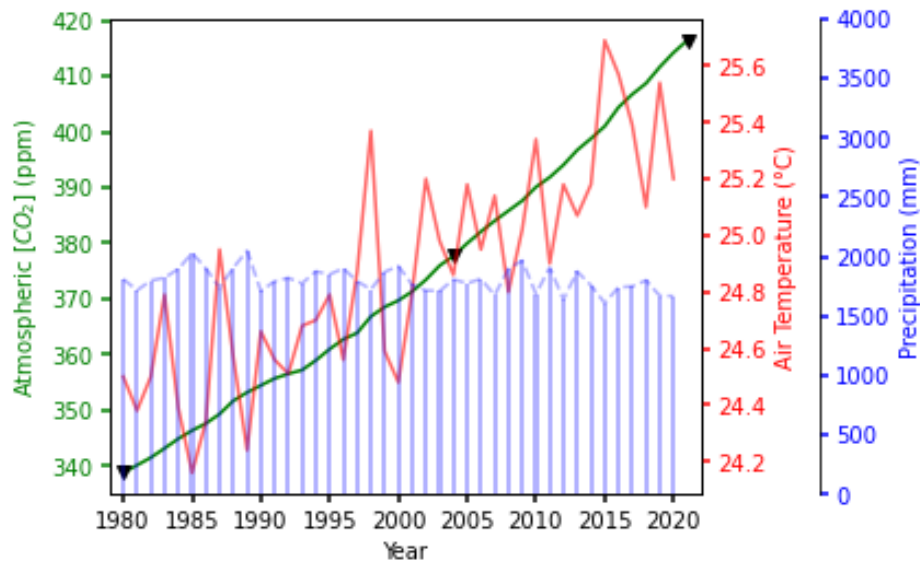


Figure 5.1 Annual average atmospheric CO<sub>2</sub> concentrations from Mauna Loa observatory (blue), and temperature (red) and precipitation (blue) over Brazil from ERA5 1980 – 2021. Black triangles indicate the selected [CO<sub>2</sub>] used in this study at years 1980, 2004 and 2021.

The VOM theory assumes the evolution of natural vegetation evolving with its environment over a long period of time resulting in a composition of plants that have optimally adapted to the given conditions (although this can be manipulated to represent crops through “switching off” perennial representation, Chapter 4). This adaptation is modelled by permitting changes of unique vegetation properties over different time scales (Schymanski et al., 2007c, 2009). Properties such as rooting depth, tree cover and water use parameters vary over decades and are therefore assumed to be static in the VOM. Trends in CO<sub>2</sub> also occur over decades meaning the model would not be able to capture these trends if dynamic CO<sub>2</sub> were used. Therefore, we can assess how far the static properties might change in response to CO<sub>2</sub> using simulations at different static CO<sub>2</sub> concentrations.

Three CO<sub>2</sub> concentrations were selected from historic yearly observations recorded at the Mauna Loa observatory; C<sub>a</sub> = 339, 377, and 416 ppm, representing 1980, the start year of the forcing data, 2004, the mean overlapping year for all flux tower observation periods and modelled concentration in Chapter 4, and 2021, present day levels, respectively. The difference

*Chapter 5: How sensitive are hydrological processes in vegetation to changes in atmospheric CO<sub>2</sub> concentration?*

between the results for 339 and 377 or 416 ppm were then taken as the response to eCO<sub>2</sub>. The same 36 years of meteorological forcing data at each site were used for each CO<sub>2</sub> concentration, simulating a similar model to the similar to the FACE experimental set up (Nowak et al., 2004; Ainsworth & Rogers, 2007; Hickler et al., 2008; Leakey et al., 2009; Norby & Zak, 2011; Norby et al., 2016). By using three static atmospheric CO<sub>2</sub> concentrations we are able to assess the long term vegetation response and link differences in maximum rooting depth, and water use efficiency as vegetation response to eCO<sub>2</sub>.

### **5.2.3 Simulating short and long-term vegetation responses**

Long-term adaptation of vegetation is modelled by optimising seven parameters to maximise NCP. These consist of four factors relating to the water-use function in both seasonal and perennial vegetation, the fractional cover of the perennial vegetation, and the maximum rooting depth of both perennial and seasonal vegetation (Schymanski et al., 2015). These are optimised using the shuffled complex evolution (Duan et al., 1994) which seeks the global optimum by repeatedly running the 36-year simulation with different parameter values. Each simulation, daily dynamically varying parameters (fractional seasonal vegetation cover, electron transport capacity of seasonal and perennial plants, and root surface areas of seasonal and perennial plants) are optimised. More detailed explanations of parameters, algorithms and plant physiological processes can be in Schymanski et al., (2007, 2009, 2015b). This model optimisation of all parameters was completed independently at each site under each C<sub>a</sub> level.

Short term responses were simulated by using the seven long-term optimised parameters for the C<sub>a</sub> = 339 ppm to re-run the model at C<sub>a</sub> = 377 and 416 ppm, only permitting parameters that vary at the daily scale to optimise. This means maximum rooting depths, fractional perennial vegetation cover, and plant water use factors, were prevented from changing at the higher C<sub>a</sub> levels but only stomatal conductance, root surface area and seasonal vegetation cover

*Chapter 5: How sensitive are hydrological processes in vegetation to changes in atmospheric CO<sub>2</sub> concentration?*

were allowed to optimise. This allows us to evaluate the short to long-term responses of hydrological quantities such as ET and runoff/discharge separately.

#### **5.2.4 Variables showing simulated response**

Variables chosen to show simulated vegetation response to eCO<sub>2</sub> were derived directly from model outputs. Maximum root depths were separated into seasonal and perennial which were kept as constant when simulating short-term adaptation. Fractional percentage cover of vegetation (FPC) was combined seasonal and perennial cover, and discharge (Q) was calculated from combined surface runoff and drainage from the model. To numerically assess the physiological effect, water use efficiency (WUE) was calculated by the mole-to-mole ratio of total carbon assimilated (CO<sub>2</sub> uptake rate,  $A_g$ ) to total transpiration ( $E_t$ ) (Equation (5-1)). The water-use efficiency (WUE) value can be a measure of stomatal closure through the ability to fix more CO<sub>2</sub> at the cost of releasing water through transpiration. Equation 1 assumes the molar mass of water as 18.015 g and 365 days in the year,  $A_g$  (mol m<sup>2</sup> year<sup>-1</sup>),  $E_t$  (mm year<sup>-1</sup>) and WUE (mmol mol<sup>-1</sup>).

$$WUE = \frac{A_g}{(E_t \times \frac{1000}{18.052} \times 1000)} \quad (5-1)$$

### **5.3 Results**

#### **5.3.1 Evapotranspiration, Discharge and Roots**

##### *Natural ecosystems*

All simulations of natural ecosystems resulted in a decrease of ET in response to an overall increase of 77 ppm in  $C_a$  (339 to 416 ppm) (Figure 5.2). ET simulated under short-term adaptation had a much greater decrease (decreasing 32-65 mm year<sup>-1</sup>), than simulated ET under

*Chapter 5: How sensitive are hydrological processes in vegetation to changes in atmospheric CO<sub>2</sub> concentration?*

long-term response (decreasing 12-46 mm year<sup>-1</sup>) (Table 5.2). The short-term response always resulted in a greater decrease than the long-term response at every site. The largest difference in ET between the two adaptations was found at the southern Amazonian forest site, RJA (54 mm year<sup>-1</sup>). Long-term adaptation at this site involved an increase in maximum perennial rooting depth (from 6.6 – 6.8 m). Maximum perennial rooting depth also increased at K83 (from 3.8 – 4 m) and PDG (from 2 – 2.2 m) under long-term adaptation.

In contrast, the wettest site, K34, long-term adaptation saw a decrease in maximum perennial rooting depth (from 4.4 – 4.2 m) accompanied by the greatest percentage decrease in ET (-2.3%, amounting to 46 mm year<sup>-1</sup>). All decreases in ET are paired with increases in discharge with long-term adaptations ranging from a 4.8% increase at K83, to a 15% increase at K34, and short-term adaptations ranging from a 13.8% increase at PDG to a 30.1% increase at RJA. The results show a magnitude in differences between percentage decreases in ET and increases in discharge, the greatest of which occur at the wettest Amazonian sites and under short-term adaptation to eCO<sub>2</sub>. Furthermore, without allowing perennials to optimally adapt or allow vegetation to maximise rooting depth decline in ET can be seen as a linear relationship with increasing C<sub>a</sub>. Long term adaptation changes this relationship across the four ecosystems.

There are no significant differences to changes in long-term responses of ET from 339 ppm to 377 ppm for any site, and there is no significant change in mean simulated ET over the entire in C<sub>a</sub> at RJA. Significant differences in the mean only occur at sites K34, K83, and PDG between 339 ppm and 416 ppm. However, there is a significant difference in simulated ET to short-term response at K34, K83 and RJA at each C<sub>a</sub> interval.

*Cultivated ecosystems*

As with the natural ecosystems, eCO<sub>2</sub> resulted in a decline in ET across all sites. With the exception of K77, this decline was less exaggerated when simulating long-term adaptation

*Chapter 5: How sensitive are hydrological processes in vegetation to changes in atmospheric CO<sub>2</sub> concentration?*

rather than short-term adaptation to eCO<sub>2</sub> (Figure 5.2). At the sugarcane site, USR, there was no significant change in annual ET when simulating long-term adaptation over an increase of 77 ppm C<sub>a</sub>. Furthermore, both USR and the soybean site, CRA, showed no significant change in ET when simulating short-term responses between an increase of C<sub>a</sub> from 339 to 377 ppm. However, both sites predicted a significant decline in ET of ~2.5% when C<sub>a</sub> increased from 339 to 416 ppm. There was invariant difference between long and short-term response of vegetation to eCO<sub>2</sub> at CRA. Maximum root depth at USR increased by 50% when C<sub>a</sub> = 416 ppm (from 0.4 – 0.6 m) but remains unaltered for CRA.

The southern Amazonian pasture site, FNS, showed a more gradual decline in ET when vegetation was allowed to respond to long-term adaptation whilst rooting depth increased by 25% overall. A faster decline was simulated when only short-term responses were permitted to adapt. However, the opposite occurred at the eastern Amazonian pasture site, K77. Significant differences in annual ET are simulated at each change in C<sub>a</sub> for both long and short-term adaptations. This is the only site where simulated long-term responses of vegetation to increased C<sub>a</sub> resulted in a greater decline in ET than when simulating short-term responses (long-term = -6%, short-term = -4%). Long-term responses at K77 included a 100% increase in maximum root depth with the first increase in C<sub>a</sub> (339 – 377 ppm) which it maintained when simulating responses at C<sub>a</sub> = 416 ppm.

Differences in discharge between both adaptation responses were much less exacerbated for the cultivated sites than at the natural sites, however, increased rooting depth and decreased ET cause a decrease in total discharge when long-term responses are taken into consideration. A similar range of increases in discharge can be seen when simulating long-term adaptation (1.9 – 8.2%) as there can be for short-term adaptation (5.1 - 7.7%).

### **5.3.2 Water Use Efficiency**

#### *Natural ecosystems*

WUE increased at every site with increasing  $C_a$  when simulating both long and short-term adaptation (Table 5.2). The lowest increases in WUE were found at the two Amazonian forest sites with the heaviest annual rainfall (K34, and RJA), which were also the least water use efficient (2.60 and 2.73 mmol mol<sup>-1</sup> respectively). The greatest increase in WUE occurred at the driest natural site in the Cerrado, PDG, which had the highest WUE at  $C_a = 339$  ppm (4.18 mmol mol<sup>-1</sup>) suggesting that increases in WUE follow the precipitation gradient as found by Schymanski et al. (2015).

Although marginal, the three Amazonian forest sites (K34, K83, and RJA), saw greater increases in WUE under short-term adaptation to eCO<sub>2</sub> (15.8% – 18.1%) than under long-term adaptation (13.7% – 15.6%). However, at PDG, there was very little difference in WUE increases between long and short-term adaptation (LT 20.4%, ST 19.4%). WUE increased linearly with eCO<sub>2</sub> at all natural ecosystem sites.

#### *Cultivated ecosystems*

WUE also increased with increasing  $C_a$  at every site under both long and short-term adaptation (Table 5.2). These increases were generally much higher than their neighbouring natural ecosystem sites (see Chapter 2, Figure 2.2 for location reference). The lowest increase occurred at the soybean site in Cruz Alta (CRA), the most southerly site, and there was little difference under long and short-term adaptations, which is reflected in the differences in ET (Figure 5.2). Similarly to the nearby Cerrado site, PDG, WUE at the sugarcane site, USR, increased more under long-term adaptation than short (LT 22.2%, ST 20.3%). The eastern Amazonian pasture site, K77, saw the largest increase in WUE under long-term adaptation (28.6%), much greater than under short-term (20.9%). FNS saw similar increases in WUE

*Chapter 5: How sensitive are hydrological processes in vegetation to changes in atmospheric CO<sub>2</sub> concentration?*

when simulating long-term adaptation as with simulating short-term (LT 20.1%, ST 20.6%). As expected, the wetter sites, FNS and K77 have a lower simulated WUE than the more seasonal sites with longer dry seasons. However, differences in WUE between long and short-term adaptations are small at FNS, USR and CRA, suggesting this is not the sole contributor to differences in ET between the two responses.

### **5.3.3 Fractional Vegetation Cover**

The mean fractional vegetation cover (FVC) responded positively to eCO<sub>2</sub> in all simulations (Table 5.2), unless the maximum cover had already been achieved at low C<sub>a</sub> (339 ppm) as with the rainforest sites K34, K83 and RJA. In general, FVC increased to a greater extent under long-term adaptation responses than it did under short-term adaptation responses. The largest increase in FVC occurred at the Cerrado sugarcane site, USR (LT +5.1%, ST +2.9%), followed closely by the eastern Amazonian pasture site, K77 (LT 4.7%, ST 2.4%). There were no differences in cover between long and short-term adaptations at CRA. Despite FVC observations lacking analysis in this study, it is important to consider that this may impact the predicted ET output of the model.



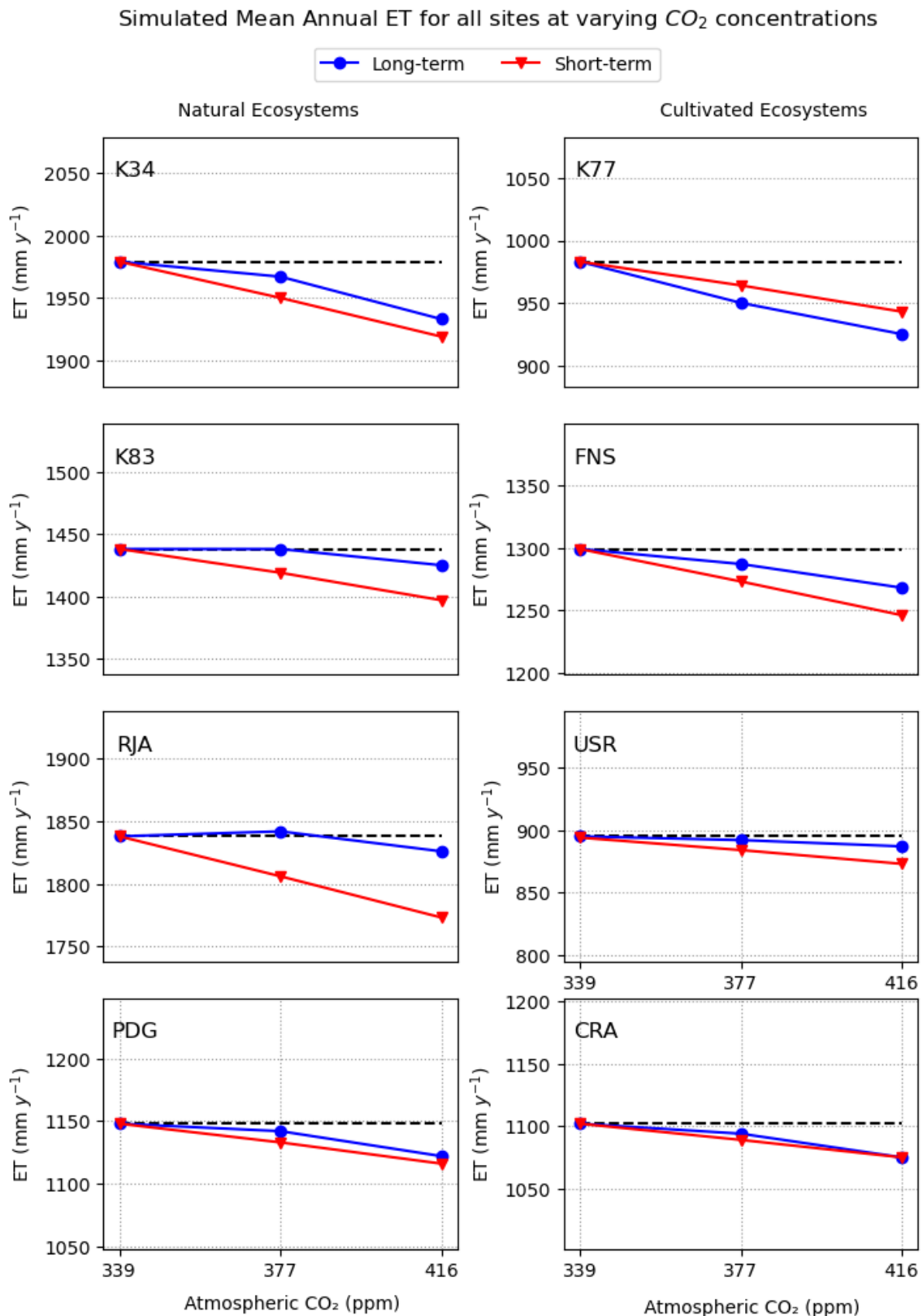


Figure 5.2 Simulated mean annual ET rates for varying  $C_a$ . 'Long-term' (blue) refers to simulations where all vegetation properties were optimised for each  $C_a$ . 'Short-term' (red) refers to simulations where 'long-term' optimised parameters for  $C_a = 339$  ppm were kept for  $C_a = 377$  and  $416$  ppm simulations. The black dashed line is ET at  $C_a = 339$  ppm simulations for reference.

Chapter 5: How sensitive are hydrological processes in vegetation to changes in atmospheric CO<sub>2</sub> concentration?

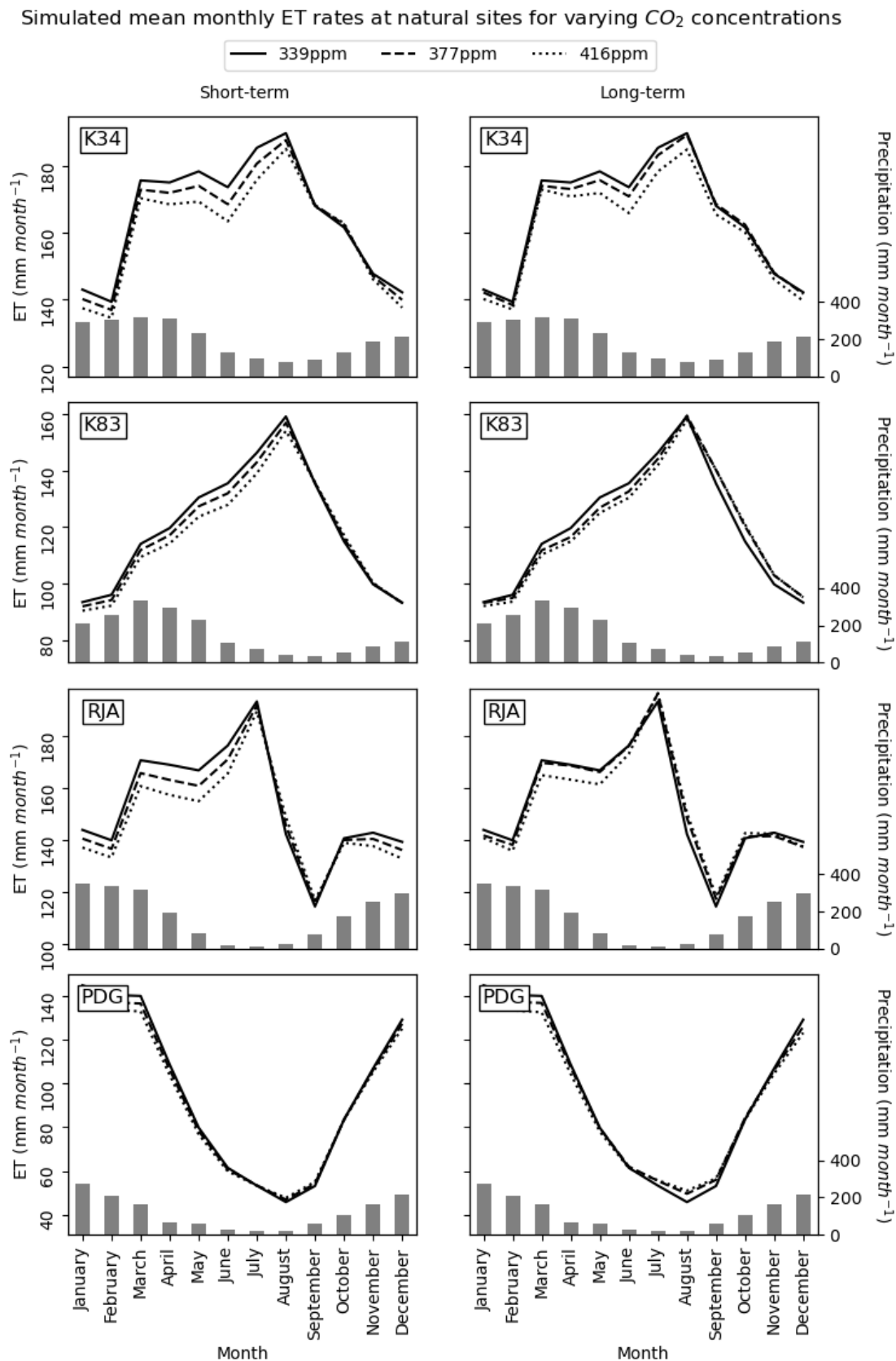


Figure 5.3 Simulated mean monthly ET rates for varying  $C_a$  at natural Brazilian ecosystems. 'Long-term' (right) refers to simulations where all vegetation properties were optimised for each  $C_a$ . 'Short-term' (left) refers to simulations where 'long-term' optimised parameters for  $C_a = 339$  ppm were kept for  $C_a = 377$  and 416 ppm simulations. Grey bars represent precipitation for reference between water limiting and energy limiting periods.

Chapter 5: How sensitive are hydrological processes in vegetation to changes in atmospheric CO<sub>2</sub> concentration?

Simulated mean monthly ET rates at cultivated sites for varying CO<sub>2</sub> concentrations

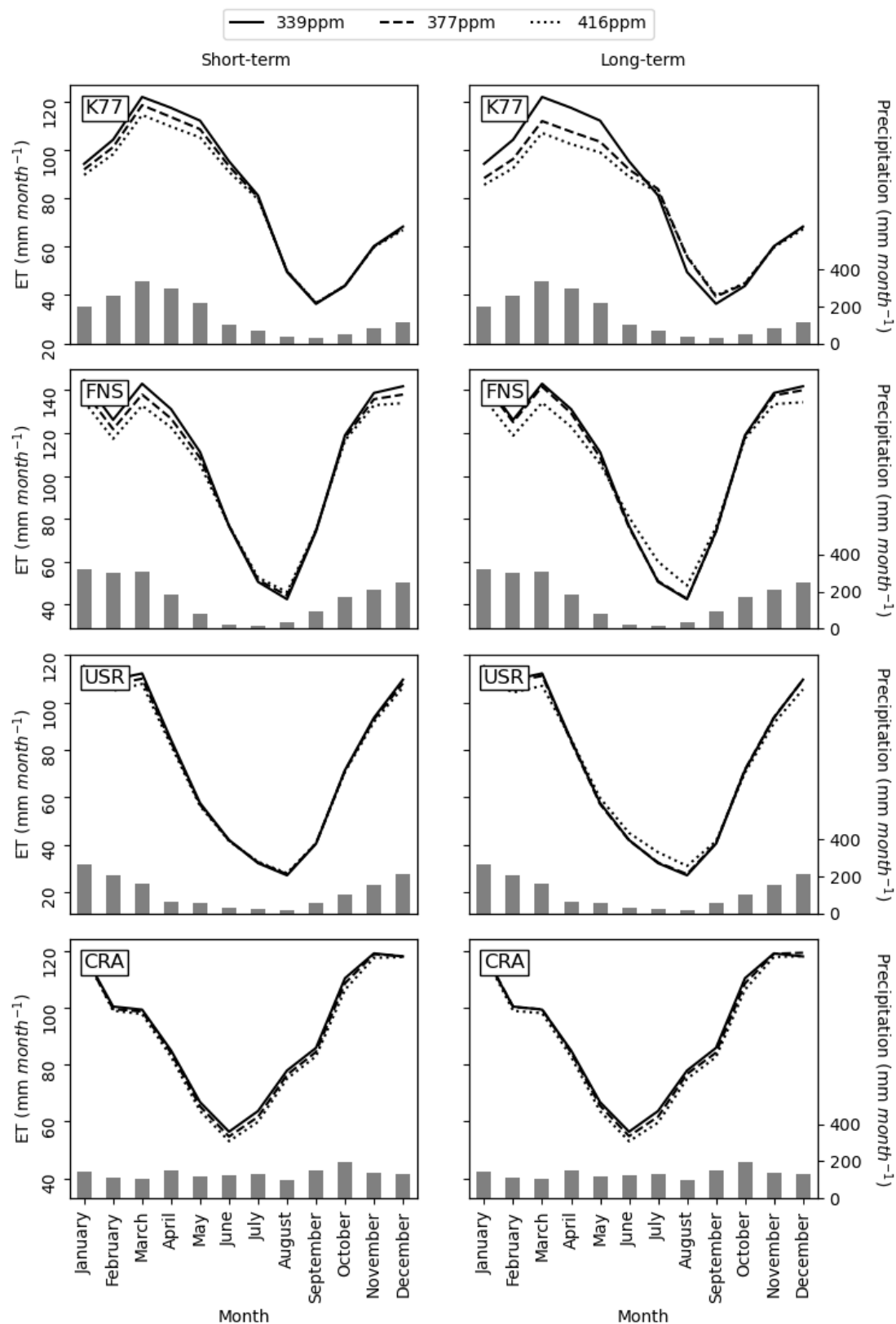


Figure 5.4 Simulated mean monthly ET rates for varying  $C_a$  at cultivated Brazilian ecosystems. 'Long-term' (right) refers to simulations where all vegetation properties were optimised for each  $C_a$ . 'Short-term' (left) refers to simulations where 'long-term' optimised parameters for  $C_a = 339$  ppm were kept for  $C_a = 377$  and  $416$  ppm simulations. Grey bars represent precipitation for reference between water limiting and energy limiting periods.

Chapter 5: How sensitive are hydrological processes in vegetation to changes in atmospheric CO<sub>2</sub> concentration?

Table 5.2 Simulated responses to increasing C<sub>a</sub>. The first column in each variable block gives actual values for C<sub>a</sub> = 339 ppm, while the subsequent columns in italics give the percentage difference from this value. Decreases, or negative differences, are shown in red. P, precipitation, ET, evapotranspiration, Q, discharge, WUE, water use efficiency (Equation(5-1), FVC, fractional vegetation cover of all vegetation (perennial and seasonal), RAI, root area index (fine root surface area per ground area), R<sub>t</sub> depth, maximum rooting depth of perennials, R<sub>g</sub> depth, maximum rooting depth of seasonal vegetation. a) shows vegetation short-term adaptation, b) shows long-term adaptation. Shaded cells indicate that the means of ET were significantly different (p<0.05) when compared to the mean of the lowest C<sub>a</sub> run (339ppm).

a)

Variable C <sub>a</sub>	P (mm year <sup>-1</sup> )	ET (mm year <sup>-1</sup> )			Q (mm year <sup>-1</sup> )			WUE (mmol mol <sup>-1</sup> )			FVC			RAI (m <sup>2</sup> m <sup>-2</sup> )		
		339	377	416	339	377	416	339	377	416	339	377	416	339	377	416
<b>Site</b>																
<b>K34</b>	2396	1979	<i>-1.5</i>	<i>-3.1</i>	316	9.8	20.5	2.60	8.0	15.8	1.00	0.0	0.0	0.04	<i>-2.0</i>	<i>-4.0</i>
<b>K83</b>	1833	1438	<i>-1.3</i>	<i>-2.8</i>	283	6.4	14.1	3.90	9.0	18.1	1.00	0.0	0.0	0.04	<i>-2.0</i>	<i>-4.2</i>
<b>RJA</b>	2124	2124	<i>-1.7</i>	<i>-3.6</i>	238	14.5	30.1	2.73	8.9	17.6	1.00	0.0	0.0	0.06	<i>-2.5</i>	<i>-4.9</i>
<b>PDG</b>	1363	1148	<i>-1.3</i>	<i>-2.8</i>	223	6.5	13.8	4.18	9.7	19.4	0.94	1.1	1.9	0.02	<i>-3.6</i>	<i>-7.9</i>
<b>K77</b>	1806	983	<i>-2.0</i>	<i>-4.0</i>	803	2.8	5.6	3.99	10.3	20.9	0.88	1.1	2.4	-	-	-
<b>FNS</b>	1993	1299	<i>-2.0</i>	<i>-4.1</i>	696	3.8	7.7	3.62	10.2	20.6	0.95	0.9	2.1	-	-	-
<b>USR</b>	1335	895	<i>-1.2</i>	<i>-2.5</i>	442	2.4	5.1	4.63	10.3	20.6	0.88	1.3	3.0	-	-	-
<b>CRA</b>	1587	1102	<i>-1.2</i>	<i>-2.5</i>	423	2.7	5.3	4.63	8.6	17.2	0.99	0.1	0.2	-	-	-

b)

Variable C <sub>a</sub>	P (mm year <sup>-1</sup> )	ET (mm year <sup>-1</sup> )			Q (mm year <sup>-1</sup> )			WUE (mmol mol <sup>-1</sup> )			FVC			RAI (m <sup>2</sup> m <sup>-2</sup> )			R <sub>t</sub> depth (m)			R <sub>g</sub> depth (m)		
		339	377	416	339	377	416	339	377	416	339	377	416	339	377	416	339	377	416	339	377	416
<b>Site</b>																						
<b>K34</b>	2396	1979	<i>-0.6</i>	<i>-2.3</i>	316	4.3	15.0	2.60	6.7	14.2	1.00	0.0	0.0	0.04	<i>-0.7</i>	<i>-4.8</i>	4.4	0.0	<i>-4.5</i>	-	-	-
<b>K83</b>	1833	1438	0.0	<i>-0.9</i>	283	0.4	4.8	3.90	7.9	15.6	1.00	0.0	0.0	0.04	1.7	0.4	3.8	5.3	5.3	-	-	-
<b>RJA</b>	2124	2124	0.2	<i>-0.7</i>	238	<i>-1.0</i>	6.0	2.73	6.7	13.7	1.00	0.0	0.0	0.06	0.7	<i>-0.2</i>	6.6	3.0	3.0	-	-	-
<b>PDG</b>	1363	1148	<i>-0.5</i>	<i>-2.2</i>	223	2.4	11.1	4.18	9.9	20.4	0.94	1.7	2.9	0.02	<i>-1.0</i>	<i>-3.5</i>	2.0	10.0	10.1	0.6	0.0	0.1
<b>K77</b>	1806	983	<i>-3.4</i>	<i>-6.0</i>	803	4.7	8.2	3.99	16.4	28.6	0.88	3.5	4.7	-	-	-	-	-	-	0.2	100.0	100.0
<b>FNS</b>	1993	1299	<i>-0.9</i>	<i>-2.4</i>	696	1.7	4.5	3.62	8.5	20.1	0.95	1.3	3.2	-	-	-	-	-	-	0.8	0.0	25.0
<b>USR</b>	1335	895	<i>-0.3</i>	<i>-1.0</i>	442	0.5	1.9	4.63	8.9	22.5	0.88	1.3	5.1	-	-	-	-	-	-	0.4	0.0	50.0
<b>CRA</b>	1587	1102	<i>-0.8</i>	<i>-2.4</i>	423	1.7	5.2	4.63	7.7	17.1	0.99	0.1	0.2	-	-	-	-	-	-	1.8	0.0	0.0

## 5.4 Discussion

The simulations presented are not climate scenarios but intended to give insight to hydrological changes through vegetation response to eCO<sub>2</sub> over different spatial and temporal scales using an optimality hypothesis. In other words, here we are focusing on evaluating the specific influence CO<sub>2</sub> has on vegetation water use enabling us to isolate potential climate change effects rather than dealing with the uncertainty future climate scenarios offer. Consequently, no changes to the model were made to improve any results through further parameter tuning. One advantage of using an optimality model is simulating plant adaptations to their environment through a principle based on natural selection which alters as the environment changes increasing the performance of future predictions.

### 5.4.1 Hydrological responses to eCO<sub>2</sub> across natural ecosystems

Modelled responses to eCO<sub>2</sub> varied depending on whether the ecosystem was either water or energy limited. RJA and K34 experience high annual rainfalls and are energy limited for most of the year. This can be seen by the low WUE values and high ET rates (Table 5.2). At these two rainforest sites, only perennial vegetation was allowed to grow to represent ecosystem composition more closely. Modelling the short-term response of vegetation to increasing C<sub>a</sub> led to less demand for water to maintain growth rate. As the adaptation of plant water use factors, and maximisation of rooting depths are prohibited in short-term responses the increase in WUE is caused by a modelled increase in stomatal closure. As perennial vegetation cover was already at 100%, water was not used for plant growth and the reduction in ET resulted in greatly increased runoff and drainage (20-30% increases).

However, at RJA, when perennial vegetation was permitted to adapt over time, increases in WUE were reduced and maximum rooting depth increased maintaining ET across the C<sub>a</sub> gradient and reducing the increase in discharge by 24%. Modelling long-term adaptations

*Chapter 5: How sensitive are hydrological processes in vegetation to changes in atmospheric CO<sub>2</sub> concentration?*

allowed perennial vegetation to access water deeper in the soil and maintain growth and ET when water started becoming the limiting factor (Figure 5.3). Similar long and short-term adaptations and differences in ET were found by Schymanski *et al.*, (2015) when modelling the effect of eCO<sub>2</sub> on a tropical rainforest site in Australia, Cape Tribulation. Long-term adaptation at RJA was predicted to lead an increase in ET from short-term modelled response by a significant amount of almost 60 mm year<sup>-1</sup>, posing important questions about the consideration of modelling long-term adaptation to future climate scenarios in similar ecosystems.

K34 is subject to a less well-defined seasonal cycle (non-water limited) and long-term adaptation to eCO<sub>2</sub> resulted in a decrease in maximum rooting depth, as growth and maintenance were possible with less water, rendering deeper roots an unnecessary cost. WUE increased at a slightly dampened rate compared with short-term adaptation resulting in a 5% decrease in discharge. Changes in root system structure and long-term adaptation to improve WUE can help vegetation maintain longer growing periods and higher rates of ET, as can be seen by the difference in soil evaporation between long and short-term adaptation simulations (Table 5.2). Another factor influencing the difference in ET between long and short-term adaptation simulations could be increased biomass such as leaf area index, however, this analysis is beyond the scope of this chapter and more information regarding why differences occur between these temporal scales at wet tropical rainforest sites can be found in Schymanski *et al.* (2015).

The eastern Amazonian forest site, K83, has a more pronounced dry season than K34. This water stress is captured by the higher initial WUE at C<sub>a</sub> = 339 ppm (Table 5.2). There is little change in WUE between long and short-term adaptations, however, increases in maximum rooting depth modelled by long-term response alleviate the change in hydrological responses modelled through short-term adaptation. Short-term adaptation simulations result in higher

*Chapter 5: How sensitive are hydrological processes in vegetation to changes in atmospheric CO<sub>2</sub> concentration?*

WUE and an overall decrease in below ground biomass over the  $C_a$  gradient implying water limitations prevent plant growth and decrease transpiration. However, when perennial vegetation properties were allowed to adapt, increases in both root area index (RAI) and maximum root depth were simulated prolonging the water availability and increasing the growing season. Despite a lack of eCO<sub>2</sub> experiments in tropical rainforests, these simulated adaptations align with results seen at other FACE experiments at water limited ecosystems which recorded increases in soil moisture, tree rooting depths and below ground biomass (Norby & Zak, 2011; De Kauwe et al., 2013).

The Cerrado site, PDG, is the most water limited of the natural sites and has the highest initial WUE and increase over the change in  $C_a$ . Short-term adaptations also show an 8% decline in RAI as less energy is needed to be spent on drawing water for photosynthesis. This was accompanied by an increase in seasonal vegetation cover of 2% supporting the greening theory of the CO<sub>2</sub> fertilisation effect (Donohue et al., 2013b). There is little change in modelled ET and WUE between long and short-term adaptations, however, perennial rooting depth and fractional vegetation cover both increase in long-term simulations. This increase in perennial plant cover causes a shift in ecosystem structure implicating eCO<sub>2</sub> as a contributor to ‘woody thickening’. Melo *et al.* (2018) reported observations on the selective advantage of a typical endemic ‘woody’ cerrado species (*Hymenaea stigonocarpa*) over a herbaceous grass (*Melinis minutiflora*) under eCO<sub>2</sub>, observing increases in biomass allocation to shoots and leaf area ratio in *H. stigonocarpa*. In the VOM, perennial vegetation can access water in deeper soils and can expand its FVC freely whilst seasonal vegetation cannot exceed a fraction of 1 minus the perennial FVC. Through its impact on WUE, eCO<sub>2</sub> alters ecosystem composition shifting water-limited environments towards energy-limited environments, where perennials have a selective advantage as observed by Melo *et al.* (2018).

#### **5.4.2 Hydrological responses to eCO<sub>2</sub> across cultivated ecosystems**

Only seasonal vegetation was prescribed at the cultivated sites, meaning the only difference between long and short-term adaptations are seasonal maximum rooting depth and water use efficiency factors. Some level of greening occurred at every cultivated site, and this was exacerbated through long-term adaptation. A shallower rooting system intensifies water stress driving the large increases in WUE with the CO<sub>2</sub> gradient across all sites (Table 5.2). Declines in ET across all sites can therefore be attributed to the physiological effect.

Despite a greater increase in vegetation cover, long-term adaptations to eCO<sub>2</sub> surprisingly caused a greater decline in ET at the eastern Amazonian pasture site, K77, than short-term adaptations did. This seemingly paradoxical result can be explained through a combination of seasonality and increased WUE. Increased WUE reduces ET during the wet season offsetting increased ET from increased FVC (Figure 5.4). However, increased ET from increased FVC and maximum rooting depth is apparent when water becomes limiting in the dry season, which is hidden in annual totals as it is offset by the reduction in ET during the wet season. At this site the VOM predicts the long-term adaptations will increase drying through the physiological effect which outweighs the contribution of greening through the CO<sub>2</sub> fertilisation effect, which is the opposite of what we see and the neighbouring natural rainforest site, K83.

Different results were predicted at the southern Amazonian pasture site, FNS, where there was almost no change in WUE between the two temporal adaptation scales. In this case short-term adaptations linked to increased stomatal closure occur in non-water limiting circumstances during the wet season. Declines in ET were more prominent under short-term adaptation than long-term as an increase in vegetation cover led to increased transpiration. A slight shift in seasonal ET occurred under long-term adaptation  $C_a = 416$  ppm which can be explained by the increase in maximum rooting depth. Despite declines in ET during the wetter months, increased access to soil moisture resulted in increased ET over the drier months,



*Chapter 5: How sensitive are hydrological processes in vegetation to changes in atmospheric CO<sub>2</sub> concentration?*

similar to K77. The increased dry season ET offsets the decrease in ET over the wet season driven by increased WUE leaving the observed difference in results between long and short-term adaptation simulations at  $C_a = 416$ .

Despite having a much lower annual rainfall increased seasonality, similar adaptation patterns to FNS occurred at the Cerrado sugarcane site, USR. Long-term adaptation responses saw that decreases in ET over the wet season through increased WUE were offset by increases in maximum rooting depth and vegetation cover increasing ET in the dry season (Figure 5.4). The long-term adaptation of maximum rooting depth in seasonal vegetation caused significantly more vegetation growth or ‘greening’ to occur at cultivated sites which can be seen by comparing results to the southern Brazilian soybean site, CRA.

Interestingly there was no increase in maximum rooting depth when modelling long-term adaptations to  $eCO_2$  at CRA. Annual precipitation is relatively stable throughout the year and seasonality in ET is driven by environmental changes in energy. As soil moisture levels are maintained over the summer months through precipitation increasing root depth becomes a waste of resources. This resulted in no substantial difference between the two temporal adaptation scales suggesting that maximum rooting depth plays an important role in regulating hydrological processes at water limited environments (Donohue et al., 2007; Fan et al., 2017).

### **5.4.3 The importance of perennial responses to $eCO_2$ on hydrological processes**

It has been shown that long-term adaptation in perennials alters the water balance under changing  $C_a$ , but it is important to look at differences in hydrological processes between these perennial dominated sites and their associated nearby cultivated sites (dominated by seasonal vegetation) (K83:K77, RJA:FNS, and PDG:USR). These sites share similar climatic pressures and thus can give us an indication on the impact of perennial cover. The most considerable difference in simulated ET under long-term adaptation of vegetation to  $eCO_2$  occurred between

*Chapter 5: How sensitive are hydrological processes in vegetation to changes in atmospheric CO<sub>2</sub> concentration?*

the eastern Amazonian rainforest site K83 and nearby pasture site K77 (an increased difference in ET of 45 mm year<sup>-1</sup> due to long-term adaptation; 455 mm year<sup>-1</sup> at C<sub>a</sub> = 339 ppm to 500 mm year<sup>-1</sup> at C<sub>a</sub> = 416 ppm). At both K83 and RJA, long-term adaptation of perennials maintained ET rates across the C<sub>a</sub> gradient, whilst decreases in ET were predicted at the associated nearby pasture sites K77 and FNS. Differences in vegetation composition between the sites suggest more exaggerated differences in ET through long-term adaptation to eCO<sub>2</sub>.

In contrast the Cerrado sites PDG and USR showed little difference in hydrological responses between long and short-term adaptations despite an increase in perennial cover at PDG. However, it is important to note that both sites showed an increase in vegetation cover which, although not enough to offset increases in WUE, prevented steeper declines in ET. A difference of 235 mm year<sup>-1</sup> was predicted at C<sub>a</sub> = 416 ppm between the two sites indicating the importance of perennials in these water-stressed environments.

#### **5.4.4 Synthesis and limitations**

In summary, the results suggest that the primary effects of eCO<sub>2</sub> are an increase in WUE irrelevant of ecosystem causing a decrease in ET. When possible, this resulted in assimilated carbon to be redistributed to growth increasing vegetation coverage at all sites. When modelling long-term adaptation, the enhanced WUE allows the production of a deeper rooting system in water-limited environments acting to allow the vegetation to maintain photosynthesis during the drier months for longer. The net effect is to maintain or enhance plant growth per unit ground area for the least amount of energy spent. It is also worth noting that, although over different gradients, WUE increases almost linearly with C<sub>a</sub>.

Although conclusions can be drawn as to the general ecosystem response to eCO<sub>2</sub>, as discussed in Chapter 4, results may not truly represent ecosystem response due to the limitations of the model. A lack of model understanding regarding groundwater hydrology and

## *Chapter 5: How sensitive are hydrological processes in vegetation to changes in atmospheric CO<sub>2</sub> concentration?*

water transport cost factors from deep roots to the canopy may cause some uncertainty. For example, if deeper roots penetrated a confined aquifer which could occur at sites similar to RJA, conditions would change to energy limiting and the distribution of carbon would ultimately be different. Furthermore, the model neglects the C<sub>4</sub> photosynthetic pathway which favours vegetation during drought conditions (i.e. in heavily water-limited environments). It is unclear and beyond the scope of this study whether increasing C<sub>a</sub> would have a comparable effect with C<sub>3</sub>-dominated vegetation, but similar responses in C<sub>4</sub> plants to elevated C<sub>a</sub> have been found. Da Faria et al. (2018) and da Silva et al. (2020) report decreased transpiration rates and stomatal conductance presenting advantages and increased plant growth in high CO<sub>2</sub> environments, whilst Bordingnon et al. (2019) present an argument that C<sub>4</sub> plants became structurally more resilient with growth under eCO<sub>2</sub> suggesting that C<sub>4</sub> plant species in different ecosystems could be expected to act similarly globally.

## 5.5 Conclusions

In this chapter we analysed the potential long and short-term vegetation responses as they optimally adapted to changes in atmospheric CO<sub>2</sub> concentrations (C<sub>a</sub>) through maximising net carbon profit (Schymanski *et al.*, 2008, 2009, 2015). We looked at how hydrological processes varied over eight key Brazilian ecosystems by focusing on changes in evapotranspiration.

Analysis shows that the economics of carbon gain and vegetation water use lead to results comparable to observed patterns leading to overall reductions in evapotranspiration (ET) at all sites. The increase in WUE was the most consistent response to eCO<sub>2</sub> across all simulations, with responses varying between 6.7% and 28.6% (Table 5.2), and generally doubling at most sites for a doubling in C<sub>a</sub>, agreeing with results found at temperate sites in Free Air CO<sub>2</sub> Enrichment (FACE) studies (De Kauwe et al., 2013). All sites supported the theory of the physiological effect (Cowan, 1978; Betts et al., 2007) as both long and short-term responses

*Chapter 5: How sensitive are hydrological processes in vegetation to changes in atmospheric CO<sub>2</sub> concentration?*

resulted in reductions in stomatal conductance and transpiration and increased discharge at all ecosystems. These predictions fall in line with multiple studies analysing the effect of eCO<sub>2</sub> on vegetation through both observations and modelling (Norby & Zak, 2011; Souza et al., 2016; Dos Santos et al., 2018; Richardson et al., 2018; da Costa Santos et al., 2020; Rezende et al., 2022; Ruv Lemes et al., 2023). It was also found that adaptations in vegetation differed with limitations. Sites that were more water-limited saw greater increases in WUE than sites that were more energy limited. These adaptations pointed towards potential shifts in seasonality of ET and ecosystem dynamics.

From the results we may also conclude that modelling the responses of perennials to eCO<sub>2</sub> at all natural ecosystem sites could ultimately change our understanding of hydrological processes in vegetation, depending on temporal scale and perennial adaptation factors. Amazonian forest sites significantly alter the hydrological processes through changes in plant water use factors and maximum rooting depth, whilst the Cerrado site caused a shift in vegetation composition towards increased perennial cover which may have implications on water availability and resources (Souza et al., 2016). The findings provide theoretical support for an elevated CO<sub>2</sub> (eCO<sub>2</sub>) – vegetation feedback which may dampen reductions in ET when maximum rooting depth is allowed to adapt optimally to its environment, concurrent with results presented by Schymanski *et al.* (2015).

Modelling long-term adaptations of ecosystems could provide insight into shifts in seasonality as increased rooting depths prolong vegetation growth during the dry season and increased WUE decreases transpiration during the wet season. Furthermore, results suggest more exaggerated differences in ET and discharge between rainforest and pasture sites under increased C<sub>a</sub> when considering long-term adaptation in vegetation.

*Chapter 5: How sensitive are hydrological processes in vegetation to changes in atmospheric CO<sub>2</sub> concentration?*

In summary, vegetation optimality modelling can be a powerful tool for predicting hydrological responses under changing environments as results suggest that model adaptations closely follow observed patterns over multiple contrasting ecosystems across Brazil. At the very least long-term adaptation of vegetation should be considered in future hydrological modelling under climate change across all ecosystems.

*Chapter 5: How sensitive are hydrological processes in vegetation to changes in atmospheric CO<sub>2</sub> concentration?*

## Chapter 6: Conclusions and Outlook

### 6.1 Summary

Understanding carbon-water dynamics is essential to accurately model and predict water availability in hydrological systems, ecosystem dynamics and the impacts of climate change, however, interrelationships over different environmental conditions make these difficult to incorporate into hydrological modelling. These interactions are especially important when trying to understand hydrological processes in vegetation dominated (sub)tropical regions. Vegetation optimality is the theory that plants adapt to given environmental conditions by maximizing their net carbon profit through CO<sub>2</sub>-water dynamics. This thesis provides evidence using vegetation optimality modelling to attempt to answer the following questions:

1. How can we use Carbon-Water mechanisms to understand hydrological fluxes particularly for (sub)tropical regions?
2. How sensitive are hydrological processes in vegetation to changes in atmospheric CO<sub>2</sub> concentration in these regions?

As a preliminary step in answering these questions we also analysed widely used, high-resolution global gridded data products for model forcing across various ecosystems over Brazil. One of the largest countries in the world, Brazil has a diverse range of hydroclimates and biomes, with a history of research at multiple sites providing potential to valuable insight into hydrological modelling. This thesis advances our knowledge in relation to the questions above improving our understanding of modelling hydrological processes in vegetation

dominated environments across Brazil. The key findings of each chapter are summarised below, succeeded by an overarching discussion and direction for future research.

**How can we choose accurate meteorological forcing data in the region? (Chapter 3)**

In the past decade, the scientific community has seen an increase in the number of global hydrometeorological products. This has been possible with efforts to push global hydrological and land surface modelling to hyper-resolution applications. As the resolution of these datasets increase, so does the need to compare their estimates against local in-situ measurements. This is particularly important for Brazil, whose large continental scale domain results in a wide range of climate and biomes. Eleven flux towers (for periods between 1999-2010) covering Brazil's main land cover types (tropical rainforest, woodland savanna, various croplands, and tropical dry forests) were used to examine the reliability and suitability of five high-resolution (0.1 - 0.25 deg) meteorological gridded products (ERA5-Land, GLDAS2.0, GLDAS2.1, Brazilian National Meteorological Database (referred here as BNMD, and MSWEPv2.2 (precipitation only)) for seven variables (precipitation, air temperature, wind speed, pressure, specific humidity and downward shortwave and longwave radiation). Data products were evaluated for their ability to reproduce the daily and monthly meteorological observations at flux towers. A ranking system for data products was developed based on the mean squared error. To identify the possible causes for these errors, contributions of correlation, bias, and variation to the MSE were analysed. Results show that, for precipitation, MSWEPv2.2 outperforms the other datasets at daily scales but at a monthly scale BNMD performs best. For all other variables, ERA5-Land achieved the best ranking (smallest) errors at the daily scale and averaged the best rank for all variables at the monthly scale. GLDAS2.0 performed least well at both temporal scales, however the newer version (GLDAS2.1) was an improvement of its older version for almost every variable. BNMD wind speed and GLDAS2.0 solar radiation outperformed the other datasets at a monthly scale. Discrepancies at the daily scale were mostly



contributed to by correlation errors, whilst at the monthly scale it was the bias contribution. ERA5-Land is recommended when using multiple hydro-meteorological variables to force land-surface models within Brazil.

**How can we use Carbon-Water mechanisms to understand hydrological fluxes?  
(Chapter 4)**

Plant growth can be understood as a carbon capture cost-benefit system. The carbon-water dynamics of this system can help us to quantify these physiological processes allowing transpiration to be calculated from a biological perspective. The Vegetation Optimality Model (VOM) attempts to describe these processes and we analyse the output of evapotranspiration (ET) at the 11 Brazilian flux tower sites using the two best performing daily gridded data products from chapter 3 to force the model. We show that through calibration of the water transport cost factor (controlling root water uptake rate) the VOM is successfully able to reproduce patterns of ET with no prior knowledge of vegetation other than seasonal or perennial growth ( $r$  values ranging 0.25 – 0.69 across sites). Stronger correlations are observed at more seasonal sites with increased water stress. Unsurprisingly the model struggles with some environments such as a seasonal flooding and some farmed sites. Root dynamics play an important role in the success of the model and minimal calibration per site credits the physiological understanding behind the model. Results prove that through modelling carbon-water mechanisms, vegetation optimality can provide a novel approach to study hydrological processes in vegetation dominated ungauged catchments. The optimality approach provides potential to predict changes in hydrological fluxes between natural and cultivated vegetation allowing future predictions of land use change on the hydrological cycle. Modelled ET predictions could further be used to force catchment runoff models lacking adequate representation. Furthermore, the model can be used to study hydrological responses to vegetation adaption under different forced climate conditions.

**How sensitive are hydrological processes in vegetation to changes in atmospheric CO<sub>2</sub> concentration? (Chapter 5)**

As atmospheric CO<sub>2</sub> concentrations continue to increase, the future impact it will have on hydrological fluxes becomes even more important to predict. The VOM allows us to analyse how vegetation might optimally adapt in response to elevated CO<sub>2</sub>. Through “switching” on or off vegetation adaptation properties thought to occur at the yearly-decadal timeframe, we analyse the potential long and short-term vegetation responses to changes in atmospheric CO<sub>2</sub> (C<sub>a</sub>). Three static C<sub>a</sub> levels are forced (291, 377, and 420 ppm) through the VOM to assess ET at eight of the flux tower sites across Brazil representing different ecosystems that performed successfully in chapter 4. ET response was validated against observations for C<sub>a</sub> = 377 ppm (C<sub>a</sub> in 2004, the mean active year for observations). Results showed that the economics of vegetation carbon gain and water use led to results comparable to observed patterns and an overall reduction in ET at all sites considering both long and short-term adaptations (reductions from 0.7-6.0% over an increase of 77 ppm CO<sub>2</sub>). Water use efficiency (WUE) rose across all simulations generally increasing linearly with C<sub>a</sub>. Long-term adaptation of vegetation tended to dampen the reduction of ET across sites except for one pasture site indicating the importance of modelling the adaptation of maximum rooting depth. Seasonal trends included decreased ET during wet periods and increased ET over dry periods. Furthermore, results underline the importance of incorporating long-term adaptation into hydrological modelling when assessing the impact of future climate changes in vegetation dominated catchments.

## 6.2 Overarching remarks

This thesis started by outlining the role of carbon-water dynamics and questioning what implications they might have on hydrological models. In Chapter 1 we discussed how the parameterisation of vegetation can be inadequate in traditional hydrological models, neglecting

important hydrosphere-biosphere interactions, especially the temporal dynamics of vegetation (Gerten et al., 2004). These temporal dynamics help capture hydrological effects resulting from variations in vegetation distribution and composition which are likely to arise in response to climate change (Gitay et al., 2001). Furthermore, we discussed how vegetation dynamics models consider these interactions, incorporating vegetation coverage, type, and rooting depth dynamically into them. However, increased understanding of biophysical processes increases complexity (Franklin et al., 2020) and many of these models need numerous parameters (Shen et al., 2013; Lei et al., 2014) decreasing in robustness, predictive power, and transparency (Prentice et al., 2015).

To avoid this, we tested a vegetation optimality model, the theory of which is based on self-organisation, natural selection, and entropy maximisation (Schymanski et al., 2009; Franklin et al., 2020). More directly, it is based on the maximisation of net carbon profit achieved through optimising water use traits such as stomatal conductance and root growth to minimise water used per carbon gained. We explored its robustness and predictive power by trying to recreate hydrological observations over multiple land uses and climates in Brazil. The model had never been tested in this region of the world before and its limitations were explored through extensive analysis of its ability to accurately model fluxes in evapotranspiration and soil moisture in Chapter 4. However, before testing the model, suitable forcing data had to be validated first.

Data underlie our theories, our understanding and hence our models. To model long term adaptation properties and vegetation composition, extensive and complete meteorological datasets are needed to force them. Therefore, we first established which gridded datasets were the most accurate to our specific observation sites, outlining a clear methodology to deliver results that could provide insight to anyone attempting to choose forcing data across Brazil (Chapter 3). The results outlined the most suitable product for each meteorological variable at

both daily and monthly temporal scales whilst also detailing the contributions to error for each data product tested. We provided insight into the performance and robustness of each product spanning multiple climates and biomes over Brazil. To our knowledge this is the first comparison of recent high-resolution meteorological datasets using representative flux towers spanning multiple climates and ecosystems in Brazil. The results from our study provide important information when a lack of data or time can prevent site-specific validation or complete datasets are needed to force models. They highlight areas where data products could improve and, less specifically, can be tools in data selection and validation, quality assurance, uncertainty estimation, model validation, decision-making processes, and climate studies across Brazil and globally.

We used our results from Chapter 3 to choose our forcing data to run our vegetation optimality model exploring its ability to recreate observed evapotranspiration across Brazil (Chapter 4). The model successfully reproduced observed patterns in evapotranspiration across Brazil and required very little parameter estimation significantly improving the objectiveness of the carbon-water flux estimates and decreasing human error. The method offers a prominent alternative to more parameter intensive and empirically based approaches, with emphasis on predicting possible consequences of environmental change. The ability to optimise and adapt root systems below ground with low computational demand combined with above-ground optimality, could make it an influential tool to simulate the impacts of long-term environmental change on water balance and vegetation (Nijzink & Schymanski, 2022; Zhu et al., 2023).

Chapter 5 looked at exploring one avenue of environmental change. We adjusted the input atmospheric CO<sub>2</sub> concentration to look at how potential adaptations of long and short-term vegetation responses affect hydrological processes (Chapter 5). We were able to study the direct impact of this isolated change and explain results through carbon-water mechanisms. We presented findings that suggested a “drying” across all sites under all scenarios and gave insight

into how modelling long-term adaptations might cause shifts in ecosystem seasonality. We highlighted differences in resilience to “drying” by comparing natural ecosystems to cultivated ones proposing that deeper roots systems from perennials play an important role in regulating water use in ecosystems. We present vegetation adaptation and water use efficiency changes as reasonable explanations of the results backed by successful model validation. Although only providing theoretical support for these scenarios, the findings underline the importance of including long-term optimisation in hydrological modelling under environmental change across multiple ecosystems over Brazil.

Predicting water availability under constantly changing land uses and climates remains one of the most challenging yet essential scientific aims presently and for the future (Biswas and Tortajada, 2022; Daneshi et al., 2021; Mishra et al., 2021; Moumen et al., 2019). Computational power, data availability, human error and understanding processes all play a part in limiting our ability to do this. Understanding carbon-water mechanisms – that is, understanding the relationship and interactions between vegetation, soil, water, and climate – would enable us to predict the distribution of water across the globe and the consequences of land use change. It would become a powerful tool in areas such as water security and agricultural planning perhaps even into the future and under different climate scenarios. It would aid model development increasing the realistic representation of vegetation-water feedbacks without having to rely on calibration. While this thesis cannot fully reach these aims, through scrutinising our available resources and testing optimality modelling over new regions, it contributes to it and provides answers that will hopefully bring us a little closer to it.

### 6.3 Directions for future research

There are many research ideas that could build or expand on this thesis. We have focused on the extent to which a vegetation optimality model works across different climates and

ecosystems over Brazil at a single point scale. Furthermore, we were only able to assess sites where data was readily available. Analysing representative sites not considered in this study would further test the resilience and limitations of the model. For example, we have already shown that it struggles in flooded environments. Further to this the model itself has some limitations that could be explored. No effect of fire or nutrient availability is considered, the former occurs either naturally or anthropogenically and has increased in size and regularity over Brazil in recent years (Andrade, 2019; Pivello et al., 2021), whilst the latter has been proven to constrain photosynthetic capacity in CO<sub>2</sub> enrichment studies (Leakey et al., 2009). However, it is remarkable that a vegetation model, never used before in this part of the world, can simulate reasonable hydrological processes to match observations with minimal calibration over a wide range of climates and land use types. This provides an opportunity to speculate on the future capability of using a vegetation optimality model in Brazil or even globally. Here we focus on examples of how understanding carbon-water mechanisms might increase our knowledge across the wider field of hydrometeorology.

### **An uncalibrated runoff model in ungauged catchments**

Catchment models are vital for understanding hydrological processes and water resources management, providing insight into how water is stored and moves through a watershed whilst responding to various topographic inputs. Currently, the VOM is one-dimensional and only describes ecohydrological processes vertically. The optimisation of biophysical processes described in the VOM could be integrated with a physically based hydrological or climate model to supply a more complete understanding of the interactions between water, vegetation, and climate. This could increase predictive power especially over vegetation dominated catchments with high evapotranspiration rates and complex root systems. Due to high information requirements, simplified empirical methods are often used to calculate potential and actual evapotranspiration in hydrological models (Zhao et al., 2013). These simplifications

cause greater uncertainty when attempting to model evapotranspiration under changing climates and environments. As the optimisation in the VOM is entirely independent of observed evapotranspiration it does not need calibration to predict it (although it does require an accurate description of soil and topographical properties). In this way it could increase the accuracy of the evapotranspiration component either integrated in models or it could be used to create a forcing dataset for models such as lumped rainfall runoff or water balance models that require estimates over data limited areas. Furthermore, optimisation naturally requires less parameterisation than other modelling techniques, decreasing the complexity of understanding parameter interactions and uncertainty.

Alternatively, lateral flow could be incorporated to create a distributed model (Chen et al., 2022) whereby VOM is run for each individual grid cell. However, this approach would be computationally intensive, and more validation studies would be needed if catchments spanned multiple land uses not yet validated. Upscaling based on representative areas within a catchment could be a less computationally expensive approach and it would be relatively simple to test reliability by comparing the discharge output against streamflow observations. Through assigning grid cells with soil properties, flow direction, and lag to each cell, optimality modelling could be a leap towards an uncalibrated runoff model increasing predictive power in ungauged basins.

### **Increasing ecosystem functionality and resilience**

Throughout this thesis we investigated a combination of sites representing both natural and agricultural ecosystems. In Chapter 4 we were able to successfully model both natural ecosystems and nearby areas that had been cultivated for crop or pasture with similar soil properties and climatic stresses. Through calibrating the VOM for cultivated sites, as outlined, it is then possible to run the naturalisation of the ecosystem to assess the depletion of water in

deforested or cultivated areas. Similarly, the reverse could be done to assess water availability in potential restoration/reforestation projects. In Chapter 5 we showed potential differences in vegetation/ecosystem response to elevated CO<sub>2</sub>. Expanding on this, future water security could be assessed by forcing the model with potential climate change scenarios and comparing the hydrological differences between ecosystems, such as changes in the water balance components (Marhaento et al., 2018). Catchment response time gives invaluable insight into the prediction of floods and droughts and is critical for assessing the future of ecosystem functionality and resilience and hence water and food security to climate change. The role of vegetation optimality in increasing ecosystem functionality and resilience underlines the importance of its application in management and policy contexts. So far, its application is predominantly in experimental research, but it may be time to assess the potential for these models for informing land management decisions including land-use optimisation, conservation planning, and vegetation restoration. By evaluating the ecological and economic repercussions of different vegetation strategies we can gain beneficial insights for sustainable water resource and land management.

### **Examining the influence of climate change through vegetation response**

In Chapter 5 we explored how the VOM responded to isolated changes in atmospheric CO<sub>2</sub>, touching on one aspect of climate change. In a similar fashion, the VOM could be used to explore the impacts of other isolated climatic variables such as changes in precipitation patterns, and temperature. Understanding how carbon-water mechanisms optimise under different environments and climates by adjusting just one climatic variable allows us to understand responses, such as increased water use efficiency under elevated CO<sub>2</sub>, which might be offset by other variables masking their impact in climate change studies. Furthermore, studying long and short-term responses to climatic variables could lead to a better understanding of how shifts in climate may influence ecosystem characteristics. In a study



focusing on Australian sites, Nijzink & Schymanski (2022) recently provided strong evidence that vegetation optimality may explain the distribution of catchments along the Budyko curve (an empirical equation for estimating mean annual runoff and evaporation from observed precipitation and net radiation, Budyko, 1974) suggesting that catchment characteristics may alter as vegetation adjusts to new climates over decades. This provides strong incentive to continue exploring climatic pressures on hydrological processes through vegetation optimality testing this theory across other climates, such as Brazil, as it could establish a new foundation for the prediction and evaluation of catchment responses to climatic shifts.

### **What is the capacity of the model outside of the tropics?**

Although the theory behind the VOM is transferable the model was developed and tested in various ecosystems in Australia (including tropical rainforests). This thesis is the first comprehensive use of the model in (sub)tropical South America, and assessed its applicability to different ecological, geographical, and climatic conditions to those it was developed under. However, very little research has been done testing the VOM outside the tropics. Environmental conditions vary greatly over the globe including precipitation patterns, temperature, vegetation composition and soil types. By evaluating the VOM's performance in diverse environments such as temperate regions with more extreme seasonal temperatures, we will be able to determine the extent to which it encapsulates fundamental ecological principles. Through integrating results from regions across the globe, we can enhance our understanding of carbon-water mechanisms driving hydrological processes.

### **Recommendations for future VOM work**

Using VOM in this study has highlighted areas for potential improvement. The application of optimality theory in this study has revealed the sensitivity of vegetation adapting to soil water stresses. The current model does not acknowledge site specific hydrological conditions

and the water balance component allows free drainage leading to an underestimation of dry season water use. A more developed groundwater component with an understanding of aquifer types could lead to a more accurate representation of water use during periods of limited rainfall and increase drought resilience of the model. Furthermore, in some cases where the water table is relatively shallow, groundwater can potentially be a primary source of hydration for plant roots and understanding its dynamics and interactions with the root zone could improve the temporal and spatial variability of water accessibility to vegetation.

It was found that the model was very sensitive to the carbon costs associated with water transport from the root system to the canopy. There is ambiguity surrounding the costs of deeper, more complex rooting systems which led to the tuning of the water transport cost factor ( $c_{rv}$ ). The model would benefit from further research into the quantification of these costs and its relationship to environmental conditions.

Another area the model might benefit from is the distinction between C3 and C4 pathways. The C4 photosynthetic pathway was not acknowledged in the model in return for greater generality. Despite positive results modelling C4 ecosystems in this study, it remains unclear if the model would still simulate coherent results under more extreme environmental or climatic stresses when modelling future climate scenarios. The model may therefore benefit from the incorporation of a C4 pathway which could be set as a parameter depending on the dominant vegetation type. However, with the addition of extra parameters the model would lose generality and transferability and potentially increase uncertainty when modelling ecosystems dominated by both C3 and C4 plants.



## A. Appendix A: Supporting Information for Chapter 3

### A.1 An overview of errors and their contribution to the MSE

Ranking systems notorious for oversimplifying complex information and causing a loss of information. They require subjective choices in defining the criteria which can introduce bias to the results. They can also be highly sensitive to small differences in data values and therefore may not reflect the significance or true difference between the datasets. Large quantities of data were analysed and compared before reaching the final ranks presented in Chapter 3 (Table 3.4). Errors were calculated for each meteorological variable when observation data for each Flux Tower sites were compared to each gridded dataset at both daily and monthly temporal scales. For purposes of transparency all errors are presented in this supporting information so that individual assumptions regarding the quality of the datasets may be drawn.

All errors have been scaled to the RMSE to conserve units (including the MSE) and for comparability with results presented graphically. The MSE has been decomposed into parts as outlined in Chapter 3 for users to acquire a better understanding of the contributions to the error. The correlation, bias and variation contributions to the MSE and the MSE for errors at the daily scale are presented below (Table A.2, Table A.3, Table A.4, Table A.5, respectively) and are associated with Figure 3.2 (Chapter 3), whilst the tables following this (Table A.6, Table A.7, Table A.8, and Table A.9) are associated with errors at the monthly scale and Figure

3.3 (Chapter 3). Only the total MSE values given in Table A.5 and Table A.9 were used in the ranking system to find the best performing dataset.

## A.2 Seasonality in errors

Seasonality in errors were assessed to gain a deeper understanding of errors between observations and the gridded products. This was achieved by looking at the average monthly contributions to errors to see if patterns occurred in line with fluctuations in seasonal patterns. Due to the quantity of data being analysed we focused on overarching trends across all sites, and datasets for each variable to explain the causes of error. Less time was spent looking at errors at individual sites. Trends in seasonal errors are easier to spot through graphical representation and useful information can be captured when presenting the MSE decomposed. For example, an increase in bias can be seen during the dry season at the Amazon sites (K34, K67, K77, RJA and FNS) when comparing observed specific humidity to GLDAS2.1 (Figure A.4d). Other important inferences may be made from the decomposition, for example, seasonal error may not appear apparent when analysing the MSE alone but shifts in the dominant contribution can change as we see for site VCP when looking at air temperature (Figure A.2). Despite maintaining a constant annual MSE the dominant contribution changes from bias in the wet summer to correlation in the dry winter. For these reasons the below graphs have been added as supporting information detailing comparisons between observations and gridded datasets for variables with the strongest seasonal signatures (precipitation, temperature, solar radiation, and specific humidity) not presented in Chapter 3.

## A.3 Gridded meteorological forcing data availability

URLs to download the gridded meteorological forcing datasets used in Chapter 3 can be found in Table A.1.

Table A.1 Data Sources for Chapter 3

Dataset	Source
GLDASv2.0 and 2.1	<a href="https://disc.gsfc.nasa.gov/datasets?keywords=GLDAS&amp;page=1&amp;temporalResolution=3%20hours&amp;spatialResolution=0.25%20%C2%B0%20x%20x%200.25%20%C2%B0">https://disc.gsfc.nasa.gov/datasets?keywords=GLDAS&amp;page=1&amp;temporalResolution=3%20hours&amp;spatialResolution=0.25%20%C2%B0%20x%20x%200.25%20%C2%B0</a>
ERA5-Land	<a href="https://cds.climate.copernicus.eu/cdsapp#!/dataset/reanalysis-era5-land?tab=overview">https://cds.climate.copernicus.eu/cdsapp#!/dataset/reanalysis-era5-land?tab=overview</a>
BNMD	<a href="https://utexas.box.com/Xavier-etal-IJOC-DATA">https://utexas.box.com/Xavier-etal-IJOC-DATA</a>
MSWEPv2.2	Personal communication through Prof Hylke Beck at <a href="mailto:hylkeb@princeton.edu">hylkeb@princeton.edu</a>

Table A.2 The correlation contribution to the MSE scaled to the RMSE of each gridded data set and the meteorological variables against all observation sites at the DAILY scale..

Correlation contribution	Flux Tower											
	K34	FNS	RJA	PDG	K67	K77	K83	BAN	CRA	VCP	USR	
<b>BMBD</b>												
Precipitation (mm)	10.65	9.16	9.85	7.13	10.04	9.16	9.11	9.64	15.60	6.11	8.74	
Air Temp (°C)	0.90	0.82	1.05	3.34	0.71	0.72	0.65	1.34	12.01	2.82	7.76	
Wind Speed (m s <sup>-1</sup> )	0.68	0.38	0.46	0.57	0.41	0.70	0.30	0.59	1.62	0.69	1.06	
Pressure (hPa)	0.00	0.00	0.00	0.00	0.00	0.00	0.00	0.00	0.00	0.00	0.00	
Solar rdn (W m <sup>-2</sup> )	267.1	619.6	598.7	1245.5	333.7	614.3	232.1	745.7	3287.5	1011.1	1213.0	
Thermal rdn (W m <sup>-2</sup> )	-	-	-	-	-	-	-	-	-	-	-	
Spec Humid (kg kg <sup>-1</sup> )	4.8E-4	8.4E-5	7.E-5	6.2E-5	2.8E-5	2.2E-5	2.5E-5	4.E-5	2.E-4	6.1E-5	2.3E-4	
<b>ERAS-Land</b>												
Precipitation (mm)	10.80	7.77	7.49	6.69	10.79	8.50	11.52	9.97	13.34	7.29	8.63	
Air Temp (°C)	1.18	1.32	1.47	1.92	0.63	0.84	1.73	1.28	6.33	1.61	6.61	
Wind Speed (m s <sup>-1</sup> )	0.26	0.24	0.26	0.19	0.25	0.41	0.42	0.28	1.47	0.39	0.67	
Pressure (hPa)	0.02	0.18	0.41	0.24	0.25	0.22	0.21	0.29	4.78	0.17	3.99	
Solar rdn (W m <sup>-2</sup> )	113.7	479.5	525.7	413.0	254.9	489.3	572.5	558.9	1909.7	366.4	896.7	
Thermal rdn (W m <sup>-2</sup> )	6.94	23.06	25.89	-	-	27.87	25.04	-	-	-	-	
Spec Humid (kg kg <sup>-1</sup> )	2.6E-4	3.1E-5	3.E-5	1.9E-5	1.6E-5	1.8E-5	1.7E-5	2.9E-5	1.1E-4	2.1E-5	2.1E-4	
<b>GLDAS2.0</b>												
Precipitation (mm)	9.20	9.13	8.79	7.26	9.14	8.29	8.36	9.64	14.57	7.72	8.36	
Air Temp (°C)	1.17	2.85	2.58	4.92	1.07	1.44	1.72	1.62	5.79	3.41	5.55	
Wind Speed (m s <sup>-1</sup> )	0.09	0.18	0.18	0.40	0.15	0.32	0.15	0.23	1.07	0.53	0.79	
Pressure (hPa)	0.07	0.36	0.54	1.31	0.32	0.46	0.24	0.38	7.81	2.13	2.52	
Solar rdn (W m <sup>-2</sup> )	136.7	703.6	526.3	737.3	217.4	437.0	353.8	516.0	1084.1	501.1	706.1	
Thermal rdn (W m <sup>-2</sup> )	9.78	48.45	43.68	-	-	38.68	20.55	-	-	-	-	
Spec Humid (kg kg <sup>-1</sup> )	1.1E-3	1.4E-4	1.1E-4	5.4E-5	4.4E-5	3.8E-5	3.E-5	5.5E-5	9.5E-5	5.6E-5	1.8E-4	
<b>GLDAS2.1</b>												
Precipitation (mm)	10.60	8.85	8.73	7.61	9.35	8.81	11.67	10.11	16.25	8.25	9.68	
Air Temp (°C)	2.38	1.94	1.63	2.02	1.26	1.52	2.23	2.40	5.13	2.54	6.80	
Wind Speed (m s <sup>-1</sup> )	0.24	0.21	0.25	0.45	0.23	0.54	0.29	0.25	1.08	0.42	0.73	
Pressure (hPa)	0.03	1.35	0.28	0.24	0.28	0.22	0.33	0.55	3.13	0.15	4.23	
Solar rdn (W m <sup>-2</sup> )	193.2	814.5	810.3	502.4	315.7	580.8	602.1	790.9	1781.9	382.2	941.7	
Thermal rdn (W m <sup>-2</sup> )	17.03	42.83	59.94	-	-	57.60	53.40	-	-	-	-	
Spec Humid (kg kg <sup>-1</sup> )	5.8E-4	7.E-5	8.2E-5	2.7E-5	7.3E-5	6.5E-5	6.1E-5	4.9E-5	8.9E-5	3.2E-5	1.9E-4	
<b>MSWEPv2.2</b>												
Precipitation (mm)	12.10	9.76	8.20	6.22	10.40	9.09	13.34	11.15	15.10	6.71	8.49	

Table A.3 The bias contribution to the MSE scaled to the RMSE of each gridded data set and the meteorological variables against all observation sites at the DAILY scale.

Bias contribution	Flux Tower											
	K34	FNS	RJA	PDG	K67	K77	K83	BAN	CRA	VCP	USR	
<b>BND</b>	Precipitation (mm)	0.03	0.01	0.06	0.02	0.05	0.03	0.00	0.04	0.01	0.10	0.10
	Air Temp (°C)	2.02	2.75	2.12	0.50	2.25	0.89	1.26	1.91	0.81	1.60	0.42
	Wind Speed (m s <sup>-1</sup> )	0.38	2.41	0.20	1.47	0.09	0.00	0.09	0.16	0.78	0.15	0.00
	Pressure (hPa)	2.23	54.56	76.90	0.24	107.56	2.11	40.22	22.37	2.71	11.38	3.68
	Solar rdn (W m <sup>-2</sup> )	2.3	51.0	80.4	15.2	419.1	103.6	183.7	15.4	2.6	0.0	19.2
	Thermal rdn (W m <sup>-2</sup> )	-	-	-	-	-	-	-	-	-	-	-
	Spec Humid (kg kg <sup>-1</sup> )	1.8E-2	2.E-3	1.6E-3	7.E-4	1.8E-3	1.8E-3	2.3E-3	2.1E-3	1.5E-4	4.8E-4	3.E-4
	Precipitation (mm)	0.20	0.00	0.09	0.01	1.00	0.43	0.43	0.03	0.00	0.02	0.04
	Air Temp (°C)	0.24	0.27	0.20	0.03	1.05	0.40	0.02	0.63	0.15	0.44	0.44
	Wind Speed (m s <sup>-1</sup> )	0.53	1.99	0.15	0.63	0.90	0.12	0.57	0.28	0.60	0.04	0.18
Pressure (hPa)	6.87	23.91	71.64	12.28	95.19	0.10	25.48	0.26	3.72	21.19	12.98	
Solar rdn (W m <sup>-2</sup> )	1.7	28.8	0.2	11.9	257.9	11.3	55.8	10.8	2.5	25.7	0.1	
Thermal rdn (W m <sup>-2</sup> )	1.99	13.09	17.40	-	-	22.63	0.03	-	-	-	-	
Spec Humid (kg kg <sup>-1</sup> )	2.7E-3	8.E-5	2.2E-4	1.3E-5	3.7E-5	5.E-5	3.1E-5	2.9E-5	1.1E-5	6.8E-6	3.2E-6	
<b>ERA5-Land</b>	Precipitation (mm)	0.07	0.00	0.06	0.03	0.06	0.06	0.01	0.02	0.01	0.13	0.18
	Air Temp (°C)	1.58	0.48	0.72	0.21	2.73	1.05	1.38	2.11	1.80	1.44	1.50
	Wind Speed (m s <sup>-1</sup> )	1.17	2.79	0.46	0.61	1.01	0.55	1.16	0.91	1.00	0.04	0.10
	Pressure (hPa)	11.96	99.85	86.49	2.57	120.94	5.39	54.54	3.64	1.02	0.13	53.66
	Solar rdn (W m <sup>-2</sup> )	0.3	9.5	20.0	3.9	323.9	41.5	93.1	12.0	49.1	34.6	2.1
	Thermal rdn (W m <sup>-2</sup> )	4.34	31.31	28.22	-	-	31.10	18.97	-	-	-	-
	Spec Humid (kg kg <sup>-1</sup> )	1.4E-3	9.9E-6	7.1E-5	2.4E-4	1.2E-4	1.E-4	3.E-4	1.5E-4	2.E-4	1.3E-4	1.4E-4
	Precipitation (mm)	0.01	0.05	0.03	0.01	0.04	0.04	0.00	0.08	0.04	0.10	0.13
	Air Temp (°C)	0.04	0.57	1.24	0.96	0.75	0.00	0.02	2.11	0.25	0.53	0.47
	Wind Speed (m s <sup>-1</sup> )	0.59	2.44	0.18	0.19	0.21	0.07	0.35	0.91	1.20	0.11	0.25
Pressure (hPa)	6.14	50.86	84.79	31.94	121.58	8.74	56.40	3.64	9.13	30.72	11.54	
Solar rdn (W m <sup>-2</sup> )	3.3	0.3	0.0	15.7	348.2	56.4	106.7	12.0	0.8	72.9	8.5	
Thermal rdn (W m <sup>-2</sup> )	4.73	30.67	16.62	-	-	32.95	18.78	-	-	-	-	
Spec Humid (kg kg <sup>-1</sup> )	2.7E-3	8.3E-5	2.7E-4	1.E-4	5.6E-5	5.9E-5	2.2E-5	1.5E-4	2.7E-5	1.4E-5	1.5E-5	
<b>MSWEPv2.2</b>	Precipitation (mm)	0.00	0.03	0.09	0.00	0.03	0.03	0.00	0.19	0.01	0.01	0.02



Table A.4 The variation contribution to the MSE scaled to the RMSE of each gridded data set and the meteorological variables against all observation sites at the DAILY scale.

Variation contribution	Flux Tower											
	K34	FNS	RJA	PDG	K67	K77	K83	BAN	CRA	VCP	USR	
<b>BMD</b>												
Precipitation (mm)	2.15	1.09	3.11	0.09	0.51	0.31	0.64	1.30	0.14	0.01	0.06	
Air Temp (°C)	0.02	0.08	0.12	0.01	0.03	0.07	0.18	0.04	0.00	0.00	0.02	
Wind Speed (m s <sup>-1</sup> )	0.00	0.35	0.00	0.05	0.11	0.01	0.06	0.00	0.59	0.01	0.18	
Pressure (hPa)	1.01	1.54	1.70	6.03	0.86	1.70	0.64	1.15	9.92	3.57	6.43	
Solar rdn (W m <sup>-2</sup> )	6.6	38.7	32.4	23.1	2.3	7.6	2.3	5.4	17.7	13.9	26.7	
Thermal rdn (W m <sup>-2</sup> )	-	-	-	-	-	-	-	-	-	-	-	
Spec Humid (kg kg <sup>-1</sup> )	5.E-4	4.5E-5	2.7E-5	1.9E-4	1.6E-5	1.5E-5	1.5E-5	7.2E-5	2.7E-4	2.2E-4	1.6E-4	
<b>ERA5-Land</b>												
Precipitation (mm)	2.05	2.31	5.36	1.60	0.01	0.37	0.18	1.60	0.37	0.47	0.27	
Air Temp (°C)	0.52	0.07	0.08	0.10	0.01	0.02	0.03	0.02	0.01	0.06	0.09	
Wind Speed (m s <sup>-1</sup> )	0.02	0.31	0.00	0.06	0.19	0.06	0.10	0.00	0.60	0.02	0.11	
Pressure (hPa)	0.00	0.06	0.17	0.00	0.04	0.00	0.00	0.00	0.00	0.00	0.01	
Solar rdn (W m <sup>-2</sup> )	13.3	28.1	33.2	8.0	6.1	6.1	1.9	0.3	18.5	0.1	2.9	
Thermal rdn (W m <sup>-2</sup> )	5.39	1.03	0.76	-	-	9.36	4.26	-	-	-	-	
Spec Humid (kg kg <sup>-1</sup> )	1.2E-4	2.4E-6	4.E-6	2.1E-6	3.9E-6	3.7E-7	2.8E-6	2.1E-5	2.3E-6	1.6E-7	3.2E-6	
<b>GLDAS2.0</b>												
Precipitation (mm)	4.16	1.91	4.92	1.92	2.33	1.66	2.06	2.34	0.29	0.89	0.81	
Air Temp (°C)	0.22	0.00	0.03	0.08	0.01	0.02	0.08	0.13	0.09	0.20	0.33	
Wind Speed (m s <sup>-1</sup> )	0.07	0.48	0.04	0.06	0.00	0.09	0.01	0.00	0.71	0.01	0.14	
Pressure (hPa)	0.01	0.16	0.35	0.06	0.14	0.07	0.02	0.03	0.34	0.05	0.05	
Solar rdn (W m <sup>-2</sup> )	78.1	194.7	194.1	250.7	24.7	110.9	72.4	78.8	215.0	123.7	213.7	
Thermal rdn (W m <sup>-2</sup> )	2.26	0.67	0.87	-	-	3.93	0.06	-	-	-	-	
Spec Humid (kg kg <sup>-1</sup> )	4.3E-5	3.3E-5	1.6E-5	3.6E-5	7.1E-6	8.7E-6	4.2E-6	1.7E-4	2.E-5	3.3E-5	3.5E-5	
<b>GLDAS2.1</b>												
Precipitation (mm)	1.89	1.38	4.09	0.45	0.42	0.12	0.27	1.11	0.13	0.03	0.02	
Air Temp (°C)	0.01	0.00	0.00	0.00	0.50	0.26	0.03	0.30	0.01	0.02	0.08	
Wind Speed (m s <sup>-1</sup> )	0.01	0.31	0.00	0.00	0.02	0.03	0.01	0.04	0.64	0.04	0.07	
Pressure (hPa)	0.00	0.00	0.09	0.00	0.03	0.00	0.02	0.04	0.00	0.02	0.00	
Solar rdn (W m <sup>-2</sup> )	7.2	41.4	17.1	28.4	17.0	2.3	1.0	21.9	53.8	3.3	0.7	
Thermal rdn (W m <sup>-2</sup> )	0.06	4.98	5.36	-	-	0.02	10.34	-	-	-	-	
Spec Humid (kg kg <sup>-1</sup> )	2.6E-4	1.5E-5	8.4E-6	9.9E-6	3.6E-6	3.4E-5	3.5E-5	4.E-5	1.3E-6	1.2E-6	3.4E-6	
<b>MSWEPv2.2</b>												
Precipitation (mm)	0.24	0.05	2.47	0.14	0.00	0.00	0.01	0.01	0.08	0.00	0.01	

Table A.5 The MSE scaled to the RMSE of each gridded data set and the meteorological variables against all observation sites at the DAILY scale

MSE	Flux Tower										
	K34	FNS	RJA	PDG	K67	K77	K83	BAN	CRA	VCP	USR
<b>BMBD</b>	Precipitation (mm)	12.83	10.26	13.02	7.24	10.61	9.50	10.99	15.75	6.22	8.90
	Air Temp (°C)	2.95	3.65	3.29	3.85	2.98	1.68	2.08	12.82	4.42	8.20
	Wind Speed (m s <sup>-1</sup> )	1.06	3.14	0.66	2.09	0.60	0.70	0.44	0.75	2.99	0.84
	Pressure (hPa)	3.23	56.10	78.59	6.26	108.41	3.81	40.85	23.53	12.63	14.95
	Solar rdn (W m <sup>-2</sup> )	276.1	709.2	711.5	1283.8	755.1	725.5	418.1	766.4	3307.8	1025.0
	Thermal rdn (W m <sup>-2</sup> )	-	-	-	-	-	-	-	-	-	-
	Spec Humid (kg kg <sup>-1</sup> )	1.9E-2	2.2E-3	1.7E-3	9.6E-4	1.8E-3	1.9E-3	2.3E-3	2.2E-3	6.2E-4	7.6E-4
	Precipitation (mm)	13.05	10.08	12.94	8.30	11.80	9.30	12.13	11.60	13.72	7.78
	Air Temp (°C)	1.94	1.66	1.75	2.05	1.69	1.25	1.78	1.93	6.49	2.10
	Wind Speed (m s <sup>-1</sup> )	0.81	2.54	0.41	0.88	1.34	0.60	1.10	0.56	2.67	0.45
<b>ERA5-Land</b>	Pressure (hPa)	6.89	24.15	72.22	12.53	95.49	0.32	25.69	8.50	21.37	
	Solar rdn (W m <sup>-2</sup> )	128.7	536.3	559.1	432.9	518.9	506.6	630.2	570.0	1930.6	
	Thermal rdn (W m <sup>-2</sup> )	14.33	37.18	44.05	-	-	59.85	29.33	-	-	
	Spec Humid (kg kg <sup>-1</sup> )	3.1E-3	1.1E-4	2.6E-4	3.5E-5	5.6E-5	6.8E-5	5.1E-5	7.9E-5	1.2E-4	
	Precipitation (mm)	13.43	11.05	13.77	9.22	11.52	10.02	10.42	12.00	14.86	
	Air Temp (°C)	2.97	3.34	3.33	5.21	3.81	2.52	3.18	3.86	7.68	
	Wind Speed (m s <sup>-1</sup> )	1.32	3.45	0.68	1.08	1.17	0.96	1.32	1.15	2.78	
	Pressure (hPa)	12.05	100.37	87.37	3.94	121.40	5.92	54.80	4.04	9.17	
	Solar rdn (W m <sup>-2</sup> )	215.1	907.9	740.5	992.0	566.0	589.5	519.3	606.8	1348.2	
	Thermal rdn (W m <sup>-2</sup> )	16.38	80.43	72.77	-	-	73.71	39.58	-	-	
<b>GLDAS2.0</b>	Spec Humid (kg kg <sup>-1</sup> )	2.5E-3	1.8E-4	2.E-4	3.3E-4	1.7E-4	1.5E-4	3.7E-4	3.1E-4		
	Precipitation (mm)	12.50	10.27	12.85	8.08	9.82	8.97	11.94	11.31		
	Air Temp (°C)	2.43	2.51	2.87	2.98	2.51	1.78	2.29	2.73		
	Wind Speed (m s <sup>-1</sup> )	0.84	2.96	0.43	0.65	0.46	0.64	0.65	0.87		
	Pressure (hPa)	6.17	52.21	85.15	32.19	121.89	8.96	56.74	0.77		
	Solar rdn (W m <sup>-2</sup> )	203.6	856.1	827.5	546.5	680.9	639.5	709.8	836.9		
	Thermal rdn (W m <sup>-2</sup> )	21.82	78.48	81.92	-	-	90.56	82.52	-		
	Spec Humid (kg kg <sup>-1</sup> )	3.5E-3	1.7E-4	3.6E-4	1.4E-4	1.7E-4	1.6E-4	1.2E-4	1.1E-4		
	Precipitation (mm)	12.34	9.85	10.76	6.36	10.43	9.12	13.35	11.34		
	<b>MSWEPv2.2</b>	Precipitation (mm)	12.34	9.85	10.76	6.36	10.43	9.12	13.35	11.34	
Pressure (hPa)		6.17	52.21	85.15	32.19	121.89	8.96	56.74	0.77		
Solar rdn (W m <sup>-2</sup> )		203.6	856.1	827.5	546.5	680.9	639.5	709.8	836.9		
Thermal rdn (W m <sup>-2</sup> )		21.82	78.48	81.92	-	-	90.56	82.52	-		
Spec Humid (kg kg <sup>-1</sup> )		3.5E-3	1.7E-4	3.6E-4	1.4E-4	1.7E-4	1.6E-4	1.2E-4	1.1E-4		
Precipitation (mm)		12.34	9.85	10.76	6.36	10.43	9.12	13.35	11.34		
Pressure (hPa)		6.17	52.21	85.15	32.19	121.89	8.96	56.74	0.77		
Solar rdn (W m <sup>-2</sup> )		203.6	856.1	827.5	546.5	680.9	639.5	709.8	836.9		
Thermal rdn (W m <sup>-2</sup> )		21.82	78.48	81.92	-	-	90.56	82.52	-		
Spec Humid (kg kg <sup>-1</sup> )		3.5E-3	1.7E-4	3.6E-4	1.4E-4	1.7E-4	1.6E-4	1.2E-4	1.1E-4		

Table A.6 The correlation contribution to the MSE scaled to the RMSE of each gridded data set and the meteorological variables against all observation sites at the MONTHLY scale.

Correlation contribution	Flux Tower												
	K34	FNS	RJA	PDG	K67	K77	K83	BAN	CRA	VCP	USR		
BMD	Precipitation	51.79	55.27	39.03	36.66	62.43	37.30	32.84	43.99	29.02	34.05	30.54	
	Air Temp	0.16	0.09	0.21	0.26	0.08	0.12	0.30	0.15	0.28	0.42	0.46	
	Wind Speed	0.07	0.02	0.10	0.06	0.06	0.36	0.10	0.05	0.07	0.19	0.25	
	Pressure	0.00	0.00	0.00	0.00	0.00	0.00	0.00	0.00	0.00	0.00	0.00	
	Solar rdn	13.3	10.8	5.3	4.2	3.0	5.8	7.3	9.2	8.7	8.4	9.6	
	Thermal rdn	-	-	-	-	-	-	-	-	-	-	-	-
	Spec Humid	1.9E-4	3.2E-4	2.3E-4	7.2E-5	7.4E-5	7.4E-5	1.1E-4	7.7E-5	2.9E-4	9.5E-5	8.5E-5	
	Precipitation	57.08	58.13	44.55	40.10	58.23	37.47	32.34	48.79	34.70	57.38	43.81	
	Air Temp	0.14	0.50	0.38	0.31	0.13	0.26	0.72	0.24	0.44	0.52	0.50	
	Wind Speed	0.04	0.04	0.04	0.02	0.05	0.20	0.06	0.05	0.06	0.26	0.16	
ERAS-Land	Pressure	0.03	0.01	0.09	0.05	0.05	0.17	0.01	0.21	0.02	0.03	0.10	
	Solar rdn	19.8	10.6	11.7	7.5	5.9	16.1	17.1	10.8	11.2	9.4	16.4	
	Thermal rdn	3.06	1.28	3.37			4.41	1.54					
	Spec Humid	1.5E-5	3.2E-4	2.8E-4	1.8E-4	1.3E-4	2.1E-4	1.5E-4	3.5E-4	2.1E-4	1.8E-4	2.6E-4	
	Precipitation	71.68	56.09	56.72	48.73	72.69	48.51	44.54	59.20	45.40	67.71	42.37	
	Air Temp	0.18	0.36	0.49	0.40	0.09	0.16	0.27	0.24	0.28	0.43	0.36	
	Wind Speed	0.02	0.02	0.02	0.06	0.03	0.18	0.03	0.02	0.13	0.33	0.22	
	Pressure	0.03	0.01	0.06	0.15	0.04	0.05	0.01	0.06	0.06	0.41	0.04	
	Solar rdn	11.2	6.3	4.8	6.3	3.4	10.2	8.1	9.7	10.9	16.0	18.0	
	Thermal rdn	4.50	1.30	3.26			6.35	1.42					
GLDAS2.0	Spec Humid	4.2E-5	7.5E-4	6.9E-4	1.6E-4	4.E-4	4.8E-4	2.6E-4	2.5E-4	2.4E-4	2.9E-4	2.7E-4	
	Precipitation	67.60	59.16	53.56	38.96	63.87	41.76	32.68	49.85	37.85	34.80	34.51	
	Air Temp	0.23	0.45	0.21	0.22	0.21	0.56	0.72	0.62	0.39	0.68	0.60	
	Wind Speed	0.05	0.03	0.03	0.07	0.06	0.39	0.06	0.03	0.06	0.23	0.13	
	Pressure	0.03	0.28	0.04	0.04	0.05	0.06	0.04	0.42	0.02	0.02	0.09	
	Solar rdn	9.5	8.6	8.1	5.2	3.9	8.7	7.6	7.8	13.2	8.0	16.2	
	Thermal rdn	5.78	1.60	4.72			4.48	2.74					
	Spec Humid	2.6E-5	2.3E-4	7.1E-4	1.E-4	8.1E-4	9.4E-4	7.4E-4	3.4E-4	1.8E-4	2.6E-4	3.1E-4	
	Precipitation	69.14	54.29	29.06	36.81	66.93	36.20	30.70	41.24	33.01	47.02	37.61	
	MSWEPv2.2												

Table A.7 The bias contribution to the RMSE scaled to the MSE of each gridded data set and the meteorological variables against all observation sites at the MONTHLY scale.

Bias contribution	Flux Tower												
	K34	FNS	RJA	PDG	K67	K77	K83	BAN	CRA	VCP	USR		
<b>BMB</b>	Precipitation	6.42	1.09	7.81	3.44	7.43	5.50	0.54	10.00	1.06	10.51	9.72	
	Air Temp	1.98	1.94	1.60	0.49	1.71	0.89	1.05	1.48	0.78	1.21	0.42	
	Wind Speed	0.38	1.78	0.32	1.26	0.15	0.00	0.16	0.28	0.82	0.24	0.00	
	Pressure	2.29	14.23	17.97	0.15	22.58	1.43	11.72	7.81	1.46	4.63	2.16	
	Solar rdn	2.1	10.5	17.6	5.0	55.0	21.2	29.7	4.6	0.9	0.0	5.5	
	Thermal rdn	-	-	-	-	-	-	-	-	-	-	-	
	Spec Humid	1.8E-2	1.6E-2	1.4E-2	7.1E-3	1.4E-2	1.5E-2	1.7E-2	1.6E-2	2.4E-3	5.8E-3	3.9E-3	
	<b>ERAS-Land</b>	Precipitation	29.58	0.03	10.03	1.90	70.57	40.57	49.17	6.05	1.00	1.95	2.19
		Air Temp	0.24	0.30	0.24	0.06	0.97	0.43	0.02	0.61	0.19	0.43	0.46
		Wind Speed	0.52	1.56	0.27	0.72	0.89	0.20	0.65	0.41	0.66	0.06	0.29
Pressure		6.85	8.28	17.18	5.32	20.82	0.16	8.65	0.38	2.44	7.62	5.30	
Solar rdn		1.8	7.1	0.0	3.4	37.1	3.0	10.8	2.9	0.7	7.1	0.1	
Thermal rdn		2.05	5.19	5.66	-	-	6.94	0.01	-	-	-	-	
<b>GLDAS2.0</b>	Spec Humid	2.6E-3	1.8E-3	3.4E-3	2.4E-4	1.1E-3	1.3E-3	8.7E-4	7.2E-4	6.7E-4	3.3E-4	4.2E-5	
	Precipitation	12.43	0.11	9.36	5.29	9.38	9.44	3.30	4.29	1.14	12.54	18.32	
	Air Temp	1.55	0.52	0.71	0.23	1.92	0.98	1.11	1.56	1.39	1.13	1.19	
	Wind Speed	1.16	1.97	0.59	0.69	1.00	0.62	1.11	0.94	0.95	0.05	0.16	
	Pressure	11.91	21.50	19.47	1.82	24.44	3.05	14.38	2.37	1.02	0.17	14.08	
	Solar rdn	0.3	2.9	6.6	1.3	45.8	10.3	18.7	3.9	11.0	7.1	0.6	
	Thermal rdn	4.38	9.56	8.12	-	-	8.63	6.59	-	-	-	-	
	Spec Humid	1.5E-3	2.7E-4	1.2E-3	3.3E-3	2.4E-3	1.9E-3	4.4E-3	2.1E-3	3.4E-3	2.4E-3	2.3E-3	
	<b>GLDAS2.1</b>	Precipitation	3.20	5.47	4.57	2.59	6.33	6.22	1.43	14.76	9.97	15.32	12.66
		Air Temp	0.03	0.54	1.07	0.88	0.64	0.00	0.03	0.04	0.31	0.49	0.44
Wind Speed		0.59	1.80	0.30	0.31	0.31	0.11	0.47	0.70	1.09	0.17	0.36	
Pressure		6.09	13.74	19.27	10.06	24.51	4.19	14.68	0.20	4.41	9.74	4.87	
Solar rdn		3.3	0.3	0.0	5.0	48.8	13.0	20.8	6.7	0.2	15.0	2.1	
Thermal rdn		4.78	9.29	5.04	-	-	9.18	6.26	-	-	-	-	
<b>MSWEPv2.2</b>	Spec Humid	2.7E-3	1.8E-3	3.8E-3	1.8E-3	1.1E-3	1.3E-3	5.7E-4	5.2E-4	1.1E-3	4.8E-4	5.1E-4	
	Precipitation	1.01	3.68	10.44	0.29	4.75	4.75	0.04	25.35	3.68	0.78	0.66	

Table A.8 The variation contribution to the RMSE scaled to the RMSE of each gridded data set and the meteorological variables against all observation sites at the MONTHLY scale.

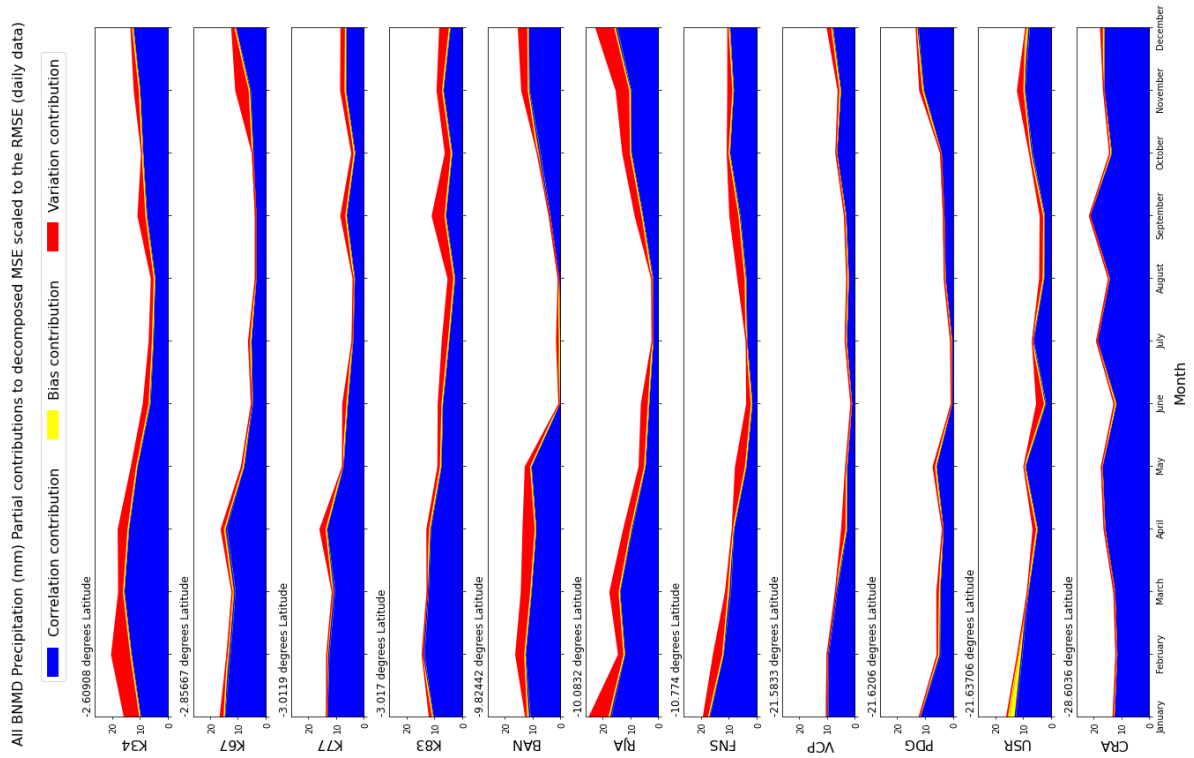
Variation contribution	Flux Tower											
	K34	FNS	RJA	PDG	K67	K77	K83	BAN	CRA	VCP	USR	
<b>BNMD</b>	Precipitation	1.46	2.05	22.02	1.57	3.30	7.45	16.20	4.68	0.12	1.71	31.35
	Air Temp	0.00	0.00	0.00	0.22	0.00	0.03	0.06	0.00	0.00	0.09	0.19
	Wind Speed	0.00	0.01	0.00	0.01	0.11	0.01	0.05	0.02	0.05	0.03	0.10
	Pressure	0.55	0.19	0.23	2.29	0.14	0.68	0.10	0.26	2.05	0.76	0.93
	Solar rdn	0.2	0.5	0.1	0.0	0.2	0.1	0.0	0.0	0.0	0.5	0.0
	Thermal rdn	-	-	-	-	-	-	-	-	-	-	-
	Spec Humid	1.6E-4	8.2E-5	6.8E-5	1.5E-3	3.1E-5	2.8E-5	4.4E-5	3.3E-4	2.6E-3	2.E-3	2.4E-3
	Precipitation	0.36	0.00	43.12	5.77	15.71	9.00	21.58	8.80	8.23	0.24	21.71
	Air Temp	0.04	0.01	0.01	0.04	0.06	0.04	0.00	0.20	0.00	0.01	0.08
	Wind Speed	0.00	0.01	0.01	0.01	0.04	0.06	0.01	0.03	0.09	0.02	0.04
<b>ERAS-Land</b>	Pressure	0.00	0.00	0.03	0.00	0.01	0.01	0.00	0.01	0.00	0.00	0.12
	Solar rdn	0.0	1.6	1.6	2.2	2.6	3.1	1.2	2.1	0.0	1.0	2.6
	Thermal rdn	3.51	0.49	0.28	-	-	1.88	1.55	-	-	-	-
	Spec Humid	4.8E-5	3.6E-5	3.E-5	1.9E-4	6.9E-5	3.3E-5	1.1E-4	5.4E-4	2.2E-5	2.E-5	1.1E-3
	Precipitation	0.14	1.63	27.42	0.54	0.04	1.18	2.40	2.34	2.15	0.05	16.10
	Air Temp	0.01	0.02	0.01	0.16	0.00	0.05	0.09	0.03	0.03	0.01	0.03
	Wind Speed	0.01	0.01	0.00	0.00	0.01	0.03	0.00	0.01	0.04	0.00	0.02
	Pressure	0.00	0.01	0.04	0.01	0.03	0.03	0.00	0.01	0.00	0.02	0.04
	Solar rdn	2.4	0.2	0.5	0.5	0.0	0.0	0.0	0.3	0.1	0.3	0.0
	Thermal rdn	1.19	0.12	0.06	-	-	0.47	0.05	-	-	-	-
<b>GLDAS2.0</b>	Spec Humid	6.7E-5	1.E-3	6.4E-4	8.E-4	1.4E-4	1.4E-4	4.7E-5	2.6E-3	4.5E-4	7.2E-4	1.6E-3
	Precipitation	1.03	2.75	23.66	0.01	0.98	5.43	11.97	10.39	0.00	0.09	20.51
	Air Temp	0.24	0.04	0.03	0.12	0.49	0.29	0.08	0.41	0.00	0.04	0.09
	Wind Speed	0.00	0.01	0.01	0.00	0.06	0.01	0.05	0.02	0.06	0.00	0.02
	Pressure	0.00	0.03	0.01	0.00	0.01	0.00	0.01	0.05	0.00	0.01	0.16
	Solar rdn	1.0	0.0	0.0	0.0	0.1	0.0	0.0	0.0	0.1	1.2	0.7
	Thermal rdn	1.77	0.04	0.00	-	-	1.40	0.01	-	-	-	-
	Spec Humid	2.E-4	4.2E-4	2.1E-4	2.3E-4	6.8E-4	5.1E-4	6.8E-4	8.6E-4	5.2E-8	9.5E-5	9.1E-4
	Precipitation	1.23	6.48	24.57	0.35	4.09	8.31	18.90	15.00	1.14	0.07	16.12
	<b>MSWEPv2.2</b>	Precipitation	1.23	6.48	24.57	0.35	4.09	8.31	18.90	15.00	1.14	0.07

Table A.9 The MSE scaled to the RMSE of each gridded data set and the meteorological variables against all observation sites at the MONTHLY scale.

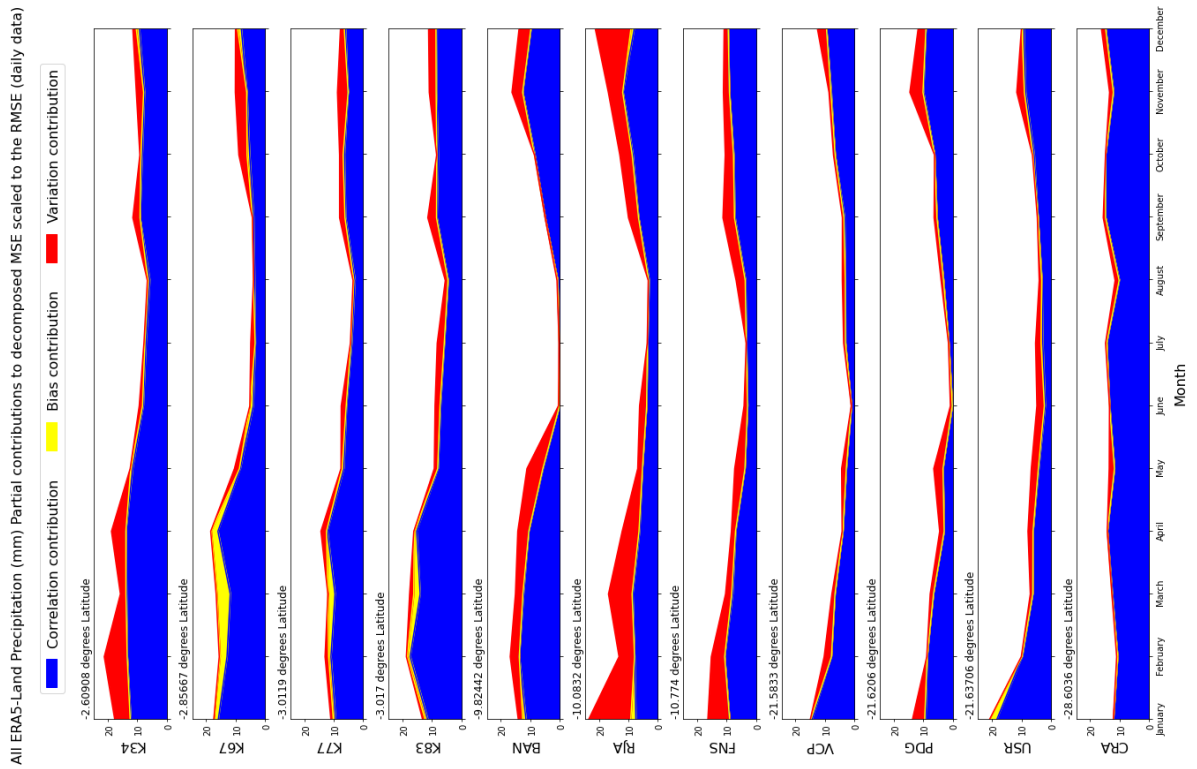
Overall MSE	Flux Tower												
	K34	FNS	RJA	PDG	K67	K77	K83	BAN	CRA	VCP	USR		
<b>BMD</b>	Precipitation	59.68	58.40	68.86	41.66	73.16	50.25	49.58	58.68	30.21	46.27	71.62	
	Air Temp	4.59	2.03	1.81	0.97	1.79	1.05	1.41	1.63	1.06	1.73	1.08	
	Wind Speed	0.21	1.81	0.42	1.33	0.33	0.37	0.31	0.35	0.93	0.46	0.36	
	Pressure	8.04	14.42	18.21	2.44	22.72	2.11	11.81	8.08	3.52	5.38	3.09	
	Solar rdn	243.3	21.8	23.1	9.2	58.2	27.1	37.0	13.8	9.7	8.9	15.1	
	Thermal rdn	-	-	-	-	-	-	-	-	-	-	-	
<b>ERAS-Land</b>	Spec Humid	3.5E-4	1.6E-2	1.4E-2	8.7E-3	1.5E-2	1.5E-2	1.7E-2	1.6E-2	5.3E-3	7.9E-3	6.4E-3	
	Precipitation	87.03	58.17	97.70	47.76	144.51	87.04	103.10	63.64	43.93	59.58	67.71	
	Air Temp	0.49	0.80	0.63	0.40	1.15	0.73	0.74	1.06	0.63	0.96	1.05	
	Wind Speed	0.31	1.62	0.32	0.75	0.98	0.46	0.72	0.49	0.81	0.33	0.48	
	Pressure	47.02	8.30	17.29	5.36	20.88	0.34	8.67	0.59	2.47	7.66	5.52	
	Solar rdn	341.1	19.2	13.3	13.0	45.6	22.2	29.0	15.8	11.9	17.5	19.1	
<b>GLDAS2.0</b>	Thermal rdn	74.33	6.96	9.31	-	-	13.23	3.10	-	-	-	-	
	Spec Humid	7.6E-6	2.2E-3	3.7E-3	6.E-4	1.3E-3	1.6E-3	1.1E-3	1.6E-3	9.E-4	5.3E-4	1.4E-3	
	Precipitation	84.25	57.83	93.50	54.57	82.12	59.13	50.24	65.83	48.69	80.29	76.79	
	Air Temp	3.14	0.90	1.21	0.79	2.02	1.19	1.47	1.83	1.70	1.57	1.58	
	Wind Speed	1.38	2.00	0.60	0.75	1.04	0.83	1.14	0.96	1.12	0.38	0.40	
	Pressure	142.16	21.52	19.58	1.98	24.51	3.13	14.39	2.44	1.08	0.59	14.16	
<b>GLDAS2.1</b>	Solar rdn	214.4	9.4	11.9	8.1	49.3	20.5	26.8	13.8	22.0	23.4	18.6	
	Thermal rdn	101.36	10.98	11.44	-	-	15.45	8.06	-	-	-	-	
	Spec Humid	3.7E-6	2.1E-3	2.5E-3	4.3E-3	2.9E-3	2.5E-3	4.7E-3	5.E-3	4.1E-3	3.4E-3	4.1E-3	
	Precipitation	71.83	67.37	81.78	41.56	71.18	53.42	46.08	75.00	47.82	50.20	67.68	
	Air Temp	0.72	1.04	1.31	1.22	1.34	0.84	0.83	1.07	0.70	1.21	1.13	
	Wind Speed	0.39	1.84	0.34	0.37	0.43	0.50	0.57	0.74	1.21	0.40	0.51	
<b>MSWEPv2.2</b>	Pressure	37.29	14.05	19.32	10.10	24.57	4.26	14.73	0.67	4.43	9.77	5.12	
	Solar rdn	209.7	8.9	8.1	10.3	52.8	21.7	28.3	14.5	13.5	24.1	18.9	
	Thermal rdn	151.99	10.93	9.76	-	-	15.05	9.02	-	-	-	-	
	Spec Humid	9.5E-6	2.5E-3	4.7E-3	2.2E-3	2.5E-3	2.7E-3	2.E-3	1.7E-3	1.3E-3	8.3E-4	1.7E-3	
	Precipitation	71.38	64.45	64.07	37.45	75.77	49.26	49.64	81.59	37.83	47.87	54.40	

### A.3.1 Seasonal errors in precipitation (mm)

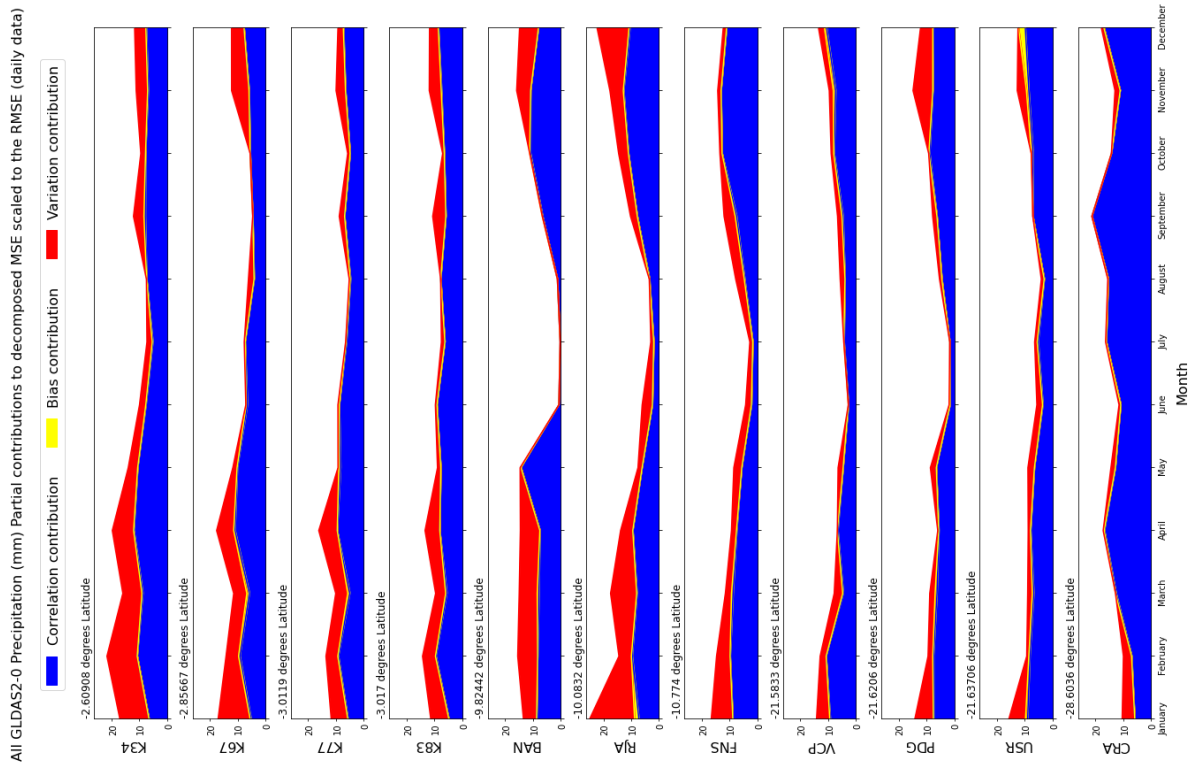
a)



b)



c)



d)

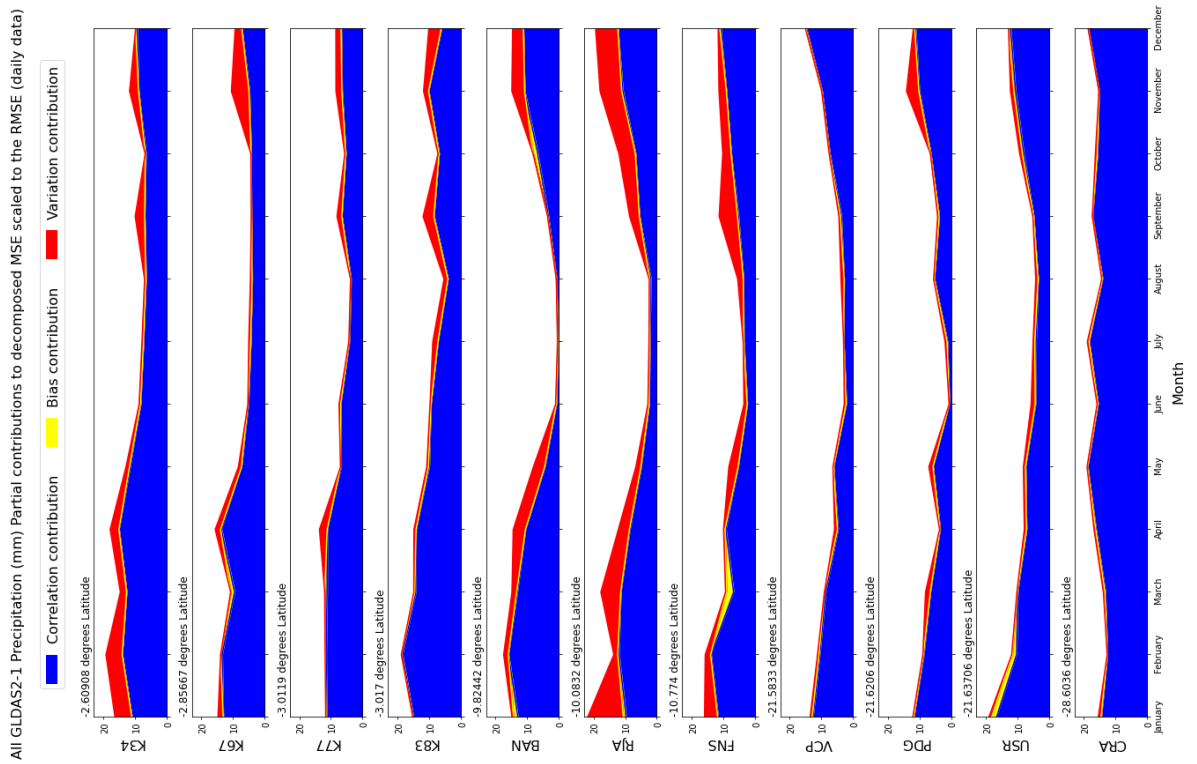
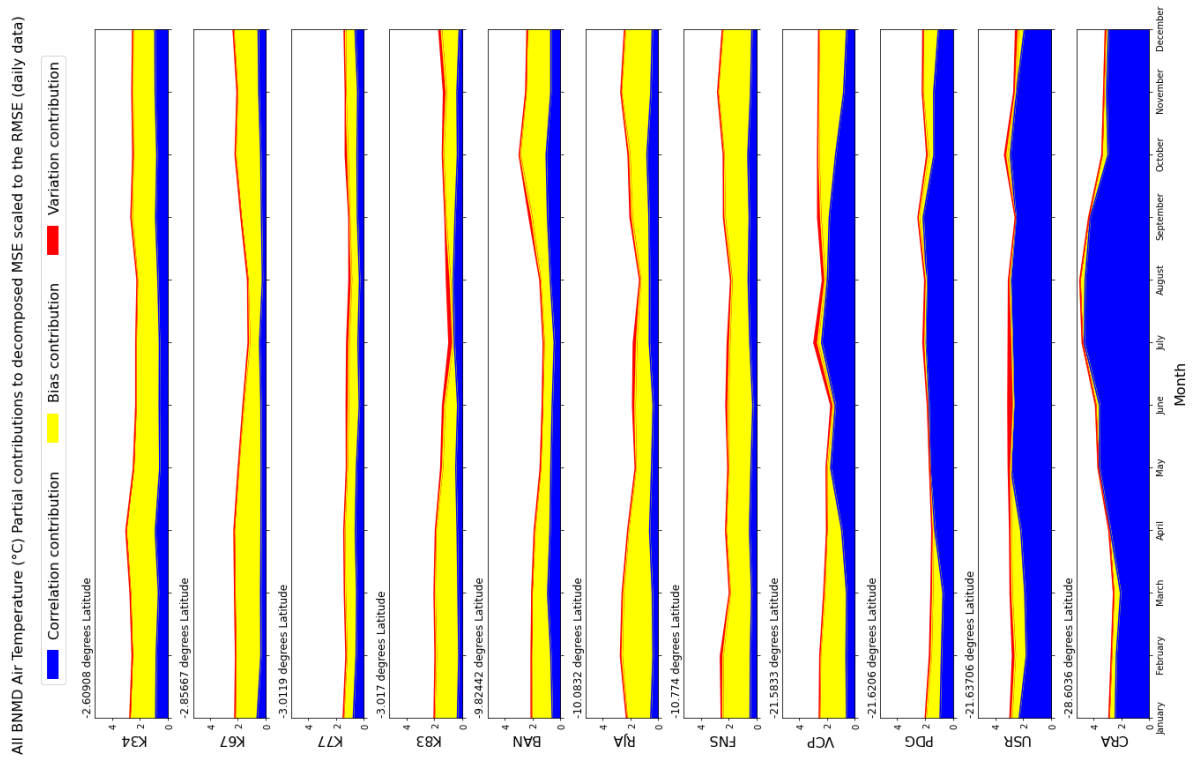


Figure A.1 Partial contributions to the MSE averaged by month over all operational observation years for precipitation across all sites for gridded datasets a) BNMD, b) ERA5-Land, c) GLDAS2.0, and d) GLDAS2.1. Sites are in descending order from distance from equator.

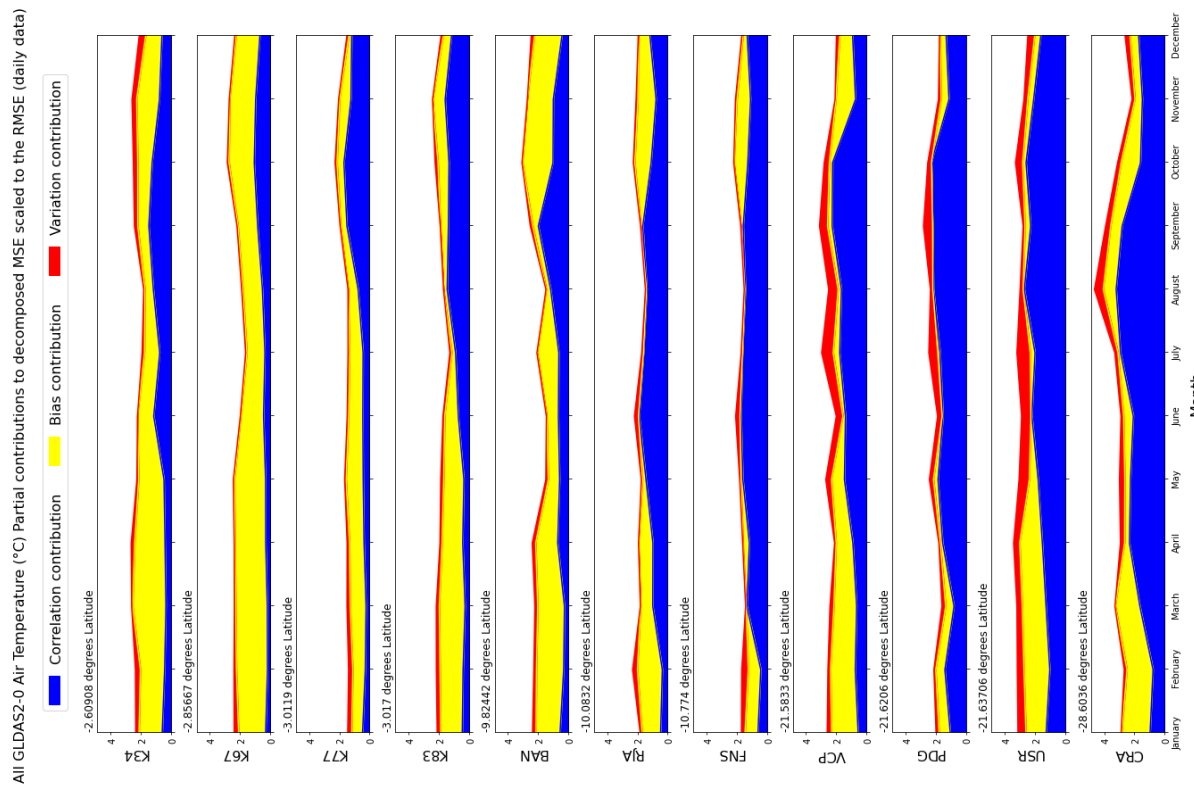


### A.3.2 Seasonal errors in Air Temperature (°C)

a)



b)



c)

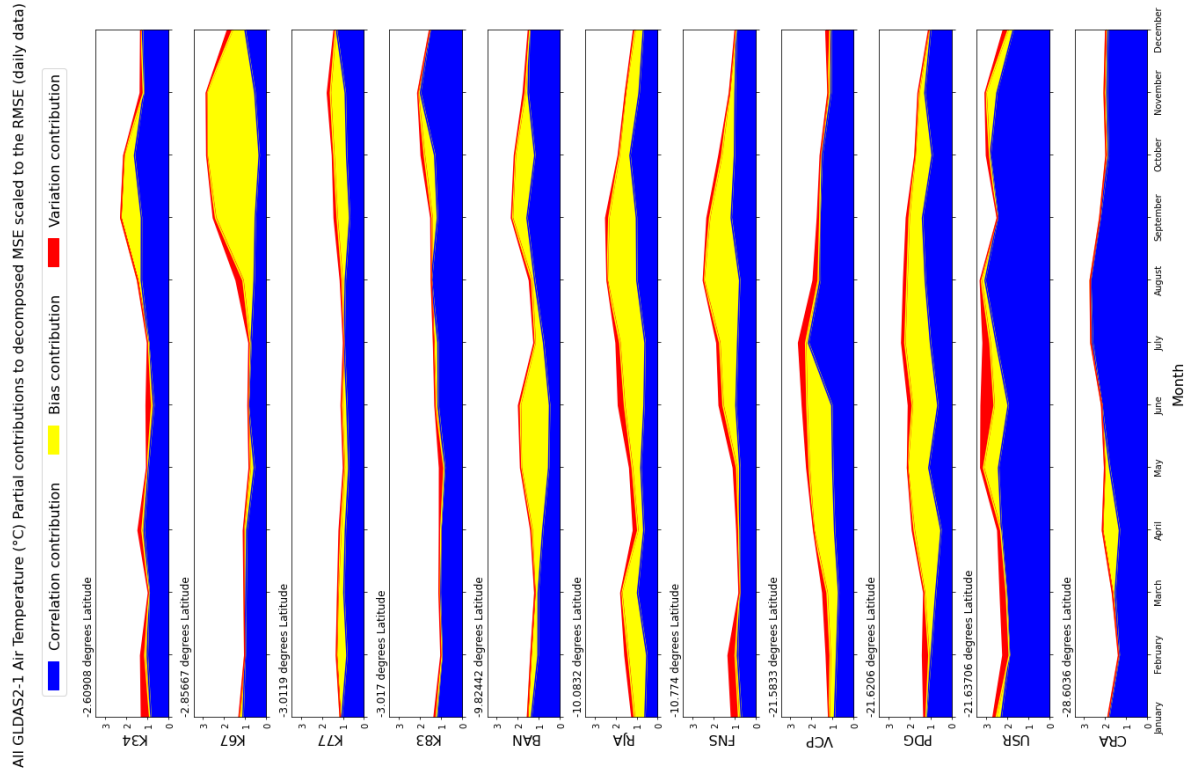
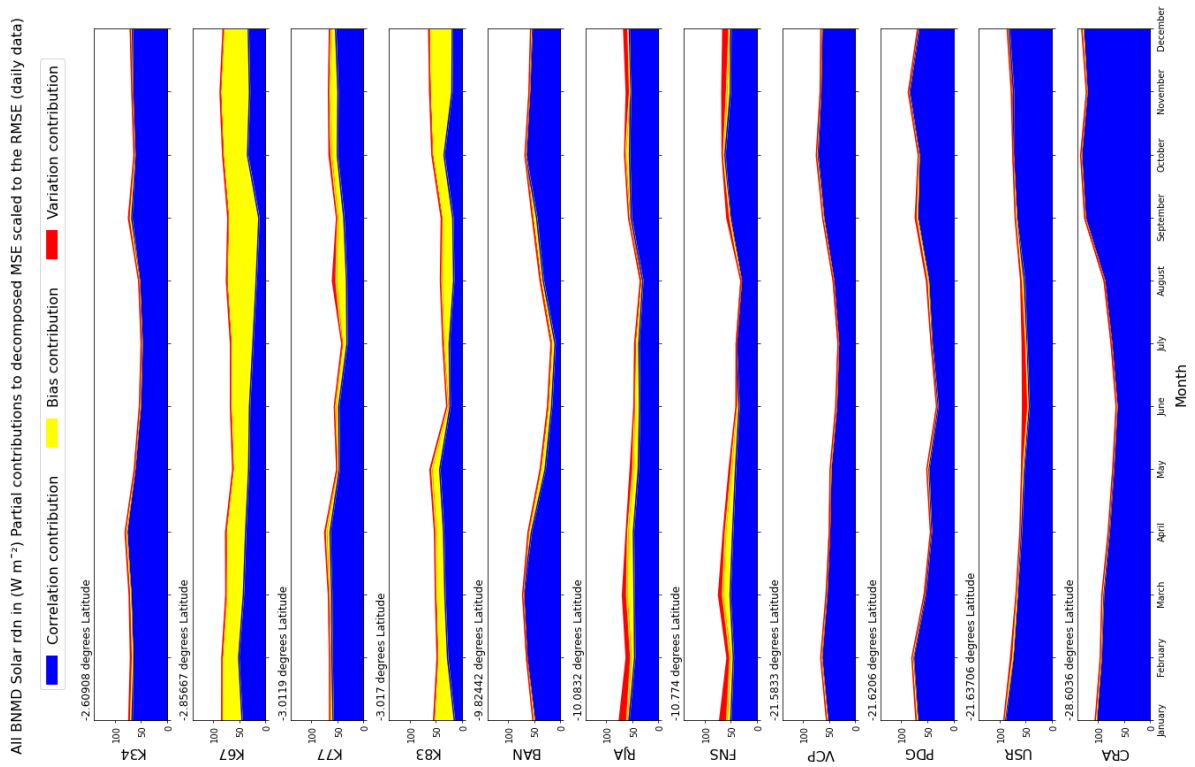


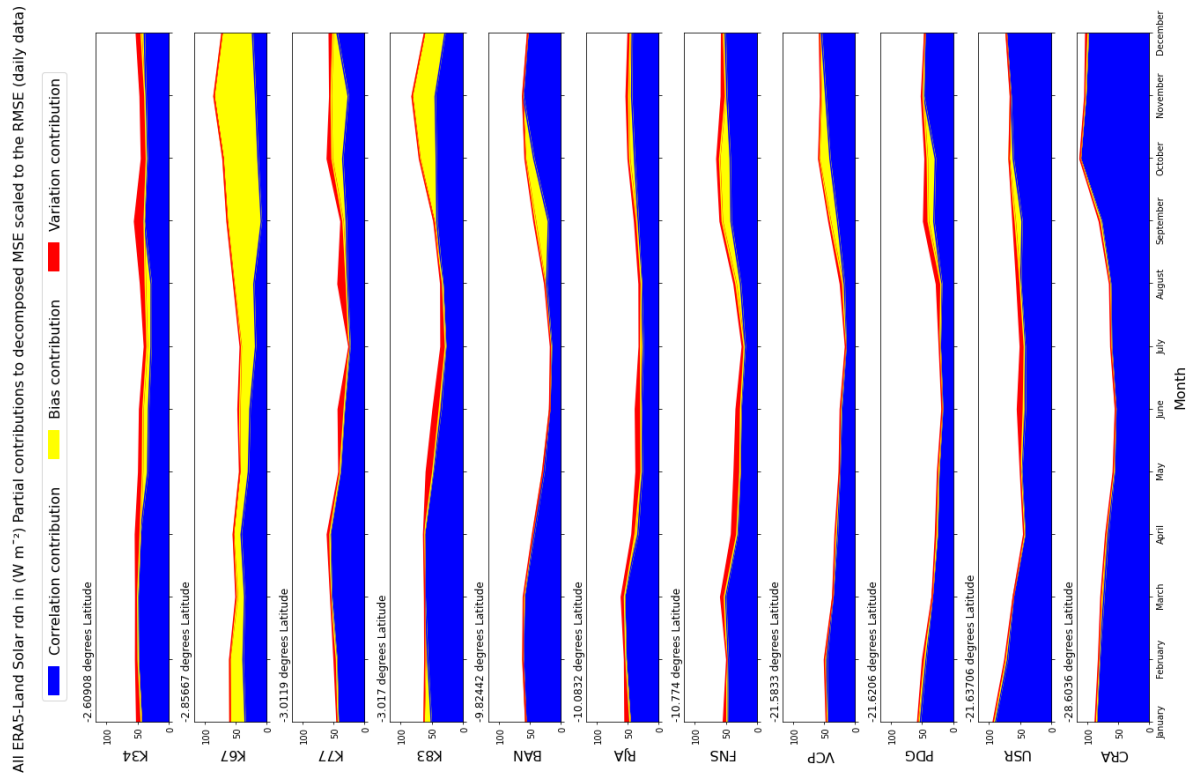
Figure A.2 Partial contributions to the MSE averaged by month over all operational observation years for Air Temperature across all sites for gridded datasets a) BNMD, b) GLDAS2.0, and c) GLDAS2.1. Sites are in descending order from distance from equator.

### A.3.3 Seasonal errors in Incoming Solar Radiation ( $W m^{-2}$ )

a)

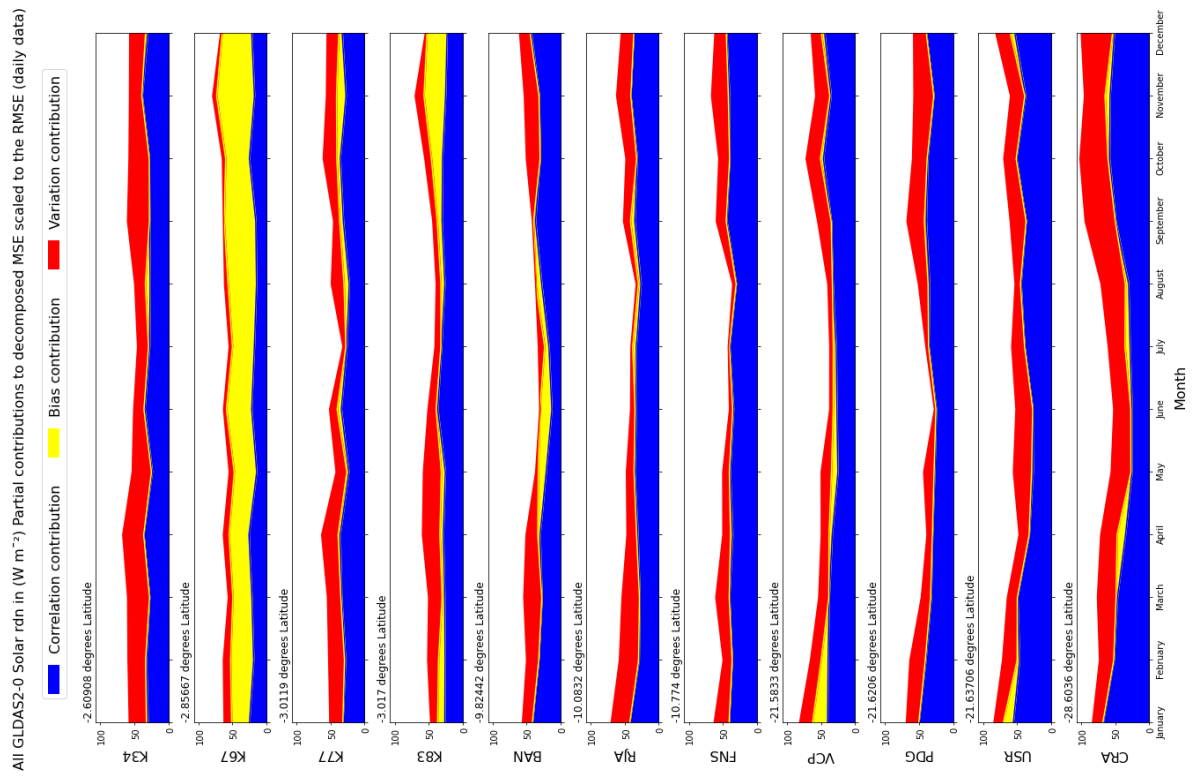


b)



## Appendix A: Supporting Information for Chapter 3

c)



d)

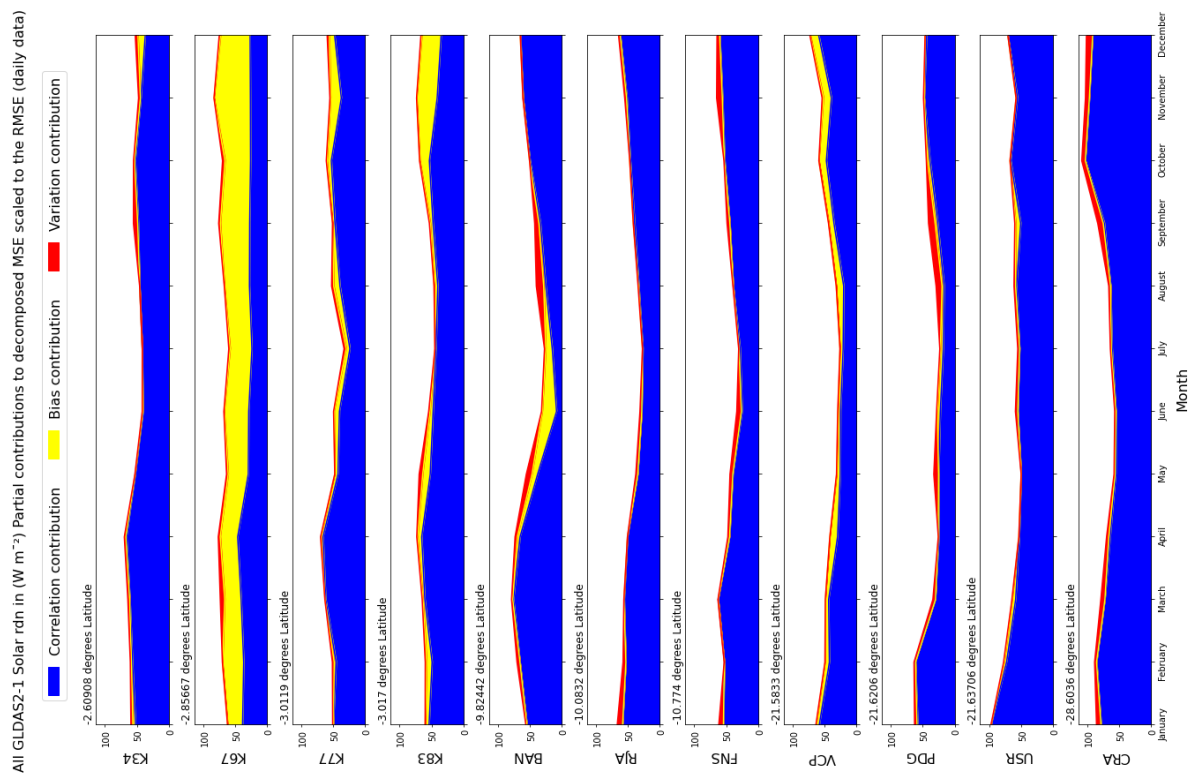
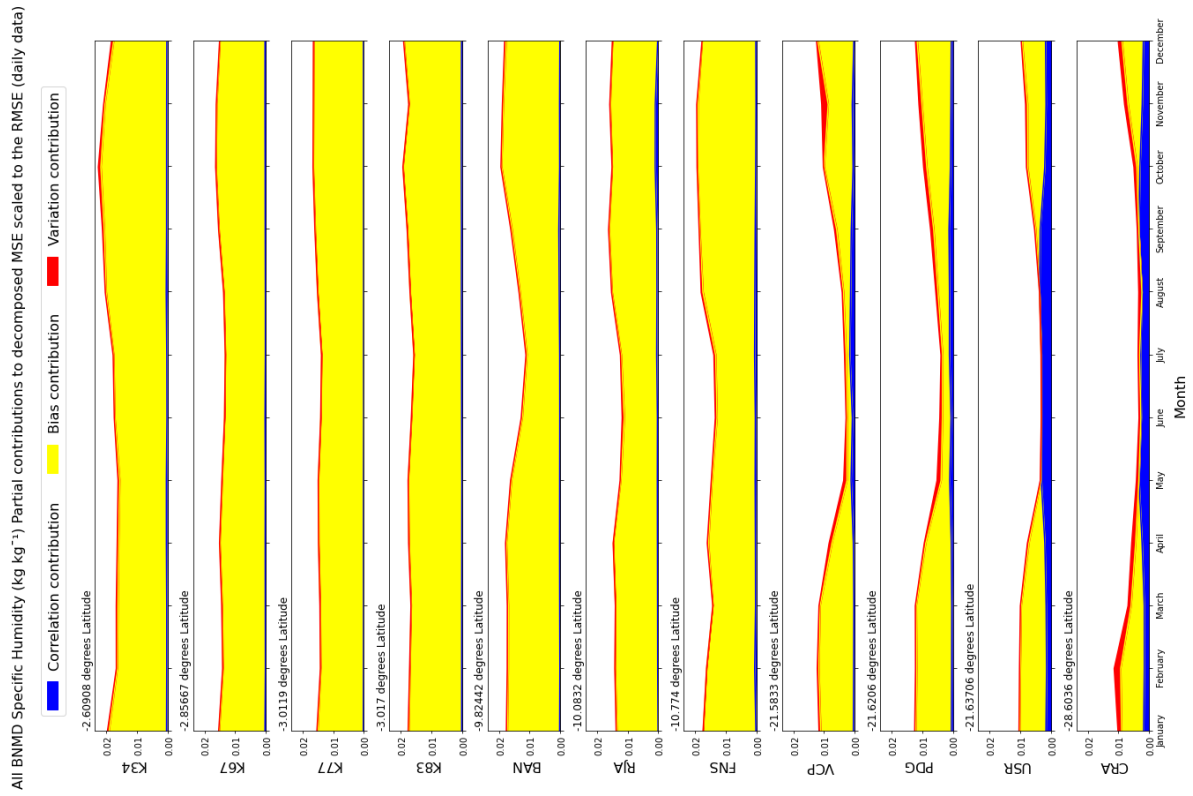


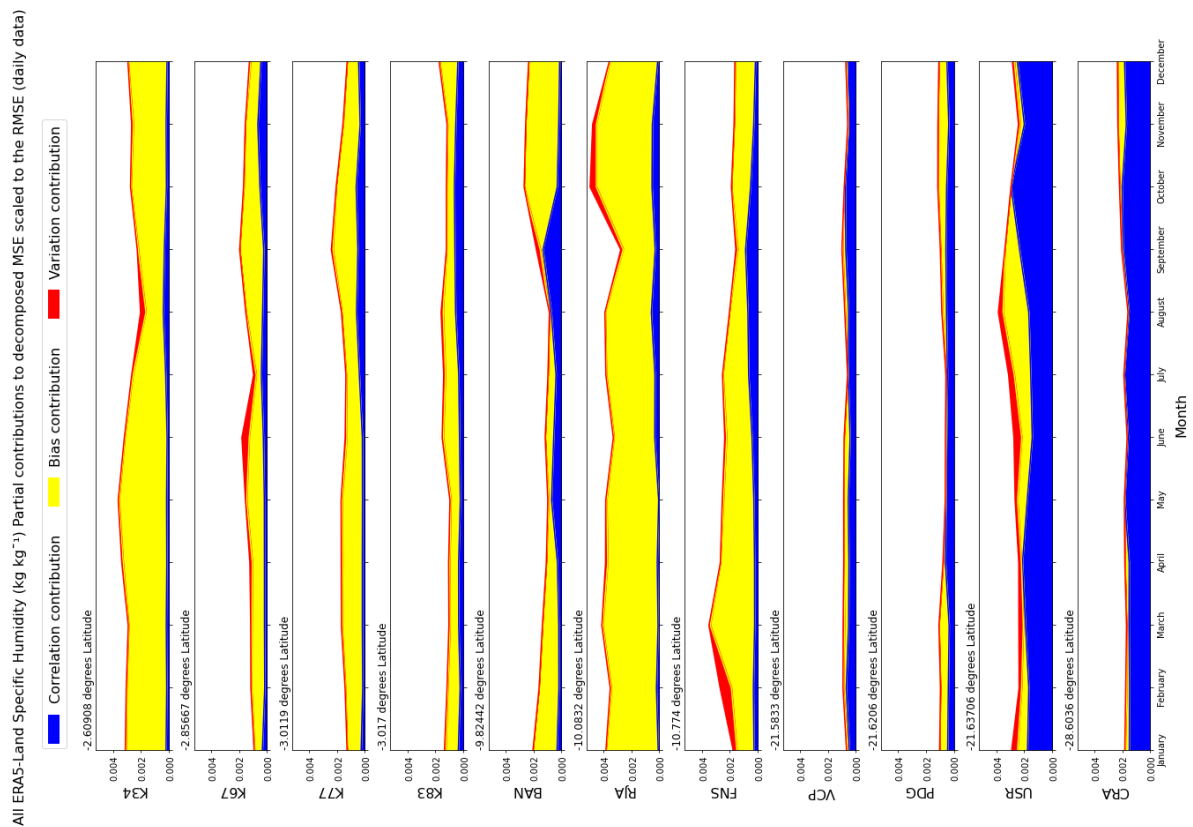
Figure A.3 Partial contributions to the MSE averaged by month over all operational observation years for precipitation across all sites for gridded datasets a) BNMD, b) ERA5-Land, c) GLDAS2.0, and d) GLDAS2.1. Sites are in descending order from distance from equator.

### A.3.4 Seasonal errors in specific humidity ( $\text{kg kg}^{-1}$ )

a)

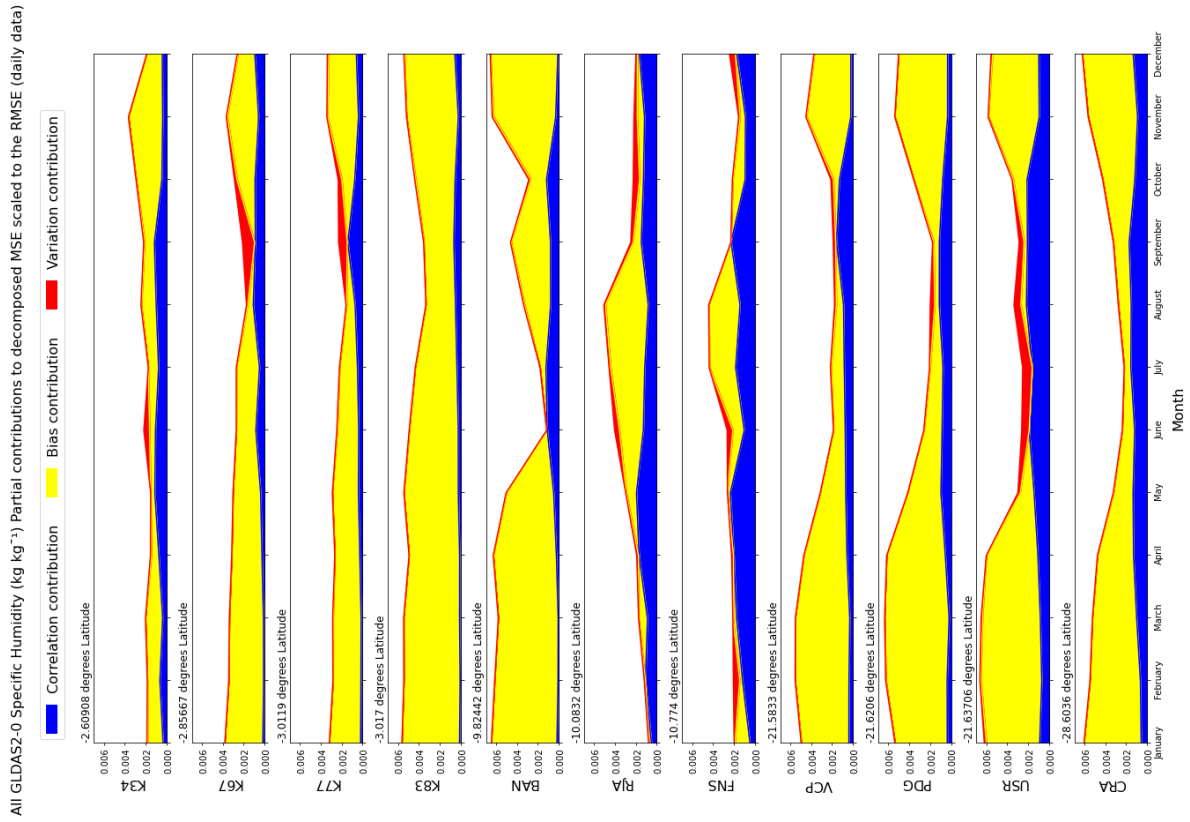


b)



Appendix A: Supporting Information for Chapter 3

c)



d)

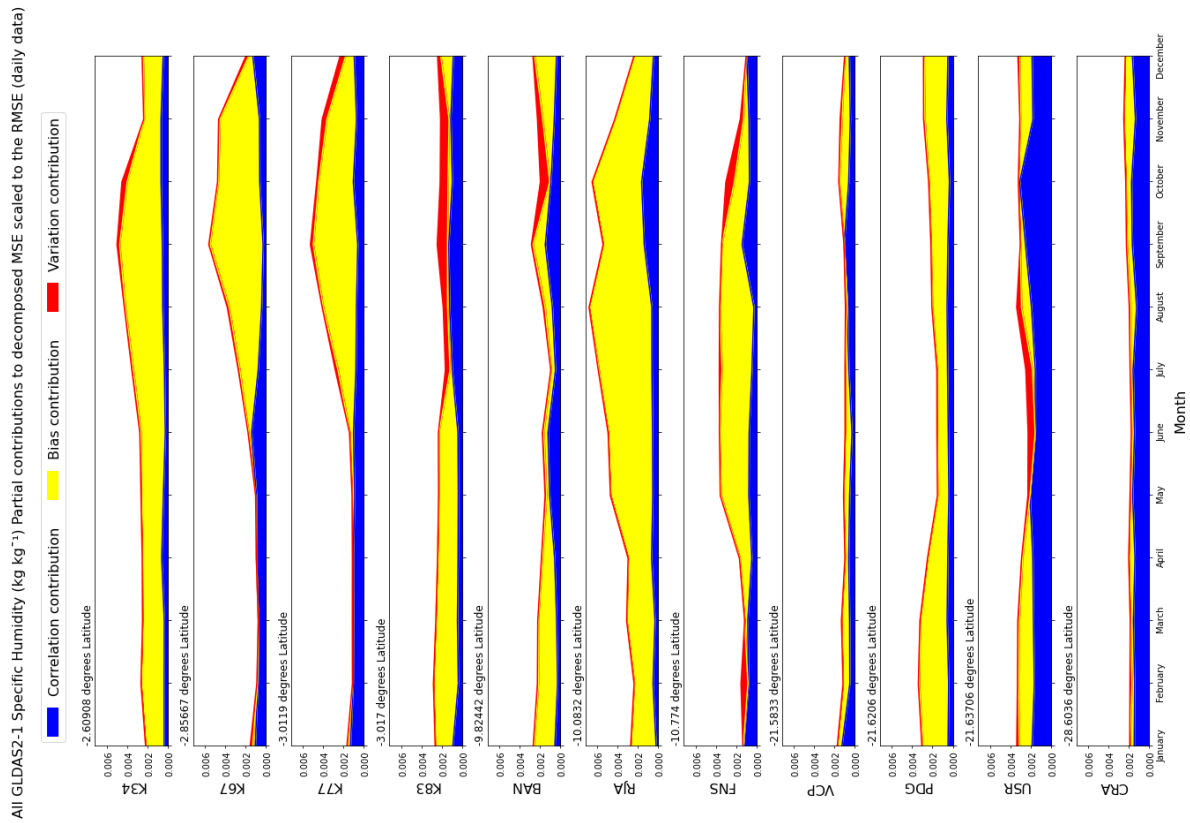


Figure A.4 Partial contributions to the MSE averaged by month over all operational observation years for specific humidity across all sites for gridded datasets a) BNMD, b) ERA5-Land, c) GLDAS2.0, and d) GLDAS2.1. Sites are in descending order from distance from equator.



## B. Appendix B: Supporting Information for Chapter 4

### B.1 Energy balance closure at RJA and FNS

In Chapter 4 we argued that the reason for a large bias between simulated and observed ET at sites K34, RJA and FNS was due to a lack of closing the energy balance causing an underprediction in observations. Through personal contact with von Randow, we acquired closed energy balance data for FNS and RJA, which involved using latent heat flux as a residue of the energy balance or the Bowen ratio to adjust sensible heat flux and latent heat flux to close the balance. Due to incomplete data, adjusted values were intermittent, and a complete dataset could not be compiled after performing closure adjustments. As such, it was only possible to assess the average diurnal cycle which we split into wet and dry seasons.

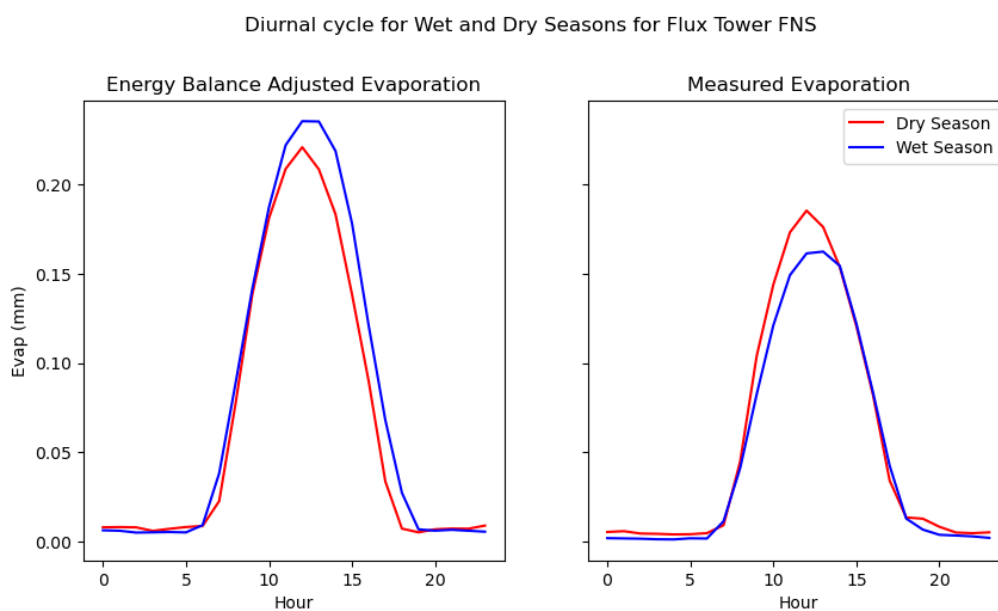


Figure B.1 Average diurnal cycles comparing evaporation after applying the energy balance closure to latent heat flux and unaltered measured latent heat flux at site FNS.



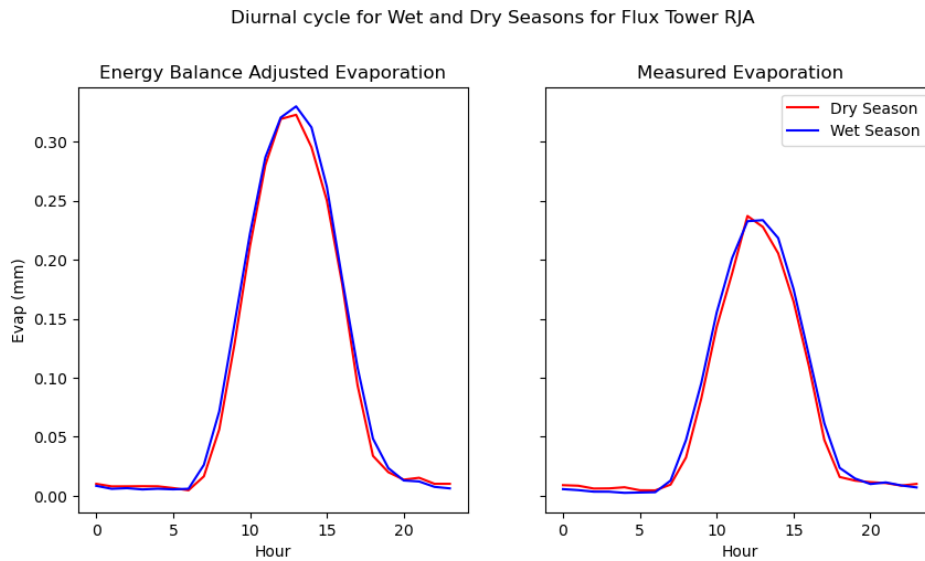


Figure B.2 Average diurnal cycles comparing evaporation after applying the energy balance closure to latent heat flux and unaltered measured latent heat flux at site RJA.

Both FNS (Figure B.1) and RJA (Figure B.2) show a large increase in evaporation after closing the energy balance explaining the bias between observed and simulated at each site. Furthermore, the seasonality of evaporation is reversed at site FNS after applying the closure again supporting modelled results.

## B.2 Parameter values for the Vegetation Optimality Model

A list of the parameters set for each site to achieve the results presented in Chapter 4 are presented in Table B.1.

## B.3 Data and model code availability

URL links to the data sources used in Chapter 4 and the Vegetation Optimality Model can be found in Table B.2.

Table B.1 Description of the parameters set in VOM to achieve the results presented in Chapter 4. From left to right the parameters are soil depth (m), capital gamma S (m), average channel bed elevation (m) (above the bottom of the profile), the slope to channel (radians), saturated hydraulic conductivity (m s<sup>-1</sup>), residual soil moisture, saturated soil moisture, the van Genuchten soil parameter n, the van Genuchten soil parameter alpha (1/m), the thickness of the soil sublayers (m), min and max tree root depth (m), min and max grass root depth (m), water transport cost factor (μmol m<sup>3</sup> s<sup>-1</sup>).

Site	Model		cz	cgs	zr	go	ksat	Θ <sub>r</sub>	Θ <sub>s</sub>	n	a	delz	rtdepth			rgdepth			crv
	Run	Run											min	max	min	max	min	max	
K34	#27		33	2	5	0.02	3.34E-7	0.18135	0.45469	1.53543	5.95964	0.2	0.05	7	0	0	0	5.00E-8	
K67	#26		40	2	5	0.02	3.34E-7	0.23003	0.51454	1.58093	4.46687	0.2	0.05	14	0	0	0	2.00E-7	
K83	#120		40	2	5	0.02	3.34E-7	0.23003	0.51454	1.58093	4.46687	0.2	1	15	0	0	0	2.00E-7	
BAN	#14		8	2	4	0.02	6.73E-6	0.18296	0.47791	1.42782	2.91314	0.2	0	4	0	1	0	2.00E-7	
RJA	#14		38	2	5	0.02	4.82E-6	0.2188	0.49146	1.4397	3.82617	0.2	0.05	12	0	0	0	1.00E-7	
PDG	#7		30	2	5	0.02	7.25E-6	0.1796	0.45422	1.49727	3.62293	0.2	1	13	0.05	2	0	8.00E-7	
K77	#6		8	2	5	0.02	7.06E-6	0.23003	0.51454	1.58093	4.46687	0.2	0	0	0.05	4	0	1.10E-6	
FNS	#31		20	2	5	0.02	7.47E-6	0.15532	0.45826	1.41704	2.80064	0.2	0	0	0.05	6	0	8.00E-7	
VCP	#14		35	2	5	0.02	7.25E-6	0.1796	0.45422	1.49727	3.62293	0.2	1	7	0.05	2	0	6.00E-7	
USR	#11		15	2	5	0.02	7.25E-6	0.1796	0.45422	1.49727	3.62293	0.2	0	0	0.05	4	0	1.20E-6	
CRA	#6		39	2	5	0.02	1.14E-5	0.14318	0.44485	1.56442	3.82237	0.2	0	0	0.05	2	0	8.00E-8	

Table B.2 Data Sources used in Chapter 4

Data	Source
Global Water Table Depths	<a href="http://thredds-gfml.usc.es/thredds/catalog/GLOBAL.WTDFTP/annualmeans/catalog.html">http://thredds-gfml.usc.es/thredds/catalog/GLOBAL.WTDFTP/annualmeans/catalog.html</a>
Global Max root depths	<a href="https://wci.earth2observe.eu/thredds/catalog/usc/root-depth/catalog.html">https://wci.earth2observe.eu/thredds/catalog/usc/root-depth/catalog.html</a>
HYBRAS database	<a href="https://geosgb.cprm.gov.br/geosgb/downloads/en.html">https://geosgb.cprm.gov.br/geosgb/downloads/en.html</a>
South American hydraulic parameter map	<a href="https://catalogue.ceh.ac.uk/datastore/eidc/hub/4078678b-768f-43ff-abba-b87712f648e9/">https://catalogue.ceh.ac.uk/datastore/eidc/hub/4078678b-768f-43ff-abba-b87712f648e9/</a>
VOM code	<a href="https://github.com/schymans/VOM">https://github.com/schymans/VOM</a>



## C. Appendix C: Supporting Information for Chapter 5

### C.1 Results for sites excluded sites

In Chapter 5, the seasonally flooded dry forest site, BAN and the Eucalyptus site, VCP were excluded from analysis as the VOM was not able to capture the correct hydrological processes. Model predictions failed because of the model's inability to account for seasonal flooding or the high ET rates of Eucalyptus trees. However, the VOM can still provide useful information and insights into trends in ET for ecosystems with similar climatic characteristics. For this reason, simulations were run on these sites to evaluate how seasonality might change in response to  $e\text{CO}_2$ . The results are presented below (Figure C.1, Figure C.2, Table C.1).

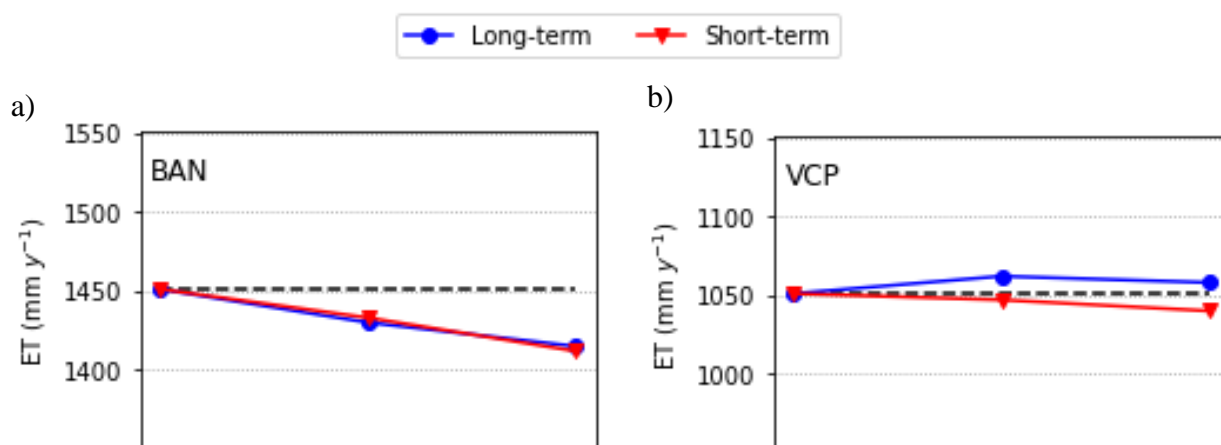


Figure C.1 Simulated mean annual ET rates for varying  $C_a$  at excluded sites BAN and VCP. 'Long-term' (blue) refers to simulations where all vegetation properties were optimised for each  $C_a$ . 'Short-term' (red) refers to simulations where 'long-term' optimised parameters for  $C_a = 339$  ppm were kept for  $C_a = 377$  and  $416$  ppm simulations. The black dashed line is ET at  $C_a = 339$  ppm simulations for reference.

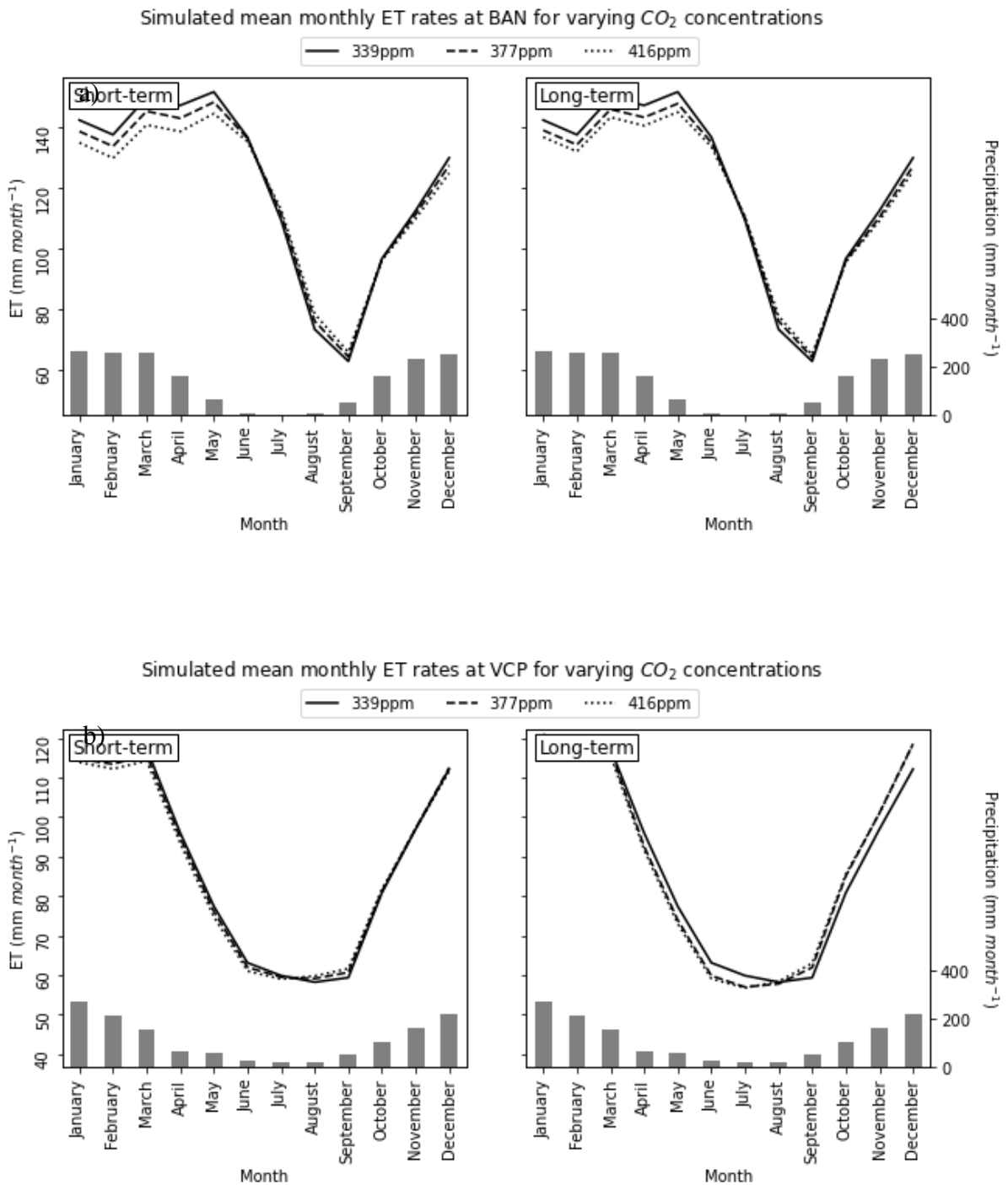


Figure C.2 Simulated mean monthly ET rates for varying  $C_o$  at excluded sites a) BAN and b) VCP. 'Long-term' (right) refers to simulations where all vegetation properties were optimised for each  $C_o$ . 'Short-term' (left) refers to simulations where 'long-term' optimised parameters for  $C_o = 339$  ppm were kept for  $C_o = 377$  and  $416$  ppm simulations. Grey bars represent precipitation for reference between water limiting and energy limiting periods.

Table C.1 Simulated responses to increasing  $C_a$  for excluded sites BAN and VCP. The first column in each variable block gives actual values for  $C_a = 339$  ppm, while the subsequent columns in italics give the percentage difference from this value. Decreases, or negative differences, are shown in red. P, precipitation, ET, evapotranspiration, Q, discharge, WUE, water use efficiency (Equation(5-1)), FVC, fractional vegetation cover of all vegetation (perennial and seasonal), RAI, root area index (fine root surface area per ground area),  $R_t$  depth, maximum rooting depth of perennials,  $R_g$  depth, maximum rooting depth of seasonal vegetation. a) shows vegetation short-term adaptation, b) shows long-term adaptation. Shaded cells indicate that the means of ET were significantly different ( $p < 0.05$ ) when compared to the mean of the lowest  $C_a$  run (339ppm).

Long-term																			
Name	P (mm year <sup>-1</sup> )	Et (mm year <sup>-1</sup> )		Q (mm year <sup>-1</sup> )	WUE (mmol mol <sup>-1</sup> )	FPC (%)	Rt depth		Rg depth										
		339	377				339	377	339	377	339	377	416	416					
BAN	1720	1451	1430	1415	278	299	314	339	377	416	339	377	416	339	377	416			
VCP	1374	1051	1062	1058	282	276	279	0.99	3.17	3.49	3.77	0.99	0.99	2.8	2.8	2.8	0.8	0.8	0.8
								0.98	5.01	5.39	5.82	0.99	0.99	2.51	2.75	2.75	0.5	1	1

Medium-term														
Name	P (mm year <sup>-1</sup> )	Et (mm year <sup>-1</sup> )		Q (mm year <sup>-1</sup> )	WUE (mmol mol <sup>-1</sup> )	FPC (%)								
		339	377				339	377	416	339	377	416		
BAN	1720	1451	1433	1412	278	296	317	0.99	3.17	3.48	3.78	0.99	0.99	1.00
VCP	1374	1051	1047	1040	282	286	292	0.98	5.01	5.47	5.93	0.99	0.99	0.99



## References

- Alijanian, M., G.R. Rakhshandehroo, A.Mishra, & Dehghani, M., (2019). Evaluation of remotely sensed precipitation estimates using PERSIANN-CDR and MSWEP for spatio-temporal drought assessment over Iran. *Journal of Hydrology*, 579, 124189.
- Allasia, D. G., Cláudio Da Silva, B., & Tucci, C. E. M. (2016). *Large basin simulation experience in South America Métodos para Estimativa de Recarga View project SAFAS-South American Flood Awareness System View project*. <https://www.researchgate.net/publication/266049080>
- Allen, Richard & Pereira, L. & Raes, D. & Smith, M.. (1998). FAO Irrigation and drainage paper No. 56. Rome: Food and Agriculture Organization of the United Nations. 56. 26-40.
- Almeida, A. C., Smethurst, P. J., Siggins, A., Cavalcante, R. B. L., & Borges, N. (2016). Quantifying the effects of Eucalyptus plantations and management on water resources at plot and catchment scales. *Hydrological Processes*, 30(25), 4687–4703.
- Alvares, C. A., Stape, J. L., Sentelhas, P. C., De Moraes Gonçalves, J. L., & Sparovek, G. (2013). Köppen's climate classification map for Brazil. *Meteorologische Zeitschrift*, 22(6), 711–728.
- Alves, L. M., Chadwick, R., Moise, A., Brown, J., & Marengo, J. A. (2021). Assessment of rainfall variability and future change in Brazil across multiple timescales. *International Journal of Climatology*, 41(S1), E1875–E1888.



## References

- Anache, J. A. A., Wendland, E., Rosalem, L. M. P., Youlton, C., & Oliveira, P. T. S. (2019). Hydrological trade-offs due to different land covers and land uses in the Brazilian Cerrado. *Hydrology and Earth System Sciences*, 23(3), 1263–1279.
- Anderegg, W. R. L., Wolf, A., Arango-Velez, A., Choat, B., Chmura, D. J., Jansen, S., Kolb, T., Li, S., Meinzer, F. C., Pita, P., Resco de Dios, V., Sperry, J. S., Wolfe, B. T., & Pacala, S. (2018). Woody plants optimise stomatal behaviour relative to hydraulic risk. *Ecology Letters*, 21(7), 968–977.
- Andrade, R. O. (2019). Alarming surge in Amazon fires prompts global outcry. Nature editorial. <https://doi.org/10.1038/d41586-019-02537-0>
- Andreae, M. O., *et al.* (2002). Biogeochemical cycling of carbon, water, energy, trace gases, and aerosols in Amazonia: The LBA-EUSTACH experiments. *Journal of Geophysical Research Atmospheres*, 107(20).
- Araújo, A. C. (2002). Comparative measurements of carbon dioxide fluxes from two nearby towers in a central Amazonian rainforest: The Manaus LBA site. *Journal of Geophysical Research*, 107(D20). <https://doi.org/10.1029/2001jd000676>
- Araújo, A. C., Nobre, A. D., Kruijt, B., Elbers, J. A., Dallarosa, R., Stefani, P., von Randow, C., Manzi, A. O., Culf, A. D., Gash, J. H. C., Valentini, R., & Kabat, P. (2002). Comparative measurements of carbon dioxide fluxes from two nearby towers in a central Amazonian rainforest: The Manaus LBA site. *Journal of Geophysical Research*, 107(D20).
- Araújo, A.C., von Randow, C., Restrepo-Coupe, N. (2016). Ecosystem–Atmosphere Exchanges of CO<sub>2</sub> in Dense and Open ‘Terra Firme’ Rainforests in Brazilian Amazonia. In: Nagy, L., Forsberg, B., Artaxo, P. (eds) *Interactions Between Biosphere, Atmosphere and Human Land Use in the Amazon Basin*. Ecological Studies, vol 227. Springer, Berlin, Heidelberg.
- Arnell, N. W. (1999). A simple water balance model for the simulation of streamflow over a large geographic domain. *Journal of Hydrology*, 217, 314–335.

## References

- Aubinet, M., Vesala, T. and Papale, D. eds., (2012). *Eddy covariance: a practical guide to measurement and data analysis*. Springer Science & Business Media.
- Ávila, L., Silveira, R., Campos, A., Rogiski, N., Gonçalves, J., Scortegagna, A., Freitas, C., Aver, C., & Fan, F. (2022). Comparative Evaluation of Five Hydrological Models in a Large-Scale and Tropical River Basin. *Water (Switzerland)*, 14(19). <https://doi.org/10.3390/w14193013>
- Avila-Diaz, A., Benezoli, V., Justino, F., Torres, R., & Wilson, A. (2020). Assessing current and future trends of climate extremes across Brazil based on reanalyses and earth system model projections. *Climate Dynamics*, 55(5–6), 1403–1426. <https://doi.org/10.1007/s00382-020-05333-z>
- Baez-Villanueva, O.M., M. Zambrano-Bigiarini, L. Ribbe, A. Nauditt, J.D. Giraldo-Osorio, & Thinh, N.X. (2018). Temporal and spatial evaluation of satellite rainfall estimates over different regions in Latin-America. *Atmospheric Research*, 213, 34-50.
- Bai, P. *et al.* (2016). Assessment of the influences of different potential evapotranspiration inputs on the performance of monthly hydrological models under different climatic conditions, *Journal of Hydrometeorology*, 17(8), 2259–2274.
- Baldocchi, D. D. and Vogel, C. A. (1996). Energy and CO<sub>2</sub> flux densities above and below a temperate broad-leaved forest and a boreal pine forest. *Tree Physiology*, 16, 5-16.
- Baldocchi, D. D., Vogel, C. A., and Hall, B. (1997) Seasonal variation of energy and water vapor exchange rates above and below a boreal jack pine forest canopy, *J. Geophys. Res.*, 102(D24).
- Baldocchi, D., and Coauthors, (2001) Fluxnet: A new tool to study the temporal and spatial variability of ecosystem-scale carbon dioxide, water vapor, and energy flux densities. *Bull. Amer. Meteor. Soc.*, 82, 2415–2434.
- Batalha, M. A. P. L. (1997). *Análise da Vegetação de ARIE Cerrado Pé-de-Gigante (Santa Rita do Passa Quatro, SP)* (Doctoral dissertation, Universidade de São Paulo).

## References

- Battisti, R., F.D. Bender, P.C. Sentelhas. (2018). Assessment of different gridded weather data for soybean yield simulations in Brazil. *Theoretical and Applied Climatology*, 135, 237-247.
- Beck, H. E., Pan, M., Miralles, D. G., Reichle, R. H., Dorigo, W. A., Hahn, S., ... & Wood, E. F. (2021). Evaluation of 18 satellite-and model-based soil moisture products using in situ measurements from 826 sensors. *Hydrology and Earth System Sciences*, 25(1), 17-40.
- Beck, H. E., Wood, E. F., Pan, M. & Fisher, C. K. (2019). MSWEP V2 Global 3-Hourly 0.1° Precipitation: Methodology and Quantitative Assessment. *Bulletin of the American Meteorological Society*, 100, 473-500.
- Bender, F.D. and Sentelhas, P.C. (2018). Solar radiation models and gridded databases to fill gaps in weather series and to project climate change in Brazil. *Advances in Meteorology*, 2018, 1-15.
- Betts, R. A., Arnell, N. W., Boorman, P. M., Cornell, S. E., House, J. I., Kaye, N. R., et al. (2012). Climate change impacts and adaptation: an Earth System view, in *Understanding the Earth System*, eds S. E. Cornell, I. C. Prentice, J. I. House, and C. J. Downy (Cambridge: Cambridge University Press), 296.
- Betts, R.A. et al. (2007). Projected increase in continental runoff due to plant responses to increasing carbon dioxide, *Nature*, 448(7157), 1037–1041.
- Betts, R.A., Malhi, Y. and Roberts, J.T. (2008). The future of the Amazon: New perspectives from climate, ecosystem and social sciences, in *Philosophical Transactions of the Royal Society B: Biological Sciences*. Royal Society, 1729–1735.
- Beven, K. (2001). How far can we go in distributed hydrological modelling? *Hydrology and Earth System Sciences*, 5(1), 1-12.
- Beven, K. and Westerberg, I. (2011). On red herrings and real herrings: disinformation and information in hydrological inference. *Hydrological Processes*, 25(10), 1676-1680.

## References

- Biswas, A.K., Tortajada, C. (2022). Ensuring Water Security Under Climate Change. In: Biswas, A.K., Tortajada, C. (eds) Water Security Under Climate Change. Water Resources Development and Management. Springer, Singapore.
- Bitencourt, M. D., De Mesquita, H. N., Kuntschik, G., Da Rocha, H. R., & Furley, P. A. (2007). Cerrado vegetation study using optical and radar remote sensing: Two Brazilian case studies. *Canadian Journal of Remote Sensing*, 33(6), 468–480.
- Blankenau, P. A., Kilic, A., & Allen, R. (2020). An evaluation of gridded weather data sets for the purpose of estimating reference evapotranspiration in the United States. *Agricultural Water Management*, 242.
- Bolton, D. (1980). The Computation of Equivalent Potential Temperature. *Monthly Weather Review*, 108, 1046–1053.
- Bonal, D., Burban, B., Stahl, C., Wagner, F., & Hérault, B. (2016). The response of tropical rainforests to drought—lessons from recent research and future prospects. *Annals of Forest Science*, 73(1), 27–44.
- Bonan, G.B. (2008). Forests and Climate Change: Forcings, Feedbacks, and the Climate Benefits of Forests, *Science, New Series*, 320(5882), 1444–1449.
- Bond, W.J. and Midgley, G.F. (2000). A proposed CO<sub>2</sub>-controlled mechanism of woody plant invasion in grasslands and savannas, *Global Change Biology*, 6(8), 865–869.
- Bordignon, L., Faria, A. P., França, M. G., & Fernandes, G. W. (2019). Osmotic stress at membrane level and photosystem II activity in two C<sub>4</sub> plants after growth in elevated CO<sub>2</sub> and temperature. *Annals of Applied Biology*, 174(2), 113-122.
- Borma, L.D.S., Da Rocha, H.R., Cabral, O.M., Von Randow, C., Collicchio, E., Kurzatkowski, D., Brugger, P.J., Freitas, H., Tannus, R., Oliveira, L. and Rennó, C.D. (2009). Atmosphere and hydrological controls of the evapotranspiration over a floodplain forest in the Bananal Island region, Amazonia. *Journal of Geophysical Research: Biogeosciences*, 114(G1).

## References

- Bortolotto, R. P., Telmo, J. C. A., Douglas, D. N., Cristiano, K., Debora, R., Jackson, E. F., Klaus, R., Mauricio, P. B. P., & Rodrigo, da S. N. (2015). Soil carbon dioxide flux in a no-tillage winter system. *African Journal of Agricultural Research*, 10(6), 450–457.
- Bosch, J. M., & Hewlett, J. D. (1982). A review of catchment experiments to determine the effect of vegetation changes on water yield and evapotranspiration. In *Journal of Hydrology* 55, 3-23.
- Brunke, M. A., Fairall, C. W., Zend, X., Eymard, L., and Curry, J. A. (2003). Which Bulk Aerodynamic Algorithms are Least Problematic in Computing Ocean Surface Turbulent Fluxes? *Journal of Climate*, 16, 4, 619-635.
- Brunner, I., Herzog, C., Dawes, M. A., Arend, M., & Sperisen, C. (2015). How tree roots respond to drought. *Frontiers in Plant Science*, 6(547) 1-16.
- Bruno, R. D., da Rocha, H. R., de Freitas, H. C., Goulden, M. L., & Miller, S. D. (2006). Soil moisture dynamics in an eastern Amazonian tropical forest, *Hydrological Processes*, 20(12), 2477–2489.
- Buckley, T.N. and Schymanski, S.J. (2014). Stomatal optimisation in relation to atmospheric CO<sub>2</sub>, *New Phytologist*, 201(2), 372–377.
- Budyko, M. (1974). *Climate and Life*, Academic Press, New York and London, edited by: Miller, D. H., ISBN 9780121394509.
- Cabral, O. M. R., Gash, J. H. C., Rocha, H. R., Marsden, C., Ligo, M. A. V., Freitas, H. C., Tatsch, J. D., & Gomes, E. (2011). Fluxes of CO<sub>2</sub> above a plantation of Eucalyptus in southeast Brazil. *Agricultural and Forest Meteorology*, 151(1), 49–59.
- Cabral, O. M. R., Rocha, H. R., Gash, J. H., Ligo, M. A. V., Ramos, N. P., Packer, A. P., & Batista, E. R. (2013). Fluxes of CO<sub>2</sub> above a sugarcane plantation in Brazil. *Agricultural and Forest Meteorology*, 182–183, 54–66.

## References

- Cabral, O.M., da Rocha, H.R., Gash, J.H., Freitas, H.C. and Ligo, M.A. (2015). Water and energy fluxes from a woodland savanna (cerrado) in southeast Brazil. *Journal of Hydrology: Regional Studies*, 4, 22-40.
- Cabral, O.M., da Rocha, H.R., Gash, J.H., Ligo, M.A., Freitas, H.C. and Tatsch, J.D. (2010). The energy and water balance of a Eucalyptus plantation in southeast Brazil. *Journal of Hydrology*, 388(3-4), 208-216.
- Cabral, O.M., da Rocha, H.R., Gash, J.H., Ligo, M.A., Tatsch, J.D., Freitas, H.C. and Brasílio, E. (2012). Water use in a sugarcane plantation. *Gcb Bioenergy*, 4(5), 555-565.
- Cantoni, E., Trambly, Y., Grimaldi, S., Salamon, P., Dakhlaoui, H., Dezetter, A., & Thiémig, V. (2022). Hydrological performance of the ERA5 reanalysis for flood modeling in Tunisia with the LISFLOOD and GR4J models. *Journal of Hydrology: Regional Studies*, 42.
- Castello, L., Mcgrath, D. G., Hess, L. L., Coe, M. T., Lefebvre, P. A., Petry, P., Macedo, M. N., Renó, V. F., & Arantes, C. C. (2013). The vulnerability of Amazon freshwater ecosystems, *Conservation Letters*, 6(4), 217–229.
- Caylor, K.K., Scanlon, T.M. and Rodriguez-Iturbe, I. (2009). Ecohydrological optimization of pattern and processes in water-limited ecosystems: A trade-off-based hypothesis, *Water Resources Research*, 45(8).
- Chavez, L. F., Amado, T. J. C., Bayer, C., La Scala, N. J., Escobar, L. F., Fiorin, J. E., & Campos, B. H. C. D. (2009). Carbon dioxide efflux in a Rhodic Hapludox as affected by tillage systems in southern Brazil. *Revista Brasileira de Ciência do Solo*, 33, 325-334.
- Chen, L., Dirmeyer, P. A., Guo, Z., & Schultz, N. M. (2018). Pairing FLUXNET sites to validate model representations of land-use/land-cover change. *Hydrology and Earth System Sciences*, 22(1), 111–125.
- Chen, L., Hu, Z., Du, X., Khan, M. Y. A., Li, X., & Wen, J. (2022). An Optimality-Based Spatial Explicit Ecohydrological Model at Watershed Scale: Model Description and Test in a Semiarid Grassland Ecosystem. *Frontiers in Environmental Science*, 10.

## References

- Christoffersen, B.O. *et al.* (2014). Mechanisms of water supply and vegetation demand govern the seasonality and magnitude of evapotranspiration in Amazonia and Cerrado, *Agricultural and Forest Meteorology*, 191, 33–50.
- Chu, H., Luo, X., Ouyang, Z., Chan, W. S., Dengel, S., Biraud, S. C., Torn, M. S., Metzger, S., Kumar, J., Arain, M. A., Arkebauer, T. J., Baldocchi, D., Bernacchi, C., Billesbach, D., Black, T. A., Blanken, P. D., Bohrer, G., Bracho, R., Brown, S., ... Zona, D. (2021). Representativeness of Eddy-Covariance flux footprints for areas surrounding AmeriFlux sites. *Agricultural and Forest Meteorology*, 301–302.
- Churkina, G., Running, S. W., & Schloss, A. L. (1999). Comparing global models of terrestrial net primary productivity (NPP): The importance of water availability. *Global Change Biology*, 5(SUPPL. 1), 46–55.
- Coe, M. T., Latrubesse, E. M., Ferreira, M. E., & Amsler, M. L. (2011). The effects of deforestation and climate variability on the streamflow of the Araguaia River, Brazil. *Biogeochemistry*, 105(1), 119–131.
- Coe, M.T., Costa, M.H. and Soares-Filho, B.S. (2009). The influence of historical and potential future deforestation on the stream flow of the Amazon River - Land surface processes and atmospheric feedbacks, *Journal of Hydrology*, 369(1–2), 165–174.
- Coe, M.T., Macedo, M.N., Brando, P.M., Lefebvre, P., Panday, P., Silvério, D. (2016). The Hydrology and Energy Balance of the Amazon Basin. In: Nagy, L., Forsberg, B., Artaxo, P. (eds) *Interactions Between Biosphere, Atmosphere and Human Land Use in the Amazon Basin*. Ecological Studies, vol 227. Springer, Berlin, Heidelberg.
- Collins, D.B.G. and Bras, R.L. (2007). Plant rooting strategies in water-limited ecosystems, *Water Resources Research*, 43(6).
- CONAB (2007). National Supply Company, Ministry of Agriculture. Acompanhamento da Safra Brasileira Cana-de-Açúcar – Safra 2007/2008, 3º levantamento. Brasília, novembro/2007. Available at <http://www.conab.gov.br/conabweb/> (last accessed 27 October 2022).

## References

- Cosby, B. J., Hornberger, G. M., Clapp, R. B., & Ginn, T. R. (1984). A Statistical Exploration of the Relationships of Soil Moisture Characteristics to the Physical Properties of Soils. *Water Resources Research*, 20(6), 682–690.
- Cowan, I.R. (1978). Stomatal Behaviour and Environment, *Advances in Botanical Research*, 4, 117–228.
- Cowan, I. R., and G. D. Farquhar (1977), Stomatal function in relation to leaf metabolism and environment, in *Integration of Activity in the Higher Plant*, edited by D. H. Jennings, pp. 471–505, Cambridge Univ. Press, Cambridge, U. K.
- Cox, P. M., Betts, R. A., Jones, C. D., Spall, S. A., & Totterdell, I. J. (2000). Acceleration of global warming due to carbon-cycle feedbacks in a coupled climate model. *Nature*, 408, 184–187.
- Creed, I. F., *et al.* (2014). Changing forest water yields in response to climate warming: Results from long-term experimental watershed sites across North America. *Global Change Biology*, 20(10), 3191–3208.
- Cruz Ruggiero, P. G., Batalha, M. A., Pivello, V. R., & Meirelles, S. T. (2002). Soil-vegetation relationships in cerrado (Brazilian savanna) and semideciduous forest, Southeastern Brazil. *Plant Ecology*, 160, 1-16.
- Cuadra, S. V, Costa, M. H., Kucharik, C. J., Da Rocha, H. R., Tatsch, J. D., Inman-Bamber, G., Da Rocha, R. P., Leite, C. C., & Cabral, O. M. R. (2012). A biophysical model of Sugarcane growth. *GCB Bioenergy*, 4(1), 36–48.
- da Costa Santos, L., José, J.V., Bender, F.D., Alves, D.S., Nitsche, P.R., dos Reis, E.F. and Coelho, R.D., 2020. Climate change in the Paraná state, Brazil: responses to increasing atmospheric CO<sub>2</sub> in reference evapotranspiration. *Theoretical and Applied Climatology*, 140, pp.55-68.
- Da Rocha, H. R., Freitas, H. C., Rosolem, R., Juárez, R. I. N., Tannus, R. N., 22, M., Ligo, A., Cabral, O. M. R., & Dias, M. A. F. S. (2002). Measurements of CO<sub>2</sub> exchange over a



## References

- woodland savanna 2 (Cerrado Sensu stricto) in southeast Brasil. *Biota Neotropica*, 2(1), 1–11.
- Da Rocha, H. R., Goulden, M. L., Miller, S. D., Menton, M. C., Pinto, L. D., de Freitas, H. C., & e Silva Figueira, A. M. (2004). Seasonality of water and heat fluxes over a tropical forest in eastern Amazonia. *Ecological applications*, 14(sp4), 22-32.
- Da Rocha, H.R. *et al.* (2009). Patterns of water and heat flux across a biome gradient from tropical forest to savanna in Brazil, *Journal of Geophysical Research: Biogeosciences*, 114(1).
- Daneshi, A., Brouwer, R., Najafinejad, A., Panahi, M., Zarandian, A., & Maghsood, F. F. (2021). Modelling the impacts of climate and land use change on water security in a semi-arid forested watershed using InVEST. *Journal of Hydrology*, 593.
- Davidson, E.A. *et al.* (2012). The Amazon basin in transition, *Nature*, 481(7381), 321–328.
- De Kauwe, M.G. *et al.* (2013). Forest water use and water use efficiency at elevated CO<sub>2</sub>: A model-data intercomparison at two contrasting temperate forest FACE sites, *Global Change Biology*, 19(6), pp. 1759–1779.
- de Oliveira Serrão, E. A., Silva, M. T., Ferreira, T. R., de Paulo Rodrigues da Silva, V., de Salviano de Sousa, F., de Lima, A. M. M., de Ataíde, L. C. P., & Wanzeler, R. T. S. (2020). Land use change scenarios and their effects on hydropower energy in the Amazon. *Science of the Total Environment*, 744.
- Decker, M., M. Brunke, Z. Wang, K. Sakaguchi, X. Zeng, & M. Bosilovich. (2012). Evaluation of the reanalysis products from GSFC, NCEP, and ECMWF using flux tower observations. *Journal of Climate*, 25, 1916-1944.
- Del Jesus, M., Foti, R., Rinaldo, A., & Rodriguez-Iturbe, I. (2012). Maximum entropy production, carbon assimilation, and the spatial organization of vegetation in river basins. *Proceedings of the National Academy of Sciences of the United States of America*, 109(51), 20837–20841.

## References

- Devia, G. K., Ganasri, B. P., & Dwarakish, G. S. (2015). A Review on Hydrological Models. *Aquatic Procedia*, 4, 1001–1007.
- Dewar, R., Maurantan, A., Mäkelä, A., Hölttä, T., Medlyn, B., & Vesala, T. (2018). New insights into the covariation of stomatal, mesophyll and hydraulic conductances from optimization models incorporating nonstomatal limitations to photosynthesis. *New Phytologist*, 217(2), 571–585.
- Díaz, M. F., Bigelow, S., & Armesto, J. J. (2007). Alteration of the hydrologic cycle due to forest clearing and its consequences for rainforest succession. *Forest Ecology and Management*, 244(1–3), 32–40.
- Döll, P., Kaspar, F., & Lehner, B. (2003). A global hydrological model for deriving water availability indicators: model tuning and validation. *Journal of Hydrology*, 270, 105–134.
- Domingues, T. F., Berry, J. A., Martinelli, L. A., Ometto, J. P. H. B., & Ehleringer, J. R. (2005). Parameterization of Canopy Structure and Leaf-Level Gas Exchange for an Eastern Amazonian Tropical Rain Forest (Tapajós National Forest, Pará, Brazil). *Earth Interactions* 9(17), 1-23.
- Donohue, R.J. *et al.* (2013). Impact of CO<sub>2</sub> fertilization on maximum foliage cover across the globe's warm, arid environments, *Geophysical Research Letters*, 40(12), pp. 3031–3035.
- Donohue, R.J., Roderick, M.L. and McVicar, T.R. (2007). Hydrology and Earth System Sciences On the importance of including vegetation dynamics in Budyko's hydrological model, *Hydrol. Earth Syst. Sci.*
- Donohue, R.J., Roderick, M.L. and McVicar, T.R. (2012). Roots, storms and soil pores: Incorporating key ecohydrological processes into Budyko's hydrological model, *Journal of Hydrology*, 436–437, 35–50.
- Dos Santos, V. *et al.* (2018). Hydrologic Response to Land Use Change in a Large Basin in Eastern Amazon, *Water*, 10(4), 429.

## References

- Doughty, C. E., & Goulden, M. L. (2009). Seasonal patterns of tropical forest leaf area index and CO<sub>2</sub> exchange. *Journal of Geophysical Research: Biogeosciences*, 114(1).
- Duan, Q., Sorooshian, S., & Gupta, V. K. (1994). Optimal use of the SCE-UA global optimization method for calibrating watershed models. *Journal of Hydrology*, 158(1), 265-284.
- Duethmann, D., Bloschl, G. and Parajka, J. (2020). Why does a conceptual hydrological model fail to correctly predict discharge changes in response to climate change?, *Hydrology and Earth System Sciences*, 24(7), 3493–3511.
- Dullaart, J. C. M., Muis, S., Bloemendaal, N., & Aerts, J. C. J. H. (2020). Advancing global storm surge modelling using the new ERA5 climate reanalysis. *Climate Dynamics*, 54(1–2), 1007–1021.
- Dunn, S. M., & Mackay, R. (1995). Spatial variation in evapotranspiration and the influence of land use on catchment hydrology. *Journal of Hydrology*, 171, 49–73.
- Dyck, S., 1985. Overview on the present status of the concepts of water balance models. *IAHS-AISH publication*, (148), pp.3-19.
- Eagleson, P. S., & Tellers, T. E. (1982). Ecological optimality in water-limited natural soil-vegetation systems: 2. Tests and applications. *Water Resources Research*, 18(2), 341-354.
- Eagleson, P.S. (1982). Ecological optimality in water-limited natural soil-vegetation systems: 1. Theory and hypothesis, *Water Resources Research*, 18(2), 325–340.
- Eagleson, P.S. and Segarra, R.I. (1985). Water-Limited Equilibrium of Savanna Vegetation Systems, *Water Resources Research*, 21(10), 1483–1493.
- Eamus, D., & Jarvis, P. G. (1989). The Direct Effects of Increase in the Global Atmospheric CO<sub>2</sub> Concentration on Natural and Commercial Temperate Trees and Forests. *Advances in Ecological Research*, 19, 1–55.

## References

- Eckhardt, K., Breuer, L., & Frede, H.-G. (2003). Parameter uncertainty and the significance of simulated land use change effects. *Journal of Hydrology*, 273, 164–176.
- Eller, C.B. *et al.* (2018). Modelling tropical forest responses to drought and El Niño with a stomatal optimization model based on xylem hydraulics, *Philosophical Transactions of the Royal Society B: Biological Sciences*. Royal Society Publishing.
- Eller, C.B. *et al.* (2020). Stomatal optimization based on xylem hydraulics (SOX) improves land surface model simulation of vegetation responses to climate, *New Phytologist*, 226(6), 1622–1637.
- Eltahir, E. A. B., & Bras, R. L. (1994). Precipitation recycling in the Amazon basin. *Quarterly Journal of the Royal Meteorological Society*, 120(518), 861–880.
- Escobar, H. (2019). Science Editorial. There's no doubt that Brazil's fires are linked to deforestation, scientists say. *Science*, 80.
- Esquivel-Muelbert, A., Baker, T. R., Dexter, K. G., Lewis, S. L., Brienen, R. J. W., Feldpausch, T. R., Lloyd, J., Monteagudo-Mendoza, A., Arroyo, L., Álvarez-Dávila, E., Higuchi, N., Marimon, B. S., Marimon-Junior, B. H., Silveira, M., Vilanova, E., Gloor, E., Malhi, Y., Chave, J., Barlow, J., ... Phillips, O. L. (2019). Compositional response of Amazon forests to climate change. *Global Change Biology*, 25(1), 39–56.
- Fan, Y., Li, H., & Miguez-Macho, G. (2013). Global patterns of groundwater table depth. *Science*, 339(6122), 940–943.
- Fan, Y., Miguez-Macho, G., Jobbágy, E. G., Jackson, R. B., & Otero-Casal, C. (2017). Hydrologic regulation of plant rooting depth. *Proceedings of the National Academy of Sciences of the United States of America*, 114(40), 10572–10577.
- De Faria, A. P., Marabesi, M. A., Gaspar, M., & França, M. G. C. (2018). The increase of current atmospheric CO<sub>2</sub> and temperature can benefit leaf gas exchanges, carbohydrate content and growth in C<sub>4</sub> grass invaders of the Cerrado biome. *Plant Physiology and Biochemistry*, 127, 608–616.

## References

- Farrion, C. E., Rodriguez-Iturbe, I., Dybzinski, R., Levin, S. A., & Pacala, S. W. (2015). Decreased water limitation under elevated CO<sub>2</sub> amplifies potential for forest carbon sinks. *Proceedings of the National Academy of Sciences of the United States of America*, 112(23), 7213–7218.
- Ferreira, J. N., Bustamante, M., Garcia-Montiel, D. C., Caylor, K. K., & Davidson, E. A. (2007). Spatial variation in vegetation structure coupled to plant available water determined by two-dimensional soil resistivity profiling in a Brazilian savanna. *Oecologia*, 153(2), 417–430.
- Field, C.B.; Jackson, R.B.; Mooney, H.A. (1995). Stomatal responses to increased CO<sub>2</sub>: implications from the plant to the global scale. *Plant, Cell and Environment* 18(10): 1214-1225.
- Filho, A. J. P., Vemado, F., Vemado, G., Vieira Reis, F. A. G., do Carmo Giordano, L., Cerri, R. I., dos Santos, C. C., Lopes, E. S. S., Gramani, M. F., Ogura, A. T., Zaine, J. E., da Silva Cerri, L. E., Filho, O. A., D’Affonseca, F. M., & dos Santos Amaral, C. (2018). A step towards integrating CMORPH precipitation estimation with rain gauge measurements. *Advances in Meteorology*, 2018(ID 2095304), 1-24.
- Fitzjarrald, D.R., and R.K. Sakai. 2010. LBA-ECO CD-03 Flux-Meteorological Data, km 77 Pasture Site, Para, Brazil: 2000-2005. ORNL DAAC, Oak Ridge, Tennessee, USA. <https://doi.org/10.3334/ORNLDAAAC/962>
- Foley, J. A., Asner, G. P., Costa, M. H., Coe, M. T., DeFries, R., Gibbs, H. K., Howard, E. A., Olson, S., Patz, J., Ramankutty, N., & Snyder, P. (2007). Amazonia revealed: Forest degradation and loss of ecosystem goods and services in the Amazon Basin, *Frontiers in Ecology and the Environment*, 25–32.
- Francis, J. R., Wuddivira, M. N., & Farrick, K. K. (2023). Reforesting degraded hillslopes with exotic pines in Trinidad and Tobago: Infiltration, repellency and implications for runoff and recharge. *Journal of Hydrology*, 622, 129650. <https://doi.org/10.1016/j.jhydrol.2023.129650>

## References

- Franklin, O. *et al.* (2020). Organizing principles for vegetation dynamics, *Nature Plants*. 6(5), 444–453.
- Fujisaka, S., Castilla, C., Escobar, G., Rodrigues, V., Veneklaas, E. J., Thomas, R., & Fisher, M. (1998). The effects of forest conversion on annual crops and pastures: Estimates of carbon emissions and plant species loss in a Brazilian Amazon colony. *Agriculture, ecosystems & environment*, 69(1), 17-26.
- Gan, G., Liu, Y. and Sun, G. (2021). Understanding interactions among climate, water, and vegetation with the Budyko framework, *Earth-Science Reviews*, 212, 1-13.
- Gash, J. C. H., C. A. Nobre, J. M. Roberts, and R. Victória (1996), Amazonian Deforestation and Climate, pp. 1–14, John Wiley, Chichester, UK.
- Gebere, S. B., Alamirew, T., Merkel, B. J., & Melesse, A. M. (2015). Performance of high resolution satellite rainfall products over data scarce parts of eastern Ethiopia. *Remote Sensing*, 7(9), 11639–11663.
- Gebrechorkos, S. H., S. Hülsmann, and C. Bernhofer, (2020): Analysis of climate variability and droughts in east africa using high-resolution climate data products. *Global and Planetary Change*, 186, 103-130.
- Gerten, D., Schaphoff, S., Haberlandt, U., Lucht, W., & Sitch, S. (2004). Terrestrial vegetation and water balance - Hydrological evaluation of a dynamic global vegetation model. *Journal of Hydrology*, 286(1–4), 249–270.
- Gitay, H., Brown, S., Easterling, W., & Jallow, B. (2001). Ecosystems and their goods and services: climate change 2001: impacts, adaptation and vulnerability contribution of Working Group II to the third assessment report of the Intergovernmental Panel on Climate Change. *J. J. McCarthy, OF Canziani, NA Leary, DJ Dokken, and KS White (Eds.), Cambridge University Press, Cambridge*, 235-342.
- Givnish, T. J. (1988). Adaptation to sun and shade: a whole-plant perspective. *Functional Plant Biology*, 15(2), 63-92.

## References

- Goulden, M. L., Miller, S. D., Da Rocha, H. R., Menton, M. C., de Freitas, H. C., e Silva Figueira, A. M., & de Sousa, C. A. D. (2004). Diel and seasonal patterns of tropical forest CO<sub>2</sub> exchange. *Ecological Applications*, 14(4), 42-54.
- Goulden, M. L., Munger, J. W., Fan, S. M., Daube, B. C., & Wofsy, S. C. (1996). Measurements of carbon sequestration by long-term eddy covariance: Methods and a critical evaluation of accuracy. *Global Change Biology*, 2(3), 169–182.
- Graham, L.P. and Bergström, S. (2000). Land surface modelling in hydrology and meteorology-lessons learned from the Baltic Basin, *Hydrology and Earth System Sciences*, 4(1), 13–22.
- Grimaldi, S., Volpi, E., Langousis, A., Michael Papalexiou, S., Luciano De Luca, D., Piscopia, R., Nerantzaki, S. D., Papacharalampous, G., & Petroselli, A. (2022). Continuous hydrologic modelling for small and ungauged basins: A comparison of eight rainfall models for sub-daily runoff simulations. *Journal of Hydrology*, 610, 1-14.
- Grishin, A.P., Grishin, A.A. and Grishin, V.A. (2019). The influence pattern of the transpiration process on plant productivity, in *IOP Conference Series: Earth and Environmental Science*. Institute of Physics Publishing.
- Guidão, P., Ruggiero, C., Antônio Batalha, M., Pivello, V. R., & Meirelles, S. T. (2002). Soil-vegetation relationships in cerrado (Brazilian savanna) and semideciduous forest, Southeastern Brazil. *Plant Ecology*, 160, 1-16.
- Guo, Z., Xiao, X., & Li, D. (2000). An assessment of ecosystem services: water flow regulation and hydroelectric power production. *Ecological Applications*, 10(3), 925-936.
- Gupta, H.V., H. Kling, K.K. Yilmaz, & Martinez, G.F., 2009. Decomposition of the mean squared error and NSE performance criteria: Implications for improving hydrological modelling. *Journal of Hydrology*, 377, 80-91.
- Guswa, A.J. (2010). Effect of plant uptake strategy on the water-optimal root depth. *Water Resources Research*, 46(9), 1-5.

## References

- Hamel, P., Riveros-Iregui, D., Ballari, D., Browning, T., Célleri, R., Chandler, D., Chun, K. P., Destouni, G., Jacobs, S., Jasechko, S., Johnson, M., Krishnaswamy, J., Poca, M., Pompeu, P. V., & Rocha, H. (2018). Watershed services in the humid tropics: Opportunities from recent advances in ecohydrology. *Ecohydrology*, *11*(3).
- Hasler, N. and Avissar, R. (2007). What controls evapotranspiration in the Amazon basin? *Journal of Hydrometeorology*, *8*(3), 380–395.
- Hawes, J. E., Peres, C. A., Riley, L. B., & Hess, L. L. (2012). Landscape-scale variation in structure and biomass of Amazonian seasonally flooded and unflooded forests. *Forest Ecology and Management*, *281*, 163–176.
- Hernandez Filho, P., Y. E. Shimabukuro, & D. C. L. Lee. (1993). Final report on the forest inventory project at the Tapajó's National Forest. Instituto Nacional de Pesquisas Espaciais, São José dos Campos, SP, Brazil.
- Hernandez Candia, C., Michaelian, K. (2010). Transpiration in plants: A thermodynamic imperative. *Nature Preceedings*, <https://doi.org/10.1038/npre.2010.5463.1>
- Hersbach, H. *et al.*, (2019). Global reanalysis: goodbye ERA-Interim, hello ERA5. *ECMWF: Newsletter*, 159.
- Hickler, T. *et al.* (2008). CO<sub>2</sub> fertilization in temperate FACE experiments not representative of boreal and tropical forests, *Global Change Biology*, *14*(7), 1531–1542.
- Hilker, T., Lyapustin, A. I., Tucker, C. J., Hall, F. G., Myneni, R. B., Wang, Y., Bi, J., De Moura, Y. M., & Sellers, P. J. (2014). Vegetation dynamics and rainfall sensitivity of the Amazon. *Proceedings of the National Academy of Sciences of the United States of America*, *111*(45), 16041–16046.
- Hodnett, M. G., & Tomasella, J., (2002). Marked differences between van Genuchten soil water-retention parameters for temperate and tropical soils: a new water-retention pedo-transfer functions developed for tropical soils. *Geoderma*, *108*, 155–180.



## References

- Hodnett, M.G., Oyama, M.D., Tomasella, J. and Marques Filho, A.D.O., (1996). Comparisons of long-term soil water storage behaviour under pasture and forest in three areas of Amazonia. *Amazonian deforestation and climate*, 287, 306.
- Hollinger, D.Y., & Richardson, A.D. (2005). Uncertainty in eddy covariance measurements and its application to physiological models. *Tree Physiology*, 25:7, 873-885.
- Hopkins, M.J.G. (2019). Are we close to knowing the plant diversity of the Amazon?, *Anais da Academia Brasileira de Ciencias*, 91.
- Huang, J. G., Bergeron, Y., Denneler, B., Berninger, F., & Tardif, J. (2007). Response of forest trees to increased atmospheric CO<sub>2</sub>. *Critical Reviews in Plant Sciences*, 26(5-6), 265-283.
- Huang, Q., Long, D., Du, M., Han, Z., & Han, P. (2020). Daily Continuous River Discharge Estimation for Ungauged Basins Using a Hydrologic Model Calibrated by Satellite Altimetry: Implications for the SWOT Mission. *Water Resources Research*, 56(7).
- Hunke, P., Mueller, E. N., Schröder, B., & Zeilhofer, P. (2015). The Brazilian Cerrado: Assessment of water and soil degradation in catchments under intensive agricultural use. *Ecohydrology*, 8(6), 1154–1180.
- Hutjes, R. W. A., Kabat, P., Running, S. W., Shuttleworth, W. J., Field, C., Bass, B., ... & Vörösmarty, C. J. (1998). Biospheric aspects of the hydrological cycle. *Journal of Hydrology*, 212, 1-21.
- Hutley, L.B. *et al.* (2022). Gross primary productivity and water use efficiency are increasing in a high rainfall tropical savanna, *Global Change Biology*, 28(7), 2360–2380.
- Hutyra, L. R., Munger, J. W., Saleska, S. R., Gottlieb, E., Daube, B. C., Dunn, A. L., Amaral, D. F., de Camargo, P. B., & Wofsy, S. C. (2007). Seasonal controls on the exchange of carbon and water in an Amazonian rain forest. *Journal of Geophysical Research: Biogeosciences*, 112(3).

## References

- Hutyra, L., S. Wofsy and S. Saleska. (2008). LBA-ECO CD-10 CO<sub>2</sub> and H<sub>2</sub>O Eddy Fluxes at km 67 Tower Site, Tapajos National Forest. Data set. Available on-line [<http://daac.ornl.gov>] from Oak Ridge National Laboratory Distributed Active Archive Center, Oak Ridge, Tennessee, U.S.A. doi:[10.3334/ORNLDAAAC/860](https://doi.org/10.3334/ORNLDAAAC/860)
- IBAMA, 2006. Plano de prevenção e combate aos incêndios florestais da reserva Biológica do Jaru (2006-2007), available at: [http://www.ibama.gov.br/phocadownload/prevfogo/planos\\_operativos/plano\\_operativo\\_reserva\\_biologica\\_do\\_jaru.pdf](http://www.ibama.gov.br/phocadownload/prevfogo/planos_operativos/plano_operativo_reserva_biologica_do_jaru.pdf), last access: 25 Oct 2022.
- IGBE (2019). 2019 Biomes and Coastal-Marine Systems of Brazil – 1:250,000, available at: <https://www.ibge.gov.br/en/geosciences/maps/brazil-environmental-information/18341-biomes.html>, last access: 06 Jun 2023.
- Intergovernmental Panel on Climate Change. (2022). *Climate Change 2022: Impacts, Adaptation and Vulnerability*. Jean.
- IPCC, 2012 – Field, C.B., V. Barros, T.F. Stocker, D. Qin, D.J. Dokken, K.L. Ebi, M.D. Mastrandrea, K.J. Mach, G.-K. Plattner, S.K. Allen, M. Tignor, and P.M. Midgley (Eds.) Available from [Cambridge University Press](https://www.cambridge.org/9781107059731), The Edinburgh Building, Shaftesbury Road, Cambridge CB2 8RU ENGLAND, 582 pp. Available from June 2012.
- Jardim, F. C. S., & Hosokawa, R. T. (1987). Estrutura da floresta equatorial úmida da estação experimental de silvicultura tropical do inpa. *Acta Amazonica*, 16/17, 411–508.
- Jepson, W., Brannstrom, C. and Filippi, A. (2010). Access regimes and regional land change in the Brazilian Cerrado, 1972-2002, *Annals of the Association of American Geographers*, 100(1), 87–111.
- Jiang, H., Y. Yang, Y. Bai, & Wang, H., (2020). Evaluation of the Total, Direct, and Diffuse Solar Radiations from the ERA5 reanalysis data in China. *Geoscience and remote sensing letters*, 17(1), 47-51.

## References

- Jiao, W., Wang, L., Smith, W. K., Chang, Q., Wang, H., & D'Odorico, P. (2021). Observed increasing water constraint on vegetation growth over the last three decades. *Nature Communications*, 12(1).
- Kauffeldt, A., Halldin, S., Rodhe, A., Xu, C.Y. and Westerberg, I.K., (2013). Disinformative data in large-scale hydrological modelling. *Hydrology and Earth System Sciences*, 17(7), 2845-2857.
- Keeley, S. C., & Johnson, A. W. (1977). A comparison of the pattern of herb and shrub growth in comparable sites in Chile and California. *American Midland Naturalist*, 97(1), 120-132.
- Keeling, C.D., S. C. Piper, R. B. Bacastow, M. Wahlen, T. P. Whorf, M. Heimann, and H. A. Meijer, (2008). Exchanges of atmospheric CO<sub>2</sub> and <sup>13</sup>CO<sub>2</sub> with the terrestrial biosphere and oceans from 1978 to 2000. I. Global aspects, SIO Reference Series, No. 01-06, Scripps Institution of Oceanography, San Diego, 88 pages.
- Keeling, R.F., S.C. Piper, A.F. Bollenbacher & J.S. Walker. (2009). Atmospheric CO<sub>2</sub> records from sites in the SIO air sampling network. In Trends: A Compendium of Data on Global Change. Carbon Dioxide Information Analysis Center, Oak Ridge National Laboratory, U.S. Department of Energy, Oak Ridge, Tenn., U.S.A.
- Keenan, T. F., Hollinger, D. Y., Bohrer, G., Dragoni, D., Munger, J. W., Schmid, H. P., & Richardson, A. D. (2013). Increase in forest water-use efficiency as atmospheric carbon dioxide concentrations rise. *Nature*, 499(7458), 324–327.
- Kergoat, L. (1998). A model for hydrological equilibrium of leaf area index on a global scale. In *Journal of Hydrology*, 212, 268-286.
- Khaleghi, M. R. (2017). The influence of deforestation and anthropogenic activities on runoff generation. *Journal of Forest Science*, 63(6), 245–253.
- Kirkby, C. A., Giudice, R., Day, B., Turner, K., Soares-Filho, B. S., Oliveira-Rodrigues, H., & Yu, D. W. (2011). Closing the ecotourism-conservation loop in the Peruvian Amazon. *Environmental Conservation*, 38(1), 6–17.

## References

- Kirkman, G. A., Gut, A., Ammann, C., Gatti, L. V., Cordova, A. M., Moura, M. A. L., Andreae, M. O., & Meixner, F. X. (2002). Surface exchange of nitric oxide, nitrogen dioxide, and ozone at a cattle pasture in Rondônia, Brazil. *Journal of Geophysical Research*, *107*(D20).
- Kleidon, A. and Heimann, M. (1998). A method of determining rooting depth from a terrestrial biosphere model and its impacts on the global water and carbon cycle. *Global Change Biology*, *4*(3), 275–286.
- Kleidon, A. and Schymanski, S. (2008) Thermodynamics and optimality of the water budget on land: A review. *Geophysical Research Letters*, *35*(20), 1–6.
- Klink, C. A., & Machado, R. B. (2005). Conservation of the Brazilian Cerrado. In *Conservation Biology*, *19*(3), 707–713.
- Kong, X., Zhou, Z. and Jiao, L. (2021). Hotspots of land-use change in global biodiversity hotspots, *Resources, Conservation and Recycling*, 174.
- Koschorreck, M. and Darwich, A. (2003). Nitrogen dynamics in seasonally flooded soils in the Amazon floodplain, *Wetlands Ecology and Management*, *11*, 317–330.
- Lammertsma, E. I., de Boer, H. J., Dekker, S. C., Dilcher, D. L., Lotter, A. F., & Wagner-Cremer, F. (2011). Global CO<sub>2</sub> rise leads to reduced maximum stomatal conductance in Florida vegetation. *Proceedings of the National Academy of Sciences of the United States of America*, *108*(10), 4035–4040.
- Lamparter, G., Nobrega, R. L. B., Kovacs, K., Amorim, R. S., & Gerold, G. (2018). Modelling hydrological impacts of agricultural expansion in two macro-catchments in Southern Amazonia, Brazil. *Regional Environmental Change*, *18*(1), 91–103.
- Lawrence, D. and Vandecar, K. (2015). Effects of tropical deforestation on climate and agriculture, *Nature Climate Change*, *5*(1), 27–36.

## References

- Leakey, A.D.B., Ainsworth, E. A., Bernacchi, C. J., Rogers, A., Long, S. P., & Ort, D. R. (2009). Elevated CO<sub>2</sub> effects on plant carbon, nitrogen, and water relations: Six important lessons from FACE, in *Journal of Experimental Botany*, 60(10), 2859–2876.
- Lei, H. *et al.* (2008). Modeling the crop transpiration using an optimality-based approach. *Science in China, Series E: Technological Sciences*, 51(SUPPL. 2), 60–75.
- Lei, H., Yang, D. and Huang, M. (2014). Impacts of climate change and vegetation dynamics on runoff in the mountainous region of the Haihe River basin in the past five decades, *Journal of Hydrology*, 511, 786–799.
- Levy, M. C., Lopes, A. V., Cohn, A., Larsen, L. G., & Thompson, S. E. (2018). Land Use Change Increases Streamflow Across the Arc of Deforestation in Brazil. *Geophysical Research Letters*, 45(8), 3520–3530.
- Liebmann, B., & D. Allured, (2005). Daily precipitation grids for South America. *Bulletin for the American Meteorological Society*, 86, 1567–1570.
- Lima, L. S., Coe, M. T., Soares Filho, B. S., Cuadra, S. V., Dias, L. C. P., Costa, M. H., Lima, L. S., & Rodrigues, H. O. (2014). Feedbacks between deforestation, climate, and hydrology in the Southwestern Amazon: Implications for the provision of ecosystem services. *Landscape Ecology*, 29(2), 261–274.
- Liu, J., Gao, G., Wang, S., Jiao, L., Wu, X., & Fu, B. (2018). The effects of vegetation on runoff and soil loss: Multidimensional structure analysis and scale characteristics. *Journal of Geographical Sciences*, 28(1), 59–78.
- Lockwood, J. G. (1999). Is potential evapotranspiration and its relationship with actual evapotranspiration sensitive to elevated atmospheric CO<sub>2</sub> levels? *Climate Change*, 41, 193–212.
- Lozano-Baez, S.E. *et al.* (2018). Previous land use affects the recovery of soil hydraulic properties after forest restoration, *Water (Switzerland)*, 10(4).

## References

- Magrin, G. O., Field, C. B., Barros, V. R., Mastrandrea, M. D., Mach, K. J., Abdrabo, M., et al (2014) “Central and South America,” in *Climate Change 2014: Impacts, Adaptation, and Vulnerability. Part B: Regional Aspects. Contribution of Working Group II to the Fifth Assessment Report of the Intergovernmental Panel on Climate Change*, eds C.B. Field, D. J. Dokken, M. D. Mastrandrea, K. J. Mach, T. E. Bilir, M. Chatterjee, et al (Cambridge: Cambridge University Press), 1499–1566.
- Maidment, D.R.. (1992). *Handbook of Hydrology*, McGraw-Hil. Inc., New York, NY.
- Makarieva, A.M. and Gorshkov, V.G. (2010). The biotic pump: Condensation, atmospheric dynamics and climate, *International Journal of Water*, 5(4), 365–385.
- Malhi, Y., Aragão, L. E. O. C., Metcalfe, D. B., Paiva, R., Quesada, C. A., Almeida, S., Anderson, L., Brando, P., Chambers, J. Q., da Costa, A. C. L., Hutyrá, L. R., Oliveira, P., Patiño, S., Pyle, E. H., Robertson, A. L., & Teixeira, L. M. (2009). Comprehensive assessment of carbon productivity, allocation and storage in three Amazonian forests. *Global Change Biology*, 15(5), 1255–1274.
- Malhi, Y., Pegoraro, E., Nobre, A. D., Pereira, M. G. P., Grace, J., Culf, A. D., & Clement, R. (2002). Energy and water dynamics of a central Amazonian rain forest. *Journal of Geophysical Research: Atmospheres*, 107(20), LBA 45-1-LBA 45-17.
- Manciu, A., Rammig, A., Krause, A., & Quesada, B. R. (2022). Impacts of land cover changes and global warming on climate in Colombia during ENSO events. *Climate Dynamics*, 1-19.
- Manciu, A., Rammig, A., Krause, A., & Quesada, B. R. (2022). Impacts of land cover changes and global warming on climate in Colombia during ENSO events. *Climate Dynamics*. Published online: <https://doi.org/10.1007/s00382-022-06545-1>
- Manzoni, S., Vico, G., Palmroth, S., Porporato, A., & Katul, G. (2013). Optimization of stomatal conductance for maximum carbon gain under dynamic soil moisture. *Advances in Water Resources*, 62(PA), 90–105.

## References

- Marhaento, H., Booij, M. J., & Hoekstra, A. Y. (2018). Hydrological response to future land-use change and climate change in a tropical catchment. *Hydrological Sciences Journal*, 63(9), 1368–1385.
- Markwitz, C. & L. Siebicke. (2019). Low-cost eddy covariance: a case study of evapotranspiration over agroforestry in Germany. *Atmospheric Measurement Techniques*, 12, 4677-4696.
- Marris, E. (2005). The forgotten ecosystem, *Nature*, 437, 944–945.
- Marthews, T. R., Quesada, C. A., Galbraith, D. R., Malhi, Y., Mullins, C. E., Hodnett, M. G., & Dharssi, I. (2014). High-resolution hydraulic parameter maps for surface soils in tropical South America. *Geoscientific Model Development*, 7(3), 711–723.
- Martinelli, L. A., Naylor, R., Vitousek, P. M., & Moutinho, P. (2010). Agriculture in Brazil: Impacts, costs, and opportunities for a sustainable future. In *Current Opinion in Environmental Sustainability*, 2(5–6), 431–438.
- Matthews, J. S., & Lawson, T. (2018). Climate change and stomatal physiology. *Annual plant reviews online*, 2(3), 713-752.
- McLaughlin, B. C., Ackerly, D. D., Klos, P. Z., Natali, J., Dawson, T. E., & Thompson, S. E. (2017). Hydrologic refugia, plants, and climate change. In *Global Change Biology*, 23(8), 2941–2961.
- McMillen, R.T. (1988). An eddy correlation technique with extended applicability to non-simple terrain. *Boundary-Layer Meteorol*, 43, 231–245.
- McVicar, T. R., Li, L. T., Van Niel, T. G., Zhang, L., Li, R., Yang, Q. K., Zhang, X. P., Mu, X. M., Wen, Z. M., Liu, W. Z., Zhao, Y., Liu, Z. H., & Gao, P. (2007). Developing a decision support tool for China's re-vegetation program: Simulating regional impacts of afforestation on average annual streamflow in the Loess Plateau. *Forest Ecology and Management*, 251(1–2), 65–81.

## References

- Medlyn, B. E., Duursma, R. A., Eamus, D., Ellsworth, D. S., Prentice, I. C., Barton, C. V. M., Crous, K. Y., De Angelis, P., Freeman, M., & Wingate, L. (2011). Reconciling the optimal and empirical approaches to modelling stomatal conductance. *Global Change Biology*, 17(6), 2134–2144.
- Melo, D.d.C.D., A.C. Xavier, T. Bianchi, P.T.S.Oliveira, B.R. Scanlon, M.C. Lucas, & E. Wendland. (2015). Performance evaluation of rainfall estimates by TRMM multi-satellite Precipitation Analysis 3B42V6 and V7 over Brazil. *Journal of Geophysical Research: Atmospheres*, 120, 9426-9436.
- Melo, N.M.J. *et al.* (2018). Rising [CO<sub>2</sub>] changes competition relationships between native woody and alien herbaceous Cerrado species, *Functional Plant Biology*, 45(8), 854–864.
- Miller, S. D., Goulden, M. L., & da Rocha, H. R. (2007). The effect of canopy gaps on subcanopy ventilation and scalar fluxes in a tropical forest. *Agricultural and Forest Meteorology*, 142(1), 25–34.
- Miller, S. D., Goulden, M. L., Menton, M. C., Da Rocha, H. R., De Freitas, H. C., Michela, A., Figueira, S., Cleilim, A., Dias, A., & Sousa, D. E. (2004). Biometric and micrometeorological measurements of tropical forest carbon balance. *Ecological Applications*, 14(4), 42-54.
- Milly, P. C. D. (1997). Sensitivity of greenhouse summer dryness to changes in plant rooting characteristics. *Geophysical Research Letters*, 24(3), 269–271.
- Miralles, D. G., Gentine, P., Seneviratne, S. I., and Teuling, A. J., (2019). Land-atmospheric feedbacks during droughts and heatwaves: state of the science and current challenges, *Annals of the New York Academy of Sciences*, 1436(1), 19-35.
- Mishra, B. K., Kumar, P., Saraswat, C., Chakraborty, S., & Gautam, A. (2021). Water security in a changing environment: Concept, challenges and solutions. *Water (Switzerland)*, 13(4).



## References

- Moreira, A.A., A.L. Ruhoff, D.R. Roberti, V.d.A. Souza, H.R. da Rocha & R.C.D. de Pavia, (2019). Assessment of terrestrial water balance using remote sensing data in South America. *Journal of Hydrology*, 575, 131-147.
- Moreira, V. S., Candido, L. A., Roberti, D. R., Webler, G., Diaz, M. B., de Gonçalves, L. G. G., Pousa, R., & Degrazia, G. A. (2018). Influence of soil properties in different management systems: Estimating soybean water changes in the agro-IBIS model. *Earth Interactions*, 22(4), 1–19.
- Moumen, Z., El Idrissi, N. E. A., & Tvaronavičienė, M. (2019). Water security and sustainable development. *Insights into Regional Development*, 1(4), 301–317.
- Muñoz-Sabater, J., (2019): ERA5-Land hourly data from 1981 to present. Copernicus Climate Change Service (C3S) Climate Data Store (CDS). (Accessed on 17-05-2021), 10.24381/cds.e2161bac
- Myers, N., Mittermeier, R. A., Mittermeier, C. G., Da Fonseca, G. A., & Kent, J. (2000). Biodiversity hotspots for conservation priorities. *Nature*, 403(6772), 853-858.
- Nature Editorial. (2018a). Brazil's new president adds to global threat to science. *Nature*, 563,5e6 <https://doi.org/10.1038/d41586-018-07236-w>
- Nature Editorial. (2018b). Brazil's sustainability needs social sciences. *Nature Sustainability*, 1, 607 <https://doi.org/10.1038/s41893-018-0183-0>
- Negrón Juárez, R. I., da Rocha, H. R., e Figueira, A. M. S., Goulden, M. L., & Miller, S. D. (2009). An improved estimate of leaf area index based on the histogram analysis of hemispherical photographs. *Agricultural and Forest Meteorology*, 149(6–7), 920–928.
- Neiff, J. J. (2003). Planícies de inundação são ecótonos. *Ecótonos nas interfaces dos ecossistemas aquáticos. São Carlos: Rima*, 29-46.
- Neilson, R. P., & Marks, D. (1994). A global perspective of regional vegetation and hydrologic sensitivities from climatic change. *Journal of Vegetation Science*, 5(5), 715–730.

## References

- Nepstad, D. C., Moutinho, P., Dias-Filho, M. B., Davidson, E., Cardinot, G., Markewitz, D., Figueiredo, R., Vianna, N., Chambers, J., Ray, D., Guerreiros, J. B., Lefebvre, P., Sternberg, L., Moreira, M., Barros, L., Ishida, F. Y., Tohlver, I., Belk, E., Kalif, K., & Schwalbe, K. (2002). The effects of partial throughfall exclusion on canopy processes, aboveground production, and biogeochemistry of an Amazon forest. *Journal of Geophysical Research*, *107*(D20).
- Nepstad, D., de Carvalho, C., Davidson, E. *et al.* (1994). The role of deep roots in the hydrological and carbon cycles of Amazonian forests and pastures. *Nature*, *372*, 666–669.
- Nepstad, D., McGrath, D., Stickler, C., Alencar, A., Azevedo, A., Swette, B., ... & Hess, L. (2014). Slowing Amazon deforestation through public policy and interventions in beef and soy supply chains. *science*, *344*(6188), 1118-1123.
- Nijzink, R. C., Beringer, J., Hutley, L. B., & Schymanski, S. J. (2022). Does maximization of net carbon profit enable the prediction of vegetation behaviour in savanna sites along a precipitation gradient? *Hydrology and Earth System Sciences*, *26*(2), 525–550.
- Nijzink, R.C. and Schymanski, S.J. (2022). Vegetation optimality explains the convergence of catchments on the Budyko curve, *Hydrology and Earth System Sciences*, *26*(24), 6289–6309.
- Nijzink, R.C. *et al.* (2022b). Influence of modifications (from AoB2015 to v0.5) in the Vegetation Optimality Model, *Geoscientific Model Development*, *15*(2), 883–900.
- Nitta, T., Arakawa, T., Hatono, M., Takeshima, A., & Yoshimura, K. (2020). Development of Integrated Land Simulator. *Progress in Earth and Planetary Science*, *7*(68), 1-14.
- Niu, J., Sivakumar, B. and Chen, J. (2013). Impacts of increased CO<sub>2</sub> on the hydrologic response over the Xijiang (West River) basin, South China, *Journal of Hydrology*, *505*, 218–227.

## References

- Norby, R.J. and Zak, D.R. (2011). Ecological and evolutionary lessons from free air carbon enhancement (FACE) experiments, *Annual Review of Ecology, Evolution, and Systematics*, 42, pp. 181–203.
- Norby, R.J. *et al.* (2016). Model-data synthesis for the next generation of forest free-air CO<sub>2</sub> enrichment (FACE) experiments, *New Phytologist*, 209(1), 17–28.
- Nowak, R.S., Ellsworth, D.S. and Smith, S.D. (2004). Functional responses of plants to elevated atmospheric CO<sub>2</sub> - Do photosynthetic and productivity data from FACE experiments support early predictions? *New Phytologist*, 162(2), 253–280.
- OECD/FAO (2020), *OECD-FAO Agricultural Outlook 2020-2029*, OECD Publishing, Paris/FAO, Rome.
- Oliveira, P. T. S., Nearing, M. A., Moran, M. S., Goodrich, D. C., Wendland, E., & Gupta, H. V. (2014). Trends in water balance components across the Brazilian Cerrado. *Water Resources Research*, 50(9), 7100–7114.
- Oliveira, P. T. S., Wendland, E., Nearing, M. A., Scott, R. L., Rosolem, R., & Da Rocha, H. R. (2015). The water balance components of undisturbed tropical woodlands in the Brazilian cerrado. *Hydrology and Earth System Sciences*, 19(6), 2899–2910.
- Oliveira, R. S., Bezerra, L., Davidson, E. A., Pinto, F., Klink, C. A., Nepstad, D. C., & Moreira, A. (2005). Deep root function in soil water dynamics in cerrado savannas of central Brazil. *Functional Ecology*, 19(4), 574–581.
- Oliveira, R. S., Dawson, T. E., Burgess, S. S. O., & Nepstad, D. C. (2005). Hydraulic redistribution in three Amazonian trees. *Oecologia*, 145(3), 354–363.
- Oliveira, V. F., Silva, E. A., & Carvalho, M. A. M. (2016). Elevated CO<sub>2</sub> atmosphere minimizes the effect of drought on the Cerrado species *Chrysolaena obovata*. *Frontiers in Plant Science*, 7(810) 1-15.

## References

- Olivier, J. G. J., & Peters, J. A. H. W. (2020). Report: Trends in global co2 and total greenhouse gas emissions, 2020 Report, [www.pbl.nl/en](http://www.pbl.nl/en).
- Olson, R. J., Holladay, S. K., Cook, R. B., Falge, E., Baldscchi, D., & Gu, L. (2004). *(ORNUM-20031204 FLUXNET: Database of Fluxes, Site Characteristics, and Flux-Community Information)*.
- Otoni, M.V., T.B. Otoni Filho, M.G. Schaap, M.L.R.C. Lopes-Assad, and O.C. Rotunno Filho. (2018). Hydrophysical database for Brazilian soils (HYBRAS) and pedotransfer functions for water retention, *Vadose Zone Journal*, 17(1).
- Overgaard, J., Rosbjerg, D., & Butts, M. B. (2006). Land-surface modelling in hydrological perspective—a review. *Biogeosciences*, 3(2), 229-241.
- Peel, M. C., Finlayson, B. L., & McMahon, T. A. (2007). Updated world map of the Köppen-Geiger climate classification. *Hydrology and Earth System Sciences*, 11, 1633-1644.
- Peel, M. C., McMahon, T. A., Finlayson, B. L., & Watson, F. G. R. (2001). Identification and explanation of continental differences in the variability of annual runoff. *Journal of Hydrology*, 250, 224–240.
- Pelosi, A., F. Terribile, G. D’Urso, & G.B. Chirico, (2020). Comparison of ERA5-Land and UERRA MESCAN-SURFEX reanalysis Data with spatially interpolated weather observations for the regional assessment of reference evapotranspiration. *Water*, 12(6), 1669.
- Penman, H. L. (1951). The role of vegetation in meteorology, soil mechanics and hydrology. *British Journal of Applied Physics*, 2, 145–151.
- Pivello, V. R., Ruggiero, P. C. G., & Oliveira Filho, F. (1996). Analise da variacao fitofisionomica na area do cerrado pe-de-gigante (santa rita do passa quatro, sp) em relacao a caracteristicas topograficas e pedologicas locais. *Manejo de Ecossistemas e Mudancas Globais: Resumos*.

## References

- Pivello, V. R., Vieira, I., Christianini, A. v., Ribeiro, D. B., da Silva Menezes, L., Berlinck, C. N., Melo, F. P. L., Marengo, J. A., Tornquist, C. G., Tomas, W. M., & Overbeck, G. E. (2021). Understanding Brazil's catastrophic fires: Causes, consequences and policy needed to prevent future tragedies. *Perspectives in Ecology and Conservation*, 19(3), 233–255.
- Postel, S.L. and Thompson, B.H. (2005). Watershed protection: Capturing the benefits of nature's water supply services, *Natural Resources Forum*, 29(2), 98–108.
- Prance, G.T. (1979). Notes on the vegetation of Amazonia III. The terminology of amazonian forest types subject to inundation. *Brittonia* 31, 26–38.
- Prentice, I. C., Liang, X., Medlyn, B. E., & Wang, Y. P. (2015). Reliable, robust and realistic: The three R's of next-generation land-surface modelling. *Atmospheric Chemistry and Physics*, 15(10), 5987–6005.
- Pugh, T. A. M., Jones, C. D., Huntingford, C., Burton, C., Arneth, A., Brovkin, V., Ciais, P., Lomas, M., Robertson, E., Piao, S. L., & Sitch, S. (2018). A Large Committed Long-Term Sink of Carbon due to Vegetation Dynamics. *Earth's Future*, 6(10), 1413–1432.
- Qian, T., A. Dai, K.E. Trenberth, & Oleson, K.W., 2006. Simulation of global land surface conditions from 1948 to 2004. Part I: forcing data and evaluations. *Journal of Hydrometeorology*, 7, 953-975.
- Quirk, J., Bellasio, C., Johnson, D. A., & Beerling, D. J. (2019). Response of photosynthesis, growth and water relations of a savannah-adapted tree and grass grown across high to low CO<sub>2</sub>. *Annals of botany*, 124(1), 77-90.
- Rakovec, O. *et al.* (2016). Improving the realism of hydrologic model functioning through multivariate parameter estimation, *Water Resources Research*, 52(10), 7779–7792.
- Raulino, J.B.S., Silveira, C.S. and Lima Neto, I.E. (2021). Assessment of climate change impacts on hydrology and water quality of large semi-arid reservoirs in Brazil, *Hydrological Sciences Journal*, 66(8), 1321–1336.

## References

- Raupach, M. R. (2005). 19 Dynamics and Optimality in Coupled Terrestrial Energy, Water, Carbon and Nutrient Cycles. *Predictions in ungauged basins: international perspectives on the state of the art and pathways forward*, (301), 223.
- Reatto, A. *et al.* (2007). Hydraulic properties of the diagnostic horizon of Latosols of a regional toposequence across the Brazilian Central Plateau, *Geoderma*, 139(1–2), 51–59.
- Refsgaard, J.C., (1996). Terminology, modelling protocol and classification of hydrologic model codes. *Distributed Hydrologic Modelling*, edited by Michael B. Abbott and Jens C. Refsgaard, 41-54.
- Reggiani, P., Sivapalan, M., & Hassanizadeh, S. M. (2000). Conservation equations governing hillslope responses: Exploring the physical basis of water balance. *Water Resources Research*, 36(7), 1845–1863.
- Resende, F. M., Cimon-Morin, J., Poulin, M., Meyer, L., & Loyola, R. (2019). Consequences of delaying actions for safeguarding ecosystem services in the Brazilian Cerrado. *Biological Conservation*, 234, 90–99.
- Resende, F. M., Cimon-Morin, J., Poulin, M., Meyer, L., Joner, D. C., & Loyola, R. (2021). The importance of protected areas and Indigenous lands in securing ecosystem services and biodiversity in the Cerrado. *Ecosystem Services*, 49(101282).
- Restrepo-Coupe, N. *et al.* (2013). What drives the seasonality of photosynthesis across the Amazon basin? A cross-site analysis of eddy flux tower measurements from the Brasil flux network, *Agricultural and Forest Meteorology*, 182–183, 128–144.
- Restrepo-Coupe, N. *et al.* (2017). Do dynamic global vegetation models capture the seasonality of carbon fluxes in the Amazon basin? A data-model intercomparison, *Global Change Biology*, 23(1), 191–208.
- Restrepo-Coupe, N. *et al.* (2021). Understanding water and energy fluxes in the Amazonia: Lessons from an observation-model intercomparison, *Global Change Biology*, 27(9), 1802–1819.

## References

- Restrepo-Coupe, N. *et al.* (2021). LBA-ECO CD-32 Flux Tower Network Data Compilation, Brazilian Amazon: 1999-2006, V2. ORNL Distributed Active Archive Center. doi: 10.3334/ORNLDAAAC/1842.
- Rezende, L.F.C. *et al.* (2022). Impacts of Land Use Change and Atmospheric CO<sub>2</sub> on Gross Primary Productivity (GPP), Evaporation, and Climate in Southern Amazon, *Journal of Geophysical Research: Atmospheres*, 127(8).
- Ricciuto, D., Sargsyan, K., & Thornton, P. (2018). The Impact of Parametric Uncertainties on Biogeochemistry in the E3SM Land Model. *Journal of Advances in Modeling Earth Systems*, 10(2), 297–319.
- Rice, A. H., Pyle, E. H., Saleska, S. R., Hutyyra, L., Palace, M., Keller, M., De Camargo, P. B., Portilho, K., Marques, D. F., & Wofsy, S. C. (2004). carbon balance and vegetation dynamics in an old-growth amazonian forest. *Ecological Applications*, 14(4), S55-S71.
- Richardson, T.B. *et al.* (2018). Carbon Dioxide Physiological Forcing Dominates Projected Eastern Amazonian Drying, *Geophysical Research Letters*, 45(6), 2815–2825.
- Rodell, M. *et al.*, (2004). The Global Land Data Assimilation System. *Bulletin of the American Meteorological Society*, 85, 381-394.
- Rodrigo, L. M. *et al.*, 2016. An extensive reef system at the Amazon River mouth. *Science Advances*, 2(4), e1501252.
- Rosolem, R., H.V. Gupta, W.J. Shuttleworth, L.G.G. de Gonçalves, & X. Zeng, (2013). Towards a comprehensive approach to parameter estimation in land surface parameterization schemes. *Hydrological Processes*, 27, 2075-2097.
- Ruggiero, P. G. C., Antônio Batalha, M., Pivello, V. R., & Meirelles, S. T. (2002). Soil-vegetation relationships in cerrado (Brazilian savanna) and semideciduous forest, Southeastern Brazil. *Plant Ecology*, 160, 1-16.

## References

- Ruiz-Vásquez, M., Arias, P. A., Martínez, J. A., & Espinoza, J. C. (2020). Effects of Amazon basin deforestation on regional atmospheric circulation and water vapor transport towards tropical South America. *Climate Dynamics*, 54(9–10), 4169–4189.
- Running, S. W., Baldocchi, D. D., Turner, D. P., Gower, S. T., Bakwin, P. S., & Hibbard, K. A. (1999). A Global Terrestrial Monitoring Network Integrating Tower Fluxes, Flask Sampling, Ecosystem Modeling and EOS Satellite Data. *Remote Sensing of Environment*, 70(1), 108–127.
- Ruv Lemes, M. *et al.* (2023). Impacts of atmospheric CO<sub>2</sub> increase and Amazon deforestation on the regional climate: A water budget modelling study, *International Journal of Climatology*, 43(3), 1497–1513.
- Sabot, M. E. B., de Kauwe, M. G., Pitman, A. J., Medlyn, B. E., Verhoef, A., Ukkola, A. M., & Abramowitz, G. (2020). Plant profit maximization improves predictions of European forest responses to drought. *New Phytologist*, 226(6), 1638–1655.
- Saha, S., *et al.*, (2010). The NCEP Climate Forecast System Reanalysis. *Bulletin of the American Meteorological Society*, 91, 8, 1015-1058.
- Sakai, R. K., Fitzjarrald, D. R., Moraes, O. L. L., Staebler, R. M., Acevedo, O. C., Czikowsky, M. J., da Silva, R., Brait, E., & Miranda, V. (2004). Land-use change effects on local energy, water, and carbon balances in an Amazonian agricultural field. *Global Change Biology*, 10(5), 895–907.
- Sakai, R. K., Fitzjarrald, D. R., Moraes, O. L. L., Staebler, R. M., Acevedo, O. C., Czikowsky, M. J., Da Silva, R., Brait, E., & Miranda, V. (2004). Land-use change effects on local energy, water, and carbon balances in an Amazonian agricultural field. *Global Change Biology*, 10(5), 895–907.
- Saleska, S. R., Miller, S. D., Matross, D. M., Goulden, M. L., Wofsy, S. C., Da Rocha, H. R., De Camargo, P. B., Crill, P., Daube, B. C., De Freitas, H. C., Hutyyra, L., Keller, M., Kirchhoff, V., Menton, M., Munger, J. W., Pyle, E. H., Rice, A. H., & Silva, H. (2003).



## References

- Carbon in Amazon Forests: Unexpected Seasonal Fluxes and Disturbance-Induced Losses. *Science*, 302(5650), 1554–1557.
- Saleska, S.R., H.R. da Rocha, A.R. Huete, A.D. Nobre, P. Artaxo, & Y.E. Shimabukuro, (2013). LBA-ECO CD-32 Flux Tower Network Data Compilation, Brazilian Amazon: 1999-2006. Data set. Available on-line [<http://daac.ornl.gov>] from Oak Ridge National Laboratory Distributed Active Archive Center, Oak Ridge, Tennessee, USA <http://dx.doi.org/10.3334/ORNLDAAAC/1174>
- Schaefli, B. *et al.* (2011). HESS Opinions: Hydrologic predictions in a changing environment: Behavioral modeling, *Hydrology and Earth System Sciences*, 15(2), 635–646.
- Schiesari, L. and Grillitsch, B. (2011). Pesticides meet megadiversity in the expansion of biofuel crops, *Frontiers in Ecology and the Environment*, 9(4), 215–221.
- Schiesari, L. *et al.* (2013). Pesticide use and biodiversity conservation in the Amazonian agricultural frontier, *Philosophical Transactions of the Royal Society B: Biological Sciences*, 368(1619).
- Schleppi, P., Conedera, M., Sedivy, I., & Thimonier, A. (2007). Correcting non-linearity and slope effects in the estimation of the leaf area index of forests from hemispherical photographs. *Agricultural and Forest Meteorology*, 144(3–4), 236–242.
- Schymanski, S. J., Roderick, M. L., & Sivapalan, M. (2015). Using an optimality model to understand medium and long-term responses of vegetation water use to elevated atmospheric CO<sub>2</sub> concentrations. *AoB Plants*, 7, plv060.
- Schymanski, S. J., Roderick, M. L., Sivapalan, M., Hutley, L. B., & Beringer, J. (2007). A test of the optimality approach to modelling canopy properties and CO<sub>2</sub> uptake by natural vegetation. *Plant, Cell & Environment*, 30(12), 1586–1598.
- Schymanski, S. J., Sivapalan, M., Roderick, M. L., Beringer, J., & Hutley, L. B. (2008). An optimality-based model of the coupled soil moisture and root dynamics. *Vegetation Dynamics*, 20.

## References

- Schymanski, S. J., Sivapalan, M., Roderick, M. L., Hutley, L. B., & Beringer, J. (2009). An optimality-based model of the dynamic feedbacks between natural vegetation and the water balance. *Water Resources Research*, 45(1).
- Schymanski, S.J. (2008). Optimality as a Concept to Understand and Model Vegetation at Different Scales, *Geography Compass*, 2(5), 1580–1598.
- Schymanski, S.J. *et al.* (2008). A canopy-scale test of the optimal water-use hypothesis, *Plant, Cell and Environment*, 31(1), 97–111.
- Schymanski, S.J., Kleidon, A. and Roderick, M.L. (2009). Ecohydrological Optimality. In *Encyclopedia of Hydrological Sciences* (eds M.G. Anderson and J.J. McDonnell).
- Serrão, E. A. de O., Silva, M. T., de Sousa, F. de A. S., de Lima, A. M. M., Dos Santos, C. A., de Ataíde, L. C. P., & da Silva, V. de P. R. (2019). Four decades of hydrological process simulation of the Itacaiúnas river watershed, Southeast Amazon. *Boletim de Ciências Geodésicas*, 25(3).
- Sheffield, J., G. Goteti, & Wood, E.F., (2006). Development of a 50-Year High-Resolution Global Dataset of Meteorological Forcings for Land Surface Modeling. *Journal of Climate*, 19, 3088-3111.
- Shen, C., Niu, J. and Phanikumar, M.S. (2013). Evaluating controls on coupled hydrologic and vegetation dynamics in a humid continental climate watershed using a subsurface-land surface processes model, *Water Resources Research*, 49(5), 2552–2572.
- Shuttleworth, W.J., (2012). *Terrestrial hydrometeorology*. John Wiley & Sons.
- Sierra, J. P., Junquas, C., Espinoza, J. C., Segura, H., Condom, T., Andrade, M., Molina-Carpio, J., Ticona, L., Mardoñez, V., Blacutt, L., Polcher, J., Rabatel, A., & Sicart, J. E. (2022). Deforestation impacts on Amazon-Andes hydroclimatic connectivity. *Climate Dynamics*, 58(9–10), 2609–2636.

## References

- Sierra, J.P. *et al.* (2022). Deforestation impacts on Amazon-Andes hydroclimatic connectivity, *Climate Dynamics*, 58(9–10), 2609–2636.
- Sikder, M. S., David, C. H., Allen, G. H., Qiao, X., Nelson, E. J., & Matin, M. A. (2019). Evaluation of Available Global Runoff Datasets Through a River Model in Support of Transboundary Water Management in South and Southeast Asia. *Frontiers in Environmental Science*, 7.
- Da Silva, R. G., Alves R. d. C., Zingaretti S. M. (2020). Increased [CO<sub>2</sub>] Causes Changes in Physiological and Genetic Responses in C<sub>4</sub> Crops: A Brief Review. *Plants*. 9(11), 1567.
- Silva Junior, C. H. L., Pessôa, A. C. M., Carvalho, N. S., Reis, J. B. C., Anderson, L. O., & Aragão, L. E. O. C. (2021). The Brazilian Amazon deforestation rate in 2020 is the greatest of the decade, *Nature Ecology and Evolution*. Nature Research, 5(2), 144–145.
- Silva, J. F., Fariñas, M. R., Felfili, J. M., & Klink, C. A. (2006). Spatial heterogeneity, land use and conservation in the cerrado region of Brazil. *Journal of Biogeography*, 33(3), 536–548.
- Silver, W. L., Neff, J., McGroddy, M., Veldkamp, E., Keller, M., & Cosme, R. (2000). Effects of soil texture on belowground carbon and nutrient storage in a lowland Amazonian forest ecosystem. *Ecosystems*, 3(2), 193–209.
- Skiles, J. W., & Hanson, J. D. (1994). Responses of arid and semiarid watersheds to increasing carbon dioxide and climate change as shown by simulation studies. *Climatic Change*, 26, 377–397.
- Smith, B., & Wilson, J. B. (2002). Community convergence: ecological and evolutionary. *Folia Geobotanica*, 37, 171-183.
- Smith, M.N. *et al.* (2020). Empirical evidence for resilience of tropical forest photosynthesis in a warmer world, *Nature Plants*, 6(10), 1225–1230.
- Solar, R. R. de C., Barlow, J., Andersen, A. N., Schoereder, J. H., Berenguer, E., Ferreira, J. N., & Gardner, T. A. (2016). Biodiversity consequences of land-use change and forest

## References

- disturbance in the Amazon: A multi-scale assessment using ant communities. *Biological Conservation*, 197, 98–107.
- Sood, A., & Smakhtin, V. (2015). Revue des modèles hydrologiques globaux. *Hydrological Sciences Journal*, 60(4), 549–565.
- Soti, V., Puech, C., Lo Seen, D., Bertran, A., Vignolles, C., Mondet, B., Dessay, N., & Tran, A. (2010). The potential for remote sensing and hydrologic modelling to assess the spatio-temporal dynamics of ponds in the Ferlo Region (Senegal). *Hydrology and Earth System Sciences*, 14(8), 1449–1464.
- Souza, J. P., Melo, N. M. J., Pereira, E. G., Halfeld, A. D., Gomes, I. N., & Prado, C. H. B. A. (2016). Responses of woody Cerrado species to rising atmospheric CO<sub>2</sub> concentration and water stress: gains and losses. *Functional Plant Biology*, 43(12), 1183–1193.
- Spera, S.A., Winter, J.M. and Chipman, J.W. (2018). Evaluation of Agricultural Land Cover Representations on Regional Climate Model Simulations in the Brazilian Cerrado, *Journal of Geophysical Research: Atmospheres*, 123(10), 5163–5176.
- Spracklen, D. V. and Garcia-Carreras, L. (2015). The impact of Amazonian deforestation on Amazon basin rainfall, *Geophysical Research Letters*, 42(21), 9546–9552.
- Sprenger, M., Stumpp, C., Weiler, M., Aeschbach, W., Allen, S. T., Benettin, P., Dubbert, M., Hartmann, A., Hrachowitz, M., Kirchner, J. W., McDonnell, J. J., Orłowski, N., Penna, D., Pfahl, S., Rinderer, M., Rodriguez, N., Schmidt, M., & Werner, C. (2019). The Demographics of Water: A Review of Water Ages in the Critical Zone. *Reviews of Geophysics*, 57(3), 800–834.
- Stape, J.L. (2002). *Production ecology of clonal Eucalyptus plantations in northeastern Brazil*. Colorado State University.
- Stephenson, N. L. (1990). Climatic control of vegetation distribution: the role of the water balance. *The American Naturalist*, 135(5), 649-670.

## References

- Stevens, N. *et al.* (2017). Savanna woody encroachment is widespread across three continents', *Global Change Biology*, 23(1), 235–244.
- Stöckli, R., (2007). LBA-MIP driver data gap filling algorithms. Technical note for LBA data. Colorado State University. url: <https://www.climatemodeling.org/lba-mip/LBAmipDriverDataFillingMethods.pdf>
- Syed, T. H., Famiglietti, J. S., Rodell, M., Chen, J., & Wilson, C. R. (2008). Analysis of terrestrial water storage changes from GRACE and GLDAS. *Water Resources Research*, 44(2).
- Tatsch JD, Bindi M, & Moriondo M, (2009). Report: A preliminary evaluation of the Cropsyst model for sugarcane in the Southeast of Brazil. *Impact of Climate Change on Agricultural and Natural Ecosystems*, 75–84. Firenze University Press, Firenze, Italia.
- Teckentrup, L. *et al.* (2021). Assessing the representation of the Australian carbon cycle in global vegetation models, *Biogeosciences*, 18(20), 5639–5668.
- Terzago, S., Andreoli, V., Arduini, G., Balsamo, G., Campo, L., Cassardo, C., Cremonese, E., Dolia, D., Gabellani, S., von Hardenberg, J., Morra Di Cella, U., Palazzi, E., Piazzzi, G., Pogliotti, P., & Provenzale, A. (2020). Sensitivity of snow models to the accuracy of meteorological forcings in mountain environments. *Hydrology and Earth System Sciences*, 24(8), 4061–4090.
- Tesemma, Z. K., Wei, Y., Peel, M. C., & Western, A. W. (2015). The effect of year-to-year variability of leaf area index on Variable Infiltration Capacity model performance and simulation of runoff. *Advances in Water Resources*, 83, 310–322.
- The World Bank (2017). World Bank Open Data, Table: Agricultural irrigated land (% of total agricultural land). Data from the Food and Agricultural Organization. Retrieved from <https://data.worldbank.org/indicator/AG.LND.IRIG.AG.ZS?locations=BR> last access: 10 Apr 2023.

## References

- Thornton, P. E., Shrestha, R., Thornton, M., Kao, S. C., Wei, Y., & Wilson, B. E. (2021). Gridded daily weather data for North America with comprehensive uncertainty quantification. *Scientific Data*, 8(1).
- Tian, S., Renzullo, L. J., van Dijk, A. I. J. M., Tregoning, P., & Walker, J. P. (2019). Global joint assimilation of GRACE and SMOS for improved estimation of root-zone soil moisture and vegetation response. *Hydrology and Earth System Sciences*, 23, 1067–1081.
- Tijerina, D., Condon, L., FitzGerald, K., Dugger, A., O'Neill, M. M., Sampson, K., Gochis, D., & Maxwell, R. (2021). Continental Hydrologic Intercomparison Project, Phase 1: A Large-Scale Hydrologic Model Comparison Over the Continental United States. *Water Resources Research*, 57(7), 1-27.
- Tladi, T. M., Ndambuki, J. M., & Salim, R. W. (2022). Meteorological drought monitoring in the Upper Olifants sub-basin, South Africa. *Physics and Chemistry of the Earth*, 128, 1-8.
- Tomasella, J., & Hodnett, M. G. (1998). Estimating soil water retention characteristics from limited data in Brazilian Amazonia. *Soil Science*, 163(3), 190–202.
- Tomasella, J., & Hodnett, M. G. (2004). Pedotransfer functions for tropical soils. In *Developments in Soil Science* 30(C), pp. 415–429.
- Tomasella, J., Hodnett, M. G., & Rossato, L. (2000). Pedotransfer Functions for the Estimation of Soil Water Retention in Brazilian Soils. *Soil Science Society of America Journal*, 64(1), 327–338.
- Tomasella, J., Hodnett, M. G., Cuartas, L. A., Nobre, A. D., Waterloo, M. J., & Oliveira, S. M. (2008). The water balance of an Amazonian micro-catchment: The effect of interannual variability of rainfall on hydrological behaviour. *Hydrological Processes*, 22(13), 2133–2147.
- Trambauer, P., Maskey, S., Winsemius, H., Werner, M., & Uhlenbrook, S. (2013). A review of continental scale hydrological models and their suitability for drought forecasting in (sub-Saharan) Africa. *Physics and Chemistry of the Earth*, 66, 16–26.

## References

- Troch, P. A., Carrillo, G., Sivapalan, M., Wagener, T., & Sawicz, K. (2013). Climate-vegetation-soil interactions and long-term hydrologic partitioning: Signatures of catchment co-evolution. *Hydrology and Earth System Sciences*, 17(6), 2209–2217.
- Troch, P. A., Martinez, G. F., Pauwels, V. R. N., Durcik, M., Sivapalan, M., Harman, C., Brooks, P. D., Gupta, H., & Huxman, T. (2009). Climate and vegetation water use efficiency at catchment scales, *Hydrological Processes*, 2409–2414.
- Tron, S., Perona, P., Gorla, L., Schwarz, M., Laio, F., & Ridolfi, L. (2015). The signature of randomness in riparian plant root distributions. *Geophysical Research Letters*, 42(17), 7098–7106.
- Twine, T.E., Kustas, W.P., Norman, J.M., Cook, D.R., Houser, P., Meyers, T.P., Prueger, J.H., Starks, P.J. and Wesely, M.L., (2000). Correcting eddy-covariance flux underestimates over a grassland. *Agricultural and forest meteorology*, 103(3), 279-300.
- Valentine, H.T. and Mäkelä, A. (2012). Modeling forest stand dynamics from optimal balances of carbon and nitrogen, *New Phytologist*, 194(4), 961–971.
- Valverde, M. C. & Marengo, J. A. (2014). Extreme Rainfall Indices in the Hydrographic Basins of Brazil. *Open Journal of Modern Hydrology*, 4, 10-26.
- Van Der Ent, R. J., Savenije, H. H. G., Schaefli, B., & Steele-Dunne, S. C. (2010). Origin and fate of atmospheric moisture over continents. *Water Resources Research*, 46(9).
- van Genuchten, M.T. (1980), A Closed-form Equation for Predicting the Hydraulic Conductivity of Unsaturated Soils. *Soil Science Society of America Journal*, 44, 892-898.
- Van Wijk, M.T. and Bouten, W. (2001). Towards understanding tree root profiles: simulating hydrologically optimal strategies for root distribution. *Hydrology and Earth System Sciences*, 5(4), 629-644.
- Viana, F. de S., J., Maria Gico Lima Montenegro, S., Barbosa da Silva, B., Srinivasan, R., Augusto Guimarães Santos, C., Cezar dos Santos Araújo, D., & Gadelha Tavares, C. (2021).

## References

- Evaluation of gridded meteorological datasets and their potential hydrological application to a humid area with scarce data for Pirapama River basin, northeastern Brazil. *Theoretical and Applied Climatology*, 145, 393-419.
- Viola, M. R., Mello, C. R., Beskow, S., & Norton, L. D. (2014). Impacts of Land-use Changes on the Hydrology of the Grande River Basin Headwaters, Southeastern Brazil. *Water Resources Management*, 28(13), 4537–4550.
- Vissa, N. K., Anandh, P. C., Behera, M. M., & Mishra, S. (2019). ENSO-induced groundwater changes in India derived from GRACE and GLDAS. *Journal of Earth System Science*, 128(115), 1-9.
- Vogel, T., van Genuchten, M. T., Cislérova, M., & Brown, G. E. (2001). Effect of the shape of the soil hydraulic functions near saturation on variably-saturated flow predictions. *Advances in Water Resources*, 24, 133–144.
- von Randow, C., Manzi, A. O., Kruijt, B., de Oliveira, P. J., Zanchi, F. B., Silva, R. L., Hodnett, M. G., Gash, J. H. C., Elbers, J. A., Waterloo, M. J., Cardoso, F. L., & Kabat, P. (2004). Comparative measurements and seasonal variations in energy and carbon exchange over forest and pasture in South West Amazonia. *Theoretical and Applied Climatology*, 78(1–3), 5–26.
- Vörösmarty, C. J., Green, P., Salisbury, J., & Lammers, R. B. (2000). Global Water Resources: Vulnerability from Climate Change and Population Growth. *Science*, 289, 284–288.
- Wagner, P. D., Bieger, K., Arnold, J. G., & Fohrer, N. (2022). Representation of hydrological processes in a rural lowland catchment in Northern Germany using SWAT and SWAT+. *Hydrological Processes*, 36(5).
- Wang A. & Zeng X., (2012). Evaluation of multireanalysis products with in situ observations over the Tibetan Plateau. *Journal of Geophysical Research*, 117:D05102.
- Wannasin, C., Brauer, C. C., Uijlenhoet, R., van Verseveld, W. J., & Weerts, A. H. (2021). Daily flow simulation in Thailand Part I: Testing a distributed hydrological model with



## References

- seamless parameter maps based on global data. *Journal of Hydrology: Regional Studies*, 34(100794).
- Weber, M., Koch, F., Bernhardt, M., & Schulz, K. (2021). The evaluation of the potential of global data products for snow hydrological modelling in ungauged high-alpine catchments. *Hydrology and Earth System Sciences*, 25(5), 2869–2894.
- Webler, G. *et al.* (2012). Evaluation of a dynamic agroecosystem model (Agro-IBIS) for soybean in Southern Brazil, *Earth Interactions*, 16(12), 1–15.
- Webler, G., Roberti, D. R., Cuadra, S. V., Moreira, V. S., & Costa, M. H. (2012). Evaluation of a dynamic agroecosystem model (Agro-IBIS) for soybean in Southern Brazil. *Earth Interactions*, 16(12), 1–15. <https://doi.org/10.1175/2012EI000452.1>
- Whitehead, D. & Beadle, C.L. (2004). Physiological regulation of productivity and water use in Eucalyptus: A review, *Forest Ecology and Management*, 193(1–2), 113–140.
- Whitley, R. *et al.* (2016). A model inter-comparison study to examine limiting factors in modelling Australian tropical savannas, *Biogeosciences*, 13(11), 3245–3265.
- Whitley, R., Beringer, J., Hutley, L. B., Abramowitz, G., De Kauwe, M. G., Evans, B., Haverd, V., Li, L., Moore, C., Ryu, Y., Scheiter, S., Schymanski, S. J., Smith, B., Wang, Y. P., Williams, M., & Yu, Q. (2017). Challenges and opportunities in land surface modelling of savanna ecosystems. *Biogeosciences*, 14(20), 4711–4732.
- Wilson, K. B., & Baldocchi, D. D. (2000). Seasonal and interannual variability of energy fluxes over a broadleaved temperate deciduous forest in North America. In *Agricultural and Forest Meteorology* (Vol. 100).
- Wilson, K., *et al.* (2002). Energy balance closure at FLUXNET sites. *Agricultural and Forest Meteorology*, 113, 223-243.
- WMO (2021). Hydromet Gap Report. Tech. rep., Geneva, 53 [https://library.wmo.int/index.php?lvl=notice\\_display&id=21912#.Yjkbud\\_rIV](https://library.wmo.int/index.php?lvl=notice_display&id=21912#.Yjkbud_rIV).

## References

- Wohl, E., Barros, A., Brunzell, N., Chappell, N. A., Coe, M., Giambelluca, T., Goldsmith, S., Harmon, R., Hendrickx, J. M. H., Juvik, J., McDonnell, J., & Ogden, F. (2012). The hydrology of the humid tropics. *Nature Climate Change*, 2(9), 655–662.
- Wolf, A., Anderegg, W.R.L. and Pacala, S.W. (2016). Optimal stomatal behaviour with competition for water and risk of hydraulic impairment, *Proceedings of the National Academy of Sciences of the United States of America*, 113(46), E7222–E7230.
- Wright, C., Kagawa-Viviani, A., Gerlein-Safdi, C., Mosquera, G. M., Poca, M., Tseng, H., & Chun, K. P. (2018). Advancing ecohydrology in the changing tropics: Perspectives from early career scientists. *Ecohydrology*, 11(3), 1-18.
- Wright, S.J. (1996). Phenological Responses to Seasonality in Tropical Forest Plants. In: Mulkey, S.S., Chazdon, R.L., Smith, A.P. (eds) *Tropical Forest Plant Ecophysiology*. Springer, Boston, MA.
- Wu, Y., Liu, S. and Abdul-Aziz, O.I. (2012). Hydrological effects of the increased CO<sub>2</sub> and climate change in the Upper Mississippi River Basin using a modified SWAT. *Climatic Change*, 110(3–4), 977–1003.
- Xavier, A. C., King, C. W. & Scanlon B. R., (2016). Daily gridded meteorological variables in Brazil (1980–2013). *International Journal of Climatology*, 36, 2644-2659.
- Xi, Y., S. Peng, P. Ciais, and Y. Chen, (2021). Future impacts of climate change on inland Ramsar wetlands. *Nat. Clim. Change*, 11, 45–51.
- Xin, F, X. Xiao, O.M.R. Cabral, P. M. White Jr., H. Guo, J. Ma, B. Li, & B. Zhao. (2020). Understanding the Land Surface Phenology and Gross Primary Production of Sugarcane Plantations by Eddy Flux Measurements, MODIS Images, and Data-Driven Models. *Remote Sensing*. 12, no. 14: 2186. <https://doi.org/10.3390/rs12142186>
- Xu, Z., Z. Wu, H. He, X. Wu, J. Zhou, Y. Zhang, X. Guo, (2019). Evaluating the accuracy of MSWEP V2.1 and its performance for drought monitoring over mainland China. *Atmospheric Research*, 226, 17-31.

## References

- Yang, D., Shao, W., Yeh, P. J. F., Yang, H., Kanae, S., & Oki, T. (2009). Impact of vegetation coverage on regional water balance in the nonhumid regions of China. *Water Resources Research*, 45(7).
- Yang, Y., Donohue, R.J. and McVicar, T.R. (2016). Global estimation of effective plant rooting depth: Implications for hydrological modeling, *Water Resources Research*, 52(10), 8260–8276.
- Yang, Y., Roderick, M. L., Zhang, S., McVicar, T. R., & Donohue, R. J. (2019). Hydrologic implications of vegetation response to elevated CO<sub>2</sub> in climate projections. *Nature Climate Change*, 9(1), 44–48.
- Zandler, H., T. Senftl, & Vanselow K.A., (2020). Reanalysis datasets outperform other gridded climate products in vegetation change analysis in peripheral conservation areas of central Asia. *Nature: Scientific Reports*, 10:22446.
- Zemp, D. C., Schleussner, C. F., Barbosa, H. M. J., Hirota, M., Montade, V., Sampaio, G., Staal, A., Wang-Erlandsson, L., & Rammig, A. (2017). Self-amplified Amazon forest loss due to vegetation-atmosphere feedbacks. *Nature Communications*, 8(14681).
- Zemp, D. C., Schleussner, C. F., Barbosa, H. M. J., Van Der Ent, R. J., Donges, J. F., Heinke, J., Sampaio, G., & Rammig, A. (2014). On the importance of cascading moisture recycling in South America. *Atmospheric Chemistry and Physics*, 14(23), 13337–13359.
- Zeng, Z., Wang, D., Yang, L., Wu, J., Ziegler, A. D., Liu, M., Ciais, P., Searchinger, T. D., Yang, Z. L., Chen, D., Chen, A., Li, L. Z. X., Piao, S., Taylor, D., Cai, X., Pan, M., Peng, L., Lin, P., Gower, D., ... Wood, E. F. (2021). Deforestation-induced warming over tropical mountain regions regulated by elevation. *Nature Geoscience*, 14(1), 23–29.
- Zhang, S., Yang, H., Yang, D., & Jayawardena, A. W. (2016). Quantifying the effect of vegetation change on the regional water balance within the Budyko framework. *Geophysical Research Letters*, 43(3), 1140–1148.

## *References*

- Zhao, L., Xia, J., Xu, C. yu, Wang, Z., Sobkowiak, L., & Long, C. (2013). Evapotranspiration estimation methods in hydrological models. *Journal of Geographical Sciences*, 23(2), 359–369.
- Zhu, Z., Wang, H., Harrison, S. P., Prentice, I. C., Qiao, S., & Tan, S. (2023). Optimality principles explaining divergent responses of alpine vegetation to environmental change. *Global Change Biology*, 29(1), 126–142.